NUMERICAL PREDICTION OF STRUCTURAL FIRE PERFORMANCE FOR PRECAST PRESTRESSED CONCRETE FLOORING SYSTEMS

A thesis submitted in partial fulfilment
of the requirements for the
Degree of Doctor of Philosophy.

By
Jeong-Ki Min

Supervised by
Professor Andrew H. Buchanan
Associate Professor Rajesh P. Dhakal
Associate Professor Peter J. Moss
Dr Anthony Abu

Department of Civil and Natural Resources Engineering
University of Canterbury
Christchurch, New Zealand
2011

Abstract

In predicting the likely behaviour of precast prestressed concrete flooring systems in fire using advanced finite element methods, an improved numerical model using the non-linear finite element program SAFIR has been developed in order to investigate the effects and the interaction of the surrounding structures and has been used extensively throughout this thesis. Note that fire induced spalling is not included in the analysis.

In the numerical investigation of the new model, the reinforced concrete topping is modelled as part of the beam elements in order to predict the behaviour of single hollowcore concrete slabs, with various support conditions, under a Standard ISO fire. It is shown that the current approach using tendons that are anchored into the supporting beams leads to a major problem for precast prestressed flooring systems. In order to resolve this problem, a multi-spring connection model has been developed to include the old and new connection systems corresponding to the New Zealand Concrete Standard NZS 3101. The connection model with hollowcore slabs is validated against a published fire test. The investigation on restrained hollowcore floors is performed with various parameters and boundary support conditions. Numerical studies on various boundary support conditions show that the behaviour of hollowcore floors in fire is very sensitive to the existence of side beams. Further investigations on the effects of fire emergency beams, which reduce the transverse curvature of floors to improve fire resistance, are made on 4x1 multi-bay hollowcore floors with different arrangements of theses beams. The numerical studies show that fire emergency beams significantly increase the fire resistance.

Code based equations which can calculate the shear resistance and splitting resistance are then introduced. The Eurocode equation can be modified with high temperature material properties to estimate the shear capacity of a hollowcore slab. The modified Eurocode equation which is fit to fire situations validated against the published literature with respect to shear tests in fire.

The structural behaviour of single tee slabs having different axial restraint stiffness as well as the variation of axial thrust in fire is then studied. SAFIR

analyses of single tee slabs show that fire performance can increase when a web support type is used that has high axial restraint stiffness.

A series of test results on prestressed flat slabs conducted in United States are used to validate a simply supported numerical model. The application of multi-spring connection elements is also investigated in order to examine the feasibility of continuity.

Acknowledgement

I would like to express my sincere gratitude to Professor Andrew Buchanan, Associate Professor Peter Moss, Associate Professor Rajesh Dhakal and Dr. Anthony Abu for all the guidance, inspiration, patience, support and constructive criticisms that they have given me during my this research. You are a great supervisory team. This research would never have been possible without the long hours and precious time they spent with me.

The financial support provided by the Future Building Systems project and Department of Civil and Natural Resources Engineering is greatly appreciated. I thank Professor Jean-Marc Franssen of University of Liège for his invaluable guidance and help with the SAFIR program throughout the project. I thank Venkatesh Kodur of Michigan State University and Linus Lim of Arup Fire for reviewing my PhD thesis with impressive comments. I thank Jerry Chang for guiding with SAFIR program when I started my research. I thank Senior Lecture Michael Spearpoint and Associate Professor Charley Fleischmann who organised Fire Research Meeting in every Friday. I thank all staff of the Department of Civil and Natural Resources Engineering, at the University of Canterbury.

I would like to thank my friends Dr. Min-Ho Chey, Hyun Chan Kim, Dongxu Li, Matthew Qu, Jakob Studhalter, Dennis Pau, James O'Neill, Phillip Spellman, MEFE students (past and present) and all colleagues (past and present) of E307. Jakob helped me translate Borgogno's PhD thesis to English for Chapter 7.

I would like to thank Professor Sang-Dae Kim and Associate Professor Young-Kyu Ju from Korea University, Assistant Professor Myeong-Han Kim from Daejin University, Korea, for all their help. They have supported me in many ways, for which I will always be grateful to them.

I would like to thank my family and parents-in-law for their understanding and devotion during my years of study. My sincere appreciation is expressed to my father, Byeong-Cheol Min, my young sister, Jeong-Hee, and young brother, Hyung-Ki, for all their encouragement and belief. I know my mother, Kyeong-Ja Kim, who passed away 7 years ago, is celebrating with me in spirit. Also, I wish to thank my wife, Eunsuk Ju, for all her love.

Table of Contents

List of Figures

List of Tables

Notation

a	Axis distance of prestressing steel from the nearest exposed surface
a	Depth of the equivalent rectangular stress block at ultimate load
A_c	Area of concrete cross section
A_p	Total cross sectional area of prestressing strands at the bottom face of the section
A_s	Cross sectional area of reinforcement
A_{ps}	Cross sectional area of prestressing steel
A_{sl}	Area of the tensile reinforcement, which extends ≥ (lbd +d) beyond the section considered, where lbd is a bond development length
A_t	Total internal area of the bounding surfaces
A_v	Area of the window opening
b	$\sqrt{\text{thermal inertia}} = \sqrt{\text{k}\rho c_\text{p}}$
b_w	Total web width
b_w	Smallest width of the cross-section in the tensile area
b_{wi}	Thickness of an individual web
c	Cover thickness
c_p	Specific heat
C	Compressive force
d	Distance between the centroid of reinforcement and extreme compression fibre
d	Effective depth
e_0	Eccentricity of the prestressing steel
$f_{bpd,fi}$	Bond strength for anchorage of the tendon at elevated temperatures
f_c	Compressive strength of concrete
f_c'	Specified Compressive strength of concrete
$f_{c,fi,m}$	Average strength of concrete at elevated temperatures
f_{ck}	Characteristic value of compressive strength of concrete
f_{ct}	Tensile strength of the concrete
f_{ctd}	Design tensile strength
f_{dt}	Design principal tensile strength of concrete
f_{pk}	Characteristic tensile strength of prestressing steel
f_{ps}	Stress in prestressing steel in flexural member at ultimate load
f_{yk}	Characteristic yield strength of reinforcement
$f_{y,T}$	Reduced yield stress

$F_{R,a,fi}$	Force capacity of prestressing and ordinary reinforcement anchored at the support
$F_{R,a,fi,p}$	Force capacity of the prestressing steel anchored at the support
$F_{R,a,fi,s}$	Force capacity of ordinary reinforcement anchored at the support
F_v	Ventilation factor
H_v	Height of the window opening
h	Thickness of a slab
k	Thermal conductivity
$k_p(\theta)$	Strength reduction factor for the prestressing steel at temperature θ
$k_s(\theta_m)$	Strength reduction factor for the ordinary reinforcement at temperature θ_m
l_{pt}	Value of the transmission length
l_{pt1}	Lower design value of the transmission length
L	Span
M	Service load bending moment
M_0	Decompression moment
M_n	Nominal moment strength
M_x	Moment in the cross section at a distance x from the theoretical support
P_0	Initial prestressing force just after release
t	Time
t^*	Fictitious time
t_{rel}	Age of the concrete at release
T	Tensile force
T_c	Concrete temperature
T_f	Temperature
T_s	Steel temperature
T_w	Surface temperature
V_x	Force in the cross section at a distance x from the theoretical support
$V_{Rd,c,fi}$	Shear flexure equation for fire situation
V_{uk}	Shear capacity of the member in the region which is cracked in flexure
w	Load
w_d	Dead load
w_f	Fire design load
w_l	Live load
w_s	Self-weight
x	Anchorage length of the tendon for the considered section

Γ	Fictitious time factor
ε_i	Initial strain
ε_{th}	Thermall strain
ε_σ	Stress related strain
ε_{total}	Total strain
ξ	1.6 - d (m)
ρ	Density
$\rho_{l,fi}$	Force-equivalent ratio of longitudinal reinforcement
$\sigma_{cp,20}$	Concrete stress due to prestressing force at normal temperature
$\sigma_{cp,fi}$	Average stress on the concrete section for fire condition
σ_{pm0}	Stress in the tendon just after release
σ_{sp}	Splitting strength
$ø$	Diameter of strand
$ø$	Revised strength reduction factor

Chapter 1

Introduction

1.1 Background

Significant improvements in structural fire engineering have taken place since the late 1990s. Improved knowledge of structural behaviour in fire from the full-scale Cardington frame fire tests (Kirby, 1997 and 2000), a better understanding of fire dynamics, and the development of advanced finite element modelling on global structural analysis have all contributed to these advances. In addition, since the collapse of the World Trade Centre towers (FEMA, 2002), the finite element analysis technique is being increasingly used as a design tool to bring greater robustness to the response of structures to fire.

Precast prestressed concrete flooring systems in multi-storey buildings have become more popular over the last 30 years in New Zealand and overseas. This is because precast prestressed concrete flooring systems provide several advantages such as high quality control, the saving of labour, and the reduction of weight without significant loss of strength or stiffness compared with traditional cast-in-situ concrete at ambient temperature (Technical reports, 2007).

During the last 15 years, New Zealand has adopted a performance-based fire code which mainly emphasises life safety rather than property protection (Buchanan, 2008). The development of a performance-based fire code has reduced the importance of structural fire engineering as well as fire resistance time requirements in New Zealand. Nevertheless, the research on structural fire engineering is still important because passive fire protection, such as fire resistance, plays an important role in controlling the spread of fire. In addition, the collapse of buildings in fire can lead to a large loss of property.

The Standard fire test has been widely used to determine the fire resistance of each structural element such as beams, slabs, columns and walls. In this manner, fire resistance of structural elements is mainly determined by the exposure in furnace conditions rather than structural interaction. Although this prescriptive approach can be useful for deciding the fire resistance time of structures, the results obtained from a standard fire test may not exactly predict structural behaviour in practice. Because of this drawback of the standard fire test, there have been many attempts to experimentally and numerically predict fire performance of reinforced concrete and steel structures with the surrounding structural elements. On the other hand, many studies on precast prestressed concrete structures in fire have mainly focused on the prestressed units alone rather than structural interaction with the surrounding structures (Andersen and Lauridsen, 1999, Schepper and Andersen, 2000, Fellinger, 2004, Jensen, 2005).

The fire performance of precast prestressed concrete floor systems is heavily influenced by the end connections and the stiffness of the surrounding structure, both of which must be considered in any analysis. Analysing floor slabs with beam or shell elements whose end nodes share the nodes of supporting beams leads to a major problem for precast prestressed flooring systems where the steel tendons terminate at the end of the flooring units because the approach of sharing nodes of the supporting beam and floor assumes that these tendons are anchored into the supporting beams. In order to obtain more accurate predictions of prestressed concrete slab behaviours in fire, a new model which can contribute to understanding several different load carrying mechanisms of precast prestressed concrete flooring systems during fire exposure is required.

1.2 Research objectives

This research programme has been initiated by Chang (2007) as part of the Future Building Systems Research Project at University of Canterbury in order to investigate the structural performance of precast prestressed hollowcore concrete flooring systems in fire. The main aim of this research is to develop an advanced

numerical model that addresses the behaviour of alternative load bearing mechanisms of precast prestressed flooring systems in fire. The three precast prestressed flooring systems investigated in this research are:

- Hollowcore slabs
- Single tee slabs
- Prestressed flat slabs

More specific objectives of this study are:

1. To develop a finite element model for the 3-dimensional behaviour of precast prestressed hollowcore concrete flooring systems and validate this against available literature test results.
2. To investigate the fire performance of precast prestressed hollowcore concrete floors connected with surrounding structures such as supporting beams, side beams and columns.
3. To extend the modelling to cover the fire performance of precast prestressed tee- and flat slabs.
4. To provide recommendations on the design and construction of precast prestressed concrete flooring systems in order to provide improved fire resistance.

1.3 Scope of thesis

As mentioned in Section 1.2, the main objective of this thesis is to develop an advanced numerical model which can be applied to precast prestressed flooring systems. Throughout this thesis, the non-linear finite element program SAFIR is used. No experimental testing was carried out in the course of this research. Due to the characteristics of the program, the research focusses on global behaviour of precast prestressed flooring systems, rather than local behaviour (such as spalling, anchorage or shear). The numerical prediction of structural fire performance on precast prestressed slabs is investigated with the scope as summarised below:

1. Hollowcore slabs: The structural fire performance of hollowcore slabs in fire can vary depending on the geometry, the height of units and the arrangement of prestressing steels. Moreover, there still exist various arguments on failure modes of hollowcore slabs in fire. Therefore, in this thesis the height of hollowcore unit is limited to 200mm, which is believed to fail in flexural bending with respect to simple supports (Fellinger, 2004).
2. Single tee slabs: Different support types, namely web support, notched web support, and flange support, on prestressed single tee slabs have been used in New Zealand. In particular, flange support has several specific details depending on developer (Hare, 2009). However, in this research reinforcement details are not included.

1.4 Organisation of thesis

In this thesis, Chapter 1 (this chapter) gives an introduction to the background, objectives, scope and organisation of the research.

Chapter 2 addresses structural fire safety of precast prestressed floors. In addition, this chapter contains a review of literature relevant to precast prestressed concrete floors, particularly hollowcore slabs and double tee slabs, in fire.

Throughout chapters 3 to 6, a series of numerical studies are performed following the modelling framework of Figure 1.1.

Temperature development of a hollowcore cross section under the Standard fire is assessed in Chapter 3. A sensitivity analysis is also performed to investigate the effect of mesh density. A preliminary investigation of the behaviour of the hollowcore slab unit (10m span, 1.2m width and 200mm depth including 65mm topping concrete) is performed using the modified grillage model which includes only beam elements. In this chapter, only one unit, as shown in 1(a) of Figure 1.1, is used to perform the numerical analysis.

Chapter 4 develops the multi-spring connection model to represent the connection behaviour between hollowcore slabs and supporting beams. Based on the multi-spring connection model, the structural behaviour of the hollowcore slab

unit restrained by supporting beams is numerically investigated by varying its topping thickness, the number of prestressing strands, and the number of starter bars. The failure mechanism in a hollowcore slab unit is studied. The investigation in this chapter covers one hollowcore unit plus supporting beams, as shown in 1(b) of Figure 1.1.

Chapter 5 describes the numerical modelling of 200mm prestressed hollowcore slabs focusing on the MacPherson's seating connection detail (MacPherson, 2005) along with the multi-spring connection model. In order to investigate the effects of surrounding structures, such as end (or support) beams on the fire resistance of hollowcore slabs, numerical studies are performed using a variable end beam length as edge support for the single hollowcore unit, without consideration of columns (2(a), 2(b) and 2(c) of Figure 1.1). In addition, the model has been extended to include columns (3(a) of Figure 1.1). The fire performance, with respect to each case, is studied and the failure mode is investigated. The effect of infill which has been adopted in the New Zealand Concrete Standard NZS 3101 (SNZ, 2006a) is investigated along with side beams and compared to the case of no infill with the first hollowcore unit placed next to the side beam (3(b) and 3(c) of Figure 1.1).

In Chapter 6, a one bay prestressed hollowcore floor model is extended such that fire performance of multi-bay (4 x 1 bay) prestressed hollowcore floor slabs is investigated (4(a) of Figure 1.1). In addition, the behaviour of multi-bay hollowcore floor slabs exposed to ISO fire including cooling has been investigated. The influence of fire emergency beams which reduce the transverse curvature of floors on multi-bay prestressed hollowcore floor slabs is compared in terms of fire resistance time (4(b) and 4(c) of Figure 1.1).

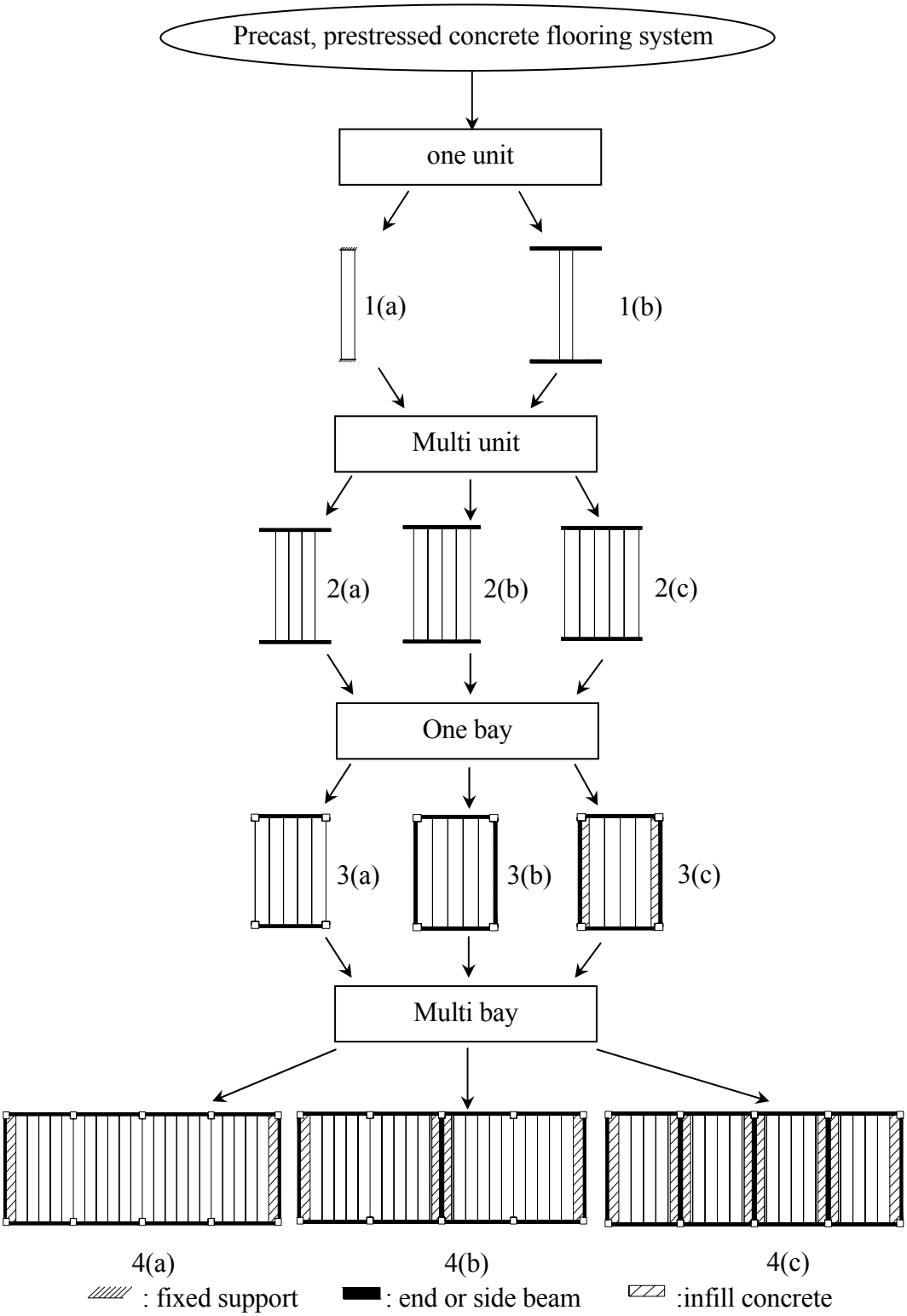

Figure 1.1 A framework of modelling of precast prestressed flooring system

Chapter 7 introduces the failure mechanism of hollowcore slabs in fire. Possible failure modes of hollowcore slab units in fire are mentioned and discussed. Some failure modes are investigated based on calculation methods given in several Codes.

In Chapter 8, the structural behaviour of a single tee slab having different restraint mechanisms is numerically investigated. The effects of prestressing level are examined. In order to simulate the restraining effect between single tee slabs and a supporting structure, analysis models are developed and assessed.

A series of laboratory test results (Gustaferro, 1967) on prestressed concrete flat slabs conducted in United States is used to validate a numerical analysis model having simply supported boundary conditions in Chapter 9. The application of multi-spring connection elements is also investigated in order to examine the feasibility of the continuity. In addition, the proprietary rating of prestressed flat slabs is compared with numerical analysis.

Finally, a summary of the major findings and suggestions for further study are presented in Chapter 10.

Chapter 2

Review of Structural Fire Safety of Prestressed Concrete Slabs

---

2.1 Introduction

This chapter introduces a variety of precast, prestressed concrete slab systems, such as hollowcore, double tee and prestressed flat slabs. A brief summary of the current approaches to assessing fire resistance of prestressed concrete slabs will be presented. A literature review of previous research on prestressed concrete slabs will be provided. Lastly, the analysis capability, structural elements and material properties regarding the finite element program, SAFIR, which is used in this study, are described.

2.2 Prestressed concrete slabs

For the purposes of this thesis, prestressed concrete slabs refer to precast pre-tensioned components for flooring, including hollowcore slabs, double tee slabs and prestressed flat slabs. Post-tensioned concrete slabs are not included. Precast prestressed concrete flooring offers an economic and versatile solution that is widely used in commercial, industrial and domestic buildings, offering both design and cost advantage over traditional methods such as in situ concrete. In this section, three common prestressed concrete floor slabs are explained.

2.2.1 Hollowcore slab

A hollowcore slab is an extruded, precast, prestressed concrete slab with continuous voids provided to reduce weight, costs and for electrical and mechanical runs, as well as a reinforced concrete topping. Standard unit width is 1,200mm and standard

unit depths are 200, 300 and 400mm. Units are cut to a customised length. A hollowcore slab is ideally suited for large floor spans with commercial loading. In New Zealand, the cast-in-situ topping is typically 65mm or 75mm thick (http://www.stresscrete.co.nz and http://www.stahlton.co.nz).

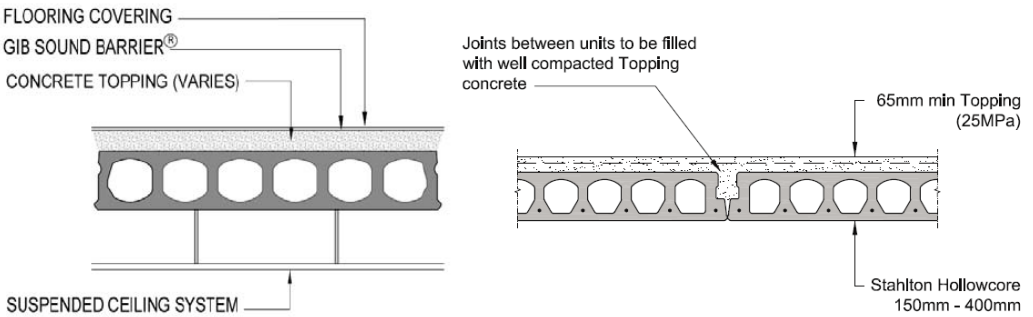

(a) Stresscrete (2011) (b) Stahlton (2011)

Figure 2.1 Typical hollowcore sections

2.2.2 Double Tee slabs

Double Tee flooring units consist of two prestressed ribs and a connecting top slab. The depth of the Double Tees can vary from 200 to 600mm. The connecting slab is usually 2,400mm wide x 50mm thick. Double Tees are ideally suited for larger spanning floors with a wide variety of services suspended from the flooring system. Double Tees can easily accommodate large ducts or other services between the webs. The cast-in-situ topping is typically 65mm or 75mm thick (http://www.stresscrete.co.nz and http://www.stahlton.co.nz).

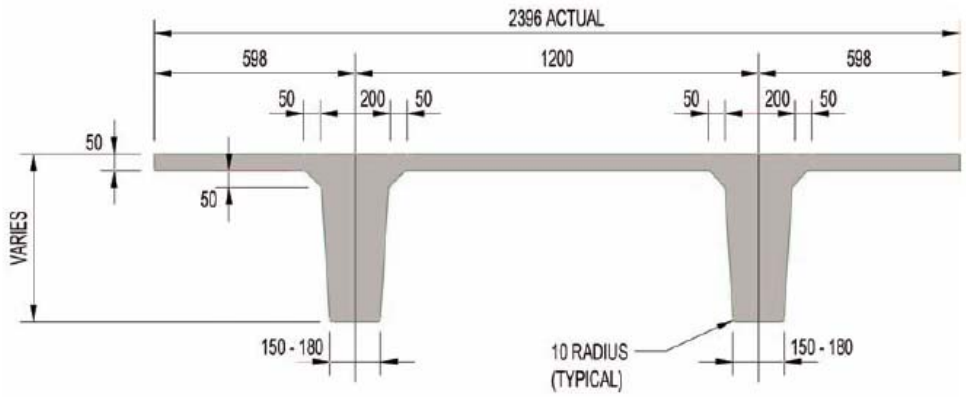

(a) Stresscrete (2011)

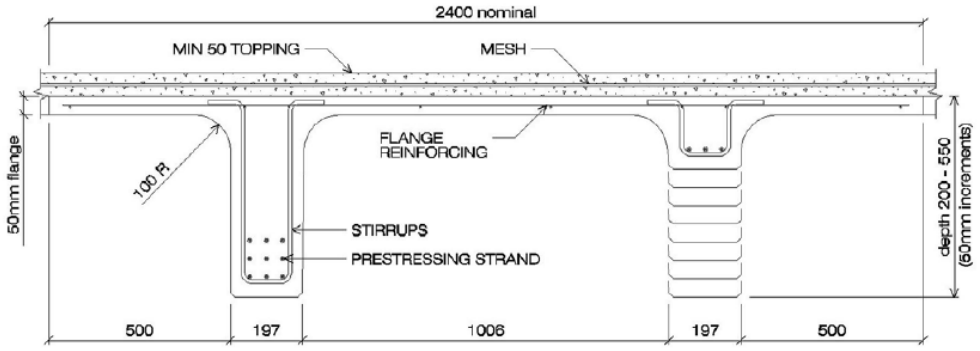

(b) Stahlton (2011)

Figure 2.2 Typical double tee sections

2.2.3 Prestressed flat slabs

The prestressed flat flooring system consists of a 75mm thick precast prestressed concrete slab with a reinforced concrete topping. This composite construction allows clear spans of up to 8.0 metres (http://www.stresscrete.co.nz and http://www.stahlton. co.nz). The terminology of prestresssed flat slabs can be different depending on the manufacturer. For instance, Stresscrete uses "unispan" slabs (Stresscrete, 2011) instead of prestressed flat slabs (Stahlton, 2011).

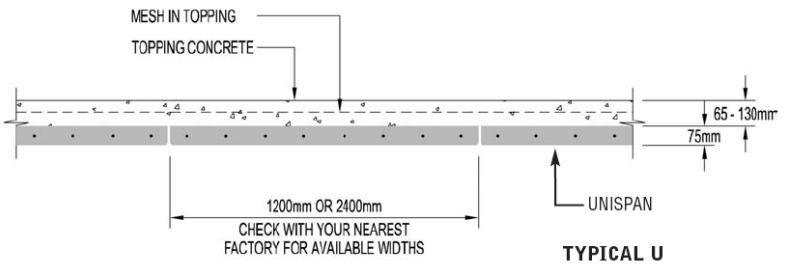

(a) Stresscrete (2011)

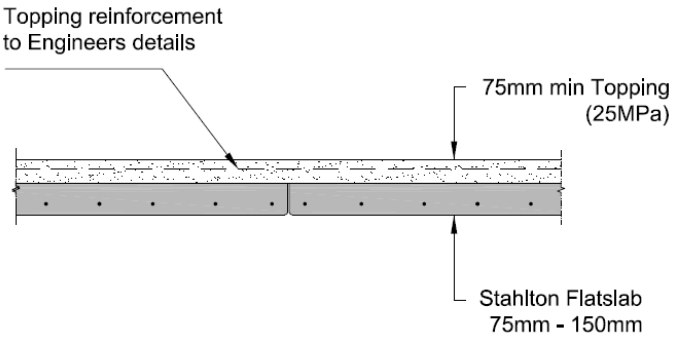

(b) Stahlton (2011)

Figure 2.3 Typical prestressed flat sections

2.3 Approaches to assessing fire resistance of prestressed concrete slabs

Various different approaches can be used to evaluate fire resistance of prestressed concrete slabs; a summary of current methods is presented.

2.3.1 Standard fire test

The current prescriptive rules for assessing the fire resistance of prestressed concrete slabs are based solely on the results and observations from standard fire resistance tests. Basically, the test involves subjecting a structural member to a heated furnace environment for the desired duration. The resulting fire resistance rating is expressed as the time (in minutes) that the member is able to withstand exposure to the Standard fire before a specified failure criteria is reached. Based on these tests, structural members are classified into fire resistance categories, for instance R30, R60, R90, R180, R210 and R240. The standard test methods for determining the fire resistance of precast prestressed concrete slabs are either the International Standard ISO 834 (ISO, 1975), BS 476 (BSI, 1987), or ASTM E119 (ASTM, 1998). Results of standard fire tests are listed by some testing authorities, for instance, Underwriters Laboratories (UL) and Underwriters Laboratories of Canada (ULC).

2.3.2 Codes and standards

Most countries throughout the world require structures to meet minimal fire safety requirements. Typically, design provisions offer a hierarchy of design methods, such as tabulated data, simplified calculations, and advanced methods. The hierarchy varies in complexity of application, with the tabulated data being the easiest and the advanced methods being the most complex. Therefore, most design provisions are typically established through either tabulated data or simplified calculations. However, in recent years performance-based methods have been introduced to offer more flexibility to designers through a rational approach. In this section, an overview of New Zealand, European and United States design provisions are presented.

New Zealand

All concrete structures in New Zealand are designed in accordance with the New Zealand Concrete Standard NZS 3101 (SNZ, 2006a). In addition, the New Zealand Concrete Standard NZS 3101 (SNZ, 2006a) offers tabulated data to establish the fire performance of a prestressed concrete slabs. The tabulated fire rating for the slabs is based on minimum concrete cover. Through this parameter the tabulated prescriptive method gives fire ratings for 0.5, 1, 1.5, 2, 3, or 4 hours for prestressed slabs.

Europe

The majority of European countries design concrete structures in accordance with the European Standards, better known as “Eurocode” (2004). All reinforced and prestressed concrete structures are governed by EN 1992-1-1 (EC2, 2003) and the fire provisions are supplied in EN 1992-1-2 (EC2, 2004). The provisions offer tabulated data, simplified calculations and advanced methods. The quickest method to crudely determine the fire resistance of a prestressed slab is through the tabulated data. The tabulated prescriptive method gives fire ratings for 0.5, 1, 1.5, 2, 3 and 4 hours for prestressed slabs. The ratings are based on minimum slab thickness and

average axis distance of tendon to the exposed surface. The tables are supplied based on support conditions; either simply or continuously supported.

United States

All concrete structures in the United States are designed in accordance with the American Concrete Institute standards (ACI 318, 2005). However, this guide references ACI 216.1 (2007) for the fire provisions of concrete structural members. The ACI provisions for prestressed concrete slabs are similar to the Precast/ Prestressed Concrete Institute Design Handbook (2004) and International Building Code (ICC, 2006). These codes offer tabulated data and simplified procedures to establish the fire performance of a prestressed concrete beam. The ratings are valid for ASTM E119 (ASTM, 1998) standard fire test. The tabulated fire ratings for the slabs are based on minimum concrete cover and depend on restraint and aggregate type. The restraint is categorized either as restrained or unrestrained. The aggregate types are classified as siliceous, carbonate, semi-lightweight or lightweight.

All the tabulated fire ratings for the prestressed concrete slabs mentioned above are summarised in Table 2.1. In terms of ACI 216.1 (2007), only results for siliceous aggregates are shown in Table 2.1.

2.3.3 Manufacturer's websites

Most precast prestressed concrete manufacturers provide the minimum fire resistance of products based on Standard fire testing results. These can be found on their web sites.

Table 2.1 A summary of fire resistance ratings for prestressed concrete slabs

FIRE RESISTANCE RATING	0.5 hour		1.0 hour		1.5 hours		2.0 hours		3.0 hours		4.0 hours		NOTES
	Width[1] or Slab depth[2] (mm)	Axis distance (mm)	Width[1] or Slab depth[2] (mm)	Axis distance (mm)	Width[1] or Slab depth[2] (mm)	Axis distance (mm)	Width[1] or Slab depth[2] (mm)	Axis distance (mm)	Width[1] or Slab depth[2] (mm)	Axis distance (mm)	Width[1] or Slab depth[2] (mm)	Axis distance (mm)	
DOCUMENT, STANDARD OR CODE													
NZS 3101:2006 (NZ) -Solid and hollow-core slabs	-	25	-	35	-	45	-	55	-	70	-	80	normal-weight 1-way simply supported
	-	25	-	25	-	30	-	35	-	45	-	55	normal-weight continuous
NZS 3101:2006 (NZ) EN 1992-1-2:2004 (Europe) -Ribbed slabs	80[1]	30	100[1] 120[1] ≥200[1]	50 40 30	120[1] 160[1] ≥250[1]	60 55 45	160[1] 190[1] ≥300[1]	750 70 55	220[1] 260[1] ≥410[1]	90 85 75	280[1] 350[1] 500[1]	115 90 85	normal-weight 1-way and 2-way simply supported
	80[1]	25	100[1] 120[1] ≥200[1]	40 30 25	120[1] 160[1] ≥250[1]	50 40 30	160[1] 190[1] ≥300[1]	60 55 45	310[1] 600[1]	75 65	450[1] 700[1]	85 75	normal-weight 1-way and 2-way continuous
NZS 3101:2006 (NZ) EN 1992-1-2:2004 (Europe) -Flat slabs	150[2]	25	180[2]	30	200[2]	40	200[2]	50	200[2]	60	200[2]	75	normal-weight
EN 1992-1-2:2004 (Europe) -Solid slabs	60[2]	25	80[2]	35	100[2]	45	120[2]	55	150[2]	70	175[2]	80	normal-weight 1-way simply supported
ACI 216.1-07: 2007 (USA) -Floor slabs	-	-	-	28	-	38	-	44	-	60	-	69	Siliceous, unrestrained
ACI 216.1-07: 2007 (USA) -Floor slabs	-	-	-	19	-	19	-	19	-	19	-	19	Siliceous, restrained

2.4 Previous studies on prestressed concrete slabs

Over the past five decades, more than one hundred hollowcore units have been tested under standard fire conditions in laboratory tests (Elliott, 2000; Fellinger, 2004; Overbeek, 2010). The majority of tests were designed primarily to check the fire resistance of individual hollowcore units rather than the structural behaviour of a system of hollowcore slabs in fire. Most test results have been briefly reported or not reported at all, as most of them are confidential (Fellinger, 2004; Overbeek, 2010). Most previous studies on prestressed concrete slabs concentrated on hollowcore slabs, although there have been a few researchers who focussed on double tee slabs.

The next section will review available literature, which has been reported as journal papers or reports, on structural behaviour of hollowcore units in fire. The reviews are chronologically ordered. Previous studies on double tee slabs are reviewed in terms of laboratory tests and numerical and analytical studies.

2.5 Hollowcore slabs

ETH Zurich, 1997 (Switzerland)

Borgogno (1997) investigated the structural behaviour of hollowcore slabs both at ambient temperature and at elevated temperatures. Possible failure modes were identified and structural models of hollowcore slabs were developed with respect to rigid supports. In terms of fire performance, bending, anchorage, shear compression, and shear tension failures are observed and compared with test results which were carried out at ETH, CTICM (France) and elsewhere as shown in Table 2.2. Among the tests, six fire tests were performed at ETH. In addition, the structural behaviour of hollowcore slabs with flexible supports, such as steel beams, was examined. The results show that the structural behaviour of the hollowcore elements is decisively influenced by the conditions at the supports. In particular, a flexible support on a beam and the transverse bending of the hollowcore slab decrease the shear resistance significantly.

Table 2.2 Listing of fire tests, which were considered for the verification of the ETH model (Borgogno, 1997)

Test[1]	Date	Slab[2]	Support[3]	S[4]	l_c[5]	Support width[6]	M/V[7]	t_u[8]
PTT	16.08.94	P16+8	flex./f	80	100/500	A_s^-/A_t	22.0/26.6	>122
B2-1	21.03.95	P20	flex./f	85	100	-	18.5/26.4	>122
B2-2	15.03.95	P20	flex./f	80	100	-	30.1/42.1	49/A
B2-3	27.03.95	P20	flex./f	80	100/500	A_t	31.1/48.1	75/P
B2-4	23.06.95	P20, PL	flex./f	89	100	-	27.4/38.1	75/A
B3-1N	05.07.95	P20	rigid/f	80	100	-	30.2/34.3	97/A
B3-1P	05.07.95	P20, PL	rigid/f	80	100	-	27.0/33.9	>97
CTICM 73	26.03.73	DCS16	rigid/f	200	100	-	32.3/34.0	55/B
CTICM 93	21.04.93	DCS16	flex./f	100	100	-	42.1/28.1	33/B
CTICM 95/1	02.11.95	DAL16+5	flex./f	90	190	A_s^-	71.0/46.6	48/B
CTICM 95/2	07.12.95	DAL16+5	flex./f	90	740	A_s^{--}/A_t	46.7/32.0	99/D
CTICM 96/1	28.08.96	DAL16+5	rigid/f-b	90	190	A_s^-	71.0/46.6	70/FC
CTICM 96/2	03.09.96	DAL16	rigid/f(-b)	90e	160	-	49.6/33.4	40/FC
HD-2/85	1985	HD14	rigid /f	225	-	-	36.5/30.4	32/B
HD-3/85	1985	HD14	rigid /f	225	-	-	21.7/18.2	50/FT
HD-3/85	1985	HD14	rigid /f	225	-	-	27.5/22.8	45/FT
Sevilla	02.92	HOR14+6	rigid /f(-b)	75	-	A_s^-	13.5/6.0	*/B

1. Tests: The tests in Zurich (PTT and Bi-k) are described in [Borgogno and Fontana (1995/6)]. The tests of Metz (CTICM *) are in [CTICM (1973)], [CTICM (1995/1)], [CTICM (1995/2)], [CTICM (1996/1)] and [CTICM (1996/2)]. The tests of Brunswick (HD*) are in [Richter (1987/2)]. The fire test in Seville has been published in [Rui-Wamba (1994)].
2. Slab: All hollowcore slabs were 1.20m wide and used round wires except for P20, PL. The first number refers to the hollowcore slab height, the second number refers to the concrete cover thickness. [cm]
3. Support: It is distinguished between flexible bottom flange steel (flex) and rigid, uniform points (rigid distinction). f stands for free expansion ability of the test specimen and b (blocked) for expansion disability in a longitudinal direction.
4. Support width: e means that the support area of the plate is completely embedded in concrete. [mm]
5. lc filling depth: length of the filling depth of concrete in the cavities. In the case of an additional reinforcement in each of two cavities per hollowcore slab, the second number is their filling depth. [mm]
6. Reinforcement: As-(-) reinforcement in cover thickness. At: cavity reinforcement (sometimes declined tensile reinforcement).
7. M / V: M is the maximum moment per a hollowcore slab, V is the maximum shear force. [KNm] and [kN]
8. Fire resistance tu: failure time [min]. Failure modes: anchorage failure (A), brittle web failure in combination with complete destruction (B), test stopping due to a rapid increase of a deformation (D), concrete failure in the bending compression zone (FC) and shear failure due to punching (P).

Danish Institute of Fire Technology, 1999 (Denmark)

Danish researchers (Andersen *et al.*, 1999) carried out three separate fire tests on hollowcore slabs, simply supported without axial restraint and subjected to the ISO 834 fire, to investigate spalling of high strength concrete. Hollowcore units were of 6.0m length and 1.2m width with three different depths (thicknesses), 185mm (SP 18), 220mm (SP 22) and 270mm (SP 27) as shown in Figure 2.4. Each test consisted of two identical slabs (Figure 2.5) and no topping concrete was included. Bond failure between the main reinforcement and the surrounding concrete was observed after approximately 10 minutes of testing on each slab. In all three tests the failure mechanism leading to collapse can be characterised as a shear failure. For the slabs SP 18 and SP 22 the shear failures occurred approximately 1m from the support and the observed rupture figures were very similar, showing a classic rupture figure with a rupture line of 45 degrees. The shear failure concerning the SP 27 slab occurred at the support as the supporting concrete snapped off.

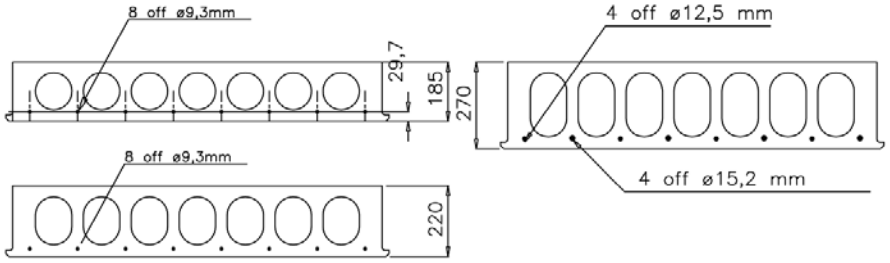

Figure 2.4 Test specimens for Danish tests (Andersen *et al.*, 1999)

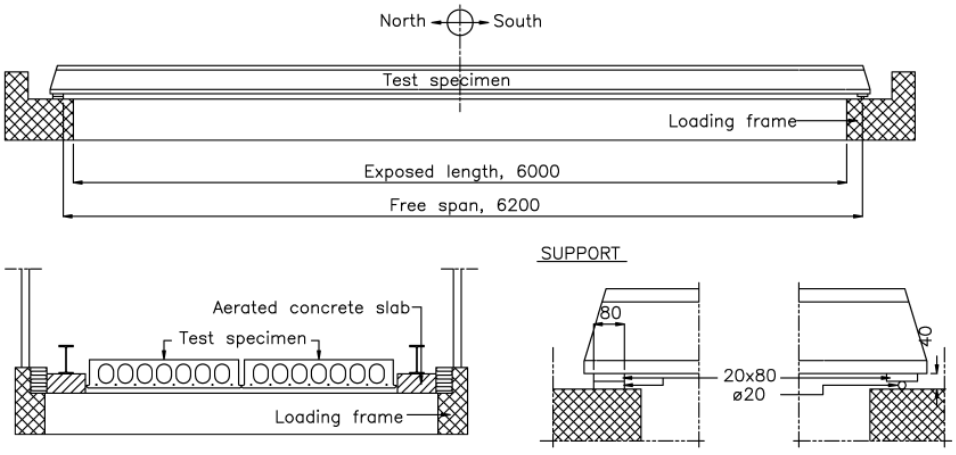

Figure 2.5 Test arrangement for Danish tests (Andersen *et al.*, 1999)

Calculations on the same test specimens were performed by four participants, DTI, DTU, FSD and PJK. More details on the four participants can be found in the literature (Andersen *et al.*, 1999). The calculations included thermal exposure conditions, temperature inside the member, and load bearing capacity at elevated temperature. Table 2.3 summarises the calculation methods of each participant.

Table 2.3 Calculation methods for four participants (Andersen *et al.*, 1999)

	DTI	DTU	FSD	PJK
Reduction of tensile strength of strands	Entire stress-strain curve is considered	Entire stress-strain curve is considered	Entire stress-strain curve is considered	Entire stress-strain curve is considered
Reduction of pressure zone	Finite element[1)]	No reduction because of low pressure load	Finite element[2)]	No reduction because of low pressure load
Shear	-	Diagonal compression force method, Θ=45° and variable (2 criteria)	-	Based on reduction of measured cold shear capacity
Spalling	-	-	-	-
Anchorage	-	Yes	-	Yes
Other	Deformation	-	-	-

1) FIRE-2D, 2) Super Tempcalc + Fire Design

According to the comparison of the calculation methods with test results, on average the calculated fire resistance time for SP 22 is 96% higher than the fire resistance time found from the tests as shown in Table 2.4. For SP 27 the average calculated value is 273% higher than the test value. In both cases the scatter is quite large, and the failure mode that leads to the calculated failure time is also different from that which led to failure in the tests. Finally, it was concluded that there was no moment capacity failure and anchorage failure was not correctly predicted, which was the primary reason for premature failure. It was also concluded that the calculated fire resistance time was higher than the actual fire resistance time (Andersen *et al.*, 1999).

Table 2.4 Comparisons of test results and calculations (Andersen *et al.*, 1999)

Failure mode		Moment failure	Shear failure	Anchorage failure	Fire Resistance Time, min.
DTI	SP18	46			46
	SP22	44	-	-	44
	SP27	64	-	-	64
PJK	SP18	55		(45)*	55/(45)
	SP22	55		(46)	55/(46)
	SP27	74		(63)	74/(63)
DTU	SP18	66	875	None	65
	SP22	65	802	None	64
	SP27	109	668	1121	108
FSD	SP18	50			50
	SP22	50	-	-	50
	SP27	78	-	-	78
Test	SP18	-	21	21	21**
	SP22	-	26	26	26
	SP27	-	21	21	21

* PJK included this part of the calculation as optional
** The test results with SP 18 were obtained with faulty loading conditions.

Danish Institute of Fire Technology & COWI, 2000 (Denmark)

Another set of fire tests on hollowcore slab elements in a deck structure were performed by COWI and DIFT to determine the fire resistance of deck structures in the strong rooms at the new National Archives in Copenhagen (Schepper *et al.*, 2000). Even though some hollowcore elements protected with fire insulation were investigated, only the test results regarding unprotected hollowcore elements exposed to the Standard ISO 834 fire were reported. In this project, the decks consisted of 220mm deep pre-stressed hollowcore concrete slabs with a 80mm cast-in-place reinforced concrete topping and partly filled hollowcores with shear reinforcement as shown in Figure 2.6. From the visual observations, the likely failure mode was compression failure on the bottom of the hollowcore slab due to the negative end restraint moment at the support as shown in Figure 2.7. The hollowcore slab elements with cast-in-place reinforced concrete topping failed at a time of around 23 minutes and the deflection was 250 mm at that time, as shown in Figure 2.8.

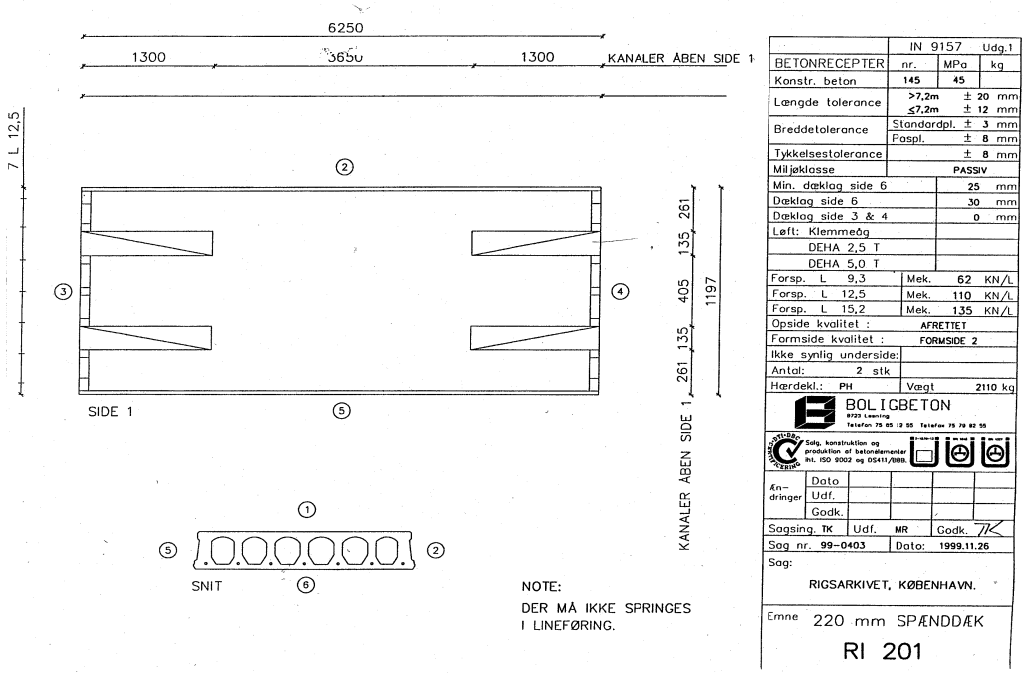

Figure 2.6 Plan view and cross section of hollowcore slab used in test element (Schepper *et al.*, 2000)

Figure 2.7 The compression failure of deck elements at the front end of the furnace after the fire test (Schepper *et al.*, 2000)

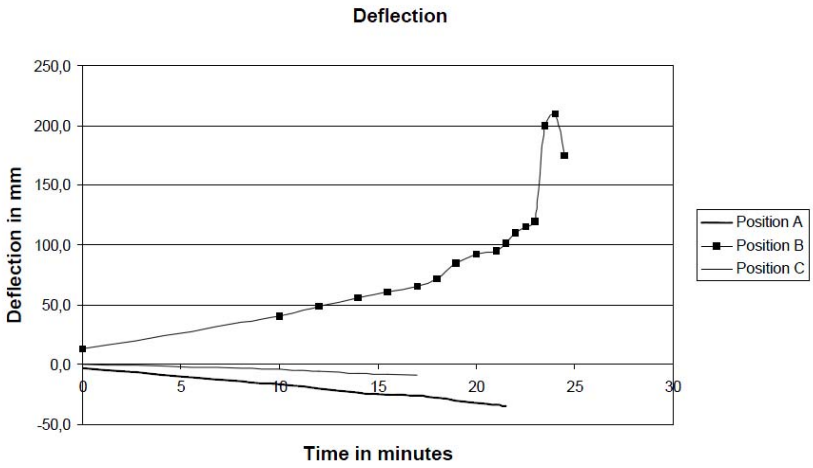

Position A: Front end of furnace; Position B: Centre; Position C: Back end of furnace

Figure 2.8 Deflection measured during the fire test (positive downwards) (Schepper *et al.*, 2000)

Universities of Gent and Liége, 2003 (Belgium)

The research project, reported by Van Acker (2003), performed four fire tests (Figure 2.9) including neighbouring structures to evaluate the magnitude and location of thermal stresses caused by the different fire exposure times, and examine the influence of parameters such as restraint to thermal expansion, the cable effect of the deflection, and the size of the cross section. The fire tests were for 2 hours according to the Standard ISO fire curve (ISO, 1975). After 2 hours of fire exposure, the load was increased until failure occurred. The loading of failure is presented in Table 2.5. Each test comprised two floor spans of 3 m, supported on three beams and a floor width of 2.4 m. The units were connected to perimeter and internal support beams using between one and four 12mm diameter bars. Two of the spans received a cast in-situ structural topping. It was observed that bending failure occurred in seven out of eight cases at load magnitudes greater than the serviceability live load by factors of 1.78-3.24, the average load factor being 2.72.

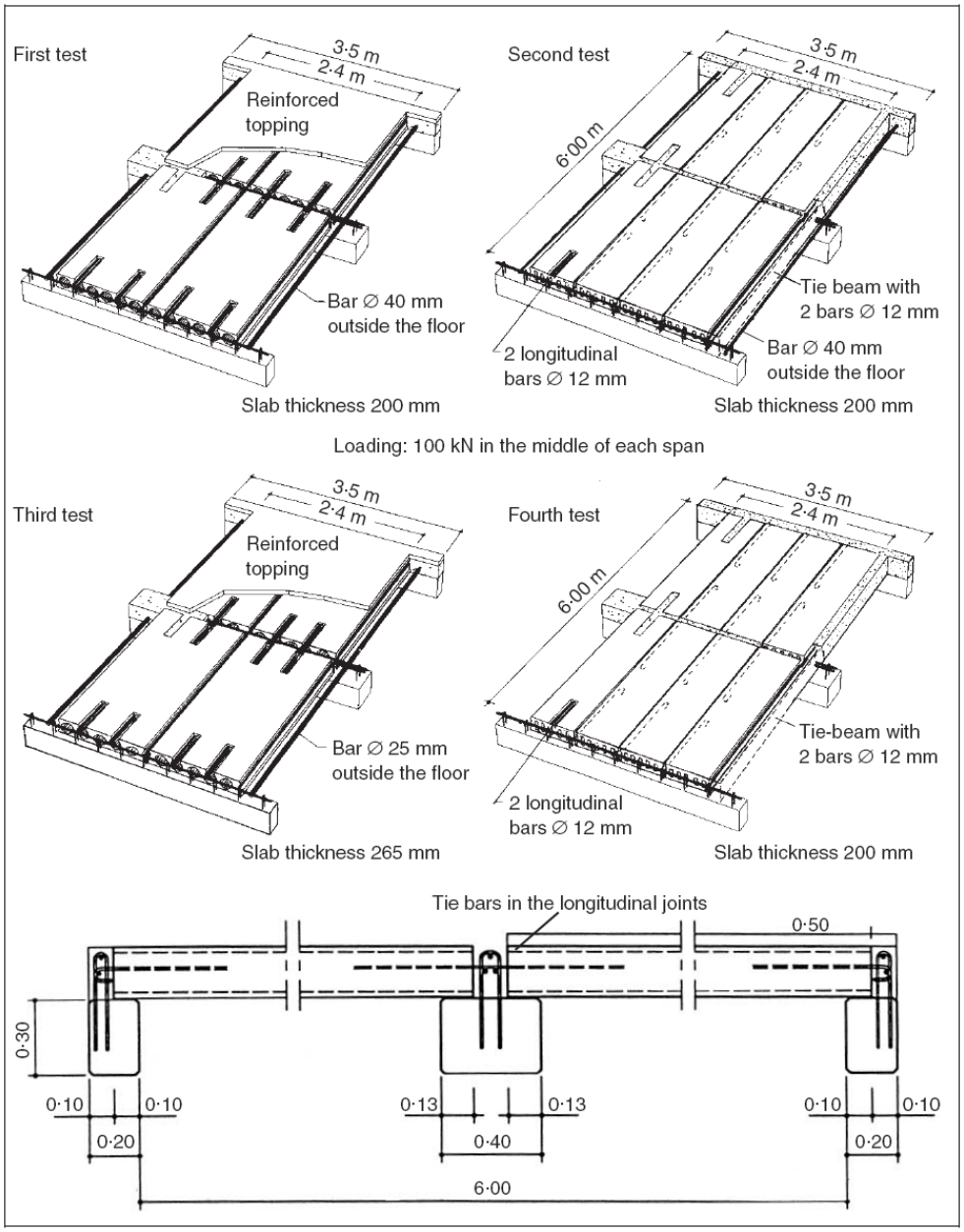

Figure 2.9 Overview of the fire tests on the shear capacity of hollowcore slabs (Van Acker, 2003)

Table 2.5 Summary of fire test results (Van Acker, 2003)

Test		Failure load: kN		Failure type
		Without topping	With topping	
First test:	Slab 1	178		Bending
	Slab 2		(50 mm)[1)] 254	Bending
Second test:	Slab 1	292		Bending
	Slab 2	324		Bending
Third test:	Slab 1	267		Bending
	Slab 2	254		Bending
Fourth test:	Slab 1	305		Bending
	Slab 2		(30 mm) [1)] 305	Shear

1) The thickness of topping concrete

Van Acker (2003) has maintained that the biggest weakness in most national and international design regulations concerning the safety of structures exposed to fire comes from a lack of understanding of global structural behaviour. Therefore, the fire resistance of concrete structures can be governed by the indirect actions resulting from thermal expansion, which can be restricted by edge columns via the supporting beams, rather than the decrease of the material properties at elevated temperature (Figure 2.10). In addition, significant shear forces can be transferred via the longitudinal joints, ranging from 0.25 to 0.40 N/mm^2. These longitudinal forces are further transferred to the prestressing reinforcement in the floor units not exposed to fire, and hence over the whole adjacent floor (Figure 2.11).

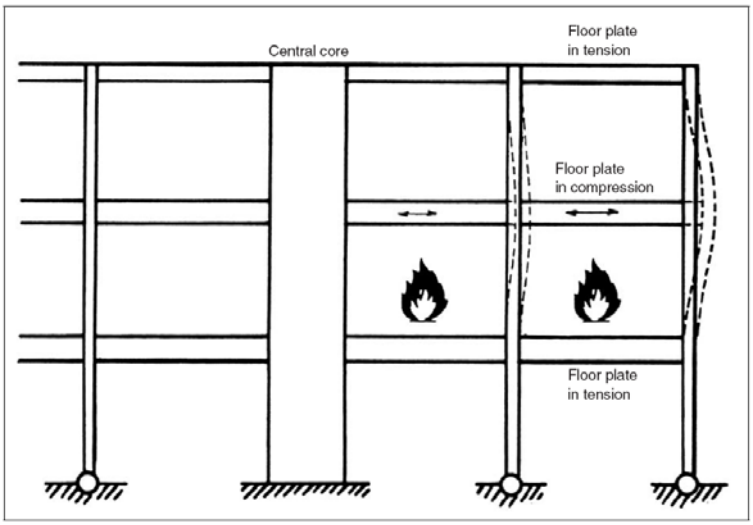

Figure 2.10 Elevation showing blocking effect of the edge construction (Van Acker, 2003)

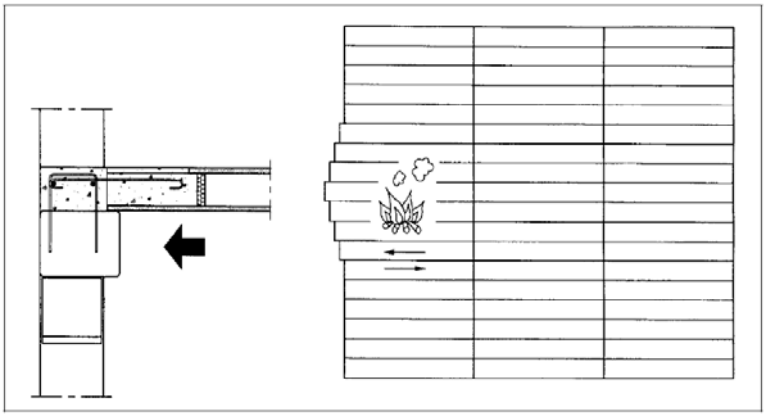

Figure 2.11 Blocking of the longitudinal expansion by the neighbouring units (Van Acker, 2003)

BRE tests, 2003 (UK)

Lennon (2003) carried out two full-scale fire tests to investigate performance with respect to spalling of the slabs and premature shear failure at the supports at Building Research Establishment (BRE)'s Cardington test facility. The test conditions and construction of the compartment were identical except for the structural topping. Two alternative approaches to providing the required restraint to the floor units were considered. One slab's joints were filled and structural topping with 50mm depth of concrete and a mesh reinforcement was used (Figure 2.12). The joints in the other slab were filled and hooked reinforcing bars were placed in the joints over the supports (Figure 2.13). The results showed no significant spalling in either of the tests despite maximum temperature in excess of 1200°C and a very rapid rate of heating. The paper concluded that there was no problem of spalling if adequate curing periods were given. It was also concluded that there was no evidence of premature shear failure of the units during the tests. In addition, the precast hollowcore floor units showed satisfactory performance under severe natural fire conditions.

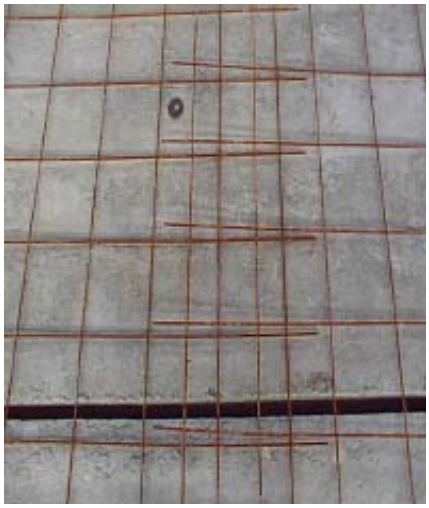

Figure 2.12 Overlap of mesh (Lennon, 2003)

Figure 2.13 Hooked bar over edge beam (Lennon, 2003)

University of Liege, 2004 (Belgium)

Numerical simulations, performed by Dotreppe and Franssen (2004), on precast hollowcore slabs in fire have been made with the computer code SAFIR developed at the University of Liege, on the basis of the fire test results of the research project by Van Acker (2003). In this research, the numerical simulations had been used to prepare the experimental fire tests and to examine the importance of some effects, i.e. the presence of cavities on the temperature distribution, the transverse cracking on the cross section due to thermal stresses, the influence of restraint on the deflections and on cracking. A summary of the numerical simulations is that: (1) the presence of cavities influences the temperature distribution on the cross section; (2) the fire

resistance corresponding to the ultimate limit state (ULS) of bending increases with the degree of restraint; (3) thermal stresses mainly developed between 0 and 30 minutes and caused the shear failures observed in some fire tests; (4) longitudinal restraint has a positive effect on the area of the cross section that cracks as well as the shear capacity of the slab so that it has a favourable effect on the ULS of bending and shear under fire conditions.

TNO Centre, 2004 (Netherland)

Fellinger (2004) investigated shear and anchorage behaviour of fire exposed hollowcore slabs. Firstly, failure modes of hollowcore slabs on the basis of 257 tests at ambient temperature and 80 tests at elevated temperatures found in the literature were assessed. From the literature, four failure modes (flexure, anchorage, shear compression and shear tension) were identified with respect to ambient temperature. On the other hand, the distinction between shear tension, shear compression and anchorage failure could not be made with respect to fire conditions as many of the fire tests were not well reported and the tests stopped when a specified fire resistance was achieved. However, the following conclusions could be drawn from the literature. Firstly, longitudinal restraint against thermal expansion could improve the shear and anchorage behaviour significantly. Secondly, the temperature of the strands is not an important indicator as the increase of the axis distance of strands had rather a detrimental than a beneficial influence on the shear and anchorage behaviour. Thirdly, shear and anchorage failure is less critical in thinner slabs.

Due to the insufficient evidence of existing fire test data, 25 new fire tests under the ISO 834 fire were performed as summarised in Table 2.6. Among the 25 new fire tests, 21 tests were conducted on double rib specimens sawn out of hollowcore slab units, in order to observe the expected cracking along the webs and measure the slip between the concrete and the strands. Several influencing parameters were considered, i.e., four types of hollowcore slabs (200, 260, 265 and 400mm deep) (Figure 2.14), production process (extrusion and slip form), support

details (simple supports, restraint in spanning direction and reinforced end beam). The other tests were carried out on complete single hollowcore units.

Table 2.6 Overview of the fire tests on HC slabs (Fellinger, 2004)

Depth - # HC (mm)	Production process	Axis dist. (mm)	Type	Support detail[1]			Load level	Failure mode[2]			Failure time (min)	Remarks
				s	r	e	(%)	S	A	F		
200-7	slip form	40	ribs	s			21		A		96	*no slip measured*
	extrusion			s			16			F	125	V_u = *30%*
		44		s			18		A		125	V_u = *34%*
					r		18			F	159	V_u = *37%*
			unit	s			19			F	117	
260-5	slip form	40	ribs	s			23		A		48	
							17		A		45	*fluctuating load*
							11		A		123	V_u = *16%*
		[3]		s			23		A		55	
							20	S	A		56	*restarted after 8 min*
							17	S	A		114	
							14	S	A		123	*loading failed*
						e	23	S	A		49	
							20	S	A		50	
							17	S	A		99	
			unit	s			23	S	A		39,40,42	
265-4	extrusion	40	rib	s				S			35	
					r			S			35	
			unit	s				S			33	
400-4	extrusion	[4]	rib	s				S			60	
				s				S			24	*low quality core filling*
			unit	s				S			33	

1) (s) = simple supports, (r) = restraint in spanning direction, (e) = reinforced end beam
2) (S) = shear failure, (A) = anchorage failure, (F) = flexural failure
3) Strand position: 4x12.5-40 + 2x12.5-76.4, for the double ribs: 1x12.5-40 +1x12.5-76
4) Strand position: 6x9.3-40 + 2x9.3-73, 5x12.5-40 + 3x12.5-88, for the double ribs: 4x9.3-40 + 1x12.5-40 + 1x12.5-88

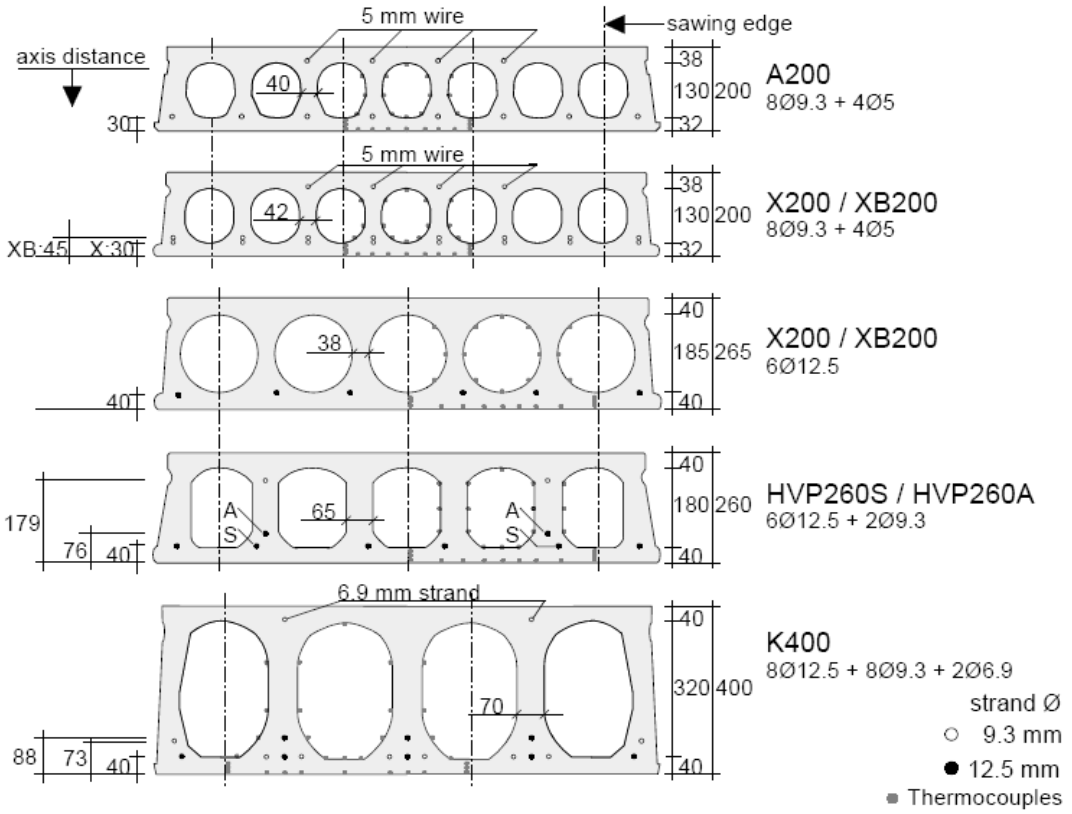

Figure 2.14 Cross section of the specimens used in the fire tests (Fellinger, 2004)

From the test results, anchorage failure, shear failure and combined shear and anchorage failure were observed in fire exposed hollowcore elements. For all slab types, the crack patterns in the webs are summarised in Figure 2.15. Due to incompatible thermal elongations, vertical cracks developed over the entire length of the specimen. For VX265 specimens, the horizontal crack developed through the smallest web width at mid depth along the entire length of the specimen. The horizontal crack developed as a splitting crack along a strand (HVP260 and K400).

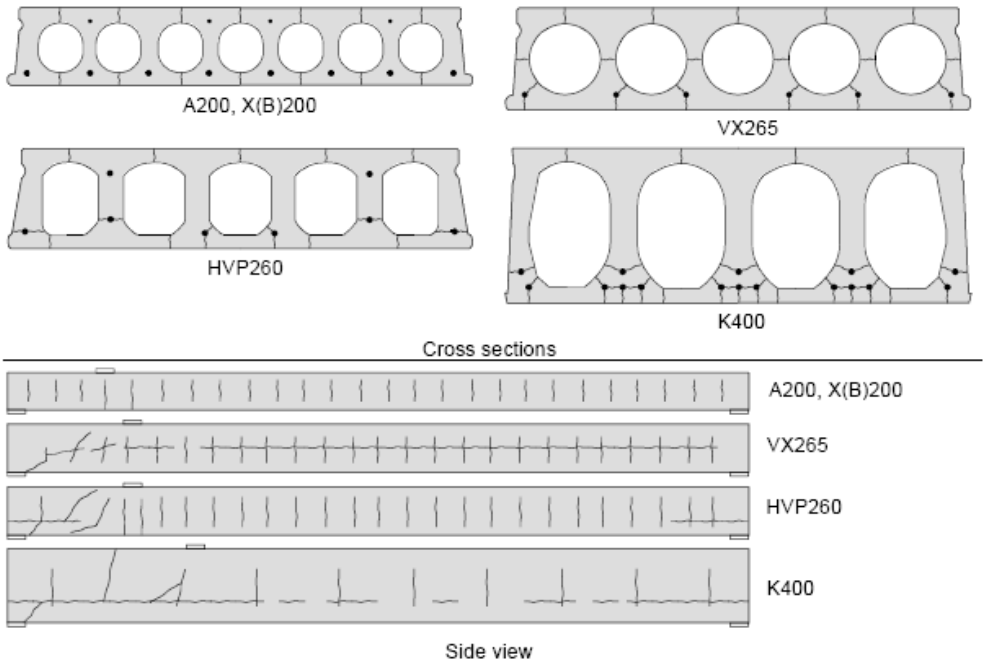

Figure 2.15 Sketch of the crack patterns for the 200mm slabs, the VX265, HVP260 and K400 slab, shown from top to bottom (Fellinger, 2004)

Based on the test results, a finite element model for the shear and anchorage behaviour of fire exposed hollowcore slabs comprising new constitutive models for concrete and bond of prestressing strands at high temperatures, was developed. The constitutive models were calibrated with 60 new small scale tests carried out at elevated temperatures up to 600°C. The finite element model was validated on the basis of the 25 full scale fire tests on hollowcore slabs loaded in shear. Finally, a parametric study was carried out with the finite element model. The results showed that the thermal expansion of concrete, the ductility of concrete in tension and the restraint against thermal expansion by the supports are the main influencing factors. It is recommended to control these factors in design in order to improve the safety level.

Danish prefab concrete association, 2005 (Denmark)

Jensen (2005) carried out a series of fire tests to confirm that 265mm deep hollowcore slabs, comprising one whole and two halves with a 2,935mm length, exposed to a 60 minutes fire according to the standard time-temperature curve and the subsequent cooling phase (Figure 2.16) can resist a displacement of at least

65% of the slabs' ultimate design shear capacity in cold conditions as determined in DS 411 (1999) based on function testing with a loading arrangement according to EN 1168 (BSI, 2005). The hollowcore element comprised a total of 8 normal ribs and two longitudinal joints, each with two adjacent side ribs in the elements as shown in Figure 2.17. The three tests were conducted at three different load levels, i.e., 65% (SP-1), 75% (SP-2) and 80% (SP-3) of the slabs' ultimate design shear capacity in cold conditions ($V_{ud(cold)}$).

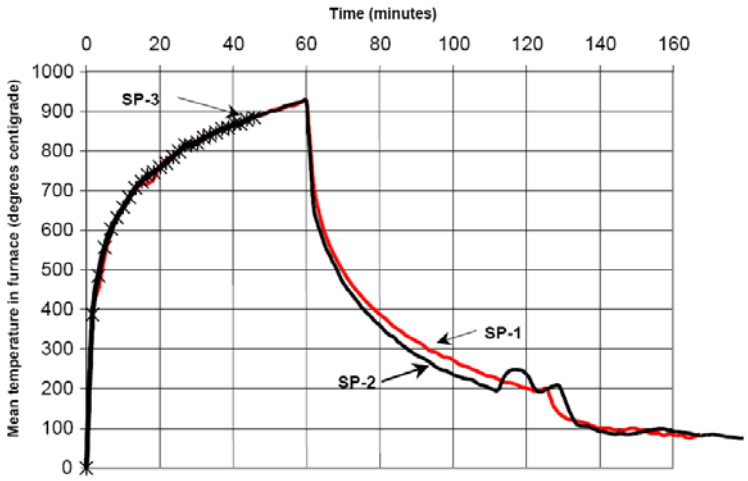

Figure 2.16 Test temperatures of SP-1, SP-2 and Sp-3 test (Jensen, 2005)

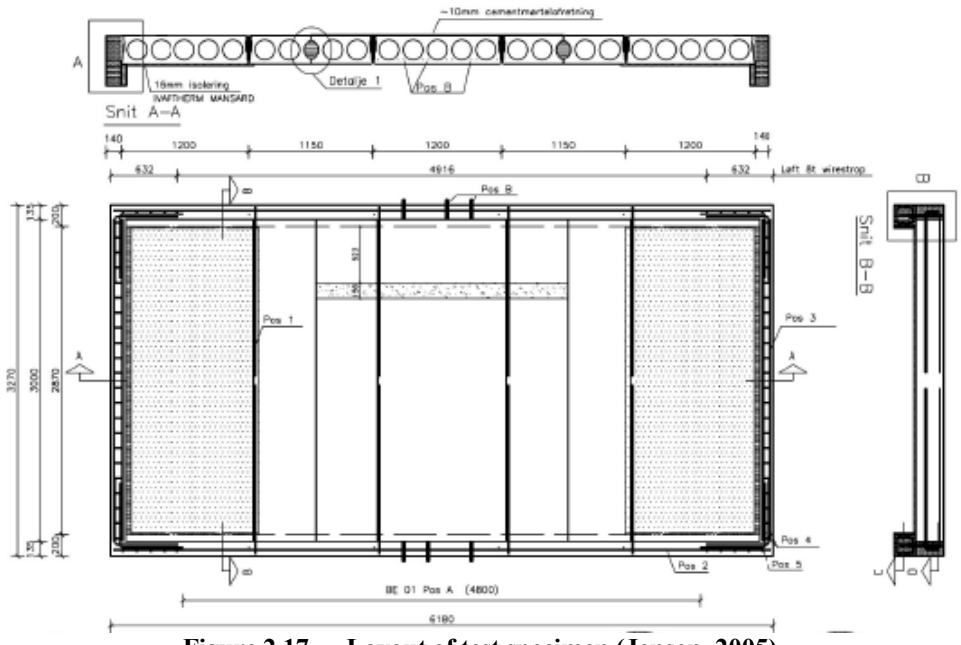

Figure 2.17 Layout of test specimen (Jensen, 2005)

With respect to SP-1 and SP-2, no breaking or spalling or other significant failure occurred during the 60 minutes fire test and the subsequent cooling phase of 90 minutes. On the other hand, SP-3 which was loaded corresponding to 80% of the ultimate design strength in cold conditions failed after 45 minutes due to shear fracture. Figure 2.18 shows the time-midspan deflection results for all tests. In these graphs, the lower curve shows the vertical deflections in the middle of the test zone. The other two curves show the deflections in the middle of the two half elements of the test zone.

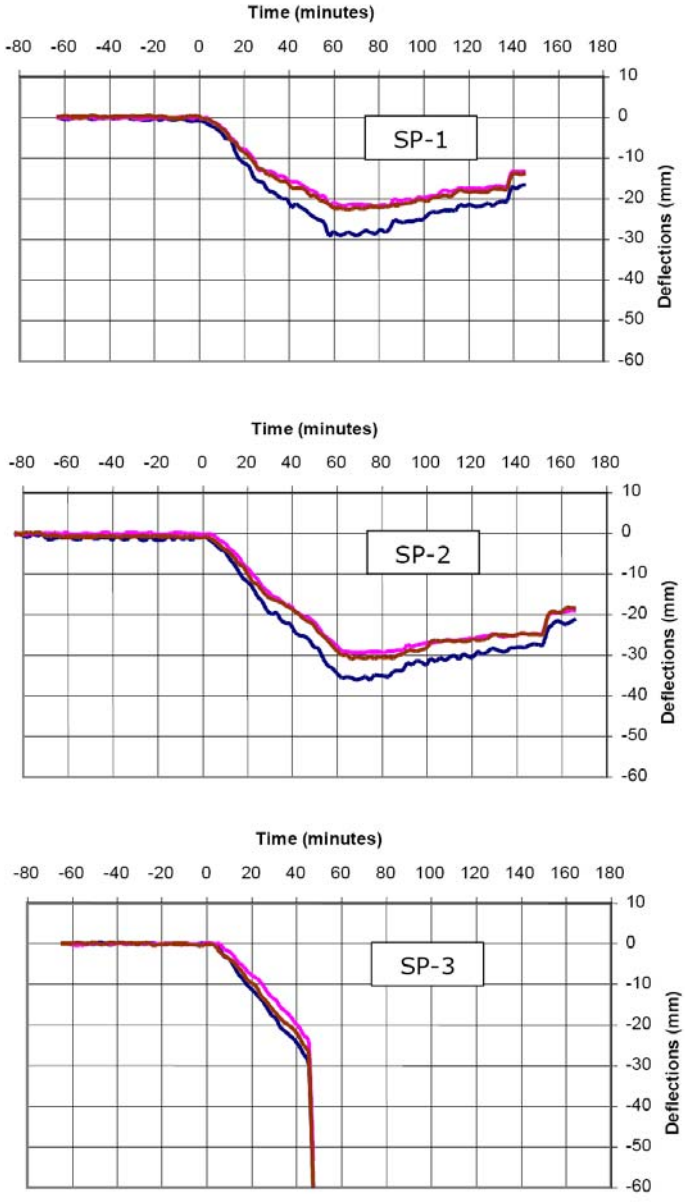

Figure 2.18 Structural behaviour of SP-1, SP-2 and SP-3 test (Jensen, 2005)

BRE tests, 2008 (UK)

Bailey *et al.* (2008) carried out further two full scale fire tests on hollowcore floors, supported on protected steel work with a very severe fire. The fire compartment was 7.02m x 17.76m, with an internal floor to soffit height of 3.6m. A total of 15 hollowcore units were used, 1200mm by 200mm deep. Except for the end restraint conditions to the hollowcore slabs, the two tests were identical. In the first test the slabs sat directly on the supporting beams with the units notched around the columns. The joints between the units, and the gaps around the columns and units, were infilled with grout comprising C25/30 concrete with 10mm aggregate. In the second test, T12-Ubars at each unit end were placed in the cores and around a 19mm diameter shear stud fixed to the steel beam. The cores housing the rebars, the end of the slab, the gap between the units, and the gap between the units and steel columns were infilled with grout. It was found that cracking behaviour around the middle edge column was observed after the test, which highlights the fact that the column was pushed out further than the units (Figure 2.19). This finding from the tests shows that the steel frame does not provide longitudinal restraint to the thermal expansion of the units which, if present, would have enhanced the unit's shear capacity. However, no shear failure occurred in the test, indicating that some other load-path mechanism was possibly occurring. It was also observed that there was evidence of a lateral compressive strip forming at the ends of the units caused by restraint to thermal expansion (Figure 2.20 and 2.21). Based on this observation, it was concluded that the compressive strip can give beneficial behaviour by enhancing the flexural capacity and shear capacity of units. It was also concluded that hollowcore floors performed well during both the hot and cooling phases of the fire.

Figure 2.19 Cracking around internal edge column (Bailey *et al.*, 2008)

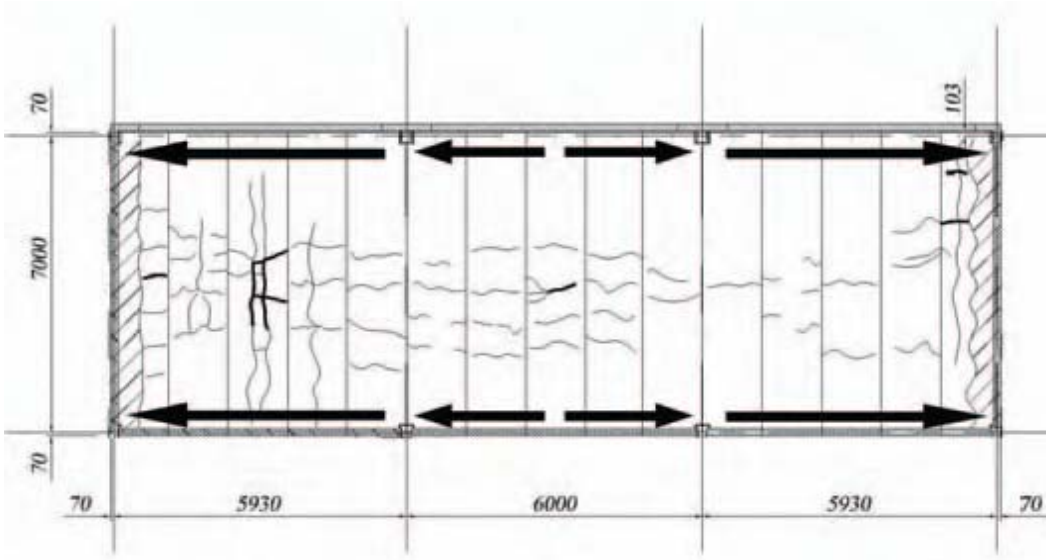

Figure 2.20 Possible restraint to slabs creating a compressive 'strip' (Bailey *et al.*, 2008)

Figure 2.21 Compressive failure of edge units due to restraint of thermal expansion (Bailey *et al.*, 2008)

2.6 Double Tee slabs

Portland Cement Association, 1972 (United States)

Abrams and Gustaferro (1972) conducted fire endurance tests on four prestressed concrete double-tee specimens with spray-applied insulation. Two different cross sections were tested under the ASTM E119 (ASTM, 1998) standard fire with unrestrained support conditions. Three specimens which had same cross section were tested with no-fire protection and 0.5 and 1 in. of sprayed vermiculite acoustical plastic. The other specimen used 0.5 in. of sprayed mineral fibre. Their fire endurances were 1 hr. 2 min., 1 hr. 50 min., 3 hr. 6 min., and 2 hr. 28 min., respectively. Both types of insulation maintained adhesion throughout the tests. For two types of double tee slabs, a prescriptive based tabulated approach was suggested for 2 and 3 hr. fire ratings, based on stem width at steel centroid, concrete cover, type and thickness of insulation (refer to Table 3.7).

Table 2.7 Thickness of sprayed insulation for unrestrained prestressed stemmed units (Abrams *et al.*, 1972)

Stem width at steel centroid, b in.	Concrete cover, u in.	Thickness of spray-applied insulation in.	
		2 hr.	3 hr.
2.5	1	1	-
3	1.25	0.75	1.25
4	1.5	0.5	0.875
5	1.75	0.25	0.625
6	1.75	0.25	0.375
8	1.75	0.25	0.375
8	2.75	0	0.25

* Governed by requirements for u

Universities of Gent and Liége, 1997 (Belgium)

Franssen *et al.* (1997) carried out standard fire tests and analysis with the nonlinear finite element program, SAFIR, on prestressed doble tee slabs in order to account for failure and to design a new specimen having 2 hours fire resistance. The prestressed double tee slabs, supported simply, had a width of 2,400mm and a depth of 700mm including 9 tendons of 100mm^2, as shown in Figure 2.22.

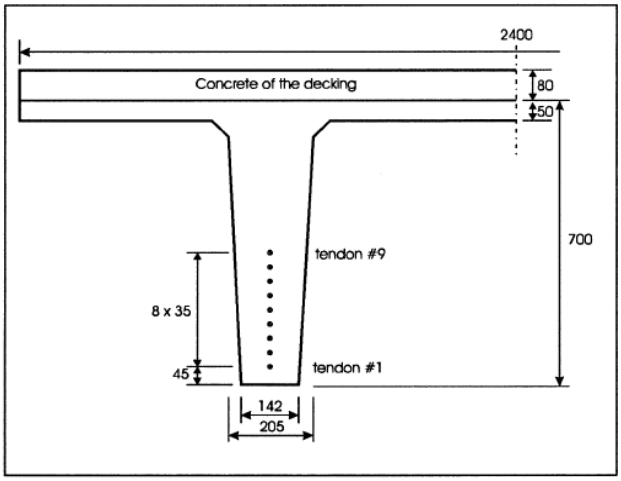

Figure 2.22 Half section in the elements (Franssen *et al.*, 1997)

The standard fire test result showed that the deflection of double tee slabs, over a length of 7,000mm due to the limitation of the furnace size, reached 90mm after 75 minutes with horizontal and inclined cracks, as illustrated in Figure 2.23. In addition, this test result was compared with the numerical analysis performed by SAFIR. In Figure 2.24, the test result showed less fire resistance time than the numerical result in the hypothesis of a bending failure mode. In order to investigate the early failure of the double tee slabs, the shear resistance calculation method in the Eurocode 2 – Part 1-1 (EC2, 1995) was adapted, with the consideration of the effects at elevated temperatures. As a result, Eurocode formula for shear resistance showed reasonable agreement with experiments result.

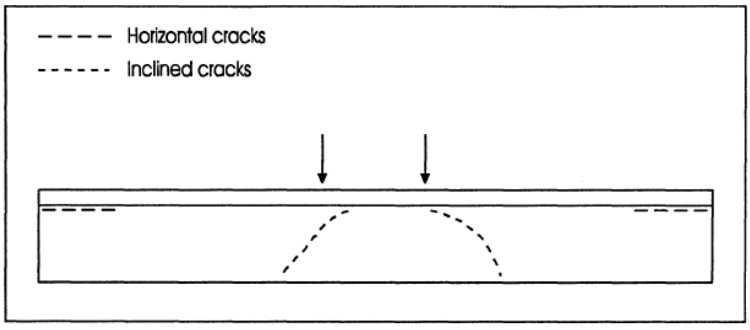

Figure 2.23 Crack pattern (Franssen *et al.*, 1997)

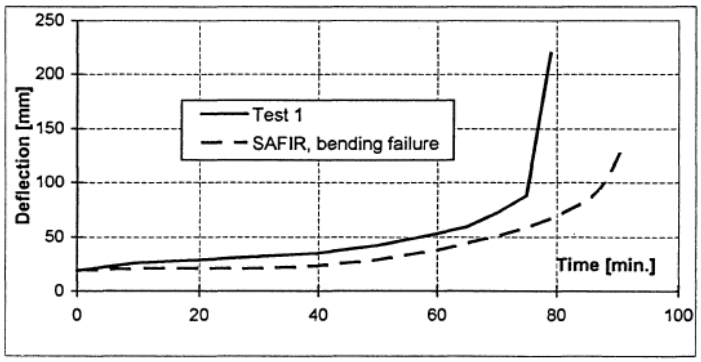

Figure 2.24 Evolution of the deflection in test 1 (Franssen *et al.*, 1997)

Thus, a new acceptable solution was proposed with a change of the web thickness from 140 to 200mm and the rearrangement of 8 tendons, as shown in Figure 2.25. With the enhanced double tee slab, a second test was performed and led to a 121 minutes fire resistance.

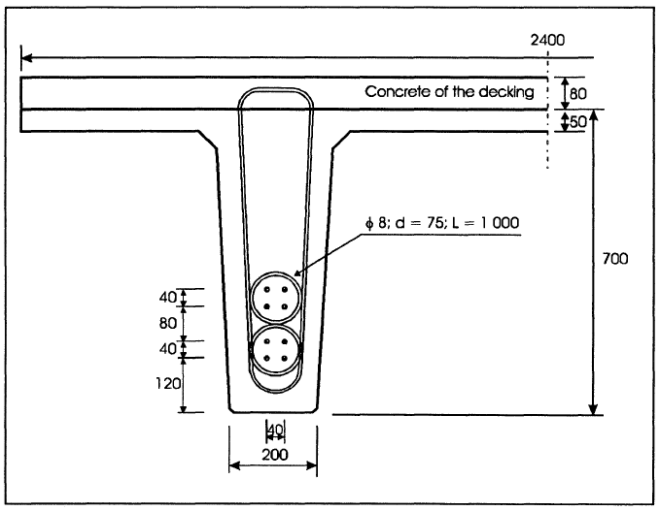

Figure 2.25 New design (Franssen *et al.*, 1997)

Danish Institute of Fire Technology, 1998 (Denmark)

Andersen et al. (1998) conducted the standard fire testing of three types of pre-fabricated TT-roof slabs subjected to ISO 834 fire and the test results was compare with the calculations performed by four different participants (DTI, DTU, FSD and PJK). The double tee roof slab consisted of two slender T-shaped beams connected with a thin concrete slab and had a 21.8m length. The beams had a width of 100mm

along the lower flange. The sides of the beams were tapered with an inclination of 1:25. The height of the section was 720mm at its highest point and sloped down with an inclination of 1:40 towards the end. Due to the limitation of the furnace size, the scaled specimen had a length of 6.36m and test specimens were modified in several ways. As a result, the number of strands was reduced from 11 to 4 in each of the beams as shown in Figure 2.26. In addition, eight single loads were applied to the test specimens instead of self weight and evenly distributed load for full length beam.

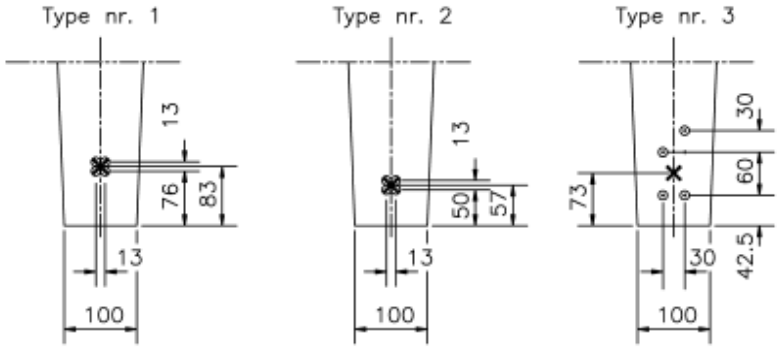

Figure 2.26 Arrangement of strands (Andersen *et al.*, 1998)

For each test specimen, constant observations during the fire tests had been made with summary. Even though in most cases spalling occurred in the middle of the concrete slab between two flanges at around 13 minutes, all three tests indicated an initial bonding failure followed by shear failure. In terms of the calculations, thermal exposure, temperature inside the member and load bearing capacity at elevated temperature were performed. The thermal exposure conditions were calculated based on ISO 834. With respect to the calculation of temperature inside the member, three out of four participants used different finite element programs, but the fourth participant (DTU) used a simplified calculation method. The more complex calculation methods for load bearing capacity of each participant are summarised in Table 2.8.

Table 2.8 Calculation methods for four participants (Andersen *et al.*, 1998)

	DTI	DTU	FSD	PJK
Reduction of tensile strength of strands	Entire stress-strain curve is considered	Entire stress-strain curve is considered	Entire stress-strain curve is considered	Entire stress-strain curve is considered
Reduction of pressure zone	Finite element	Reduced section	Finite element	No reduction because of low pressure load
Shear	-	Diagonal compression force method, θ=45° and variable (2 criteria)	-	Diagonal compression force method, θ=26-45°
Spalling	-	-	-	-
Anchorage	-	Method by K. Hertz	-	Drafts DS 411, 9.2.6 (14)
Other	Deformation	-	-	-

For each different failure mode, the calculation results as well as test results summarised in Table 2.9. For Type 2, the test terminated due to the failure of integrity. The result of Type 2 was not included in Table 2. DTI-DTU-PJK calculations were good agreement with each other while a FSD calculation showed high fire resistance time. For Type 3, calculations showed a good agreement with the test result. On the other hand, calculations in average showed 25% high fire resistance time for Type 1. It can be concluded that test specimens only achieved 40 minutes fire resistance even though the TT-beams were required 60 minutes fire resistance. Additional test, therefore, was required, with the consideration of factors which can improve or degrade the fire resistance.

Table 2.9 Comparisons of test results and calculations (Andersen *et al.*, 1998)

Failure mode		Moment failure	Shear failure	Anchorage failure	Fire Resistance Time, min.
DTI	Type 1	47	-	-	47
	Type 3	37	-	-	37
PJK	Type 1	52	50	>60	50
	Type 3	45	40	>60	40
DTU	Type 1	56	91	110	55
	Type 3	39	40	24*	(24)/38

FSD	Type 1	77	-	-	77
	Type 3	63	-	-	63
Test	Type 1	-	-	-	42
	Type 3	-	-	-	41

* Time when requirements for anchorage can no longer be met for assumed 45° inclination of the diagonal compression force. The beam has a physical capacity beyond this time.

2.7 Prestressed flat slabs

To date, no research has been reported in the literature relating to the structural behaviour at elevated temperatures of prestressed flat slabs having the same properties as in New Zealand even though some research on prestressed flat slabs has been performed in United States. Fire test results (Gustafero, 1967) with simple supports under ASTM E119 fire are described and used for validation of the numerical model in Chapter 9.

2.8 Finite element program, SAFIR

2.8.1 Introduction

SAFIR is a special purpose computer program for the analysis of structures subjected to fire. The program, which is based on the Finite Element Method (FEM), can be used to study the behaviour of one (1D), two (2D) and three-dimensional (3D) structures. The program (SAFIR) was developed at the University of Liège, Belgium. In this section, a brief description of the program SAFIR and the finite elements used are presented.

2.8.2 Analysis capability of SAFIR

SAFIR was originally written for analysing steel and composite structures exposed to fire. Some studies have explored the possibility of also using SAFIR to analyse concrete structures with satisfying results. SAFIR includes two calculation modules: one for thermal analysis, and another one for the mechanical analysis. The geometrical non-linearity caused by large displacements, as well as the

material non-linearity in the thermal and mechanical properties, are considered in the analyses. Different types of elements, various calculation procedures, as well as several material models, are built into the program. Even though SAFIR was developed for analysing structural behaviour under fire conditions, it can also be used to analyse structures at ambient temperatures.

2.8.3 Analysis procedure

SAFIR is able to run two types of analyses, which are the thermal analysis and structural analysis. In the thermal analysis, the non-uniform temperature evolution is calculated for two-dimensional section elements in the structure. Subsequently, the mechanical module of the program reads these temperatures and determines the thermo-mechanical behaviour of the structures. An additional torsional analysis is required prior to use of the three-dimensional beam elements.

In the thermal analysis, the temperature distribution can be non-uniform over the 2D cross section. The heat transfer in the plane section is by conduction, with no heat transfer along the member axis. The evaporation of moisture in the material can be modelled by modifying the thermal properties of the materials. Radiation in internal cavities of the section can also be considered in the thermal analysis such as in hollowcore concrete members. The temperature evolution of the cross section is defined as a function of time. With respect to the temperature evolution, the Standard ISO 834 curve or any other curves defined by the user can be used. In addition, the program allows the consideration of a cooling phase.

For a 3D analysis with beam elements, torsional analysis of the beams must be performed prior to the structural analysis to determine the torsional stiffness and the warping function of the beam elements. In this analysis, the elastic phase material properties at ambient temperature are taken into account.

The structural analysis in fire conditions is performed after the temperature histories in the elements have been defined. In the structural analysis, SAFIR program includes truss elements, 2D and 3D beam elements and shell elements. Among those elements, 3D beam elements and shell elements allow the modelling of three-dimensional structures.

SAFIR uses a calculation strategy based on an incremental procedure (step by step) allowing equilibrium to be found between the external load and the internal stress at every time step. For each iteration, the tangent stiffness matrix is evaluated and the system of equations is solved using the Newton-Raphson method.

The iterations are repeated for every time step until convergence is achieved. When convergence is achieved, the following data can be output:
i) Displacements of the structure at each node;
ii) Axial and bending moments at each integration point in each element;
iii) Stresses, strains and the tangent modulus of each element in each fibre and each longitudinal integration point of the beam element;
iv) Stresses, strains, bending and membrane stiffnesses of the shell elements.

The procedure repeats successive time steps and halts when the specified final time is reached or when the structure fails. In a static analysis, the failure criterion of a structure is defined as the instant when the stiffness matrix is no longer positive definite, thus becoming impossible to establish the equilibrium of the structure. However, in hyperstatic structures, local failure of a structural member does not lead to overall structural failure. Beyond local failure, part of the internal forces that cannot be supported by the local element are redistributed to other structural elements using the arc-length method, leading to a new equilibrium position. In this method, when an unstable situation occurs, the temperature remains constant and another equilibrium point is found. However, the arc-length method still fails in many cases (Franssen *et al.*, 2004).

In order to cope with this failure, a dynamic analysis option (Franssen *et al.*, 2004) has been introduced. In this process, an acceleration term counterbalances the negative stiffness matrix during the structurally unstable states. Thus, it can handle a local failure that does not endanger the safety of the whole structure. The time step is automatically adapted when no convergence is achieved, by coming back to the previous converged point and trying again with a smaller time step. Finally, the structural calculation continues until the time step is smaller than the minimum time step (value defined by the user). The numerical results presented in this thesis

were obtained using this dynamic analysis.

2.8.4 Truss element

The truss element is straight with two end nodes as shown in Figure 2.27. The geometry is defined by the position of these end nodes. The truss element is completely defined by its cross sectional area and the material type. Only one material, one temperature and one strain are present in each element.

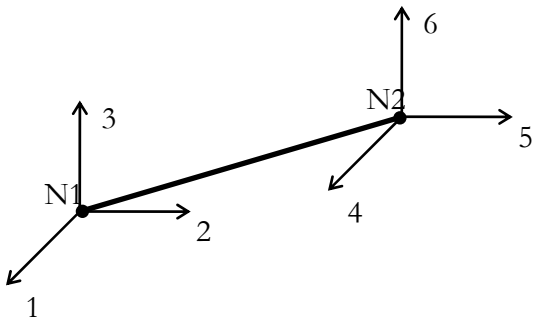

Figure 2.27 Truss element - degrees of freedom at nodes (Franssen *et al.*, 2002)

2.8.5 Beam element

The 2D beam element is defined by three nodes (Figure 2.28). N1 and N2 represent the end nodes and define the position of the beam in space. A third node, N3, lies between the two end nodes and supports the non-linear component of the longitudinal displacement. The longitudinal displacement of the node line is a second order power function of the longitudinal co-ordinate, while the transverse displacement of the node line is described by a third order power function of the longitudinal coordinate. The end nodes of the 2D beam element, N1 and N2, have three degrees of freedom comprising two displacements and one rotation.

The 3D beam element has an additional node, N4, to define the position of the local y-axis of the beam. The end nodes of the 3D beam have seven degrees of freedom, three displacements, three rotations and a warping degree of freedom.

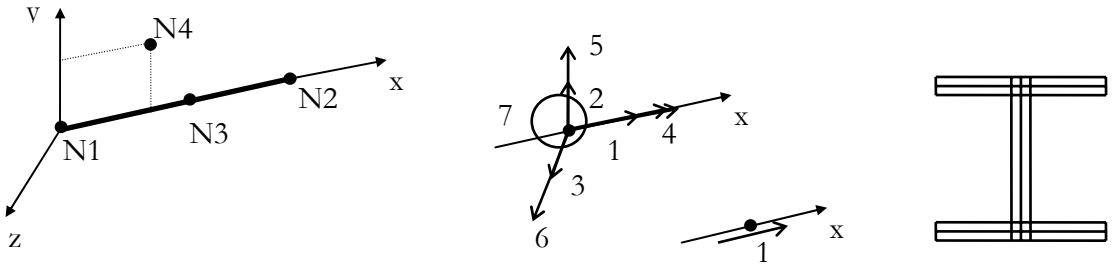

(a) (b) nodes N1,N2 node N3 (c)

Figure 2.28 Beam element: (a) local axes (b) degrees of freedom at nodes (c) cross section (Franssen *et al.*, 2002)

The cross section of the beam element is discretized by the fibre model, consisting of quadrilateral and/or triangular shaped elements. The integration along the length of the beam is performed with Gaussian integration. The number of Gaussian integration points along the length of each beam varies from one to three. Typically, two integration points are used. At every longitudinal point of integration, all the variables such as temperature, strain and stress are uniform in each fibre. Each fibre in the beam can have its own material, allowing composite sections to be made and analysed.

There are several assumptions made in the beam element that were incorporated in the program:

1. Plane sections remain plane under bending.
2. Shear energy is not considered as per Bernoulli's hypothesis.
3. In the case of strain unloading, the material behaviour is elastic with the elastic modulus equal to the Young's modulus at the origin of the stress-strain curve.
4. The plastic strain is not affected by the increase in temperature.
5. Plastifications are only considered in the longitudinal direction of the member; i.e.: uniaxial constitutive models.
6. The non-linear portion of the strain is averaged on the length of the elements to avoid locking.
7. Non-uniform torsion is considered in the beam element.
8. Local buckling of steel fibres in the beam element cannot be accounted for.

2.8.6 Material properties in SAFIR

Numerous material models are available in the SAFIR program subroutines for analysis at elevated temperatures. The strength of SAFIR lies in its ability to perform 2D and 3D thermal and structural analysis of fire exposed members with various thermal and mechanical material models.

The available models for thermal analysis of concrete include calcareous and siliceous concrete based on EC2 (2004). Reinforcing, prestressing and structural steel models based on EC3 (2002) are available to model various types of steel. Insulation materials such as gypsum and user defined material properties can also be specified for the thermal analysis.

Several different uniaxial and plane stress analysis models are available for structural analysis at elevated temperatures. These material models are available for different types of steel and concrete. Their mechanical properties are based on the Eurocodes. The steel and concrete mechanical models can also be used for analysis at ambient conditions. The stress-strain relations for steel are linear-elliptic models, while the relations are non-linear for concrete. In structures exposed to fire, the materials are subjected to initial strains (ε_i), thermal strains (ε_{th}) and stress related strains (ε_σ). The stresses are, therefore, caused by the difference between the total strain (ε_{total}), obtained from nodal displacements, and the initial and thermal strains.

2.8.7 Limitations of SAFIR

Material models included in the SAFIR program have some inherent assumptions, as is the case with all analytical models. The assumptions made by the SAFIR finite element model are as follows:

1) There is perfect bond between steel and concrete and there is no account for slippage between them.

2) Spalling of concrete cannot be predicted.

3) The beam finite element cannot detect shear failure as the software is based on the Bernoulli hypothesis.

Chapter 3

Numerical Model of a Single Hollowcore Concrete Slab

3.1 Introduction

A recent study (Chang, 2007) on prestressed hollowcore slabs used a 3-dimensional (3D) beam grillage system for modelling hollowcore units and shell elements for modelling the reinforced concrete topping to simulate the behaviour of hollowcore concrete slabs in fire. In this method, the cross section including the topping concrete in the beam elements has been used for thermal analysis, but the topping part of the beam element is regarded as a non-load-bearing material, so additional shell elements were needed for structural analysis as illustrated in Figure 3.1. This method, therefore, requires a lot of computer resources (Moss *et al.*, 2009). In order to reduce this computational effort, this chapter investigates the feasibility of a method without using shell elements. In the new method, the reinforced concrete topping is modelled as part of beam elements; shell elements are not used in the model.

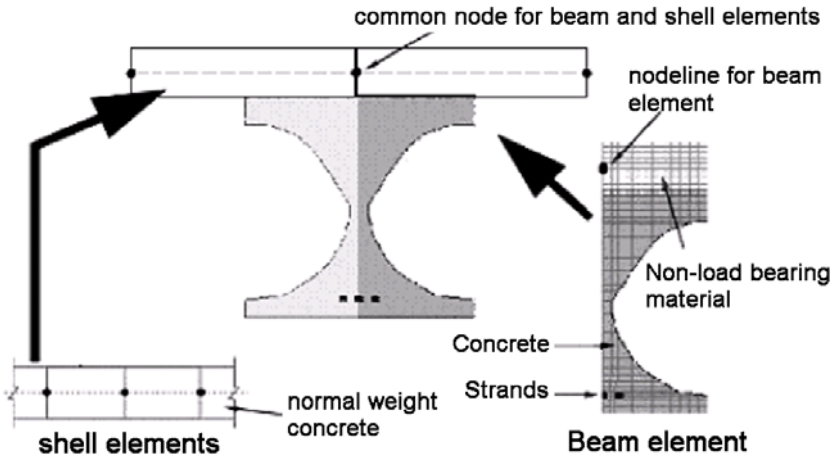

Figure 3.1 Discretisation of the cross section of hollowcore unit in the original method (Moss *et al.*, 2009)

The hollowcore unit has a 200mm depth and is exposed to the Standard ISO 834 fire. A sensitivity study is conducted with a 200mm deep hollowcore slab cross section including a reinforced concrete topping slab, to investigate the mesh sensitivity of this cross section as well as temperature development. Each structural analysis is also compared with different mesh density. Four different boundary conditions: Pin-Pin, Pin-Roller, Fixed-Fixed, Fixed-Slide are used and the failure modes of the prestressed hollowcore unit slabs are also examined. With respect to the Pin-Roller end support, three alternative methods (such as tabulated data, simplified calculation methods and advanced calculation methods) (EC2, 2004), were used to calculate and compare the fire resistance of hollowcore slabs. Figure 3.2 shows the organisation of Chapter 3.

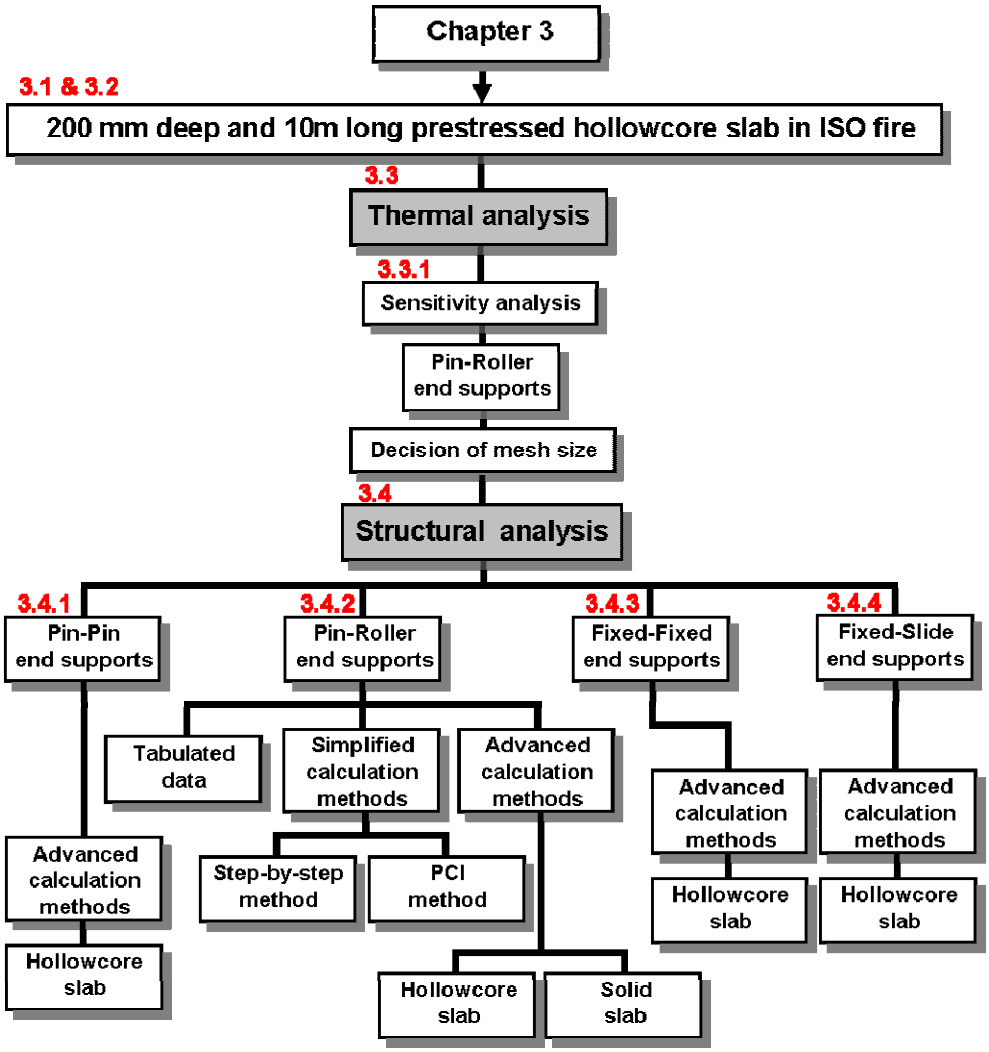

Figure 3.2 Organisation of Chapter 3

3.2 Description of a 200mm hollowcore unit slab

In New Zealand, the depths of standard hollowcore units are 200, 300 and 400 mm. Throughout this study, a 200mm deep hollowcore unit has been considered. Table 3.1 describes the material properties of the 200mm deep hollowcore unit used in this study. Figure 3.3 shows the cross section dimensions of the 200mm deep hollowcore unit, which was modelled numerically, including a 65mm thick reinforced topping slab. The thickness of the reinforced topping slab is typically 65mm, but that can be varied up to 75mm (Stresscrete products, 2011). As shown in Figure 3.3, a 200mm deep hollowcore unit has six voids with seven prestressing strands.

Table 3.1 Material properties of 200mm deep hollowcore unit

200 hollowcore	
Cross sectional area	0.121 m^2
Self weight	3.88 kPa
Compressive strength	45 MPa
Prestressing strands	
Type	Stress relieved 7-wire strand
Strength	1.87 GPa
Prestressing level	70%
Cross sectional area/strand	100 mm^2
Reinforced concrete topping slab	
Concrete compressive strength	30 MPa
Reinforcement strength	450 MPa

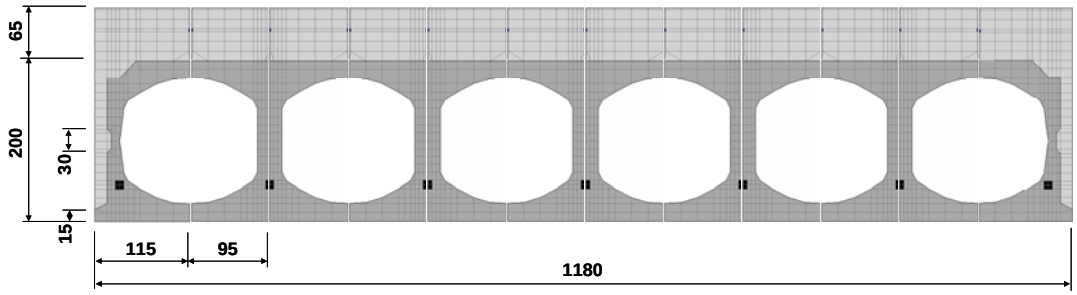

Figure 3.3 200mm deep hollowcore unit cross section

The cross section of a prestressed hollowcore unit with six voids can be represented by several longitudinal beam elements. In this chapter, seven longitudinal beams, i.e. five internal and two external, are used to represent the full cross section of a hollowcore unit. More details on cross sections used in the analyses will be explained in Section 3.3.

3.3 Temperature assessment of a 200mm hollowcore unit

The grillage system used in this chapter consists of full length longitudinal beams connected to transverse beams which are 1.2 m long (width of hollowcore units). The grillage system allows the model to expand thermally in both the lateral and longitudinal directions so that the effects of the restraints on these displacements from the surrounding structure can be captured. The longitudinal beams address the thermal gradient around the voids correctly and include the effect of the prestressing tendons. The transverse beams comprise the top and bottom flanges as well as the reinforced concrete topping slab and span only within the width of each hollowcore unit.

The nonlinear finite element program, SAFIR, was used to perform the thermal analyses for the cross sections of longitudinal and transverse beams on a prestressed hollowcore unit in a Standard ISO 834 fire. In the thermal analysis of the SAFIR program, triangular (3 nodes) and quadrilateral (4 nodes) solid elements are used to define the cross section of the structure and each cross section is discretised into a number of fibres. The heat transfer analysis of a prestressed hollowcore slab, taking into account cavities, is crucial because a 200mm hollowcore slab has 6 voids and these voids play an important role in temperature distribution. Therefore convection at the boundaries and radiation in the internal cavities of the cross section are considered. Figure 3.4 shows the thermal gradients across the depth of three different longitudinal and one transverse beam obtained numerically after 4 hours Standard ISO 834 fire exposure. As shown in Figure 3.3, there is no symmetry in terms of left and right side longitudinal beams (a, b), but each internal beam (c) has its symmetry.

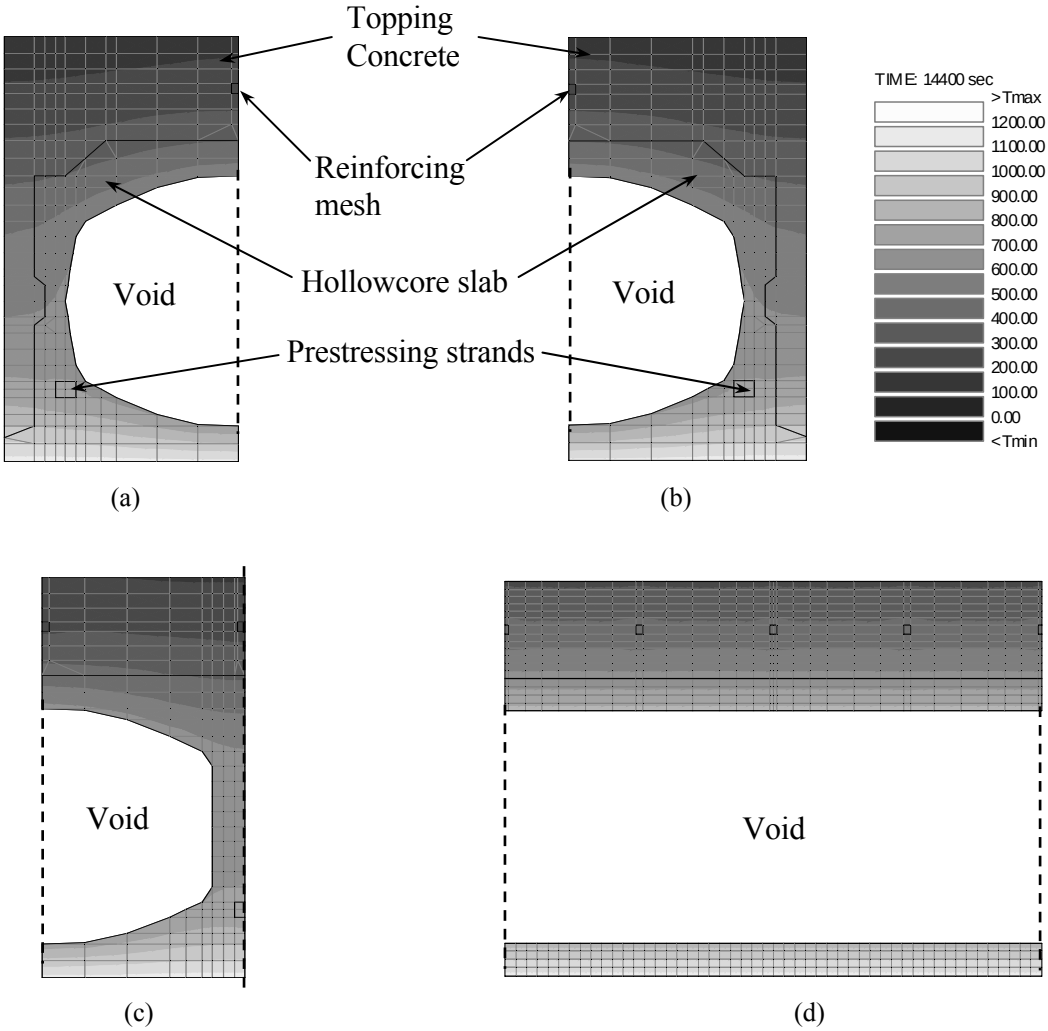

Figure 3.4 Temperature distribution of a 200mm hollowcore unit from (a) left side longitudinal beam (b) right side longitudinal beam (c) internal longitudinal beam (d) transverse beam

3.3.1 Sensitivity study

In order to investigate the effect of different finite element meshes on the temperature distribution in a prestressed hollowcore unit slab, a comparison of simulation results has been made by using three different meshes. In generating the mesh size, the bottom part of the central longitudinal element is divided more finely than the top section, because the thermal gradient of the bottom part, which is exposed to fire directly, is steeper than that of the top section. Figure 3.5 shows the temperature gradients of a central longitudinal beam, having different mesh densities, after 4 hours fire exposure. As explained above, a prestressed 200mm hollowcore unit slab is comprised of three different longitudinal beams and one

transverse beam. Amongst these elements, the behaviour of a prestressed hollowcore unit slab is mainly resisted by internal longitudinal elements which contribute to the load carrying capacity of hollowcore slabs. Here, a comparison of only the central longitudinal beam has been made for simplicity.

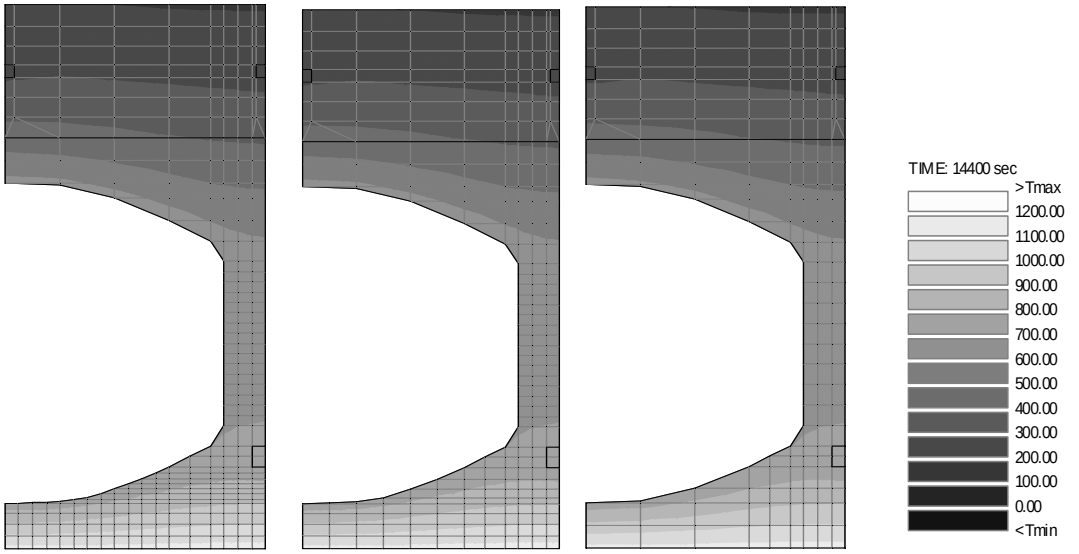

(a) (b) (c)

Figure 3.5 Temperature gradients of a central longitudinal beam from (a) fine mesh (b) medium mesh (c) coarse mesh

Figure 3.6 plots the temperature development at different locations of a central longitudinal beam. To compare the results, four points; the bottom of the element (1); a prestressing strand (2); the top of a cavity (3) and the reinforcing mesh (4), are measured. From the results, it can be seen that there is no effect of mesh size in terms of temperature and the coarse mesh is sufficient to model a prestressed hollowcore unit slab.

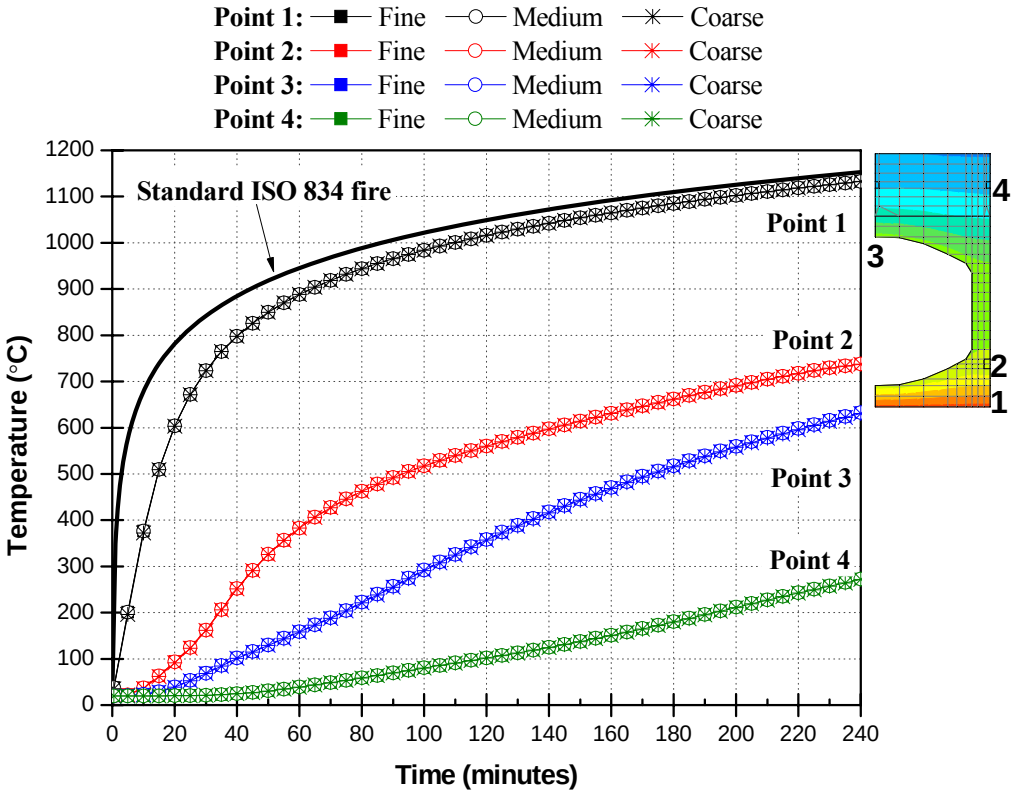

Figure 3.6 Comparisons of temperature over central longitudinal beam element

The temperature distribution of concrete structures is affected primarily by the shape of the concrete member and the type of concrete. From a fire safety perspective, the normal weight concrete aggregates are divided into two groups: siliceous aggregates and calcareous aggregates (Harmathy, 1993). All concrete products in New Zealand are made of siliceous aggregates (Chang, 2007). At the location of 25.4mm (1in.) from the bottom, the temperature developments (black dots) obtained from heat transfer analysis were compared with Prestressed Concrete Institute (PCI) experimental data as shown in Figure 3.7. PCI documentation (Gustaferro *et al.*, 1989) includes data on temperatures within solid or hollowcore concrete slabs on a basis of a standard fire test. The numbers shown in parentheses in Figure 3.7 give the Celsius temperatures corresponding to the given Fahrenheit temperatures.

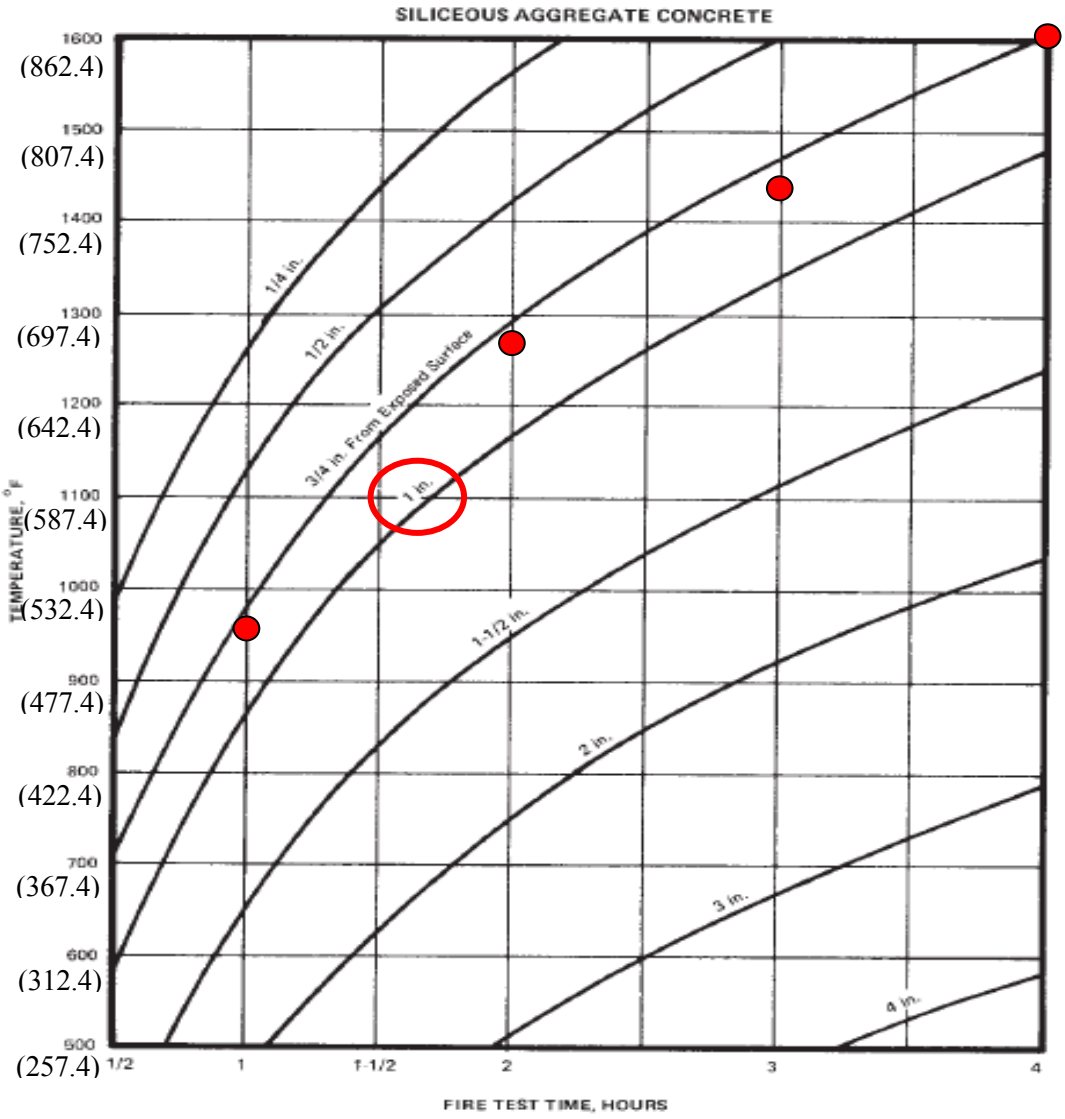

Figure 3.7 Temperatures within solid or hollowcore concrete slabs during a fire test – SILICEOUS AGGREGATE (Gustaferro, 1989)

Figure 3.8 indicates the measured point, 25.4mm (1in.) from the bottom, and its temperature at each time. The measured temperatures on a central longitudinal beam were compared with the PCI chart as shown in Figure 3.7. It can be seen that the numerical temperature results are slightly higher than the PCI test temperature results with a difference of about 50°C.

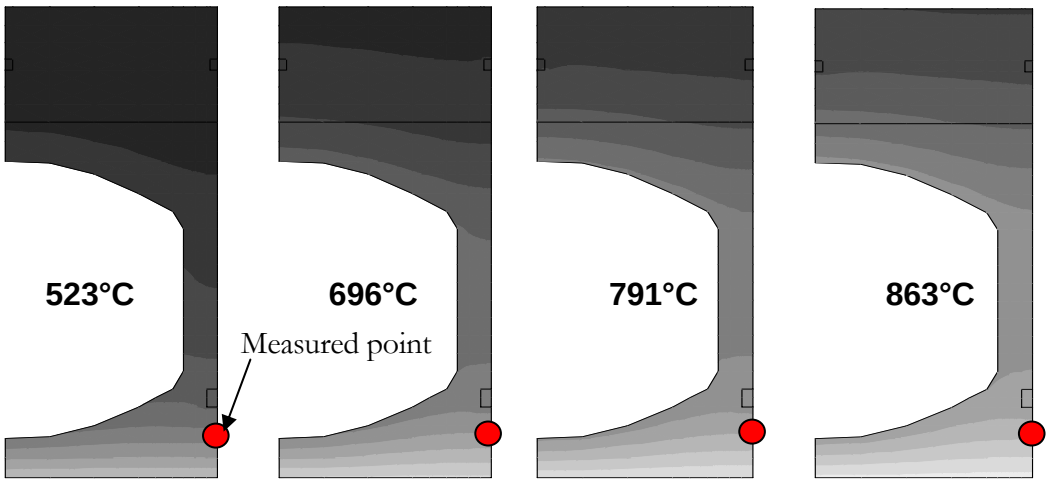

(a) 1 hour (b) 2 hours (c) 3 hours (d) 4 hours

Figure 3.8 Location of measured point with temperature distribution at each time

In order to ascertain the effect of different finite element mesh densities on the structural fire response, structural analyses are performed on a prestressed 200mm hollowcore unit by using a variety of boundary conditions, namely, (1) Pin-Pin, (2) Pin-Roller, (3) Fixed-Fixed and (4) Fixed-Slide with exposure to a Standard ISO 834 fire. The structural fire behaviour of a single prestressed hollowcore unit is dealt with in this section. Failure modes of a prestressed hollowcore unit, including the reinforced topping slab, are investigated in Section 3.4. A prestressed hollowcore slab, having 10m length, as shown in Figure 3.9, is used to investigate mesh sensitivity effects. From the load/span table of the manufacturer (Stresscrete products, 2011), a 200mm hollowcore unit with 65mm thick concrete topping can sustain a live load (Q) of 3.3 kPa under the ambient conditions and it is assumed that other superimposed dead load is not considered. The self-weight (G) of the slab is 3.88 kPa, as specified in Table 3.1. According to the New Zealand loading code (AS/NZS 1170, 2002), the load combination for the ultimate limit state condition in fire is 1.0G + 0.4Q, where G is the dead load and Q is the live load. The fire design load, therefore, is 5.2 kPa and this value is applied to the 200mm hollowcore unit slab.

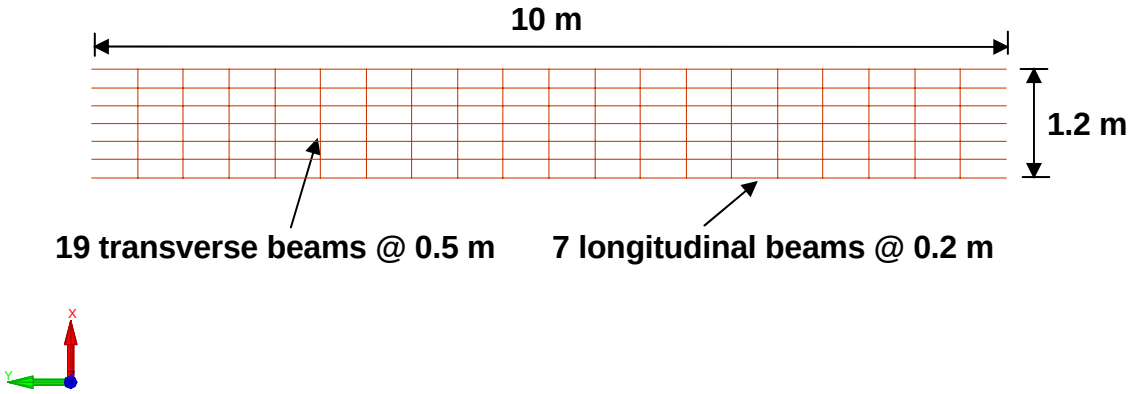

Figure 3.9 Plan view of a prestressed hollowcore grillage unit slab used for analyses

Figure 3.10 compares the vertical deflection of a 10m long hollowcore unit slab obtained using different finite element meshes. As shown in the thermal analysis results, the structural analyses of the hollowcore unit slab are almost identical and insensitive to the mesh changes, so the use of a coarse mesh is possible to investigate the structural behaviour of prestressed hollowcore slabs.

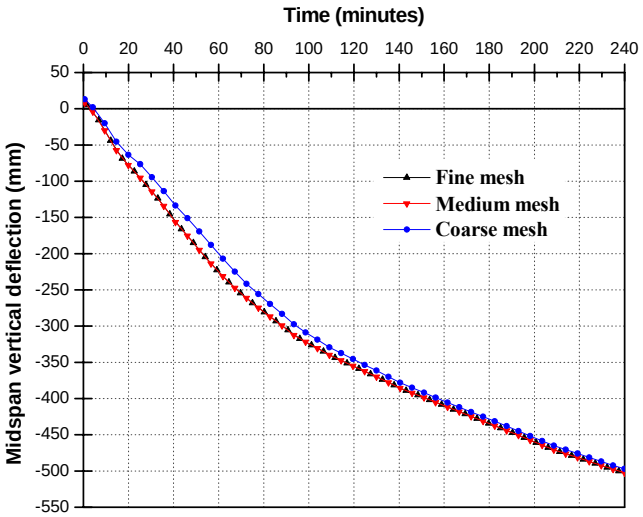

(a) Pin-Pin

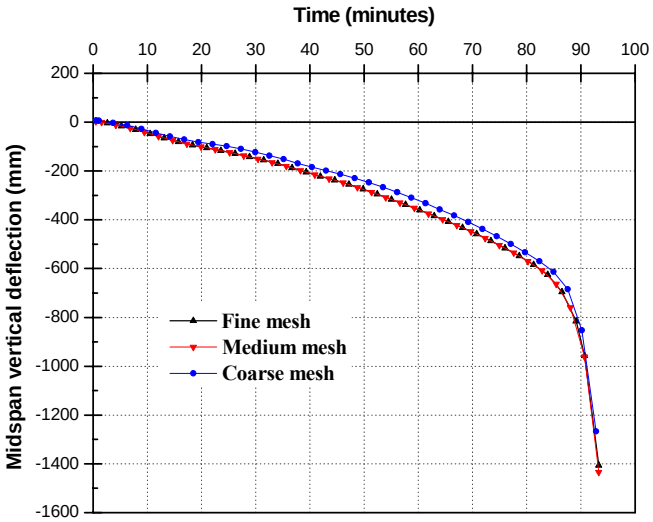

(b) Pin-Roller

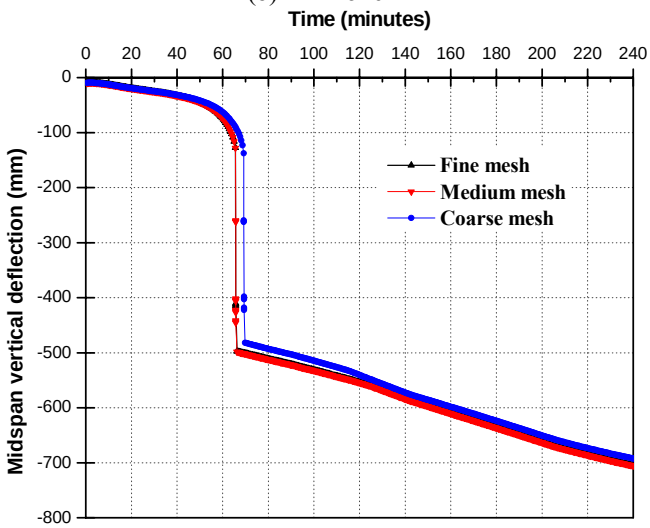

(c) Fixed-Fixed

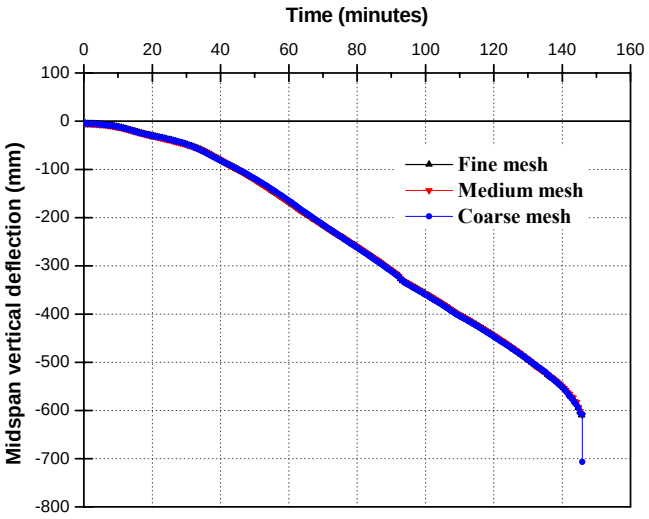

(d) Fixed-Slide

Figure 3.10 Comparison of structural behaviour depending on boundary conditions as well as different finite element mesh

3.4 Preliminary analyses of a hollowcore unit slab including reinforced topping slab

In order to identify both the fire resistance and the failure mechanism of a 200mm hollowcore unit slab, including a reinforced concrete topping, the results of the preliminary analysis, performed in Section 3.3, are investigated in this section. A coarse mesh is employed throughout this section.

3.4.1 Pin-Pin end supports

In Section 3.3.1, the nodeline for hollwocore slabs with pin-pin supports is defined at the height of the centre of reinforcement as it is assumed that only the reinforcement is anchored to end beams. In order to examine the effect of the location with respect to nodelines, three different nodelines, i.e the centre of reinforcement, the mid-depth of the slab and the bottom of the slab, are considered.

Figure 3.11 shows the comparison of the vertical deflections with time at the centre of one 200mm hollowcore concrete slab unit for different nodelines. In those cases, where the slab was exposed to Standard ISO 834 fire, it was observed that the slabs including pin supports located at near the top and the mid-depth of the slab did not fail during 4 hours of fire exposure time which is the end of the simulation. On the other hand, the slabs with pin supports located at the bottom stopped at around 87 minutes.

In order to ascertain the result with pin-pin supports at the centre of reinforcement, the prestressing strand in the centre of the hollowcore unit at midspan, and the reinforcing steel stress history are plotted against time together with their temperature dependent yield and proportional limits calculated on a basis of Eurocode 2 (EC2, 2004), in Figure 3.12 and Figure 3.13, respectively. Due to the low temperature development (less than 300°C), there is no variation in terms of the yield stress limit of reinforcement in the topping slab. After around 20 minutes, the tensile stress of a prestressing strand reached the temperature-reduced proportional limit and started to behave inelastically. However, the tensile stress did not ever reach the yield limit in the four hours fire exposure.

This result shows that although prestressing steels lost their strength against time, the tensile strength of prestressing steels did not play an important role in determining the failure of a hollowcore slab unit, supported by Pin-Pin end conditions at the centre of reinforcement.

When the supports are located at the mid-depth of the hollowcore slab, the behaviour of the slab shows a sudden increase of deflection rate after 28 minutes due to snap-through of the slab. Nevertheless, the slab survived during four hours fire exposure without collapse.

The slab with pin-pin supports at the bottom showed downward deflection through the slab at the initial stages. As fire progressed, the endspan of the slab developed upward deflection due to the restraint of thermal expansion while the midspan of the slab remained sagging deflection. As a result, the failure of reinforcement happed at the end of analysis.

In the Pin-Pin support conditions at the center of reinforcement and the mid-depth of hollowcore slabs, all the longitudinal reinforcing steels (prestressing strands and topping reinforcements) are assumed to be attached to the pin support, so that catenary action can occur.

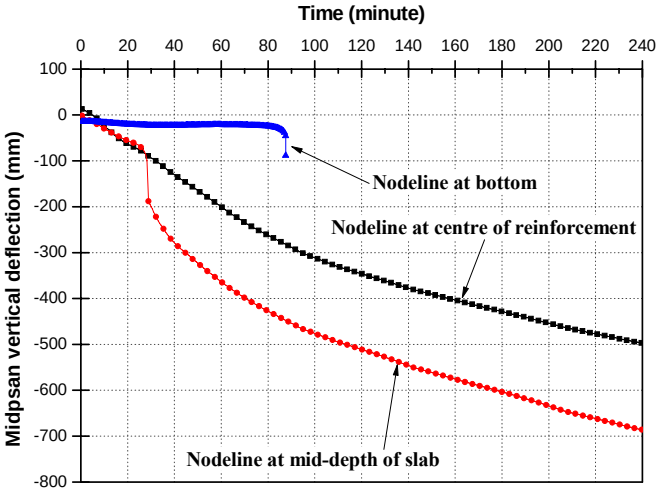

Figure 3.11 Time-deflection behaviours of one hollowcore concrete unit supported by Pin-Pin end conditions with different nodelines under an ISO 834 fire

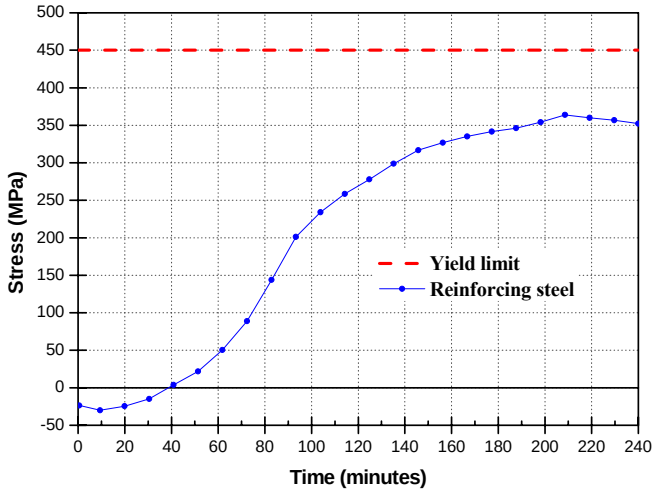

Figure 3.12 Topping reinforcement stress history of a hollowcore concrete unit with Pin-Pin end conditions under an ISO 834 fire

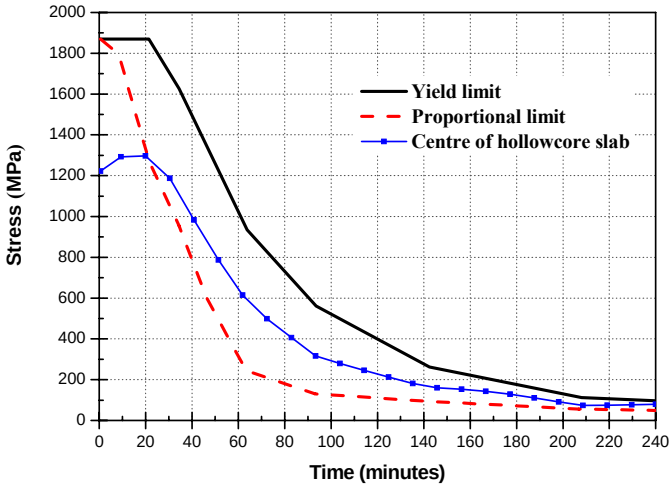

Figure 3.13 Prestressing strand stress history of a hollowcore concrete unit with Pin-Pin end conditions under an ISO 834 fire

3.4.2 Pin-Roller end supports

Figure 3.14 illustrates the time versus vertical deflection relationship with respect to Pin-Roller end supports and the run-away failure that occurred after around 90 minutes of fire exposure time. Run-away failure occurs with large deflections due to the forming of plastic hinges near to the centre of the slab. The hollowcore slab, having Pin-Roller end conditions, failed with large deflections (about 140 cm) due to the failure of prestressing strands as shown in Figure 3.15. In order to make sure the reason for the failure, the strand stress histories were plotted as shown in 3.16. At around 20 minutes, all the prestressing strands near to the midspan reached the

temperature-reduced proportional limit and the prestressing strand which is in the side beam reached the yield limit as shown in Figure 3.16. After that, the other prestressing strands suddenly lost their stress at the same time. Due to the instability of the simulation caused by the failure of a prestressing strand, the overall simulation was stopped by the analysis.

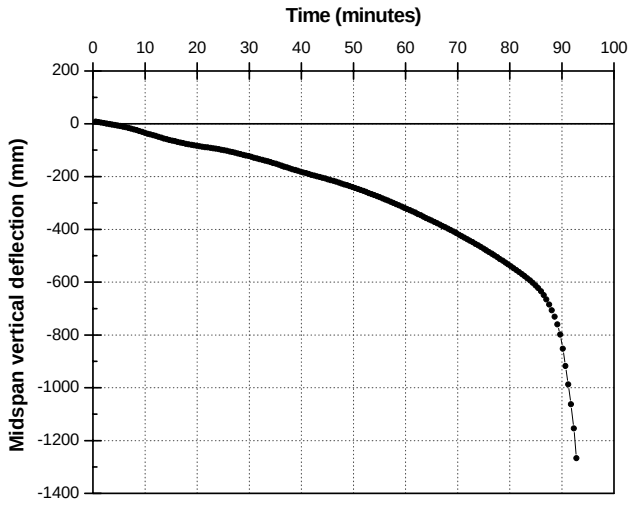

Figure 3.14 Time-deflection behaviour of a hollowcore concrete unit supported by Pin-Roller end conditions under an ISO 834 fire

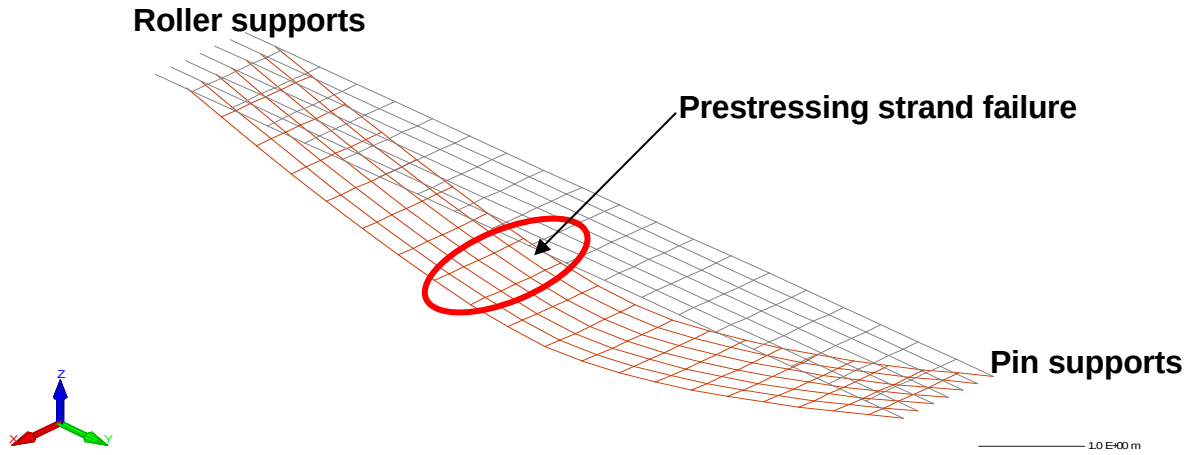

Figure 3.15 Deflected shape of one 200mm hollowcore slab supported by Pin-Roller end conditions

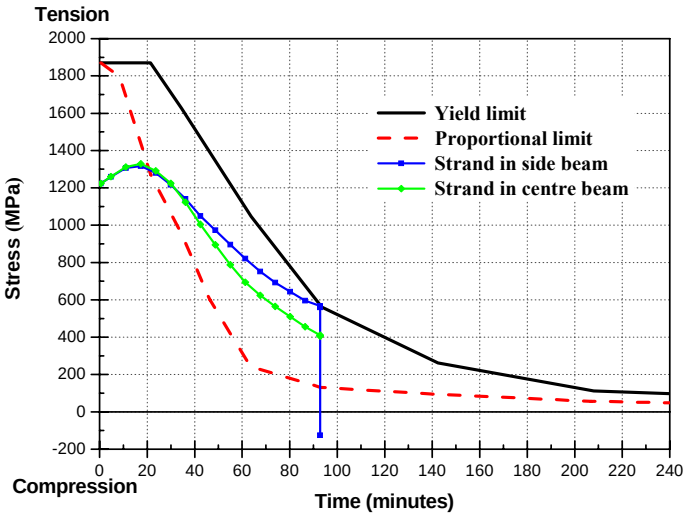

Figure 3.16 Strands stress history of a hollowcore concrete unit with Pin-Roller end conditions under an ISO 834 fire

PCI (Gustaferro *et al.*, 1989) performed a series of fire tests on simply supported prestressed concrete slabs and found no shear failure. In addition, for the design aids of simply supported prestressed hollowcore slabs, PCI documentation includes the method which determines the fire resistance using hand calculations and charts. In order to compare the fire resistance between simulation results and hand calculations, the comparison was made with the PCI method as indicated in Appendix A. For 45mm axis distance, the comparison showed that the SAFIR grillage model incorporating reinforced concrete topping slab predicted more fire resistance (93 minutes) than the PCI method (135 minutes). Also, other simple hand calculations for determining fire resistance of one unit hollowcore slab are provided in Appendix B (step-by step method) and Appendix C (moment capacity method). In these methods, the voids of a hollowcore slab are not considered as the fire resistance is only determined by the reduced moment capacity caused by the reduced tensile stress of the prestressing strands. The results show that simple hand calculations, i.e. the PCI and the step-by-step methods, do not properly predict the fire resistance of a one unit hollowcore slab.

Table 3.2 Fire resistance of a single 200mm deep prestressed slab

	Tabulated data	Simplified calculation methods		Advanced calculation methods (SAFIR)	
Axis distance, NZS 3101 concrete code	Solid or hollowcore slab	Solid slab		Hollowcore slab	Solid slab
		Step-by-step method	PCI method		
25 mm	30	71	65	54	67
35 mm	60	106	85	72	98
45 mm	90	146	135	93	135
55 mm	120	188	150	111	178
70 mm	180	255	200	Not available (geometric problem)	
80 mm	240	299	230	Not available (geometric problem)	

3.4.3 Fixed-Fixed end supports

The vertical deflection at the midspan of a 200mm hollowcore slab, incorporating Fixed-Fixed supports, is plotted against time in Figure 3.17. It is observed that the midspan vertical deflection suddenly increases at around 66 minutes. In order to determine the reason for the sudden deflection increase, the prestressing strand and reinforcing steel stress histories are plotted for mid and end spans as shown in Figures 3.18 and 3.19, respectively. Inspection of the reinforcement stress histories shown in Figure 3.18 shows that the sudden downward movement of the slab happened due to a significant reduction of stress in the reinforcement, once it reached the yield stress. Following the release of stress by the topping reinforcement, redistribution of forces within a hollowcore slab drove the arch action like the pin-ended connection model due to the anchorage of the prestressing strands into the supports. As shown in Figure 3.19, the stresses of prestressing strands at the end span abruptly increase at this time, after which they decreased gradually. This is due to the restraint of rotation at the end supports and anchorage of prestressing strands to the end supports. In practice, prestressing strands of hollowcore slabs are not anchored into the surrounding structure and the prestressed hollowcore slabs sit on end beams.

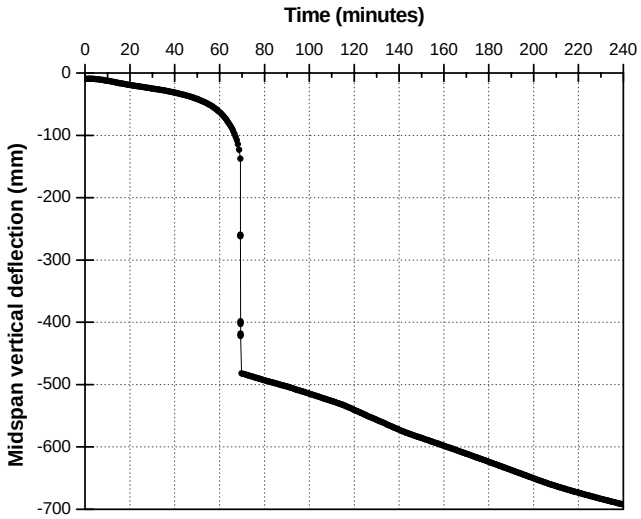

Figure 3.17 **Time-deflection behaviour of a hollowcore concrete unit supported by Fixed-Fixed end conditions under an ISO 834 fire**

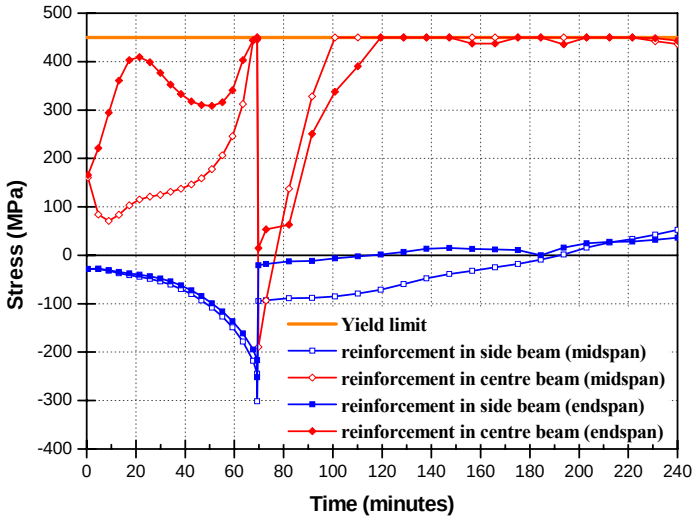

Figure 3.18 **Topping reinforcement stress history of a hollowcore concrete unit with Fixed-Fixed end conditions under an ISO 834 fire**

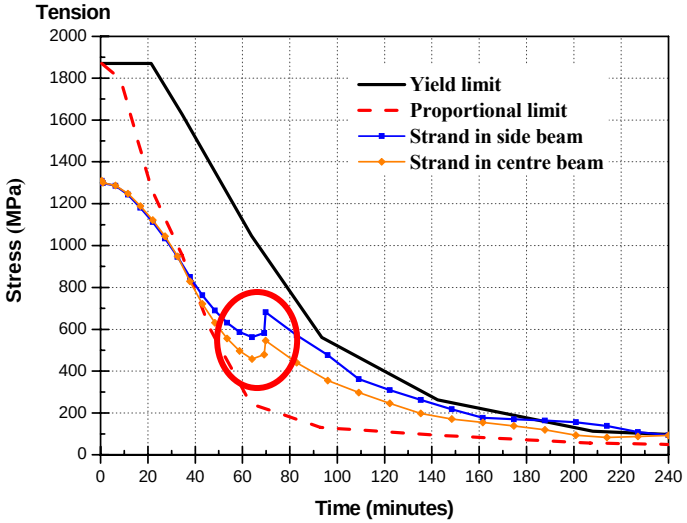

(a) Mid span

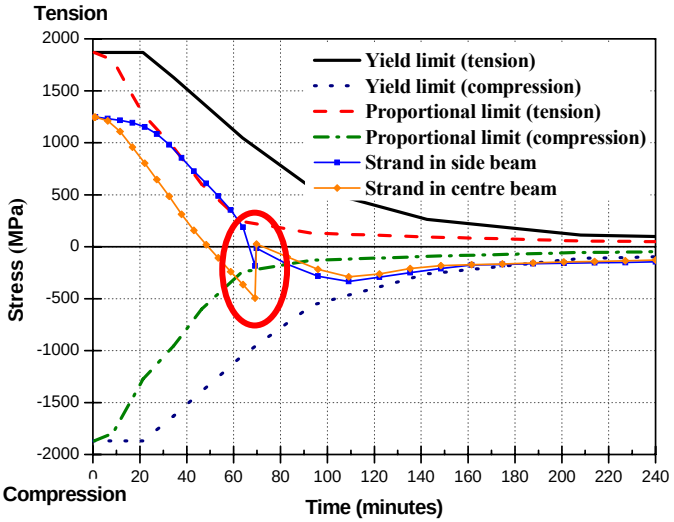

(b) End of span

Figure 3.19 Prestressing strand stress history for a hollowcore concrete unit with Fixed-Fixed end conditions under an ISO 834 fire

The axial force and bending moment histories of a fully fixed hollowcore slab are plotted against time in Figure 3.20 and Figure 3.21, respectively. It can be seen that the axial force and bending moment are increasing with time but suddenly reduce at around 66 minutes. It is evident that the load carrying mechanism of the fully fixed hollowcore slab changed from flexural to catenary action.

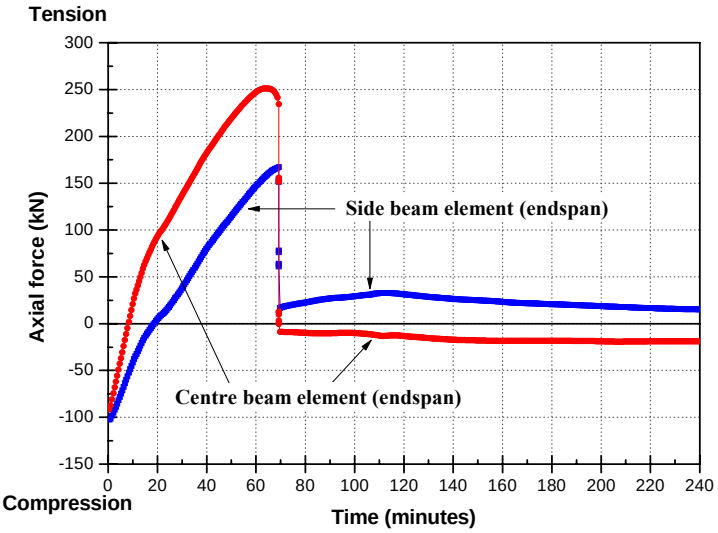

Figure 3.20 Axial force history of a hollowcore concrete unit with Fixed-Fixed end conditions under an ISO 834 fire

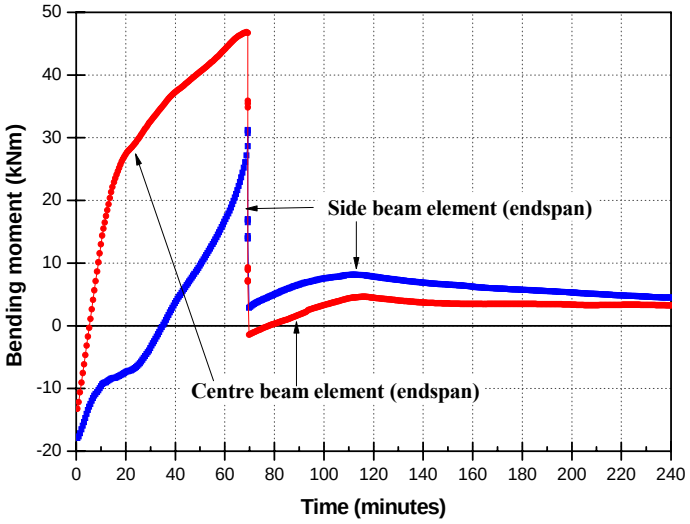

Figure 3.21 Bending moment history of a hollowcore concrete unit with Fixed-Fixed end conditions under an ISO 834 fire

In order to check the catenary action, the deflected shapes of hollowcore slab unit, before and after the sudden increase of the deflection, are shown in Figure 3.22. The deflected shape of a hollowcore slab is primarily governed by the moments developed at the end supports. During the fire exposure, fixed end conditions prevent large deflections and the prestressing strands at the end of the span forming high stresses. In addition, prestressing strands at the ends of the span were subjected to compressive stresses due to the kink near the end of the span as shown in Figure 3.22 (b) when the hollowcore slab loses the bending moment at the endspan suddenly. As

a result, the Fixed-Fixed hollowcore slab behaved like a hollowcore slab with pin-ended connections and the kinked deflected shape remained until the end of the simulation.

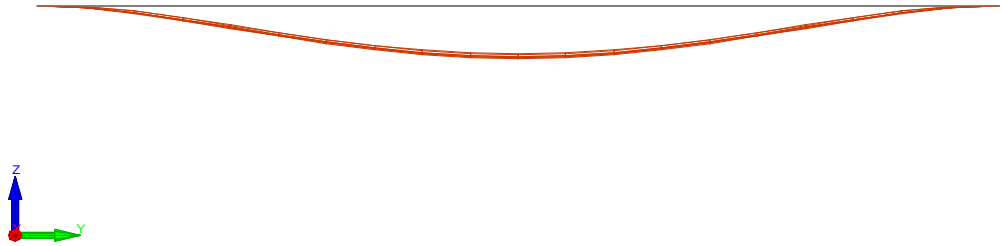

(a) Before sudden increase of the deflection

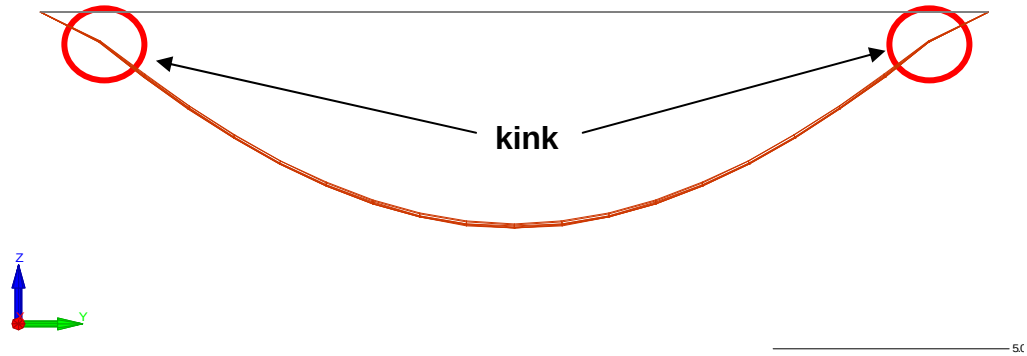

(b) After sudden increase of the deflection

Figure 3.22 Deflected shape of one 200mm hollowcore slab supported by Fixed-Fixed end conditions, scale factor = 5

This result shows that although the simulation lasted until the end of four hours fire exposure time, the deflection after 66 minutes is deemed not to be realistic due to the recovery of the prestressing strands stresses at elevated temperatures in spite of the yielding of the prestressing strands at 66 minutes and the anchorage of the prestressing strands to the end supports, which does not exist in reality.

3.4.4 Fixed-Slide end supports

Figure 3.23 shows the structural behaviour of a 200mm hollowcore slab, having Fixed-Slide supports. In this model, horizontal movement due to a thermal expansion is possible at the slide end support. The simulation stopped at around

140 minutes due to the failure of the reinforcement in the topping concrete slab next to the fixed end support as illustrated in Figure 3.24.

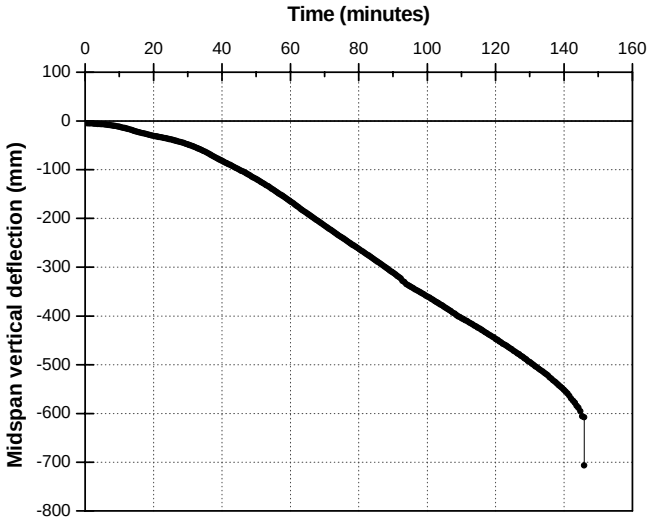

Figure 3.23 Time-deflection behaviour of a hollowcore concrete unit supported by Fixed-Slide end conditions under an ISO 834 fire

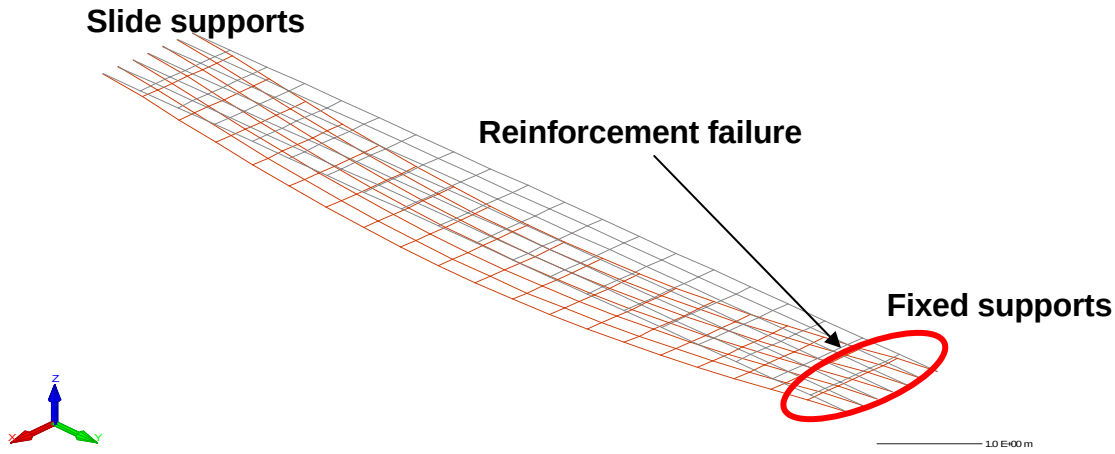

Figure 3.24 Deflected shape of one 200mm hollowcore slab supported by Fixed-Slide end condition

In order to understand the mechanism behind the failure, the stress history of the prestressing strands and the reinforcing steel was investigated. In SAFIR, the stress-strain relationship of reinforcing steel at elevated temperature follows the Eurocode mathematical model as shown in Figure 3.25 and the limiting strain for the yield strength is 0.15. Once reinforcing steels reach their limiting strain, they lose their strength rapidly.

Prestressing strand stress histories as plotted in Figure 3.26 do not show any evidence of failure, but topping reinforcement stress histories clearly indicate failure as shown in Figure 3.26. At around 20 minutes, all reinforcement in the concrete topping slab at the fixed support reached the yield limit. After yielding of reinforcement, the strain of reinforcing steels increased until about 140 minutes. After that, reinforcing steels in the end span reached the limiting strain of 0.15, so they lost their strength, hence the analysis stopped.

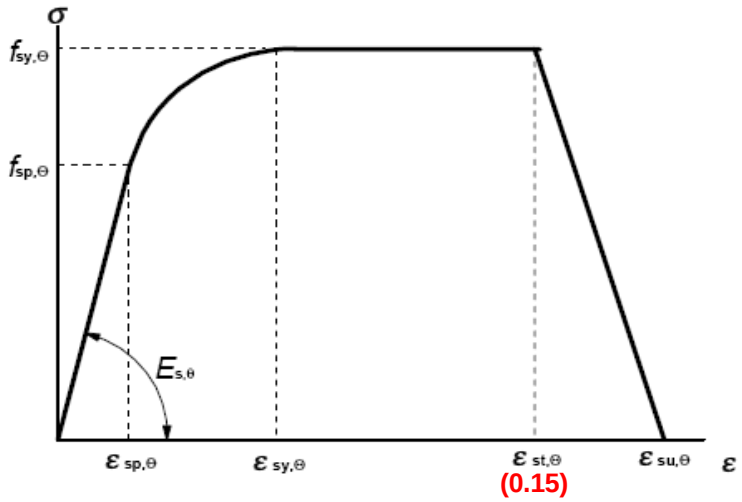

Figure 3.25 Mathematical model for stress-strain relationships of reinforcing steel at elevated temperature (EC2, 2004)

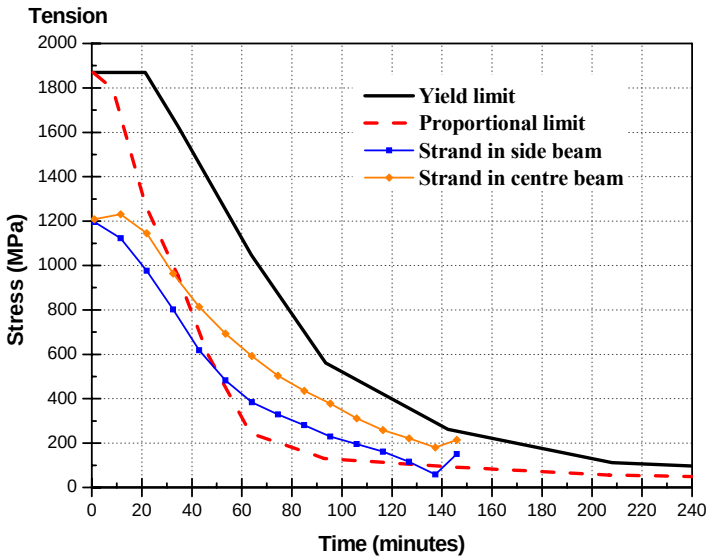

Figure 3.26 Strands stress history of a hollowcore concrete unit with Fixed-Slide end conditions under an ISO 834 fire

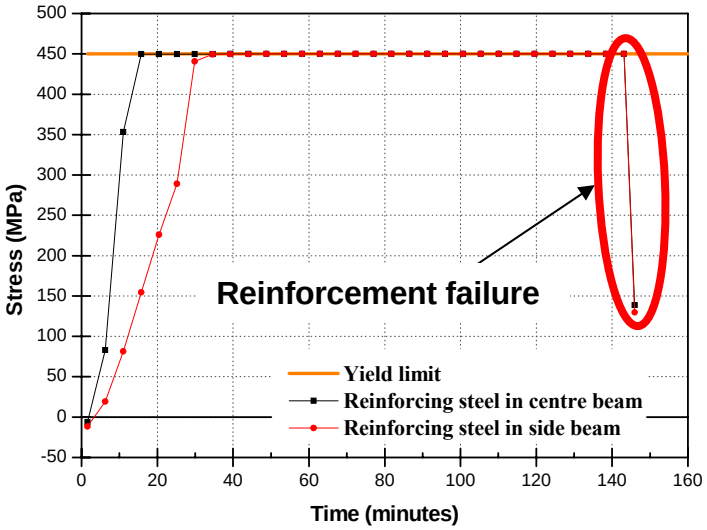

Figure 3.27 Reinforcement stress history of a hollowcore concrete unit with Fixed-Slide end conditions under an ISO 834 fire

3.5 Summary

Based upon a grillage model, a numerical model of a 200mm hollowcore concrete slab including a reinforced concrete topping slab, exposed to a Standard ISO 834 fire, was developed and investigated using the nonlinear finite element program, SAFIR.

In the thermal analysis of a 200mm hollowcore concrete slab, the effect of mesh density of cross sections was assessed and a coarse mesh was found to be satisfactory for modelling a prestressed hollowcore slab. The temperature development in the cross section was compared with the PCI temperature profile. The result shows that the temperature obtained from a numerical program was slightly higher than the PCI temperature.

The structural behaviour of a 200mm hollowcore concrete slab, uniformly exposed to a Standard ISO 834 fire, was investigated using a range of ideal support conditions. The reasons for analysis termination for all cases were investigated. Nevertheless, the application of ideal support conditions in simulating building frames with prestressed precast flooring system has some limitations, i.e. the difficulty of modelling the gap between hollowcore slabs and the end beams, and difficulty in accurately representing the end conditions for the prestressing tendons of the precast flooring units.

The analyses using idealised end supports assume that the prestressing strands

and topping reinforcing steels are anchored into the supports, for pinned and fixed end conditions. This assumption is inappropriate as it does not represent reality, so the modelling will be improved in the next chapter, with development of a multi-spring connection model.

Chapter 4

Numerical Model Development of a Single Hollowcore Concrete Slab in Fire

---

4.1 Introduction

This chapter presents the development and validation of a new multi-spring model which is able to take into account the discontinuity of prestressing steel strands between hollowcore slabs and their supporting end beams. The analysis in Chapter 3 is appropriate only if the prestressing strands were anchored into the end supports. The multi-spring model also models the role of concrete and starter bars in the topping slab during a fire. The validation of the multi-spring model was made by using a series of fire tests performed by Belgian researchers (Van Acker, 2003). The structural behaviour of a single hollowcore unit is investigated to take into account the influence of two different restraint conditions; fully restrained and restrained with end beams.

A parametric study is conducted to consider the effect of the number of prestressing strands and starter bars for a single hollowcore unit. All fire exposure in this Chapter is the Standard ISO 834 fire with no decay phase.

Two connection details, known as Matthews' and MacPherson's connection (Matthews, 2004; MacPherson, 2005), are selected to apply to the multi-spring connection model. The Matthews connection has no concrete filling and no reinforcing steel in the core. The MacPherson connection has concrete infill 1,000mm long in two of the six cores of the hollowcore slabs, with reinforcing bars in these two infills. In the application of the multi-spring connection model, the basic concept of MacPherson's connection is similar to the approach of Matthews' connection. Matthews' connection detail will be exploited throughout this Chapter

in order to investigate structural behaviour of single prestressed hollowcore slab. Then, the application will be extended to MacPherson's connection detail in the next chapter. Figure 4.1 shows the organisation of Chapter 4.

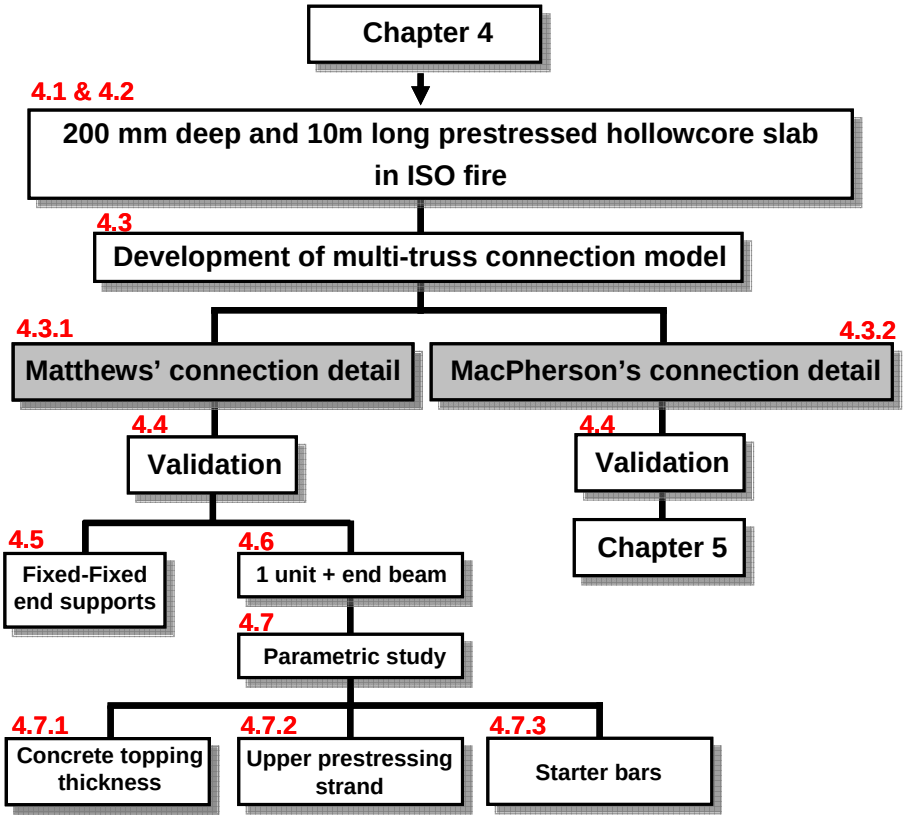

Figure 4.1 Organisation of Chapter 4

4.2 Hollowcore slabs seating connection

Precast, prestressed hollowcore floor units seated on reinforced moment resisting frames have been widely used as one of most common construction types in New Zealand during the last few decades (MacPherson, 2005). In order to investigate the seismic adequacy in different construction types, a series of experiments have been performed (Matthews, 2004; Lindsay, 2004; MacPherson, 2005). As a result, two acceptable solutions for hollowcore seating connections, i.e. Lindsay (2004) and MacPherson (2005) connection details, have been implemented in Amendment 3 within NZS3101:1995 (SNZ, 2004) and NZS3101:2006 (SNZ, 2006a) for 'new' construction practice in New Zealand (Jensen, 2006).

Previous research, using a grillage of beam elements and rigid elements, on three different kinds of hollowcore seating connections, namely Matthews', Lindsay's and MacPherson's specimens, showed that the fire performance of hollowcore floor units which have Matthews' and MacPherson's end connections was much better than Lindsay's case (Chang, 2007). In this Chapter, two end connection details, i.e. Matthews and MacPherson, will be used to describe and investigate details of seated connections of the hollowcore floor units in order to develop a new model which takes into account the effect of the influence of different seating conditions.

Traditionally, simply supported precast, prestressed hollowcore slabs in New Zealand have been widely used as shown in Figure 4.2 (Herlihy, 1999; Lim, 2003). The traditional connection details comprised of the floor unit seated on a mortar bed, core end plugs to prevent concrete from entering the cores, and conventional continuity starter bar reinforcement in the topping slab (Matthews, 2004). In a typical seating detail, starter bars connected between topping slabs and supporting beams provide rotational restraint and allow some redistribution of the bending moments in the slabs (Lim, 2003). In addition, the hollowcore slab is not anchored to the supporting beam and only starter bars in the topping concrete are connected to the supporting beam. The gap between the supporting beam and the hollowcore slab is filled with normal weight concrete in order to provide flexibility of lateral movement for earthquakes.

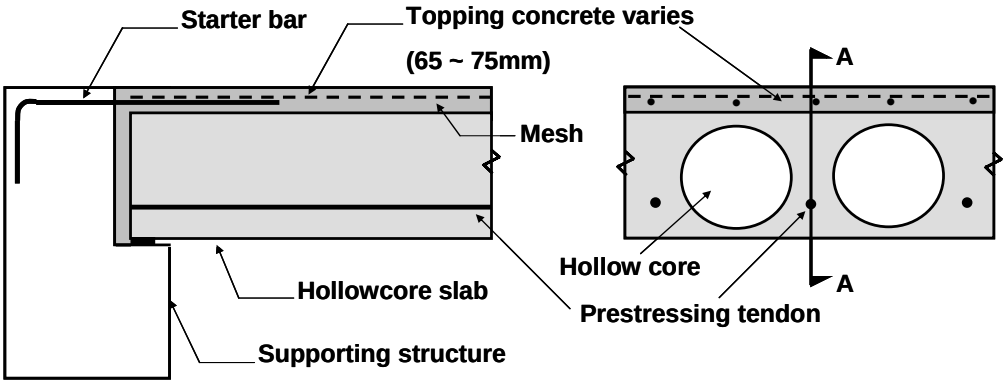

Figure 4.2 Typical floor-end beam connection detail of hollowcore floors

While the traditional connection detail of prestressed hollowcore floors has been widely used, a new floor-end beam connection solution has been proposed in order to improve seismic performance as shown in Figure 4.3. This new connection features hollow cores reinforced and filled with concrete (MacPherson, 2005). For 200mm deep hollowcore slabs, two cores of the six hollow cores are reinforced with hooked bars placed close to the bottom of the cores. The topping slab contains reinforcement which is lapped with the starter bars. To construct the new connection, more effort, such as pre-cut cores and the placing of extra reinforcement, are required in comparison to Matthews' connection detail. However, the new connection provides redundancy by being tied into the supporting beams (MacPherson, 2005).

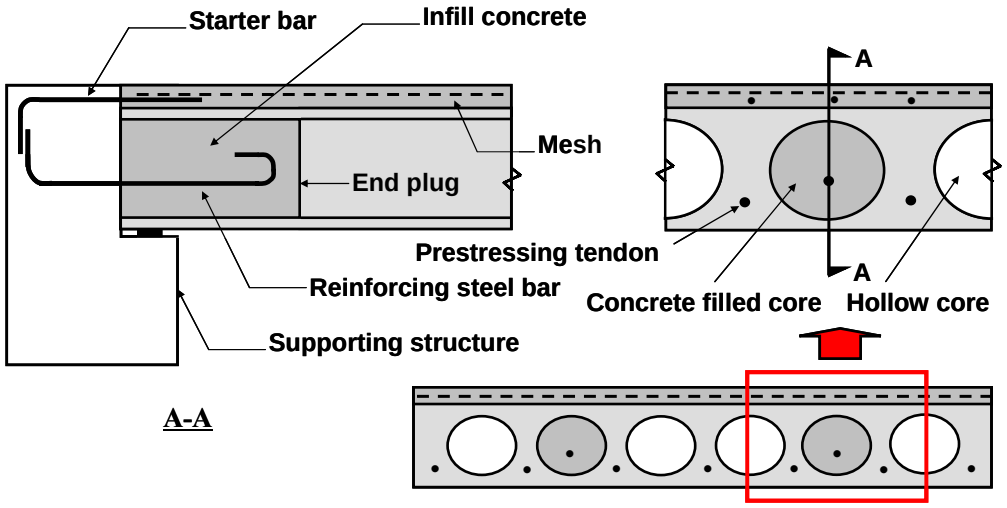

Figure 4.3 New floor-end beam connection detail of hollowcore floors

4.3 Multi-spring connection model

As explained in Section 4.2, there exists a huge difference between current modelling using ideal support conditions and construction practice in terms of the relation between hollowcore slabs and neighbouring structures. A new numerical model called a multi-spring connection, therefore, has been developed in order to better predict and understand the behaviour between hollowcore core slabs and supporting beams in fire, for Matthews' and MacPherson's connection detail.

4.3.1 Multi-spring connection model for Matthews' detail

As discussed in Chapter 3, hollowcore slabs including a reinforced concrete topping slab can be modelled by grillage systems. Nevertheless, the connection detail where the hollowcore slabs is fully connected to end supports still has a significant problem to predict the structural behaviour of hollowcore slabs in fire.

A schematic of the multi-spring connection model for Matthew's connection is shown in Figure 4.4. In the use of the grillage model, beam elements, as shown in Figure 4.4, are only expressed as fibres which include the mechanical properties of the hollowcore cross section, as well as the thermal properties at elevated temperature. Here, the vertical faces either side of a gap between hollowcore slabs and seating beams were modelled as a rigid surface, assuming that it was sufficiently rigid and connected to the starter bars. The use of rigid beam elements is able to avoid unnecessary small displacements at the vertical faces. In addition, both rigid beam elements are vertically supported at the bottom and can move horizontally and rotate freely to identify the variation of the gap at the end of the hollowcore slabs. On the other hand, the rigid beam element at the vertical surface of the seating beam can be assumed to be either fully fixed at the end boundary or connected to the supporting beam depending on the conditions.

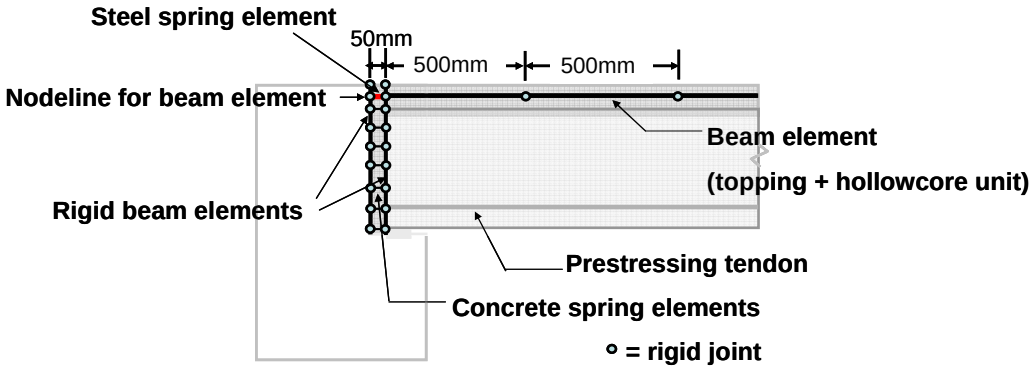

Figure 4.4 Schematic of multi-spring connection model for Matthews' detail

In the SAFIR program, the geometry of the spring elements is determined by the position of the two end nodes and spring elements are completely defined by their cross sectional areas and the material types. In order to employ spring elements into the new connection model, the cross section of the gap between

hollowcore slabs and seating beams was divided into nine segments as shown in Figure 4.5.

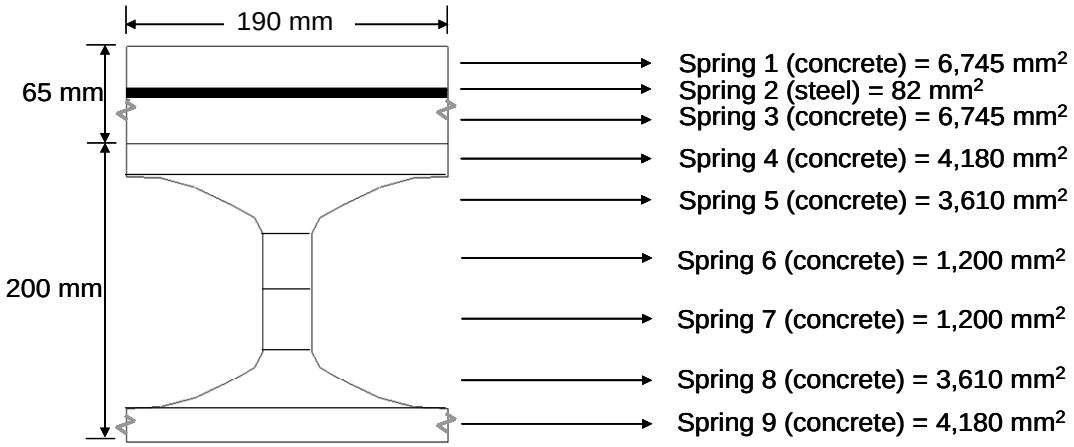

Figure 4.5 Division of the hollowcore slab cross section for Matthews' connection (white segment: concrete; black segment: steel)

In order to investigate the temperature of spring elements, the thermal analysis was conducted on an end beam. Figure 4.6 shows the dimension of the end beam with 75mm seating analysed.

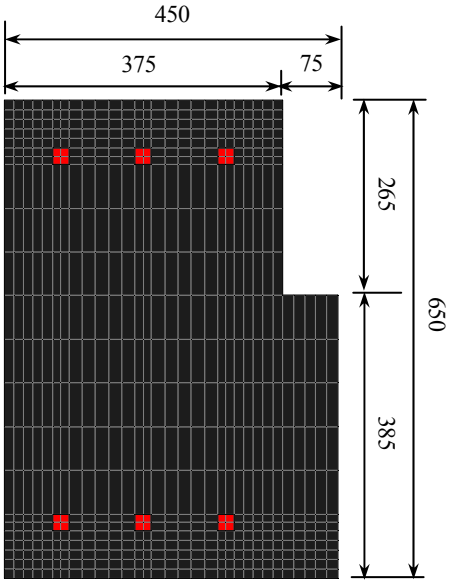

Figure 4.6 Dimension of an end beam

The temperature contours of the 450 x 650mm end beam at 60, 120, 180 and 240 minutes, obtained from SAFIR thermal analysis, are shown in Figure 4.7. In this analysis, it is assumed that the end beam is exposed to Standard ISO fire for 4 hours only on the bottom and the inner surface. In Figure 4.8, the bottom temperature (node 411) at the vertical surface of the seating beam is evaluated and indicates less than 300°C during 4 hours fire exposure. Conservatively, the temperature of nine spring element is assumed to keep ambient temperature during 4 hours fire exposure time.

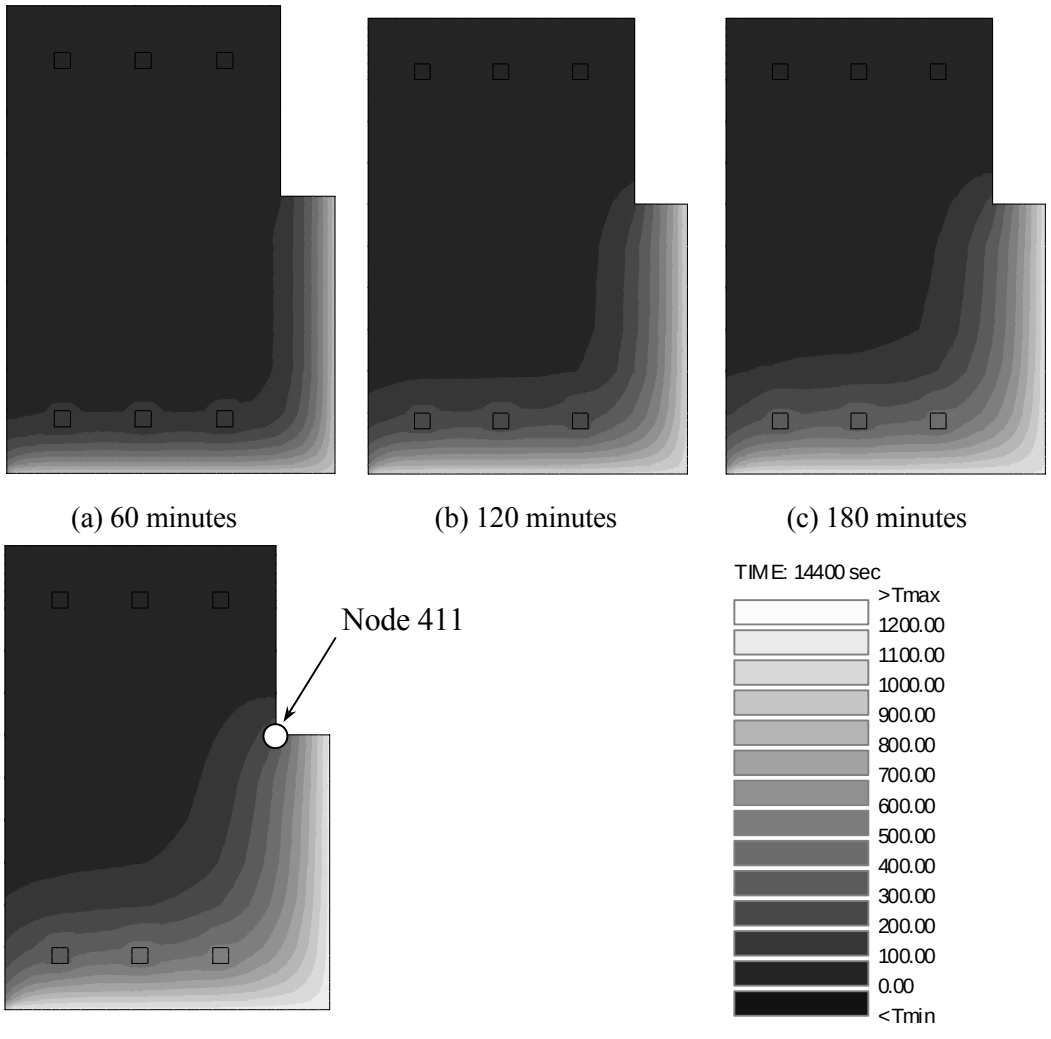

Figure 4.7 Temperature contours of the 450 x 650mm end beam at 60, 120, 180 and 240 minutes

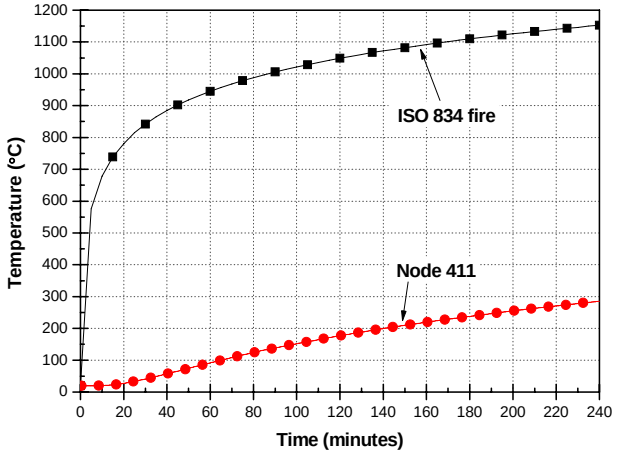

Figure 4.8 Temperature variation with time for node 411

4.3.2 Multi-spring connection model for MacPherson's detail

Most of the details in terms of the multi-spring connection model for MacPherson's case were principally based on the multi-spring connection model used for Matthews' case as described in Figure 4.4. As explained in Section 4.2, the new end connection called MacPherson's detail has some differences compared with Matthews' detail as shown in Figure 4.9. Two steel spring elements (second from top and third to bottom spring element) were used to model the starter bar and reinforcing bar within the core. In addition, the core filling was extended to 1.0 m long rather than the 800mm (greater of 800mm or 3 x depth of hollowcore) used by MacPherson to coincide with the length of the beam elements for ease of modelling. The cross section of the hollowcore slab was modified, as shown in Figure 4.10, in order to take into account the reinforcement within the filled core in the modelling and the number of longitudinal beams is reduced from 7 to 6. In MacPherson's connection detail, the gap between the hollowcore slabs and the end beams is filled with concrete. Each area of the spring elements, therefore, is modified as shown in Figure 4.11. In addition, the temperature of the modified spring elements applies to ambient temperature during 4 hours fire exposure time.

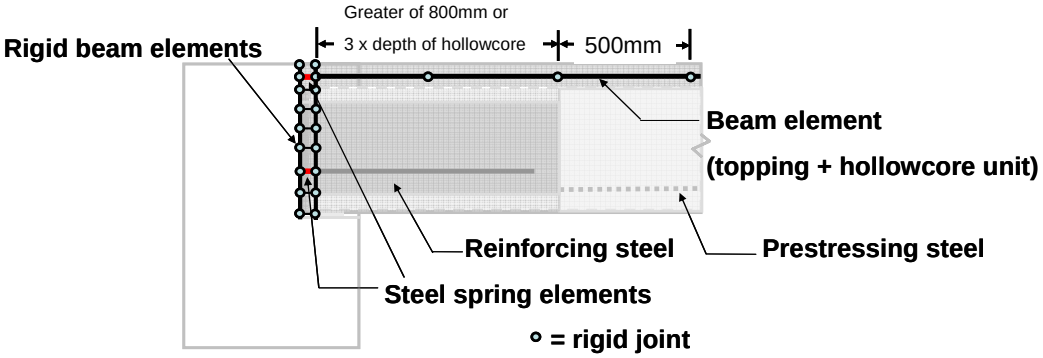

Figure 4.9 Schematic of multi-spring connection model for MacPherson's detail

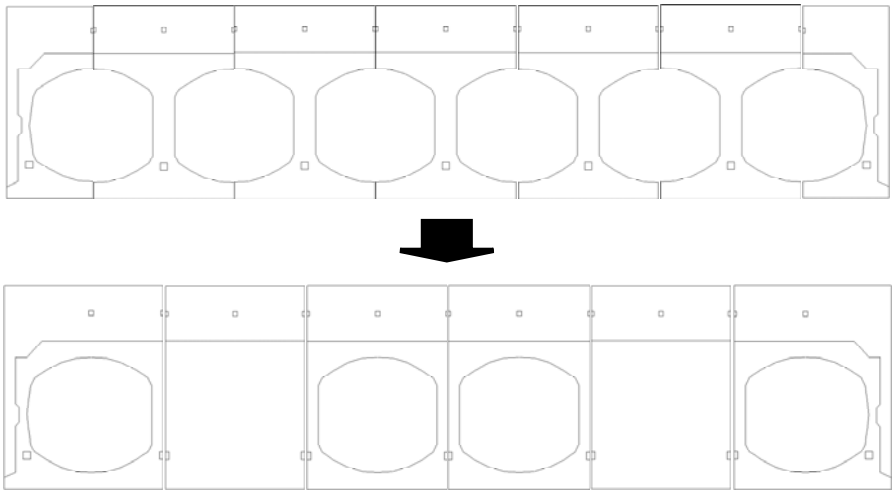

Figure 4.10 Modified hollowcore unit cross section

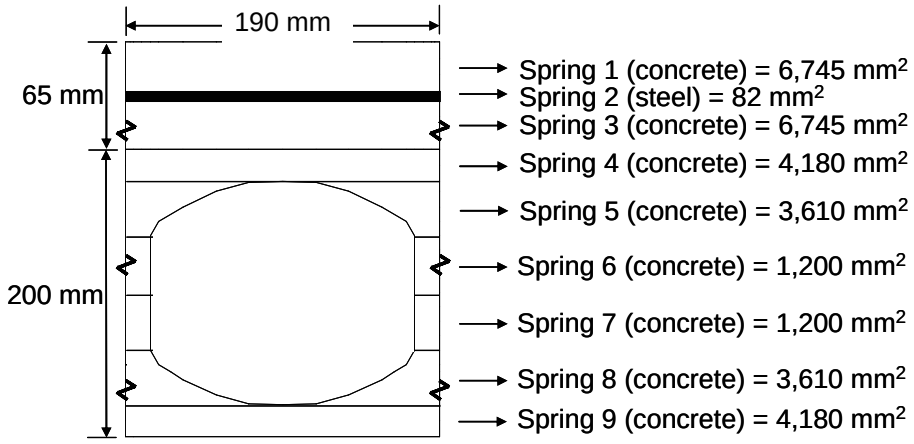

(a) cross section with unfilled core

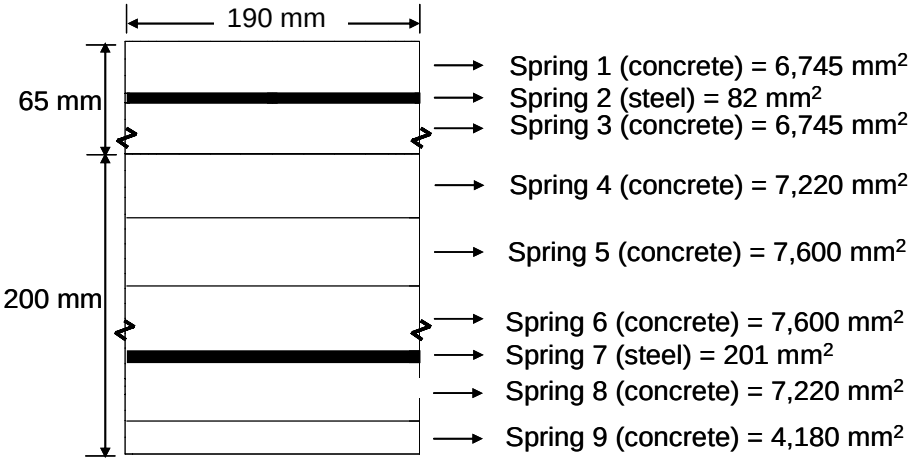

(b) cross section with filled core

Figure 4.11 Division of the hollowcore slab cross section for filled and unfilled core of MacPherson's connection (white segment: concrete; black segment: steel)

4.4 Validation against experimental data in Standard ISO 834 fire

Four full-scale fire tests were performed at the Technical Universities of Liège and Gent in Belgium, taking into account the influence of connections and surrounding structure on the fire resistance of prestressed hollowcore slabs. Among these test results, one fire test result (Van Acker, 2003) which includes a similar hollowcore profile and reinforced concrete topping, as shown in Figure 4.12, was considered for the validation of the multi-spring connection model. The connection features two out of six hollow cores in each precast slab reinforced and filled with concrete. Even though the test consisted of two sets of prestressed hollowcore units of 1.2m width supported on three beams, the one prestressed hollowcore floor span covered with a reinforced topping was selected.

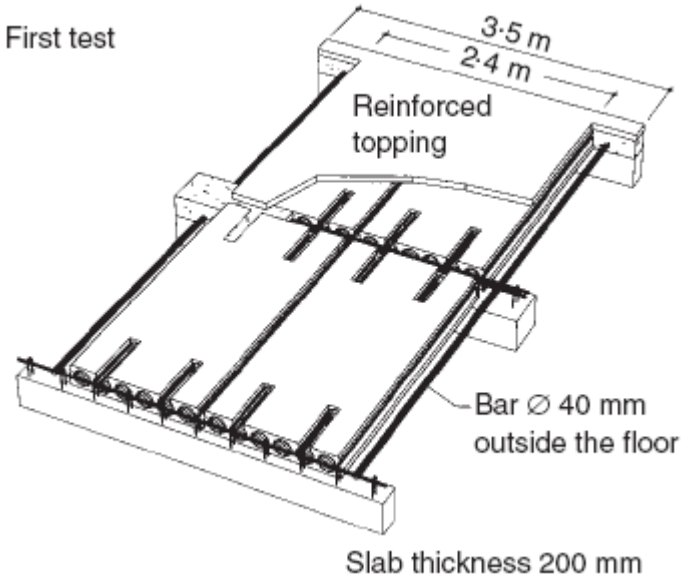

Figure 4.12 Fire test set-up (Van Acker, 2003)

The hollowcore units were 250mm thick with a 50mm reinforced concrete topping slab and the cross section and dimensions were as shown in Figure 4.13. Every 2nd and 5th core was filled near the supporting beams, and four 500mm length bars of 12mm diameter were cast in these cores and anchored in the supporting beam. A reinforcement mesh of 150 x 150 x 4mm was cast over half of the test floor. The reinforcing bars of 40mm diameter which were used to simulate the influence of the neighbouring structure were not considered in this analysis. The cube strength of the joint concrete and topping was 45 N/mm^2. The imposed load for the test was a line load of 100 kN across the middle of each of the two spans. This loading is reported (Van Acker, 2003) to correspond with the frequent part (ψ_2 in EC2 (EC2, 2003)) of the normal loading of a floor of 7.5m span, including the self-weight. The fire test was interrupted after 83 minutes "because of the appearance of a hole in the slab right under the pressure vessel" (Van Acker, 2003) and failed in bending with subsequent failure loading.

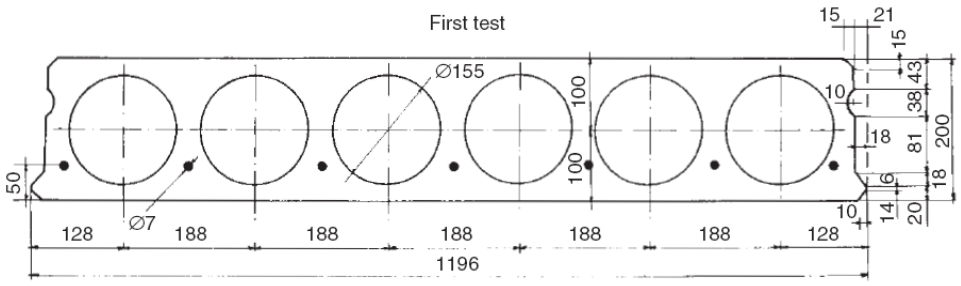

Figure 4.13 Cross section of the chosen test unit (Van Acker, 2003)

The multi-spring connection model was used to carry out the simulation of the experimental work, using the MacPherson's connection model. In this model, grillage beam elements were connected to reinforcing steel bars within the cores as shown in Figure 4.14.

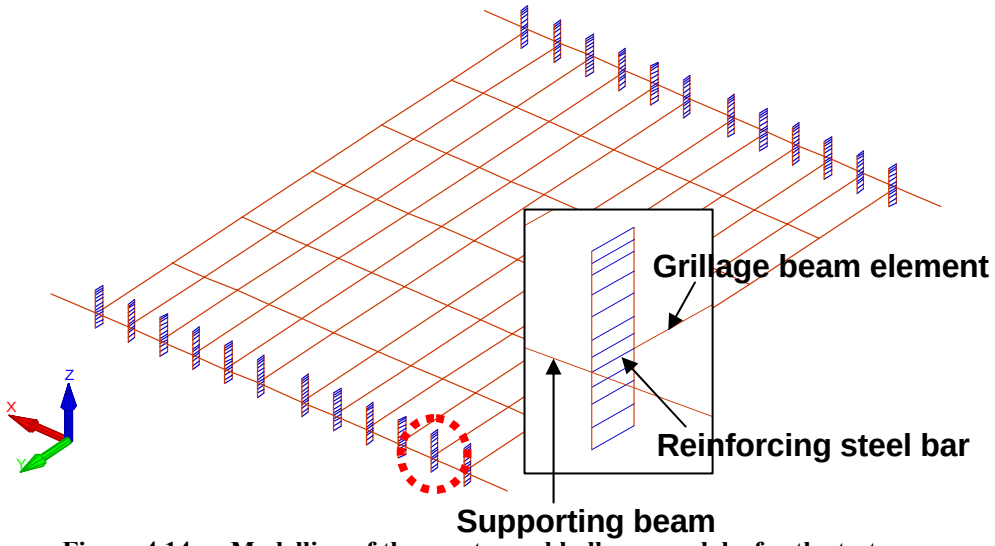

Figure 4.14 Modelling of the prestressed hollowcore slabs for the test

Figure 4.15 shows the comparison between the experimentally measured and analytically predicted structural behaviours of the slab including multi-spring connections as well as fixed and pinned connections which were studied previously (Change, 2007). As can be seen, the numerical results for the prestressed hollowcore slab with multi-spring connections are in reasonable agreement with the experimental behaviour of the prestressed concrete slabs in terms of fire resistance time, while the fixed-fixed and pinned-pinned connections (Chang, 2007) either over or underpredict the behaviour. On the other hand, the experimental and

numerical midspan vertical deflections are different. Basically, beam elements in SAFIR program adopt the Bernoulli's hypothesis which means plane section remains plane so that shear deformation is not captured; bond slips are also not taken into account (Chang, 2008). The difference with respect to vertical deflections is attributed to the factors.

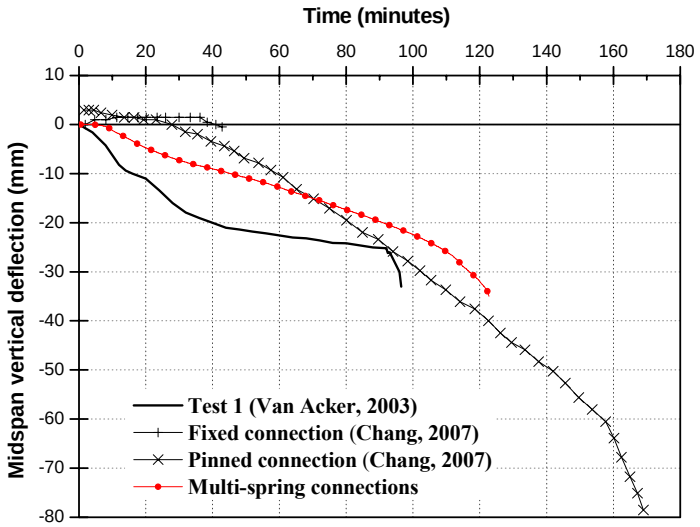

Figure 4.15 Comparison of structural behaviour against time for the reported test result (Van Acker, 2003) and the different analytical models

4.5 Structural behaviour of a fully restrained hollowcore slab unit in Standard ISO 834 fire

Based upon the multi-spring connection model as described in Section 4.3, the structural behaviour of a prestressed 200mm hollowcore slab unit, which is restrained against horizontal and vertical movements, was numerically investigated using the nonlinear finite element program, SAFIR. In this study, the material properties and geometry are same as the values used in Chapter 3. The analysis of Section 3.4.3 (Fixed-Fixed end supports) assumed that prestressing strands in hollowcore slab anchor with supports such that the result indicated unexpectedly large deflections. In order to avoid this inappropriate result, the newly developed multi-spring model was considered with respect to the Fixed-Fixed end condition. Figure 4.16 shows an isometric view of a prestressed 200mm hollowcore slab unit

incorporating multi-spring connection models at each end support. This result for this model is plotted in Figure 4.17 against time with the previous result and makes a comparison in terms of vertical deflections. This shows that the analysis using the newly developed multi-spring connection model stopped around 66 minutes without the abrupt increase of deflection that was found previously.

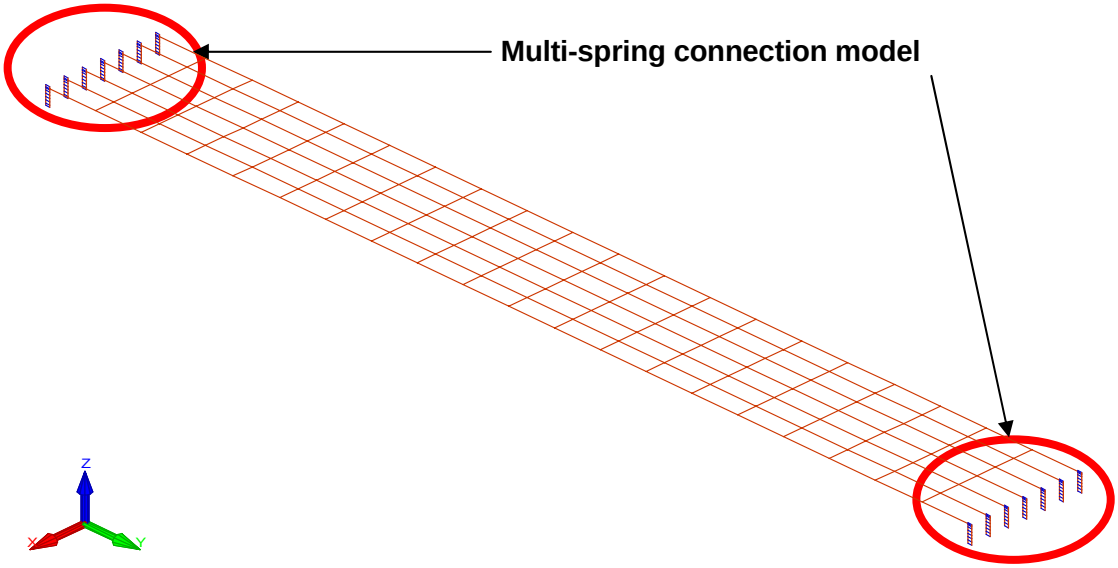

Figure 4.16 **Isometric view of a prestressed hollowcore grillage unit slab incorporating multi-spring connection models used for analysis**

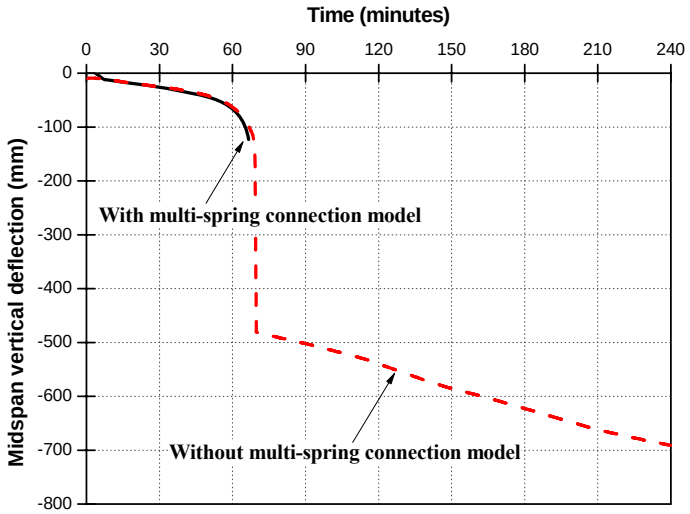

Figure 4.17 **Comparison between vertical deflections of a 200mm hollowcore slab with and without the multi-spring connection model with respect to Fixed-Fixed end conditions**

In order to identify the contribution of the spring elements to the fire performance of a prestressed hollowcore slab incorporating the multi-spring connection model, the variation of axial force for each spring element is plotted in Figure 4.18 until the simulation stops. The axial force variations in respect to the bottom concrete parts (springs 8 and 9) were compared with the material capacity. Compression force starts at the bottom of the hollowcore slab and with the increase of fire exposure time, the location of the compressive force develops from the spring 9 element.

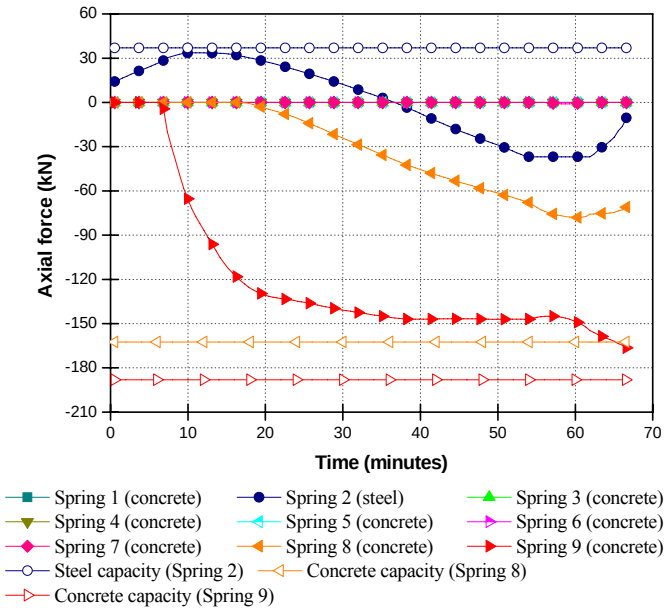

Figure 4.18 Variations of axial force (kN) for each spring element (fully restrained)

The spring 9 element which is positioned at the bottom of the multi-spring connection model indicates negative axial force due to compressive force caused by vertical deflection. Around 20 minutes, the spring 8 element starts to develop axial force. The spring 9 element did not reach its yield limit at the end of analysis. In conclusion, in case of the fully restrained situation, hollowcore slabs failed due to the failure of convergence around 66 minutes.

In order to ascertain the role of a multi-spring connection model in fire, the deflected shapes of a prestressed 200mm hollowcore slab at two different stages were studied. Figure 4.19 shows the deflected shape of a fully restrained

hollowcore slab at the beginning of the simulation. Because of the effect of prestress, the hollowcore slab deflects upwards at the initial stage. At that time, all multi-spring elements would be subjected to tension as illustrated in Figure 4.19. Prestress is applied to the hollowcore slab at the beginning of simulation, whereas the vertical loads were gradually applied to hollowcore slab over the first 20 seconds of fire exposure. After vertical loads were fully applied to hollowcore slab, the hollowcore slab starts to increase in vertical deflection with increasing time. At the end of the simulation, the steel is subjected to tension while compressive force is applied to the lower parts of multi-spring connection as shown in Figure 4.20.

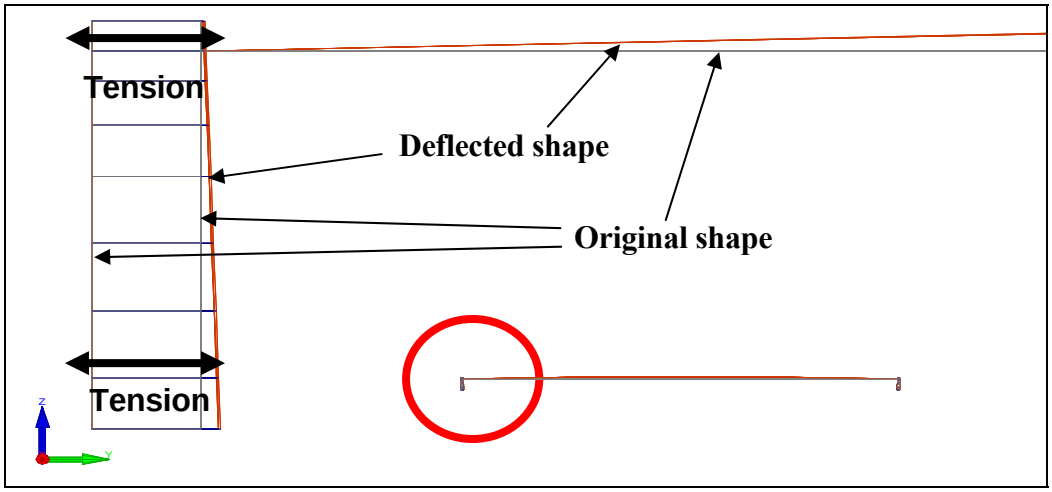

Figure 4.19 Deformation shape of a multi-spring connection at the beginning of the simulation in the fully restrained case, scale factor = 5

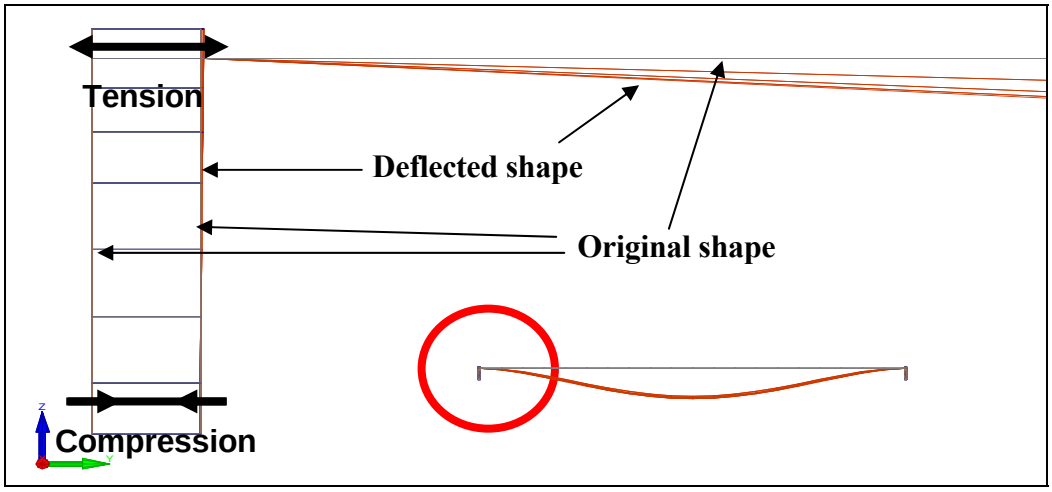

Figure 4.20 Deformation shape of a multi-spring connection at the end of the simulation in the fully restrained case, scale factor = 5

4.6 Structural behaviour of a hollowcore unit restrained with end beam in fire

In order to investigate the structural behaviour of a hollowcore unit restrained by end beams compared to the fully restrained case, a subassembly was chosen as shown in Figure 4.21. To simplify the failure mechanism of the hollowcore slab during a fire, it was assumed that only one hollowcore unit, located at the centre of subassembly, was connected to supporting beams directly and the ends of supporting beam are fully fixed against displacements and rotations (Cross-hatched region).

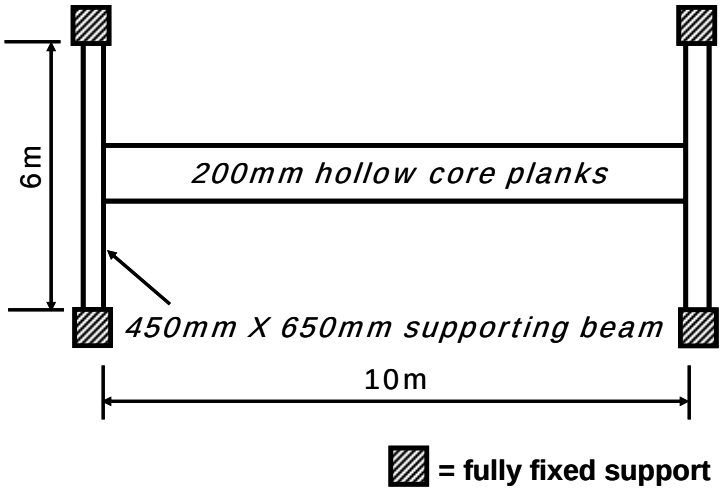

Figure 4.21 Schematic drawing of the hollowcore slab subassembly

The end beams used in this model were 650mm deep by 450mm wide with 3-D25 bars at the top and bottom. Figure 4.22 shows the discretised beam cross section used in SAFIR. It was assumed that the supporting beam was subjected to Standard ISO 834 fire exposure.

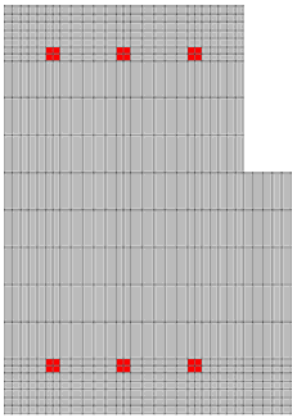

Figure 4.22 Discretised supporting beam in SAFIR

Figure 4.23 shows the comparison of the central vertical deflections of the fully restrained hollowcore slab and the hollowcore slab restrained by end beams during a Standard ISO 834 fire exposure. It can be seen that there is a great difference in terms of vertical deflections and fire resistance times.

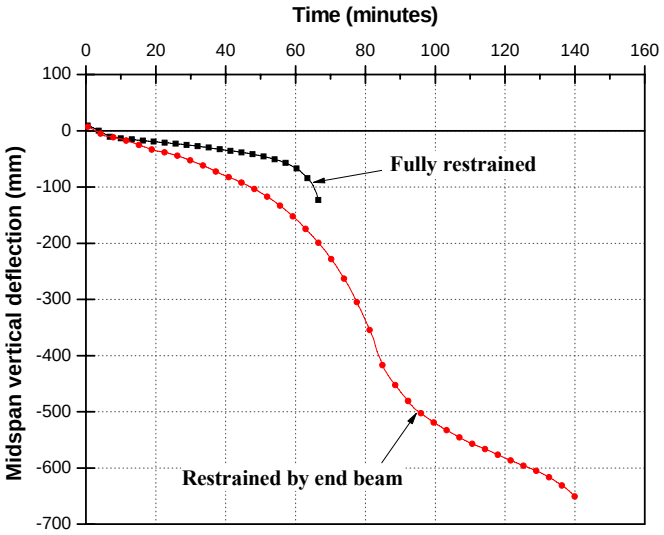

Figure 4.23 Comparison of the midspan vertical deflections

In the fully restrained case, as shown in Figure 4.20, the outside surface, expressed as rigid elements, does not move horizontally. As a result, the lower parts of the multi-spring connection model develop compressive forces significantly (Figure 4.18). In the case restrained by end beams, the bottom spring element develops compressive force in the initial stage as well as tensile force developing in a starter bar. In the contribution of the spring elements, compressive force is

concentrated in the bottom spring element as shown in Figure 4.24. As a result, the development of bottom concrete spring element does not lead to the simulation stopping.

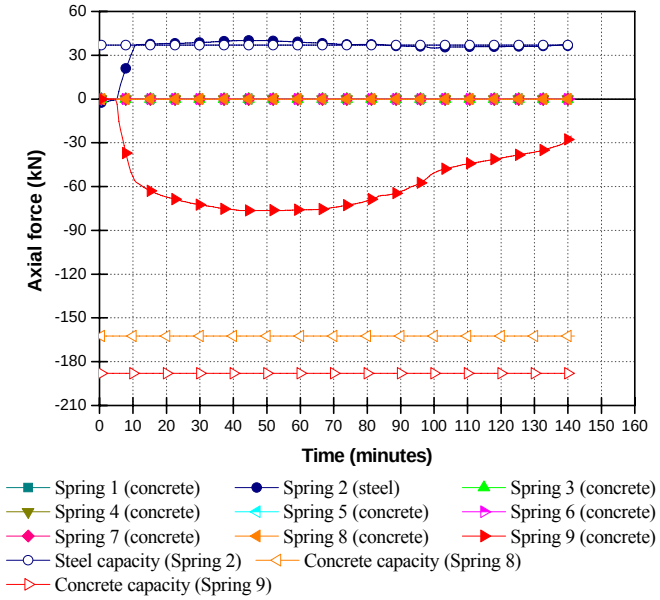

Figure 4.24 Variations of axial force of each spring element (restrained by supporting beam)

In order to examine the failure reason, strain histories of steel spring element and reinforcement at the end of a span are plotted in Figures 4.25 and 4.26 respectively. In Figure 4.25, the steel spring element reached the strain of 8% at around 45 minutes and remained the same strain at the end of analysis due to rotation restraint. On the other hand, the reinforcement started to increase the strain after around 40 minutes. After that, the analysis stopped when the reinforcement is beyond the limiting strain of 15% at around 140 minutes as shown in Figure 4.26. In addition, the stress history of reinforcement at the end of the hollowcore slab span, as shown in Figure 4.27, underlies the failure reason of the analysis. In addition, Figure 4.28 represents the stress-strain relationship of reinforcement at elevated temperatures. Figure 4.29 shows the deflected shape of the hollowcore slab where a high strain occurs.

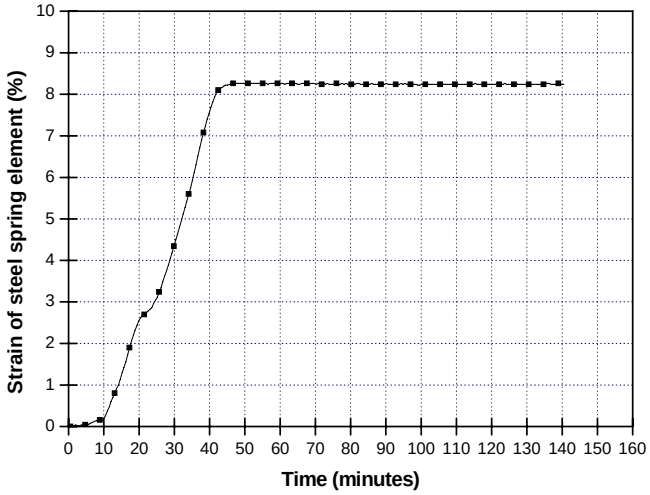

Figure 4.25 Strain history of steel spring element

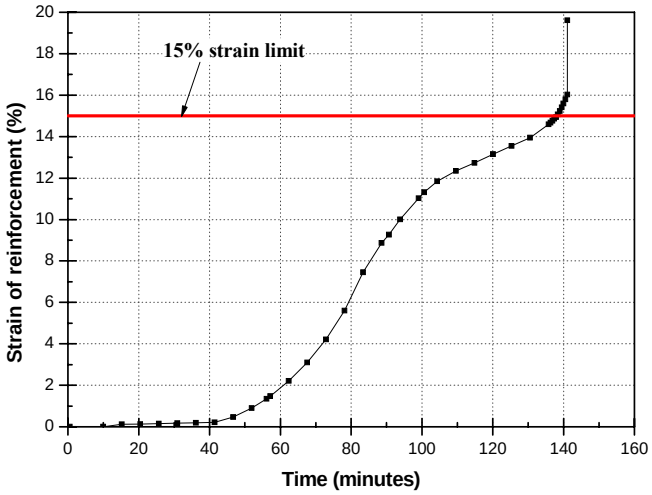

Figure 4.26 Strain history of reinforcement at the end of a span

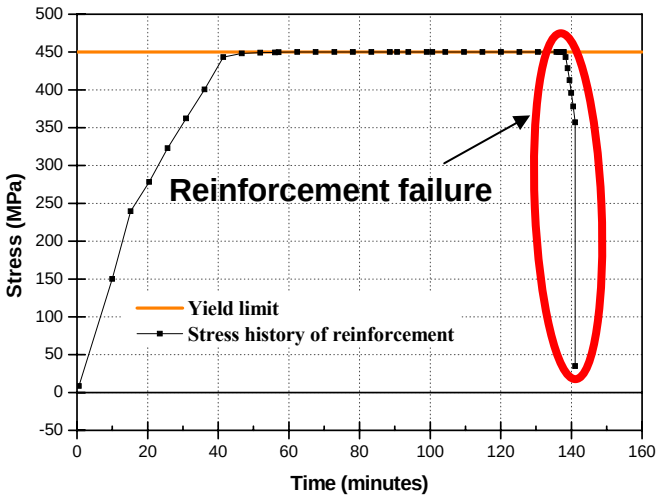

Figure 4.27 Stress history of reinforcement at the end of a span

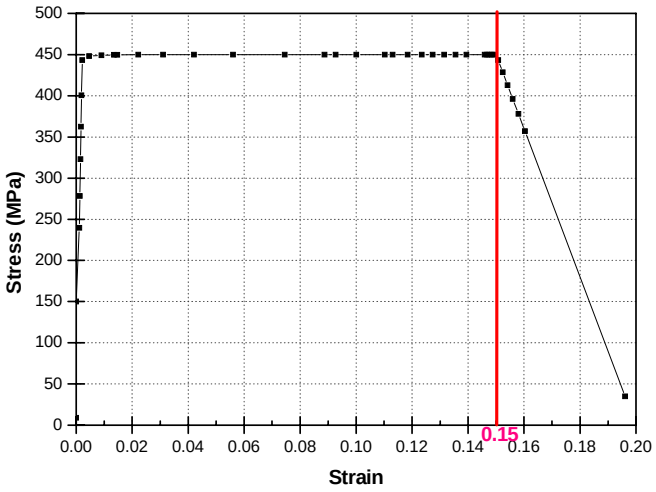

Figure 4.28 Stress-strain relationship of reinforcement at elevated temperatures

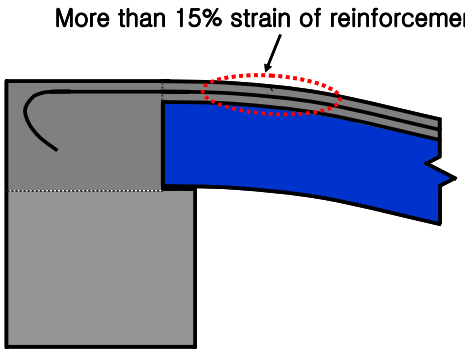

Figure 4.29 Deflected shape of a hollowcore slab at failure

4.7 Parametric study

The structural behaviour of a single prestressed 200mm hollowcore slab with various parameters, such as reinforced concrete topping thickness, upper prestressing strand and the amount of starter bars, subjected to a Standard ISO 834 fire, has been investigated in order to identify the effect of each parameter. As demonstrated in Section 4.6, it was assumed that the single prestressed hollowcore slab is connected to supporting beams throughout the parametric studies.

4.7.1 Effect of reinforced concrete topping thickness

The thickness of the cast-in-situ topping slab on prestressed hollowcore slabs is typically 65mm, but that can be varied up to 75mm (Stresscrete products, 2011). In order to assess the effect of the topping thickness on the fire resistance of single

prestressed hollowcore slab, an analysis with 75mm topping slab was performed. The comparison of midspan vertical deflection results with those for the 65mm topping slab is plotted against time in Figure 4.30. It can be seen that, by modifying the thickness of topping slab, the structural behaviour of single prestressed hollowcore slab can be improved slightly, up to around 80 minutes, but a single prestressted hollowcore slab with a 75mm topping slab gives more deflection than a hollowcore slab with 65mm topping slab. In this analysis, the hollowcore slab terminated at around 131 minutes due to the high strain at the end of the span as shown in Figure 4.31.

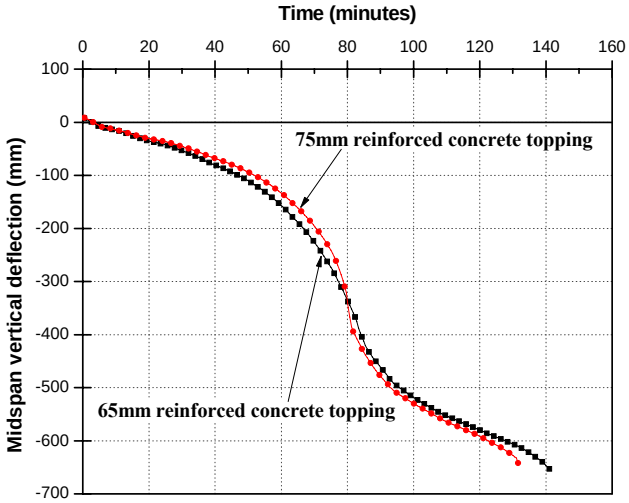

Figure 4.30 Comparison of midspan vertical deflection between 65 and 75mm reinforced concrete topping

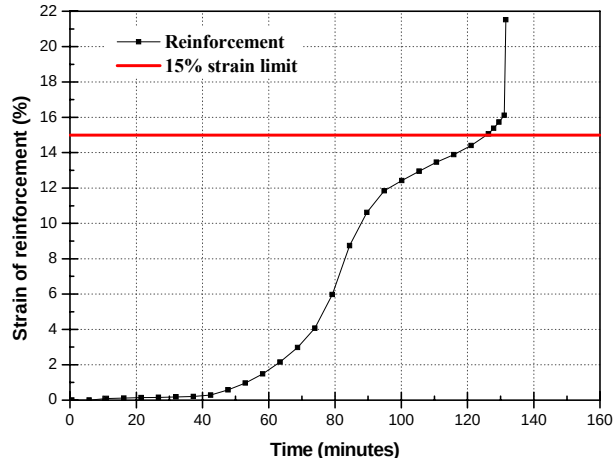

Figure 4.31 Strain history of reinforcement at the end of a span with 75mm topping

As seen earlier for the single hollowcore slab model restrained by end beams, the axial force variation in the multi-spring connection was investigated as

shown in Figure 4.32. The result shows that the bottom spring element develops a compressive force, but the axial force does not reach the yield limit at the end of analysis.

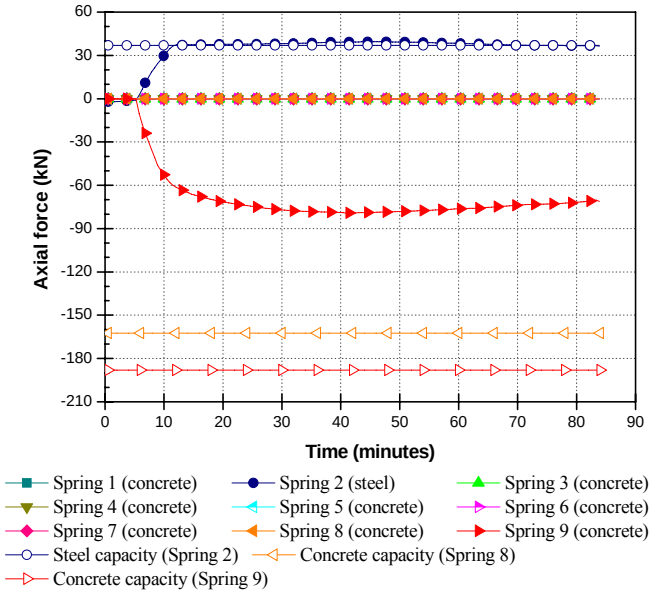

Figure 4.32 Variations of axial force of each spring element for 75mm topping slab

4.7.2 Effect of upper prestressing strand

The prestressed hollowcore slabs which have bottom prestressing strands have been widely used in New Zealand. However, for certain sections, the strands can be placed in the compression part as well as in the tension part as shown in Figure 4.33 (Lin, 1963).

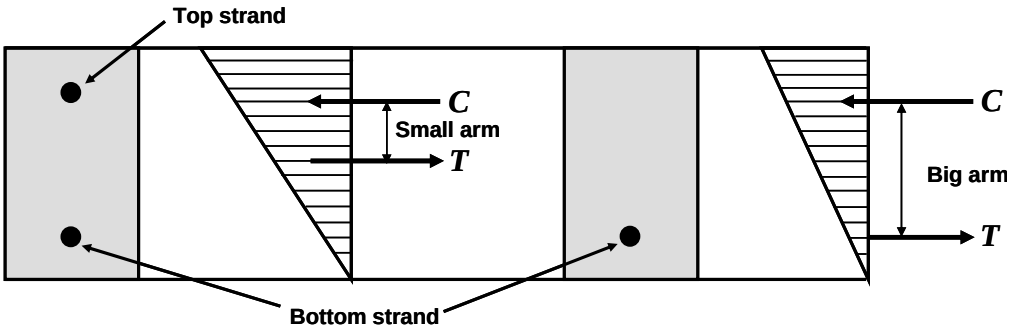

Figure 4.33 Prestressing steel in both flanges reduces lever arm for resisting moment

Even though this method is not an economical arrangement due to the decreased resisting lever arm, under certain circumstances it may be necessary to

put tendons in both flanges in spite of the resulting disadvantages. These conditions are:

1. When the member is to be subject to loads producing both $+M$ and $-M$ in the section.
2. When the member might be subject to unexpected moments of opposite sign, during its handling process.

In order to assess the effect of upper prestressing strands in fire, a prestressed 200mm hollowcore slab with upper prestressing strands which are located at 155mm from the bottom was analysed. The results are plotted in Figure 4.34 as the midspan vertical deflection against time to compare with the structural behaviour of a prestressed hollowcore slab with only bottom prestressing tendons. It can be seen that some reduction in vertical deflection occurs as a result of the changes of the lever arm length. The variation of axial force in the multi-spring connection model, for the case of top and bottom prestressing strands, is shown in Figure 4.35. The simulation stopped due to the failure of the top steel spring element at around 63 minutes.

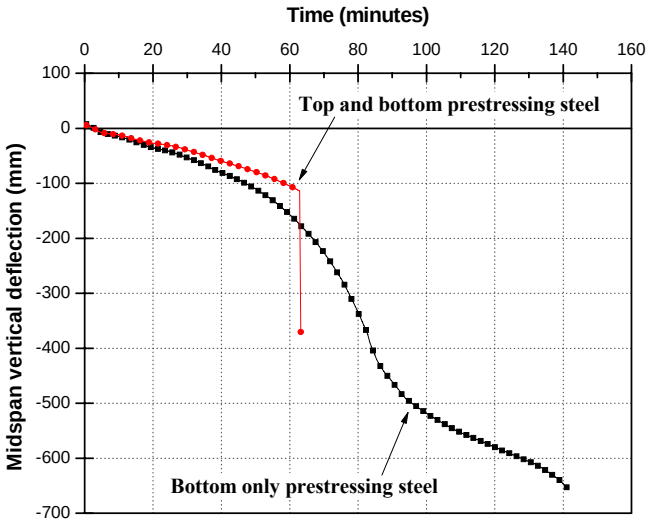

Figure 4.34 Comparison of vertical deflection for only top prestressing steel and for top and bottom prestressing steel

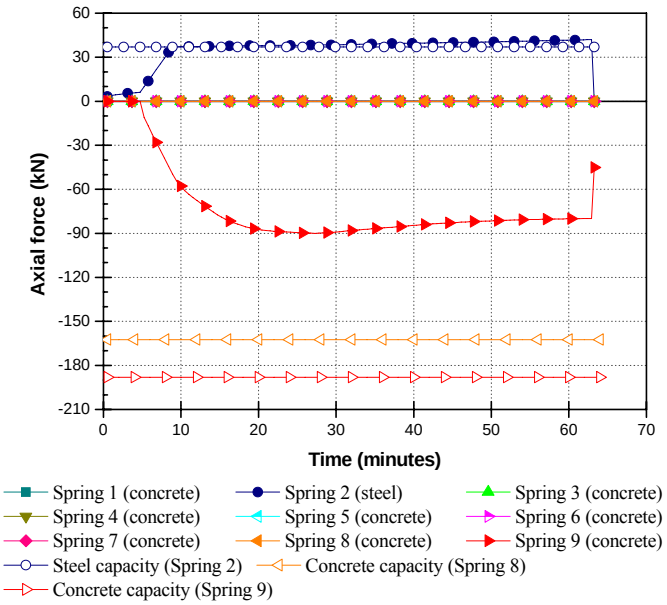

Figure 4.35 Variations of axial force of each spring element for top and bottom prestressing steel hollowcore slab multi-spring connection

4.7.3 Effect of starter bars

The role of starter bars connected between the reinforced concrete topping slabs and supporting beams has not been investigated yet. In order to examine the effect of starter bars, prestressed hollowcore slabs with different numbers of starter bars have been analysed while keeping the topping slab reinforcement the same as normal (i.e., 12mm bars with 300mm spacing). To represent the increase in the amount of steel, the area of the steel spring element in the multi-spring connection model was increased to 1.5 times the normal. These increased steel amounts are also applied to 500mm long beam elements at the ends of the slab. Figure 4.36 shows the resulting maximum deflections of these single prestressed hollowcore slabs. It can be seen that the structural behaviour of the single prestressed hollowcore slab in fire is sensitive to the amounts of starter bars, with a significant increase of fire resistance in 1.5 times starter bars case. As can be seen Figure 4.37, the strain of reinforcement at the end of the span did not reach 15% strain limit at the end of the analysis.

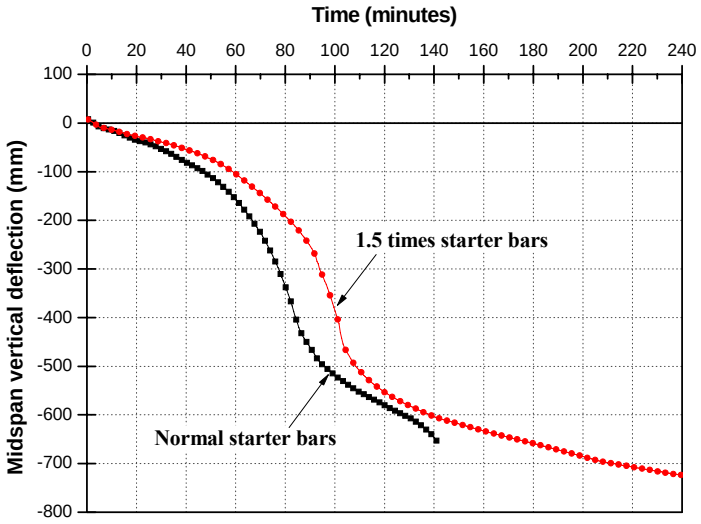

Figure 4.36 Comparison of vertical deflection according to the quantity of starter bar reinforcement

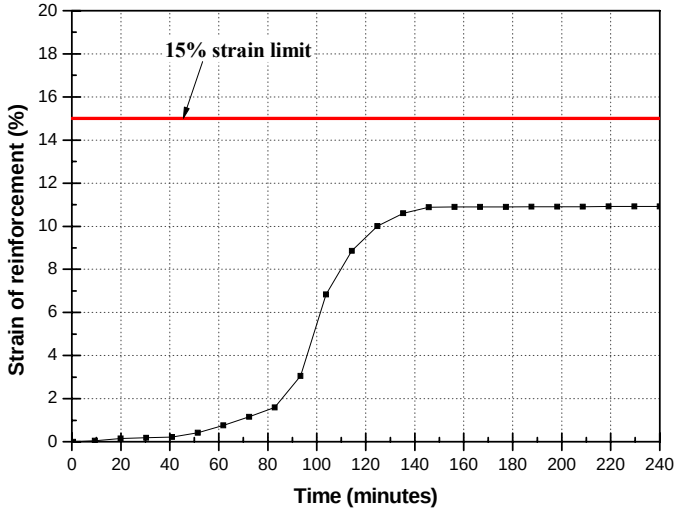

Figure 4.37 Strain history of reinforcement at the end of a span with 1.5 times starter bars

The axial force variation in the multi-spring connection was investigated as shown in Figure 4.38. The result shows that the bottom spring element develops a compressive force, but the axial force does not reach the yield limit at the end of analysis.

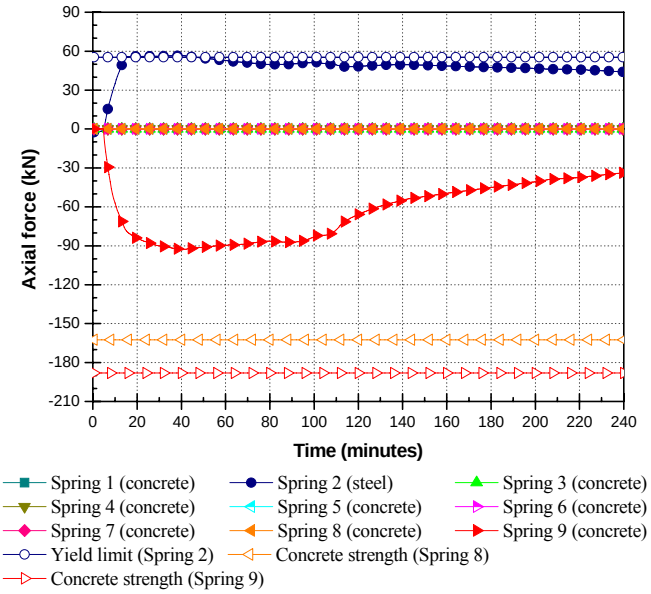

Figure 4.38 Axial force for 1.5 times the normal starter bars

4.8 Summary

A multi-spring model has been developed to predict the end connection behaviour of a single prestressed hollowcore slab under a Standard ISO 834 fire. With the multi-spring connection model, the structural behaviour of the gap between prestressed hollowcore slabs and supporting beams is captured well and understood clearly. It was demonstrated that surrounding structures such as supporting beams play a crucial role in modifying structural behaviour of a single prestressed hollowcore slab in fire. In addition, the validation has been made against an experiment and showed reasonable agreement with the experimental result available in the literature.

The effect of several parameters on the structural response of the prestressed hollowcore slab was examined. It was shown that the increase in topping thickness improved the structural behaviour slightly, but the fire resistance was more or less the same. The addition of top prestressing strands reduced the fire resistance due to the reduced lever arm length compared with bottom strands only. Finally, the 1.5 times starter bars results in the increase of the fire resistance of a single prestressed hollowcore slab.

Chapter 5

Fire Resistance of Hollowcore Slabs Restrained by Surrounding Structures

---

5.1 Introduction

This chapter describes the numerical modelling of 200mm prestressed hollowcore slabs focusing on the MacPherson's seating connection detail using the multi-spring connection model. In order to investigate the effects of the end (or support) beams on the fire resistance, numerical studies were carried out without end beams and with end beams of variable length, ranging from 1.45m to 6m long, without consideration of columns. The analyses were extended to where the columns included. The fire resistance was investigated with respect to each case and failure modes were examined. The effect of an infill strip parallel to the hollowcore units was investigated along with side beams and compared to the case of no infill where the first hollowcore unit is placed next to the side beam. Figure 5.1 illustrates the organisation of Chapter 5.

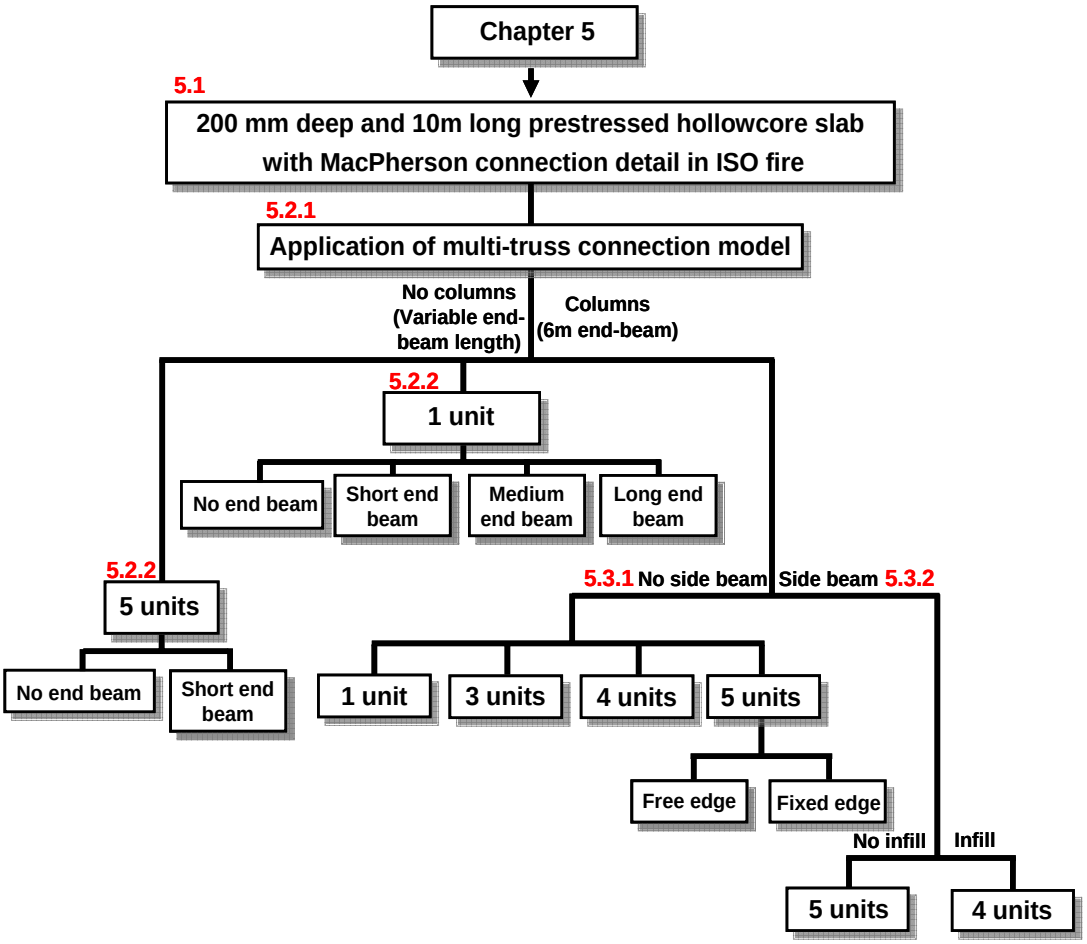

Figure 5.1 Organisation of Chapter 5

5.2 Hollowcore concrete slabs without column supports

The prediction of the fire resistance of a single 200mm deep, 1200mm wide and 10m long hollowcore slab with 75mm reinforced concrete topping without column supports is reported in this section. Hollowcore concrete slabs were analysed under the exposure of a Standard ISO fire. In order to simplify modelling a prestressed hollowcore slab which has a MacPherson's seating connection, some variables, i.e. the concrete filling location and concrete filling in beam elements, are investigated and discussed through analyses in this section.

5.2.1 Concrete filling of cores

As explained in Chapter 4, the current New Zealand Concrete Structures Standard (NZS 3101: 2006) requires a new type of seating connection detail, known as MacPherson's seating connection. This seating connection detail will be used throughout this chapter.

MacPherson's seating connection detail consists of a hollowcore unit, hooked reinforcing steel bars, a ductile mesh centrally positioned in a topping concrete and with concrete filling in two of the six hollow cores, as illustrated in Figure 4.3. One variable in the modelling of a prestressed hollowcore slab incorporating MacPherson's seating detail is the consideration of the concrete filling in the beam elements. A previous seating detail which was widely adopted in structural designs (Matthews) has showed behavioural deficiencies such as snapping action against lateral loadings as shown in Figure 5.2 and resulted in premature collapse of precast, prestressed hollowcore flooring systems both locally and globally (Jensen, 2006).

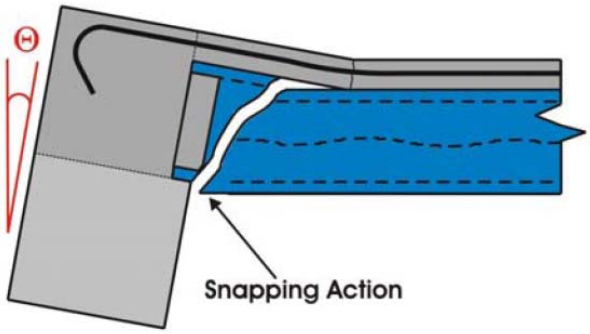

Figure 5.2 Flexure-shear failure mechanism from Matthews (Jensen, 2006)

In order to avoid flexure-shear failure mechanism from Matthews' seating detail, MacPherson's seating detail which includes two rigid cores filled with concrete out of six cores, as well as reinforcing bars passing along the bottom of the core, was developed. In the application of concrete infill cross section, the length of the concrete infill beam elements should be at least 800mm for any depth of hollowcore slab (SNZ, 2004) as illustrated in Figure 5.3. To simplify the modelling, 1.0m long concrete filling beams were applied to the 2nd and 5th longitudinal beam elements of a prestressed hollowcore slab.

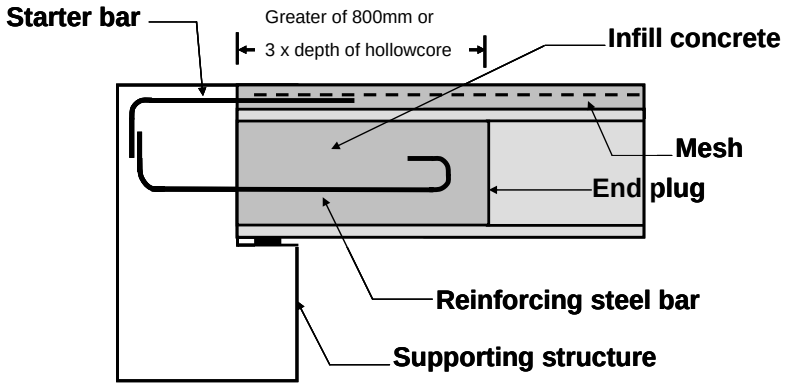

Figure 5.3 Requirements with respect to concrete infill cross section

5.2.2 Effect of concrete filling

Although two cores of six hollow cores are filled with concrete, there is no explanation in terms of the location of the concrete filling. In order to investigate the effect of different concrete filling locations, a single prestressed hollowcore unit together with 6 m long end beam was analysed with respect to three possibilities, as shown in Figure 5.4. In these analyses, a single hollowcore slab was assumed to be exposed to a Standard ISO fire, but the 6m long end beams were assumed not to be exposed to fire and were fully fixed against displacements and rotations at the ends of the beams. Midspan vertical deflections of the numerical results of the slabs with concrete filling in 3 different locations are plotted in Figure 5.5. It can be seen that the effect of concrete filling location is negligible. The 2nd and 5th core filling, therefore, was used in the analysis of MacPherson's seating connection.

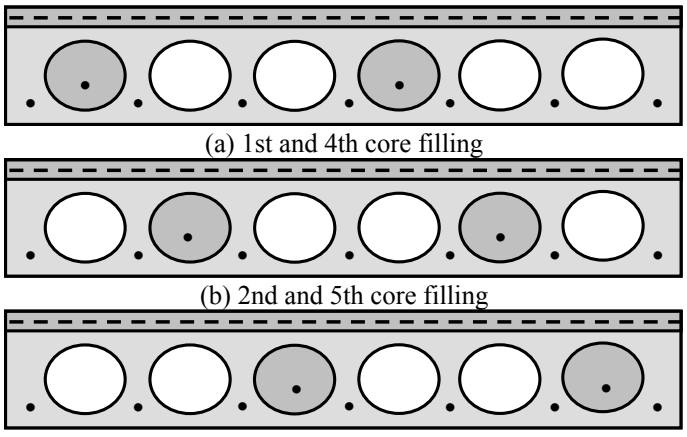

(a) 1st and 4th core filling

(b) 2nd and 5th core filling

(c) 3rd and 6th core filling

Figure 5.4 Location of concrete filling

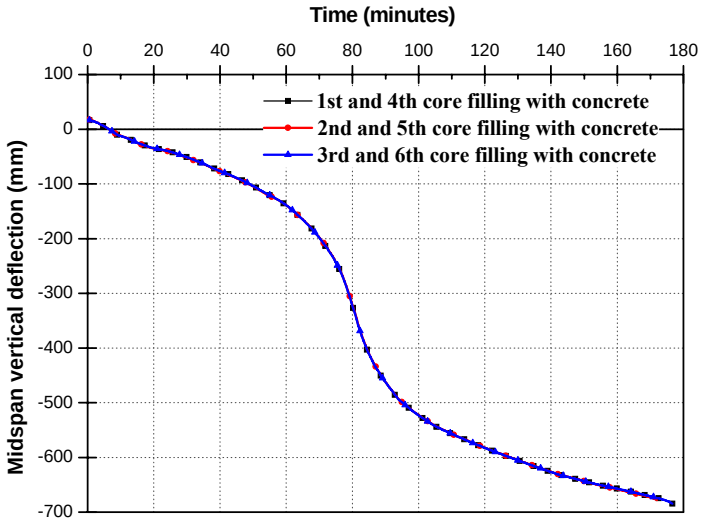

Figure 5.5 Comparison of midspan vertical deflection with respect to three different concrete filling locations

The vertical deflection of the prestressed hollowcore slab filled with concrete under a Standard ISO fire was compared to a prestressed hollowcore slab filled with no concrete. Figure 5.6 shows the comparative result of the midspan vertical deflections of a single prestressed hollowcore slab with 75mm concrete topping. It can be seen that the midspan vertical deflection of the two slabs are similar up to around 131 minutes, when the single hollowcore slab with no concrete filling fails while the single hollowcore slab with concrete filling has more fire resistance. Even though the difference of the fire resistance between concrete filling and no concrete filling cases is significant, the modelling of the prestressed hollowcore slab which includes concrete infill for 2nd and 5th hollow cores is more realistic and close to current practice in New Zealand. The model that incorporates concrete filling in beam elements up to 1.0 m at 2nd and 5th hollow cores is used in the analyses from now on.

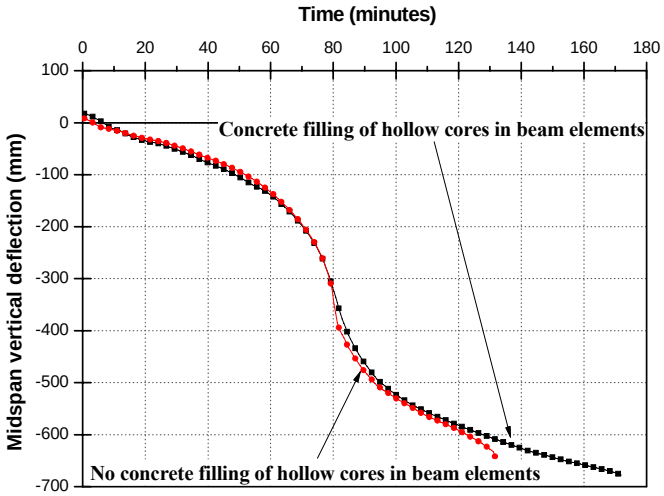

Figure 5.6 Comparison of midspan vertical deflection with respect to concrete filling of hollow cores

5.2.3 Effect of end beam length

A Standard fire test is the traditional method to evaluate the fire resistance of any type of structure. In this method, the interaction between the main structure and the surrounding structures is not likely to be considered due to the limitations such as the size of the furnace or specimens, loading conditions and edge or end restraint. As a result, most studies have been restricted to simply supported, axially restrained and continuous end conditions. With the development of computer modelling, it is possible to take into account the effect of the surrounding structures. In this section, numerical investigations of variable length end beams: 1.45m, 3.35m and 6m; fully fixed supports (no end beam), along with the effects of horizontal, vertical and rotational restraints at the ends of the end beams on the fire resistance of prestressed hollowcore slabs are reported. It was assumed that the surrounding structures, i.e. end beams, were not exposed to fire and used the corresponding modelling of the prestressed hollowcore slabs as reported in Section 5.2.1 and 5.2.2.

Figure 5.7 shows the results predicted by the analyses. It can be seen that the degree of end restraint may affect the fire resistance of a single prestressed hollowcore slab. With the 6m long end beam length, the fire resistance of a single prestressed hollowcore slab increased significantly due to the failure of a serise of reinforcement and the end beam. However, in other cases hollowcore slabs shows around 72 minutes fire resistance due to the failure of further analysis. The degree

of horizontal axial restraint can be checked by the horizontal displacements, as shown in Figure 5.8. The horizontal displacement for the fully fixed case is zero throughout the analysis. For the other cases, even though the horizontal displacement is not large, different length end beams show different horizontal displacement. The differences of horizontal displacement associated with the variation of end beam length could alter the failure modes of a single prestressed hollowcore slab. Figure 5.9 shows the axial force history, for the unfilled and filled concrete parts. For the fully fixed and short end beams, large compressive forces developed in an unfilled and filled concrete core. For a single hollowcore slab restrained by medium beams, the only bottom spring developed compressive forces in an unfilled and filled concrete core. In terms of a single hollowcore slab restrained by long beams, the bottom spring force measured over the first 76 minutes grows up, but the compressive forces decrease due to the further increase of reinforcement at the endspans.

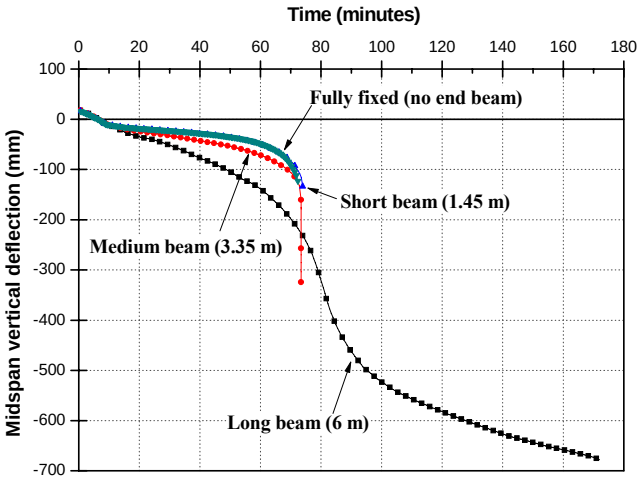

Figure 5.7 Comparison of midspan vertical deflection with respect to variable end beam length

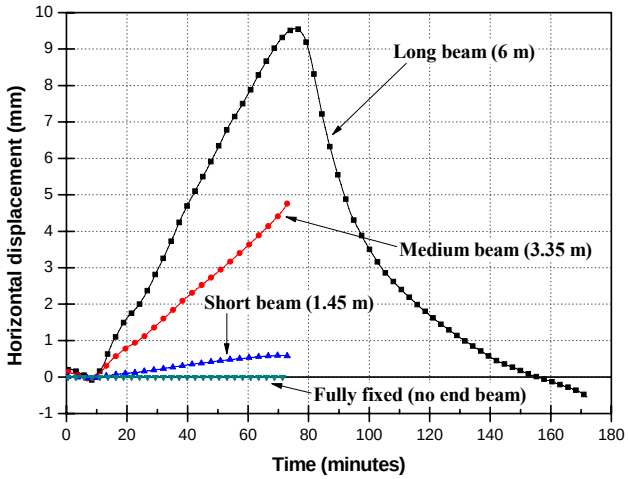

Figure 5.8 Comparison of horizontal displacement at the middle of the end beam with respect to variable end beam length

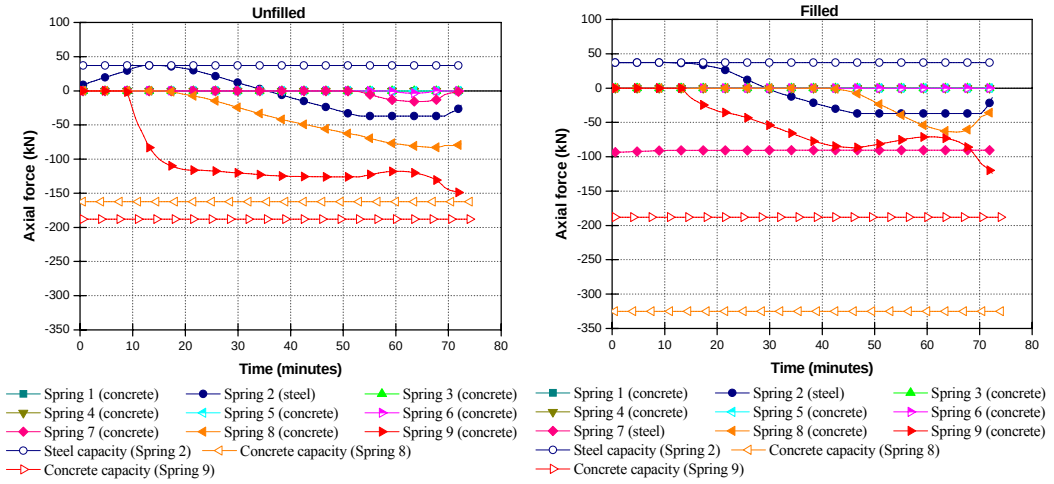

(a) fully fixed

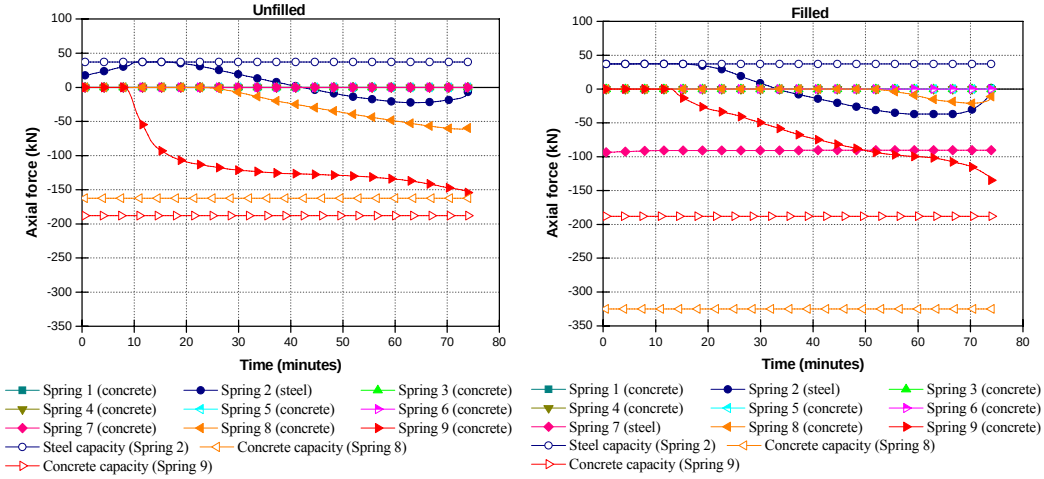

(b) short beam

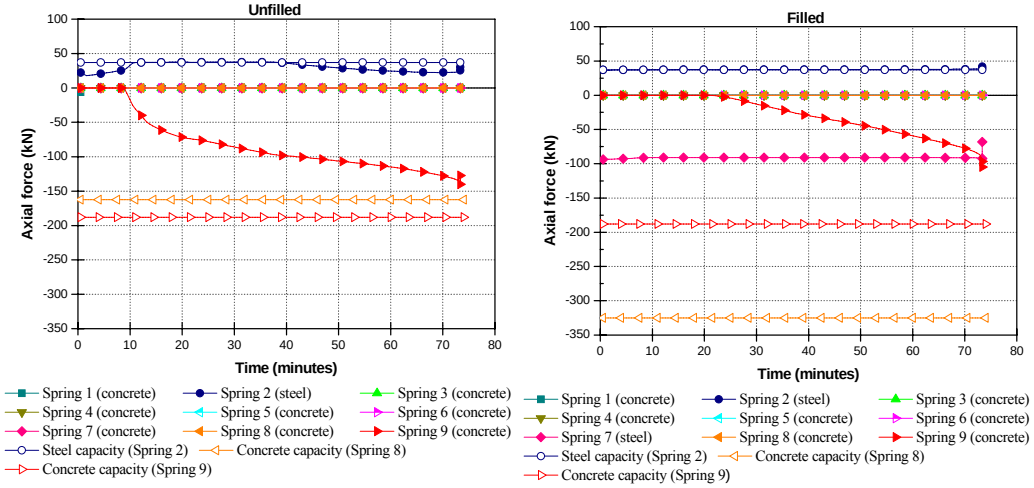

(c) medium beam

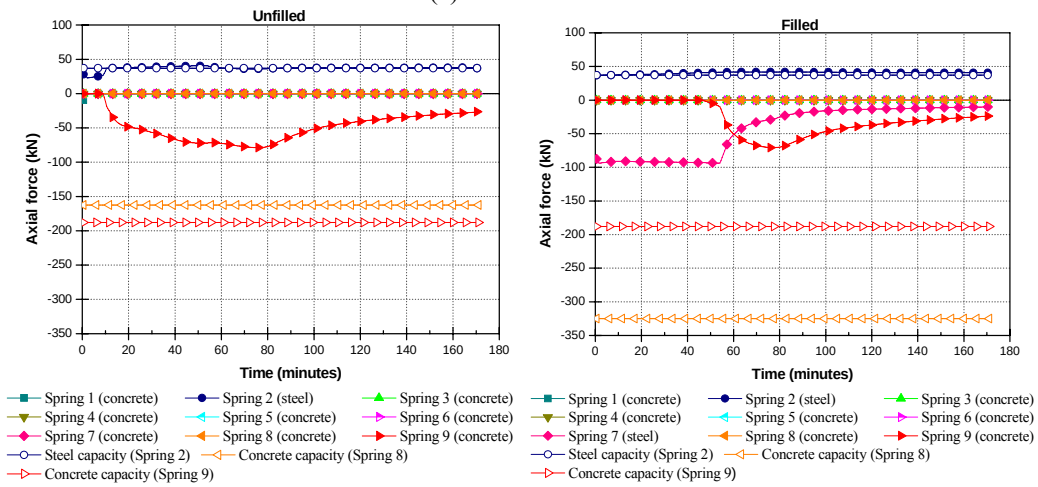

(d) long beam

Figure 5.9 Axial force history with respect to variable end beam length

An extension of the floor size up to five prestressed hollowcore units has been carried out to look into the effect of axial restraints in multi-unit floors. Each prestressed hollowcore slab unit was connected to the adjacent unit by small beam elements which represent the reinforced concrete topping slab. The basic concept in terms of an extension of prestressed hollowcore units is identical to a single hollowcore unit. Firstly, without consideration of the thermal expansion, five prestressed hollowcore units were modelled along with fully fixed end supports. Secondly, 6m long end beams were used to provide end restraint. Even though the end beams had a 6m long length, five units with 6m is similar to one unit with a short beam. Figure 5.10 shows an isometric view of the floor assembly with five prestressed hollowcore units.

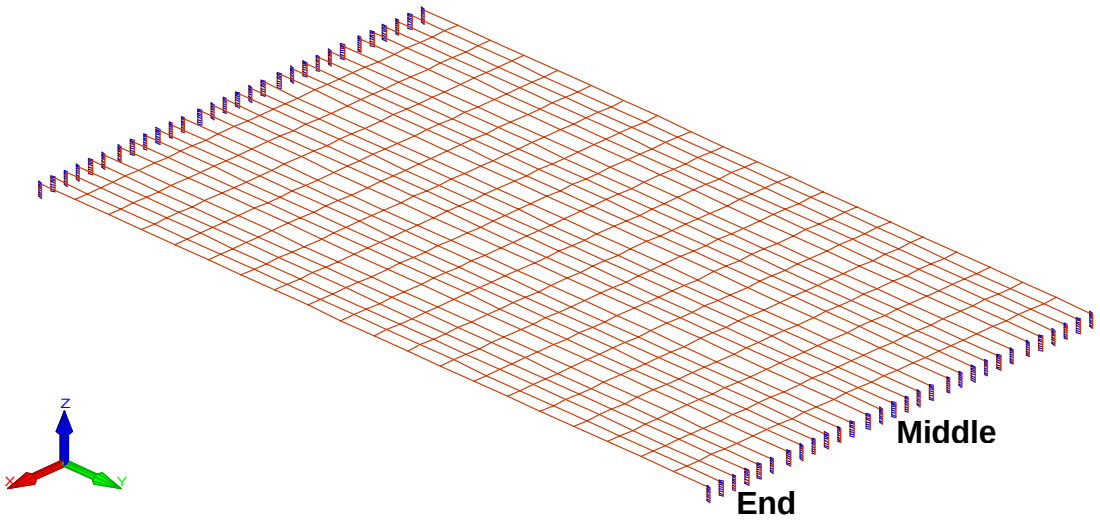

(a) Fully fixed

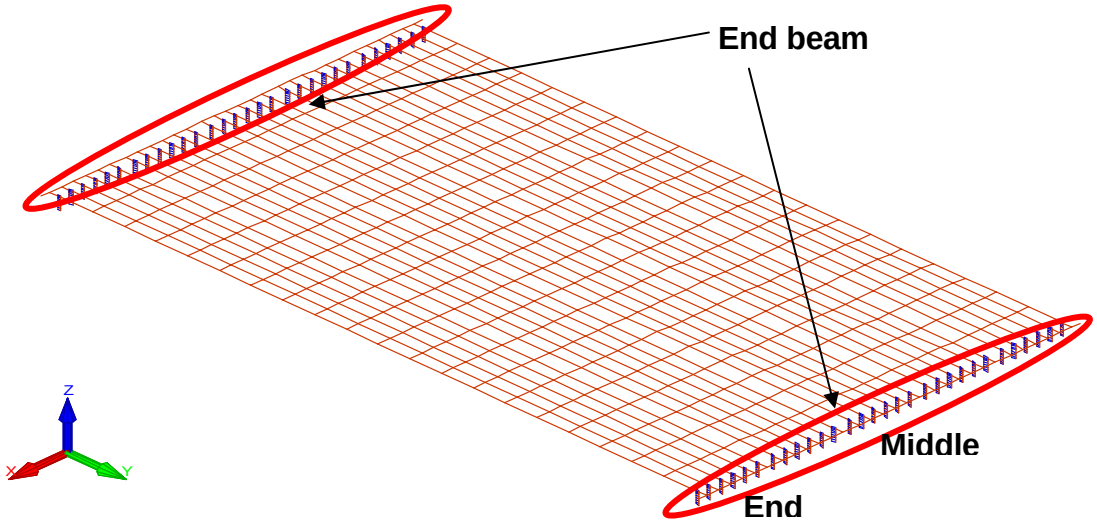

(b) Short end beam

Figure 5.10 Isometric view of five prestressed hollowcore units

The midspan vertical deflection of five prestressed hollowcore units which include different end conditions is plotted in Figure 5.11. For the fully fixed case, the failure happened slightly earlier than that with a 6m end beam due to the restraint to thermal expansion with respect to the longitudinal direction. In order to examine the difference of axial force history between the middle and end positions as illustrated in Figure 5.10, axial force histories are compared for fully fixed and 6m long end beams, as shown in Figures 5.12 and 5.13. The axial force history for fully fixed hollowcore units shows high compressions in the middle and end positions. On the other hand, the axial force history of five hollowcore units

including a 6m long end beam demonstrated a different history pattern for middle positions, as shown in Figure 5.13 (a). Only bottom spring elements develop over the time. For both cases, there is no evidence of failures in spring elements, but the analyses stopped due to the negative stiffness of the slab.

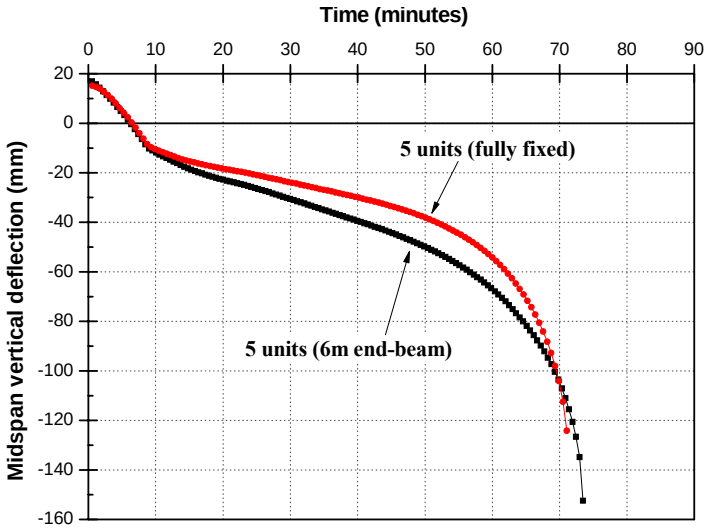

Figure 5.11 Comparison of midspan vertical deflection with respect to variable end beam length in 5 units

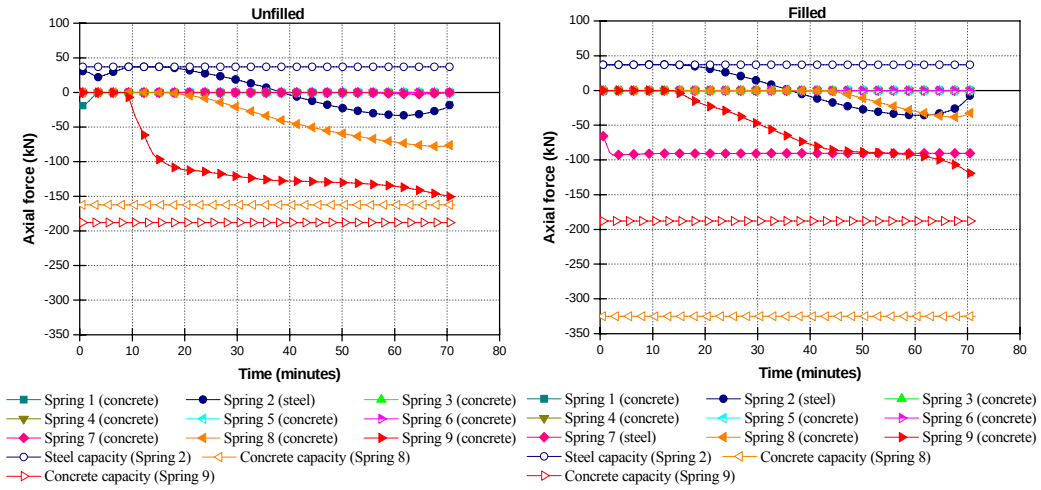

(a) middle

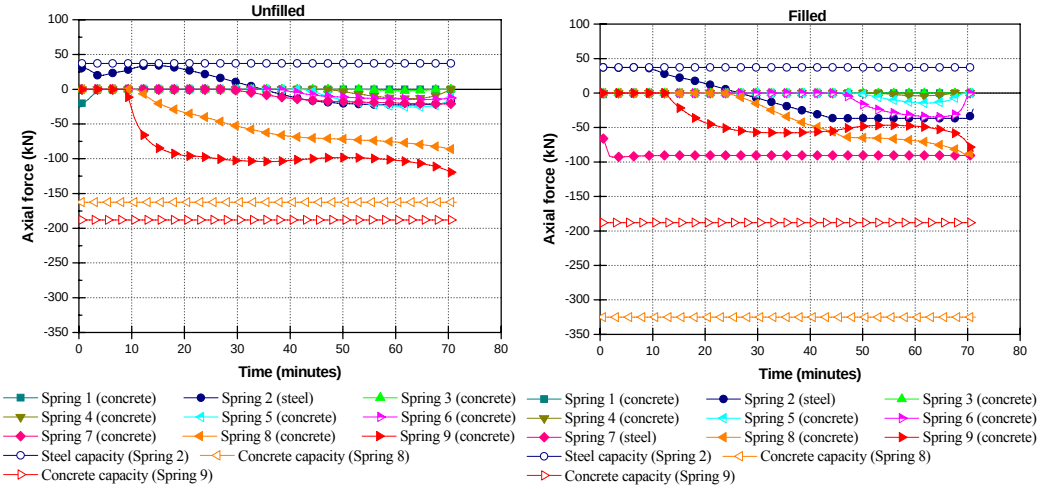

(b) end

Figure 5.12 Axial force history for 5 units (Fully fixed)

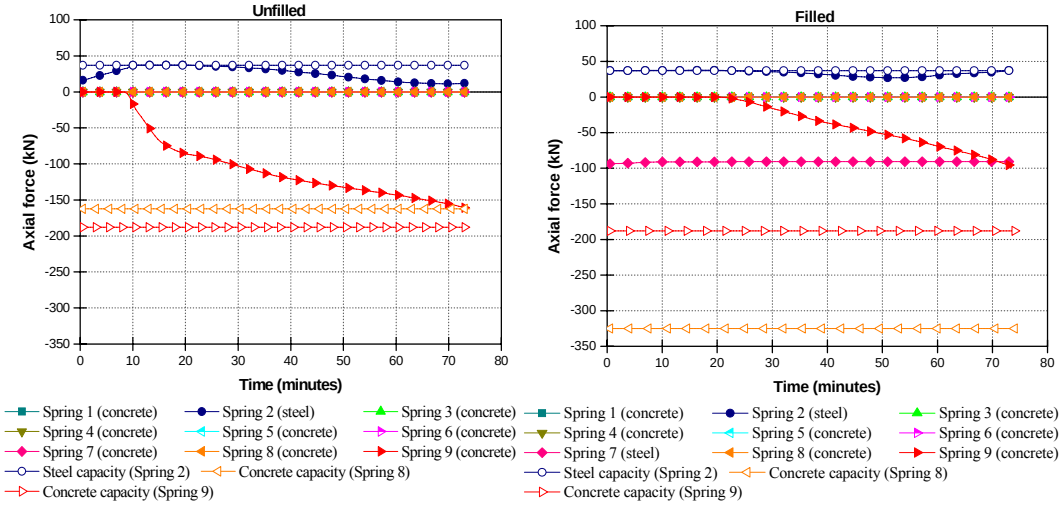

(a) middle

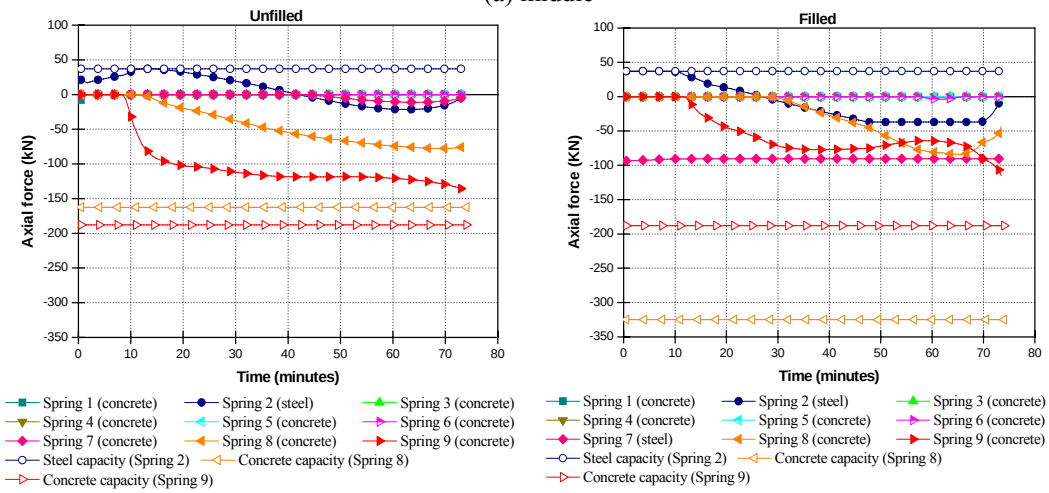

(b) end

Figure 5.13 Axial force histories for 5 units (6m long end beam)

5.3 Hollowcore concrete floor with column supports

5.3.1 Multi-unit prestressed hollowcore floor with no side beam

The structural behaviour of multi-unit prestressed hollowcore slabs with no side beams under a Standard ISO fire were studied with respect to variation of units, i.e. 1 unit, 3 units, 4 units and 5 units. Figure 5.14 only illustrates the plan view of a one bay hollowcore flooring system including five hollowcore planks. In this model, 750 by 750 mm columns were used to take into account the longitudinal and transverse movements. It was assumed that the columns and end beams were not exposed to fire and the top and bottom ends of the columns were fully fixed against horizontal and vertical displacements and rotations. Only the prestressed hollowcore slabs were subjected to fire. The Standard ISO fire was used.

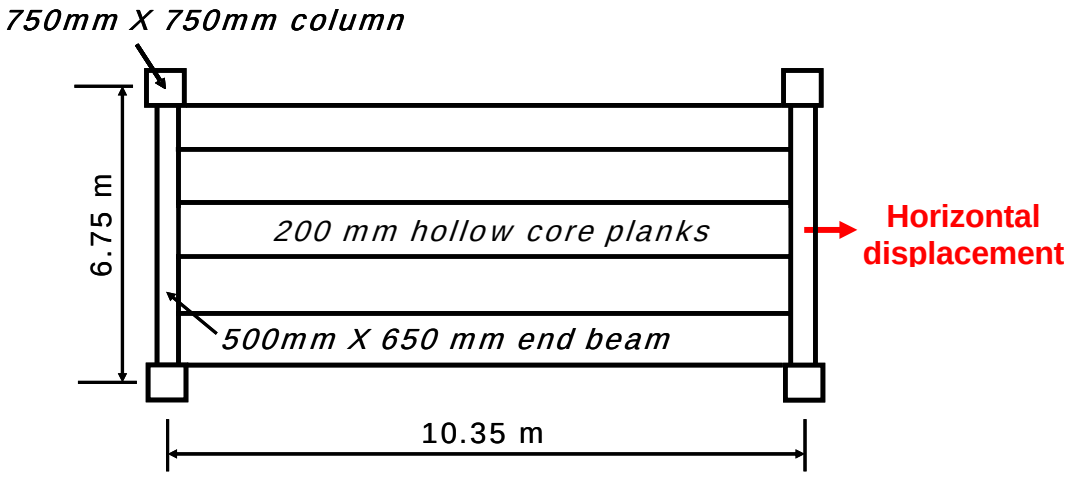

Figure 5.14 Plan view of one bay hollowcore flooring system with no side beam

The comparative results with respect to the variation of the number of prestressed hollowcore units were plotted in Figure 5.15. It can be seen that the fire resistances in terms of the variation in the number of units were nearly the same such that the increase of prestressed hollowcore units without transverse restraint could not significantly affect the behaviour of prestressed hollowcore slabs.

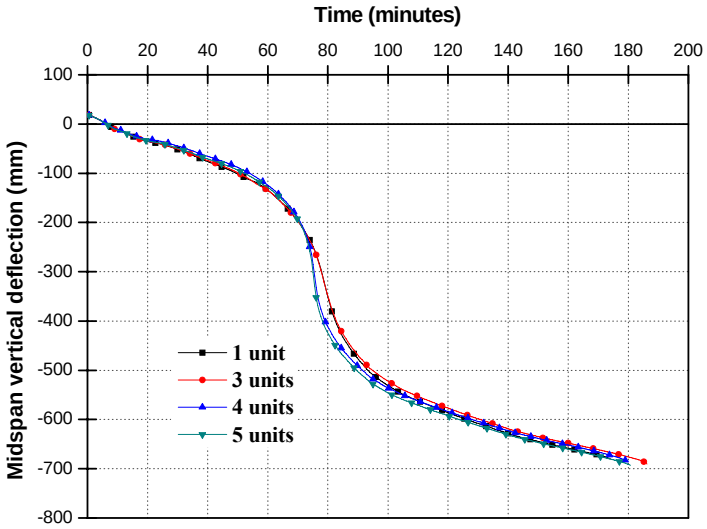

Figure 5.15 Comparison of midspan vertical deflection with respect to variation of the number of units

In order to assess the degree of restraint induced by the columns, the horizontal displacements along longitudinal directions were looked into for total displacements and beam displacements, as shown in Figure 5.16. In the measurements of horizontal displacements, total displacements include beam displacements and column displacements along longitudinal directions. For most of the analyses, total displacements of the prestressed hollowcore flooring system with no side beam show almost the same results. On the other hand, beam displacements at the middle of the end beam which do not include column horizontal displacements indicate the differences in the horizontal displacements as the increased number of prestressed hollowcore units are stiffer and the horizontal movements of five prestressed hollowcore slabs become smaller, as shown in Figure 5.16(b).

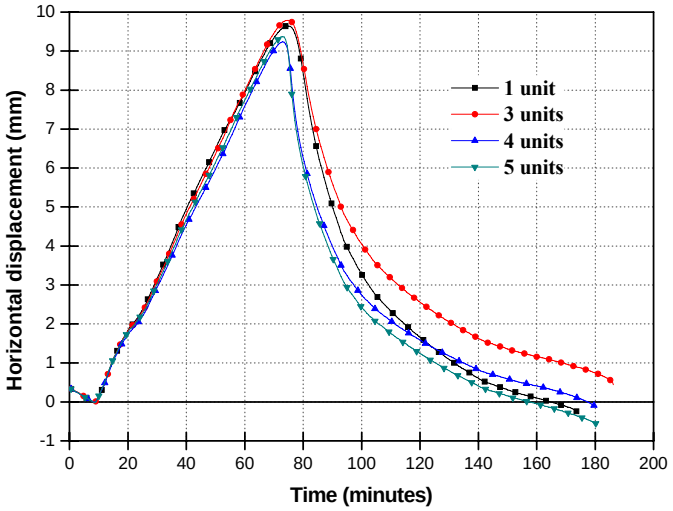

(a) Total displacements

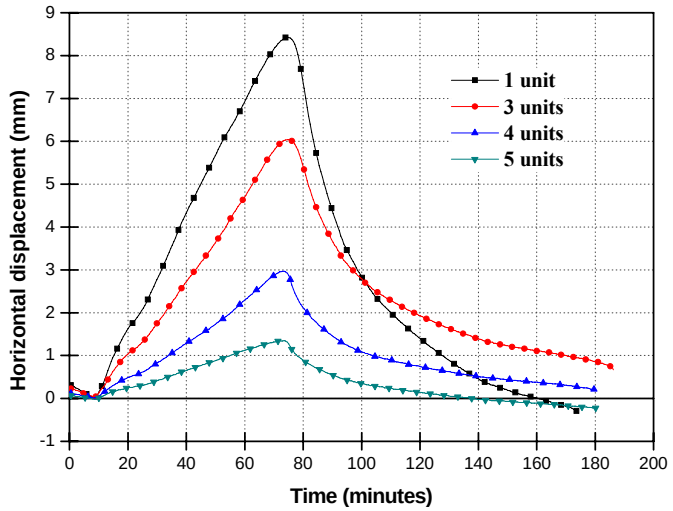

(b) Beam displacements

Figure 5.16 Comparison of horizontal displacement with respect to variation of the number of units

The failure modes of the multi-unit prestressed hollowcore slabs are examined as shown in Figure 5.17. It is observed that the consideration of columns for modelling prestressed hollowcore flooring systems may change the failure modes as the modelling of columns can provide more flexibility for framed structures compared to fixed end conditions. In all cases, the reinforcing steel failure in the topping concrete slab was indentified. After the reinforcing steel fails, concrete crushing occurred at the bottom of hollowcore slabs for 4 and 5 unit cases. As a result of the steel yielding and the concrete crushing, the analysis stopped.

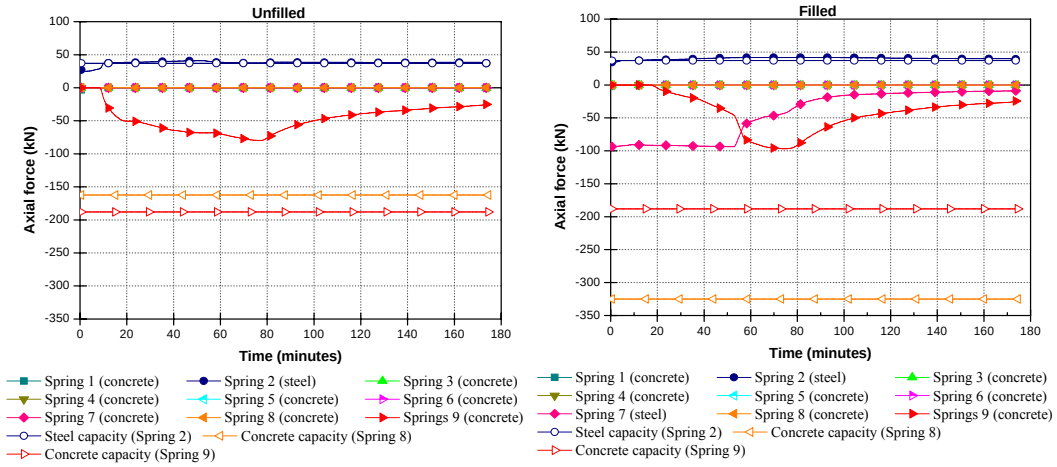

(a) 1 unit

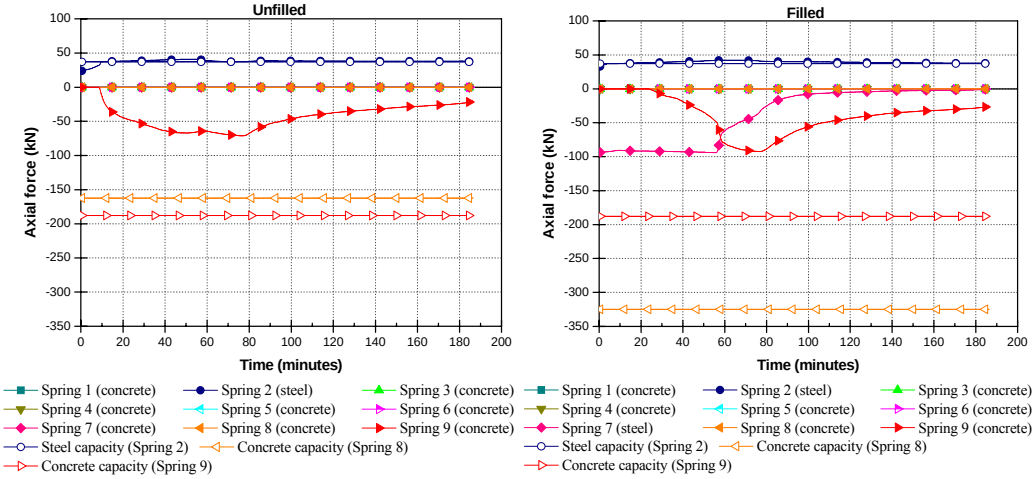

(b) 3 units

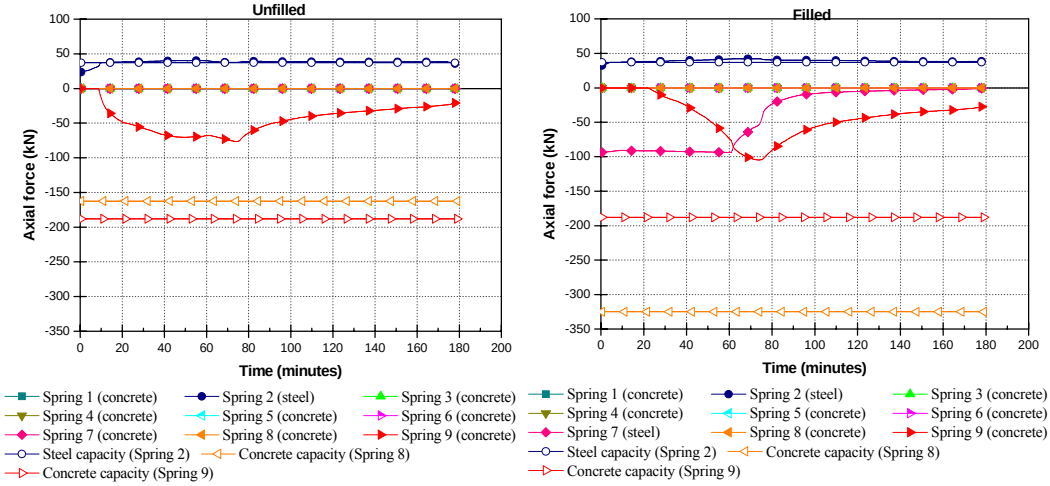

(c) 4 units

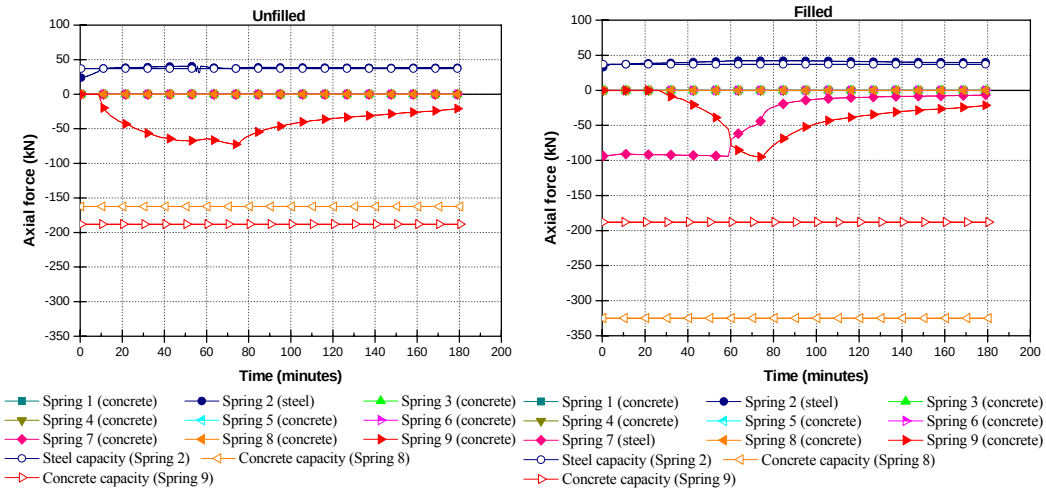

(d) 5 units

Figure 5.17 Axial force histories with respect to variation of the number of units

The vertical support conditions with respect to each edge were taken into account in order to provide a simple assessment of the effect of vertical restraints. While the vertical movements in terms of each edge are restrained, horizontal movements which consider the thermal expansions are free. The result for a vertically fixed edge was compared to the case of no vertical support in Figure 5.19. It can be seen that the vertical supports at the sides significantly reduce the vertical deflections at the middle point of the prestressed hollowcore floor.

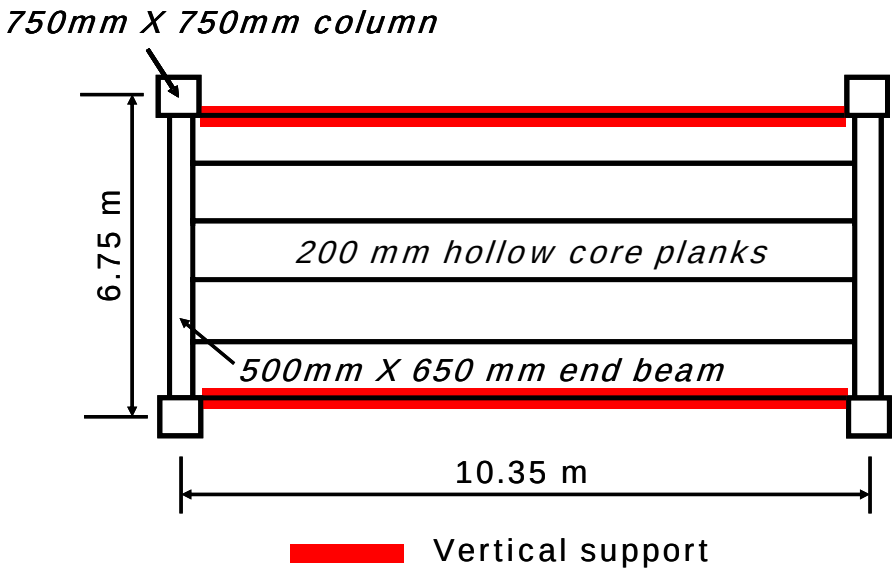

Figure 5.18 Plan view of one bay hollowcore flooring system including vertical supports

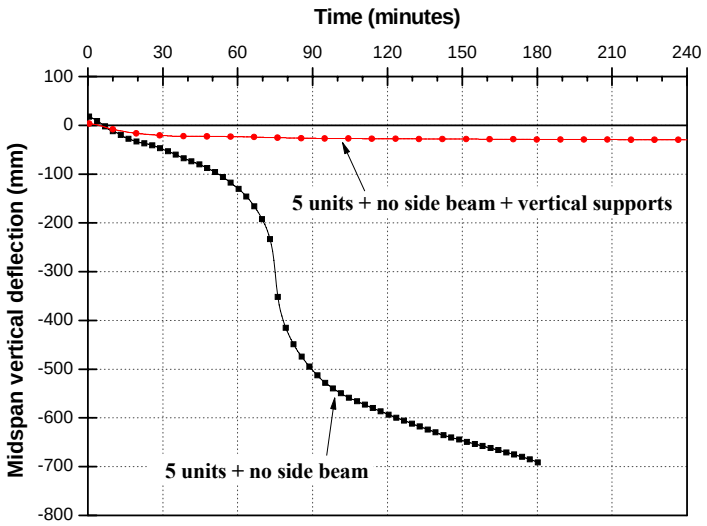

Figure 5.19 Comparison of midspan vertical deflection with respect to fixed edges

5.3.2 Multi-units prestressed hollowcore slab with side beams

There are two possible lateral connection details which were investigated by Matthews and Lindsay to model hollowcore floor systems including side beams, as shown in Figure 5.20. While the Matthews' lateral connection detail was widely used, Lindsay's lateral connection detail was developed in order to improve the seismic performance of the hollowcore floor system (Lindsay, 2004). The use of timber infill with in situ concrete topping provides a more flexible interface between the side beam and the first hollowcore unit such that unexpected displacement incompatibility may be avoided.

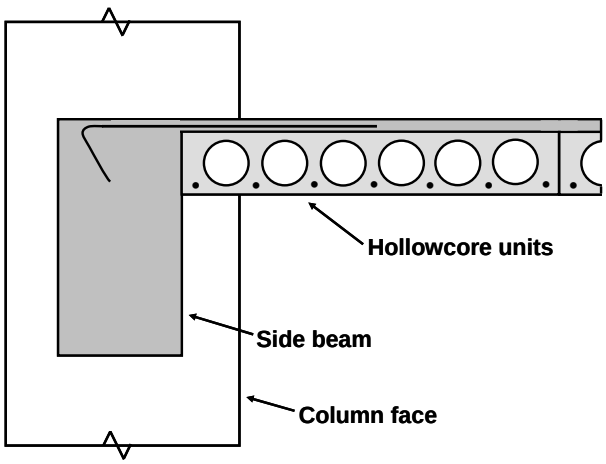

(a) Matthews (2004)

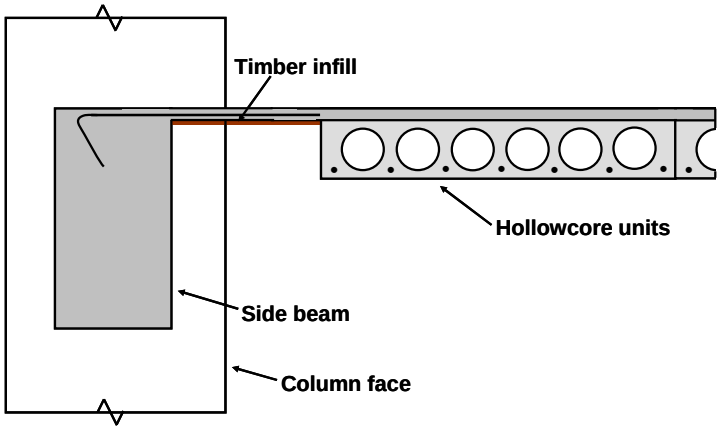

(b) Lindsay (2004)

Figure 5.20 Lateral connections to side beam

First of all, a five unit hollowcore floor adjacent to the side beams as shown in Figure 5. 21(a) was considered to assess the fire performance of a one bay hollowcore flooring system under a Standard ISO fire. The columns of the one bay hollowcore flooring system were 750 mm x 750 mm square. The side beams are 400 mm wide and 750 mm deep. It was assumed that the columns, end beams and side beams were not exposed to fire during the analyses.

For the numerical modelling of a one bay hollowcore flooring system, there are two issues to take into account as illustrated in Figures 5.21(b) and (c). The first issue is the discontinuity region and the second issue is the consideration of column width. When five hollowcore slabs are used for numerical analysis, the interaction between the hollowcore unit and side beam due to the thermal expansion can be one of the crucial factors to investigate in the fire performance. However, the width of the side beam is smaller than that of the column such that the undefined region, as shown in Figure 5.21(b), is not taken into account during an analysis. In order to consider the undefined region without changing the total frame stiffness, the cross section of the side beam has been modified based on the same torsional stiffness ($\frac{6EI}{L^2}$) as illustrated in Figure 5.22.

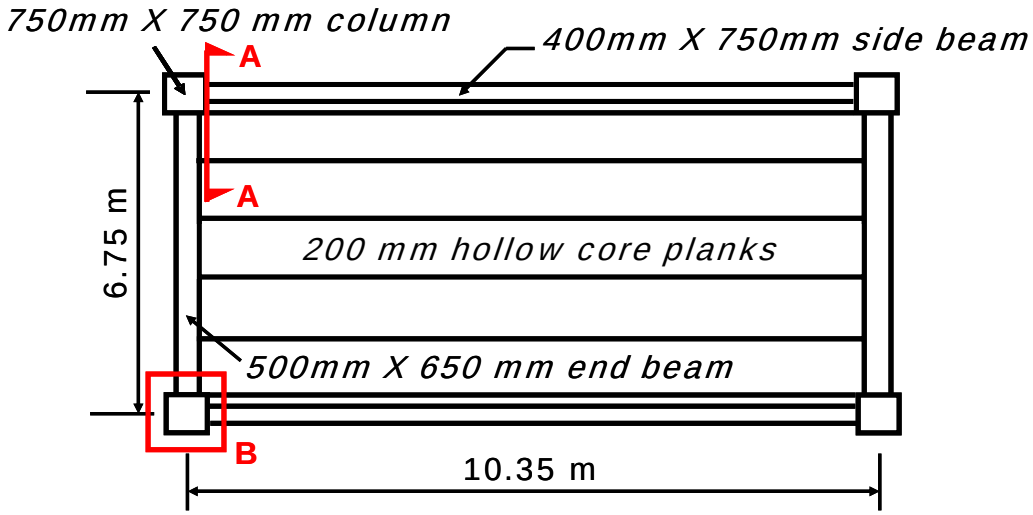

(a) Plan view of floor

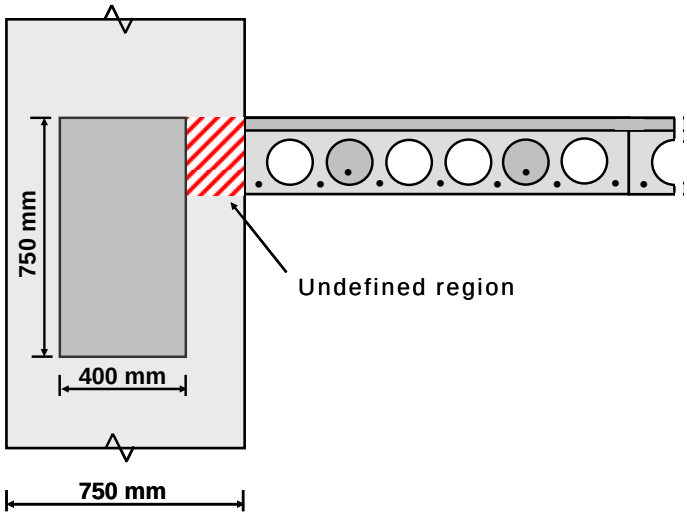

A-A

(b) Cross section

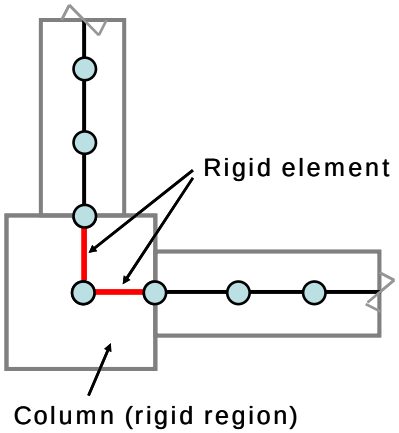

(c) Rigid elements

Figure 5.21 One bay hollowcore flooring system with side beams

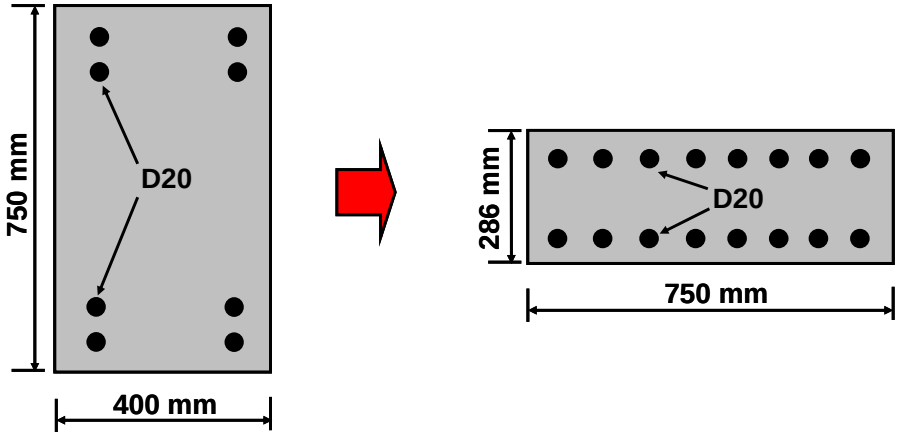

Figure 5.22 Modification of the side beam configuration

With respect to the frame structure modelling using beam elements, beams and columns are represented by line elements. Therefore, the effect in the beam-column intersection of the frame which behaves like a stiff diaphragm should be accurately considered through the modelling. As a result, rigid elements which cannot move independently from each other were exploited for each corner throughout this analysis.

The one bay hollowcore flooring system with infill, as shown in Figure 5.23, was considered to compare to the fire performance of hollowcore floors having no infill. In the thermal analysis of the infill which consists of the concrete slab and timber infill, the assumption has been made that the concrete slab was protected by the timber infill and is not affected by a Standard ISO fire. Figure 5.24 shows the comparison result between no infill and infill cases. The result shows that a large increase in deflection occurs as a result of the use of infill. Nevertheless, one bay prestressed hollowcore flooring systems with no infill and with infill did not fail during the analyses. The use of infill in hollowcore flooring system contributes to better performance against seismic effects. On the other hand, the frame incorporating infill is likely to collapse during a long duration fire due to the excessive deflection of the infill. For both cases, the transverse movements at the mid point of side beams are compared in Figure 5.25. The results show that the difference of transverse movements between infiil and no infill cases are not large.

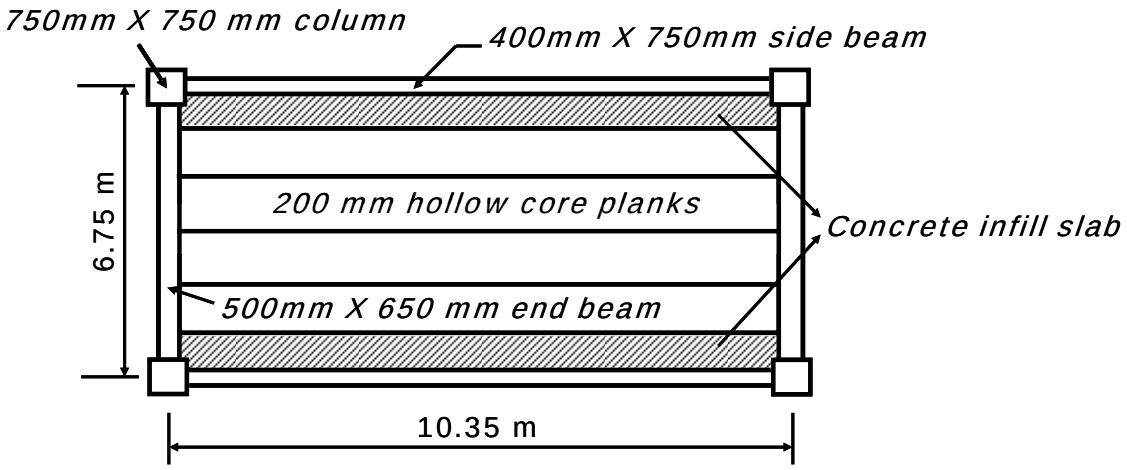

Figure 5.23 Plan view of one bay hollowcore flooring system with infill

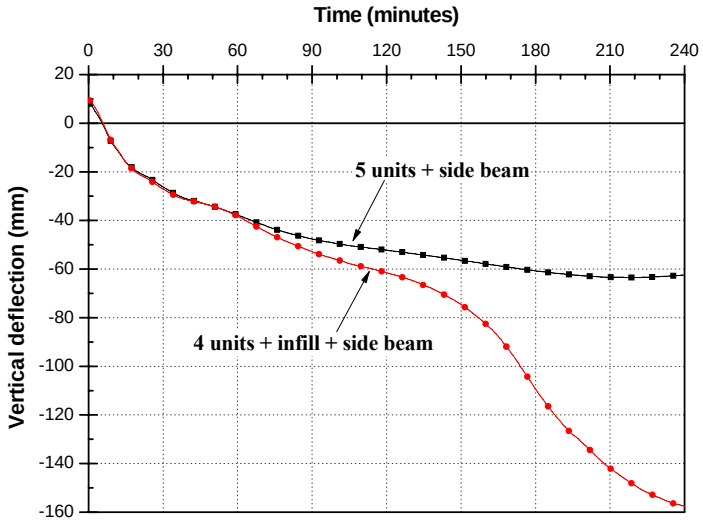

Figure 5.24 Comparison of midspan vertical deflection of one bay hollowcore flooring system

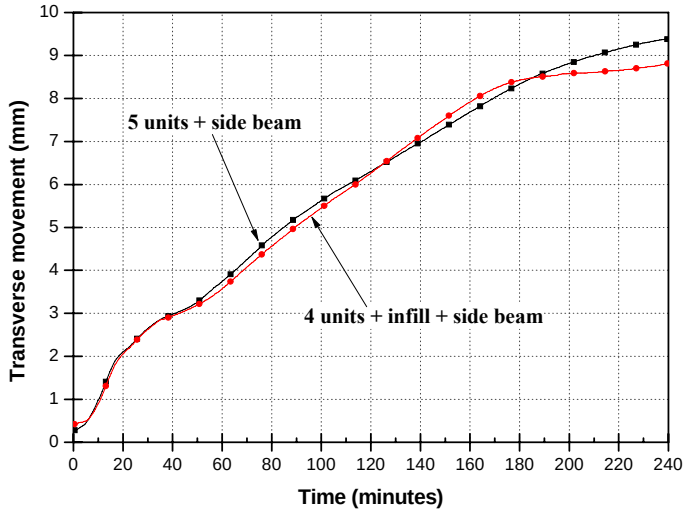

Figure 5.25 Comparison of transverse movements of one bay hollowcore flooring system

5.4 Summary

Based upon the MacPherson's multi-spring connection model developed in Chapter 4, the fire performance of prestressed hollowcore floors restrained by surrounding structures under a Standard ISO 834 fire was investigated.

The effect of concrete filling was assessed and applied to the numerical model. In addition, the effect of end beam length with respect to a single prestressed hollowcore slab as well as a five unit prestressed hollowcore floor was evaluated. The results show that the fire resistance of prestressed hollowcore slabs is highly affected by the restraint from end beams as the variable length of end beam may provide flexibility against thermal expansion.

An extension of a prestressed hollowcore slab model has been made with up to 5 units with columns. The fire performance with respect to various units was examined and compared. It was shown that the increase in the number of hollowcore slab units did not affect the fire resistance significantly. As shown in Figure 5.15, the midspan vertical deflections of the prestressed hollowcore slab in Standard ISO 834 indicated similar trends.

Two different side beam details for hollowcore floors were explained and examined. It was demonstrated that the previous lateral connection detail where a hollowcore unit is connected next to the side beam shows better fire performance than the latest lateral connection detail due to reduction of transverse curvature. Although the prestressed hollowcore floor with the latest lateral connection detail in the numerical analysis shows 4 hours fire resistance without the sign of failure, care should be taken for practical situations due to the excessive deflection after 150 minutes. Nevertheless, it was concluded that fire performance of prestressed hollowcore floors may be enhanced by considering more realistic restraint conditions.

Chapter 6

Fire performance of Multi-Bay Hollowcore Floors

6.1 Introduction

In the previous chapter, numerical models and methods were developed for predicting the fire resistance of prestressed hollowcore floors restrained by surrounding structures. In this chapter, the one bay prestressed hollowcore floor model is extended to a multi-bay (4 bays by 1 bay) model. The fire performance of the multi-bay prestressed hollowcore floor, exposed to Standard ISO fire, is investigated. In addition, a series of analyses of multi-bay models exposed to parametric fire curves, i.e., ISO fires with decay after 30, 40, 50 and 60 minutes, is carried out. The contribution of starter bars to the overall performance of the multi-bay prestressed hollowcore floor is examined to identify the possibility of catenary action. An initial model is created based on drawings of a typical building and is then modified by adding fire emergency beams, which reduce the transverse curvature to improve fire resistance. Figure 6.1 shows the organisation of Chapter 6.

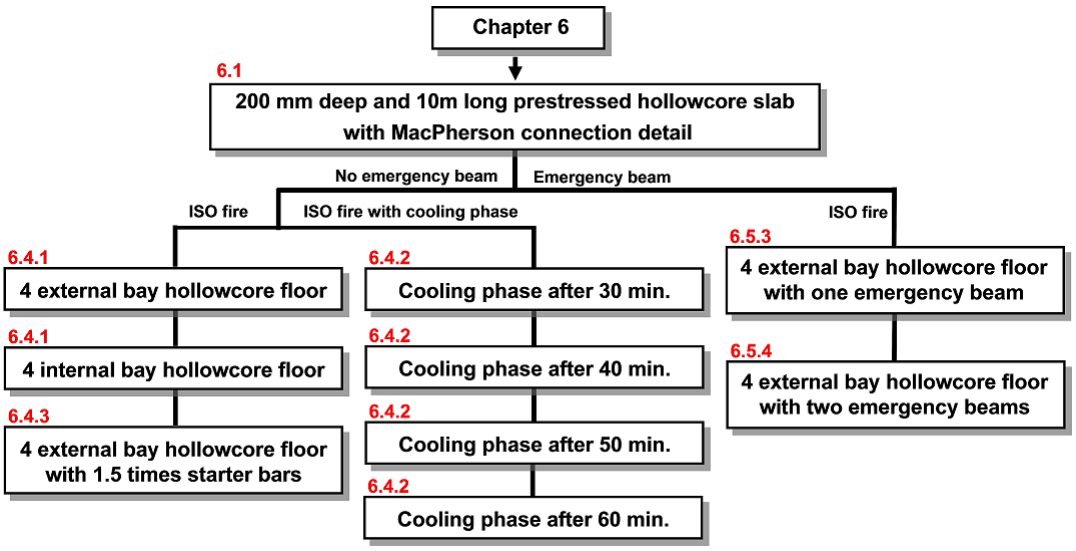

Figure 6.1 Organisation of Chapter 6

6.2 The reinforced concrete frame building

A four bay by five bay moment resisting reinforced concrete frame building (28.4m x 50m), including prestressed hollowcore floor slabs, was designed by a local design consultancy in New Zealand as part of the Future Building Systems research programme. The building is six stories high and designed to resist earthquake actions. The floor plan and frame elevations are given in Figures 6.2 to 6.4. In this study, a 28.4m x 10m precast prestressed hollowcore floor is considered (indicated by the dashed rectangular area in Figure 6.2). It consists of four bays.

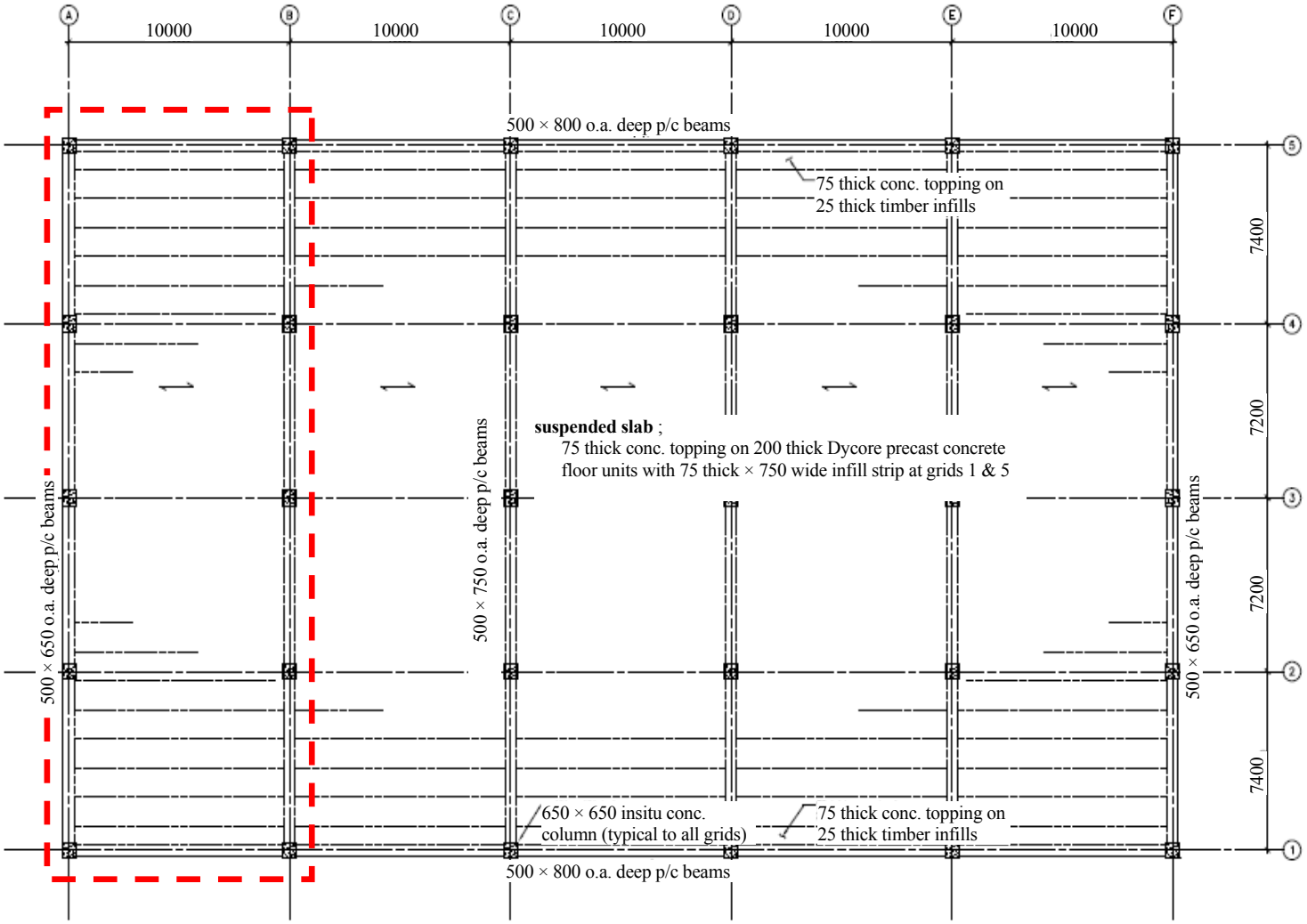

Figure 6.2 Typical floor plan of the reinforced concrete building

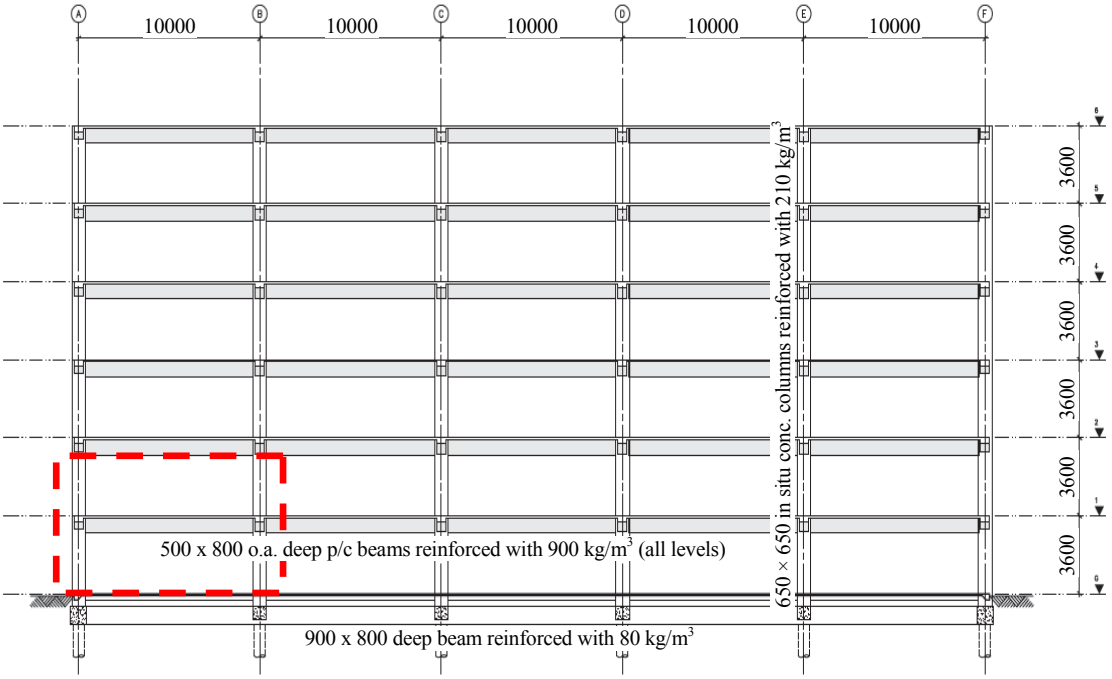

Figure 6.3 Elevation of frame, grid 1 and 5

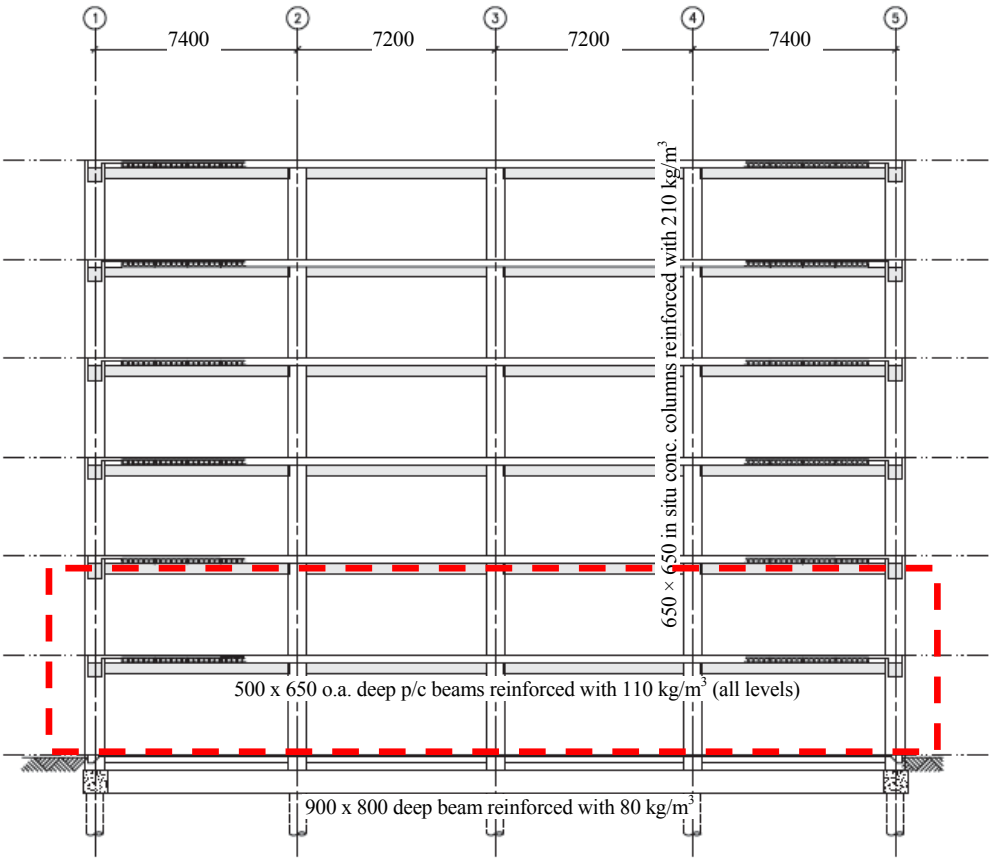

Figure 6.4 Elevation of frame, grid A to F

6.3 Model description

Figure 6.5 shows the general arrangement of the hollowcore flooring system with supporting columns. A 200mm prestressed hollowcore slab with 75mm of reinforced concrete topping was used. Each column has a cross section of 650mm x 650mm and is not exposed to fire in the analyses that follow. In addition, each of the 7.2m high columns extends over 2 storeys and is fully fixed at both ends.

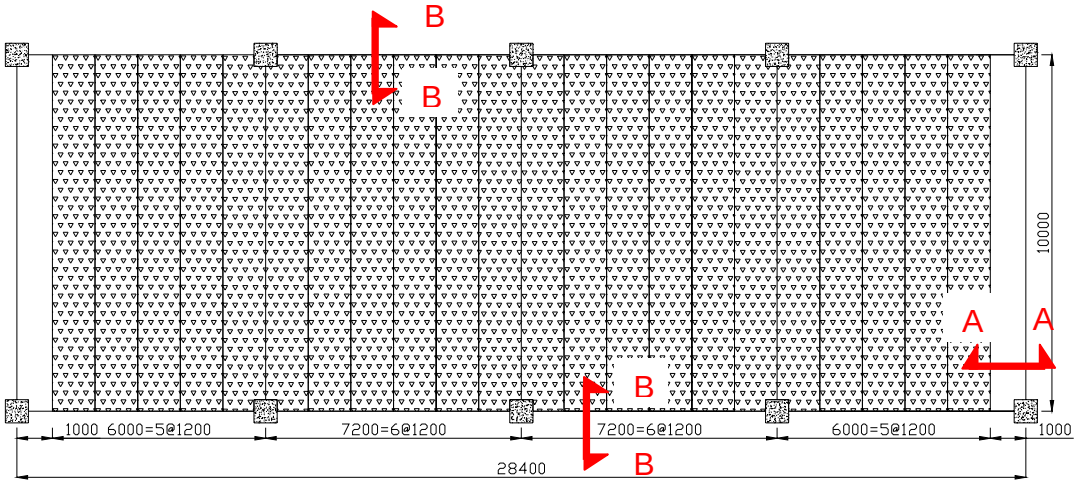

Figure 6.5 The original arrangement of hollowcore flooring system including no intermediate beams (22 hollowcore units)

The two inner bays of the slab consist of six hollowcore slabs between the column lines (see Figure 6.5). The two outer bays are made up of 5 hollowcore slabs and 75mm deep in-situ infill connections, 750mm wide (see Figures 6.5 and 6.6). In the analyses, it is first assumed that the 75mm topping concrete is not exposed to fire due to the insulation effect of the 25mm thick timber infill used as formwork. And then, the effect of ISO fire exposure on 75mm topping concrete is also investigated.

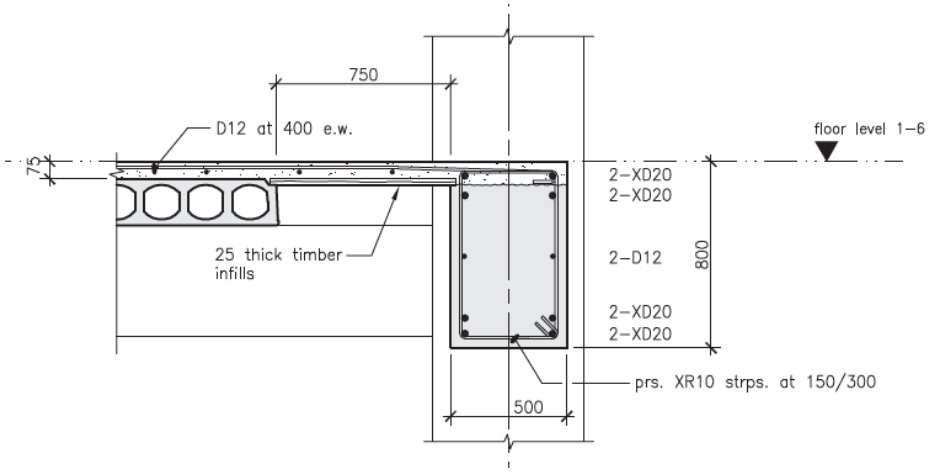

Figure 6.6 Infill side connection (A-A)

For modelling the connection to both end beams (Figure 6.7(a)), the MacPherson's multi-spring connection model developed in Section 4.3.2 is used. Depending on the location of the hollowcore slabs, their cores are filled with concrete and round bars are placed in the 2nd and 5th cores. It is assumed that the side and end beams are exposed to fire only on the bottom and inner surfaces.

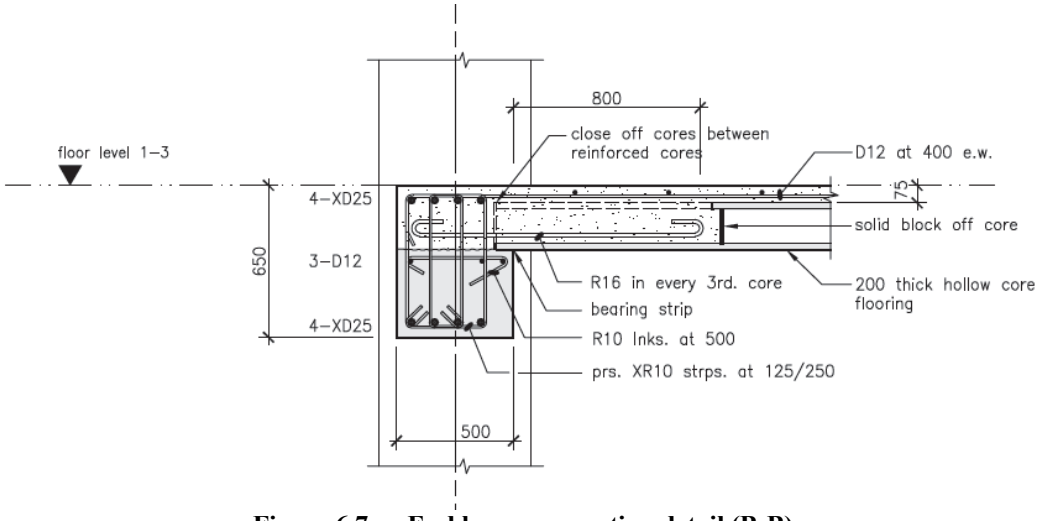

Figure 6.7 End beam connection detail (B-B)

6.4 Fire performance of multi-bay prestressed hollowcore floor

6.4.1 Fire performance of multi-bay prestressed hollowcore floor exposed to ISO fire

The multi-bay prestressed concrete hollowcore floor studied in this section consists of 4 x 1 bays. The floor is 28.4m wide and 10m long. Figure 6.8 shows the layout of the floor investigated.

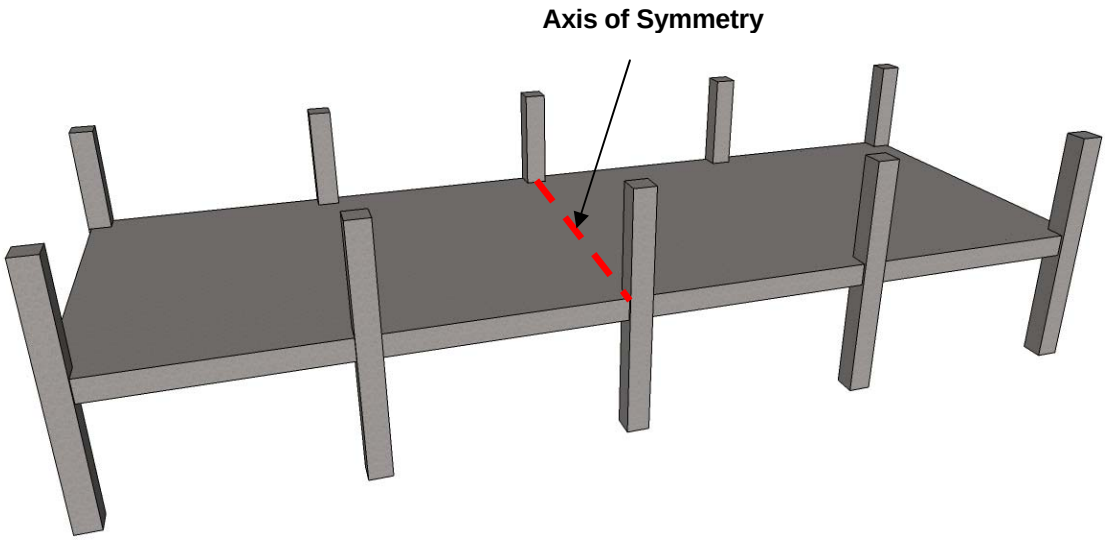

Figure 6.8 The model used for hollowcore flooring system

Figure 6.9 shows the top view of half and the reference diagram of the 4 x 1 bay hollowcore floor model used in this study. In order to save computing time, a symmetry scheme was used to enable only half of the floor to be numerically modelled. Consequently, the floor is 14.2m wide and 10m long, in the numerical model.

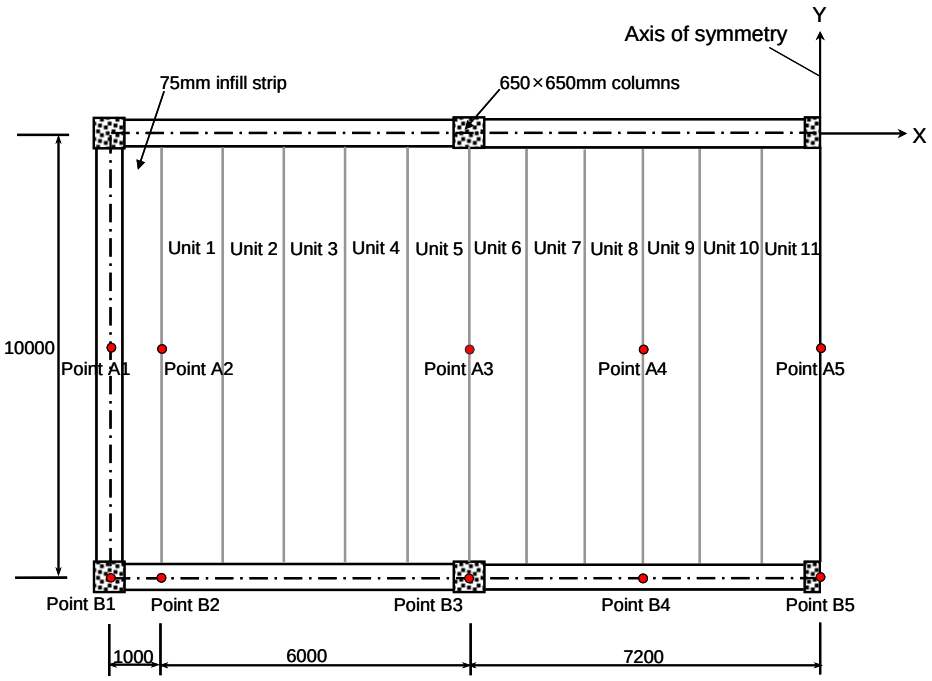

Figure 6.9 Reference diagram for the four-bay hollowcore flooring system showing the half of the slab

In order to investigate the vertical deflections of the multi-bay prestressed hollowcore floor, a number of reference points were monitored. These were the midspan of side beam (point A1), the mid-point between infill slab and unit 1 (point A2), quarter length of the multi-bay (point A3), the middle of the inner bay (point A4) and the centre of the multi-bay (point A5) (see Figure 6.9). The reference points illustrated in Figure 6.9 are used throughout this chapter, and the results are presented mainly as graphs of deflection against time.

Figure 6.10 shows the vertical deflections of the multi-bay prestressed hollowcore floor at points A1, A2, A3, A4 and A5. The deflection at point A1 was very small because of the large flexural stiffness of the side beams, which were also partially exposed to the fire while point A2 indicated a large deflection compared to point A1. For the first 8 minutes, the vertical deflection of points A2, A3, A4 and A5 indicated upward deflection due to the prestressing effects of the tendons. After this time, points A3, A4 and A5 showed a rapid increase of vertical deflections. The largest vertical deflection was at point A4, the middle of the inner bay. The vertical deflection of the hollowcore floor at point A4 is 133mm at 60 minutes. Normally, many standard fire tests have a limitation on deflection or rate of deflection for load

carrying capacity. Commonly specified failure criteria are a deflection of $L/20$ of the span, or a limiting rate of deflection ($L^2/9000d$; where L is the beam length and d is the beam depth) when the deflection exceeds $L/30$ of the span (Buchanan, 2001). In this simulation, the maximum deflection of 133mm is much less than the deflection criterion, $L/30$ (333mm). Nevertheless, the analysis terminated at 60 minutes, due to non-convergence of the non-linear solution.

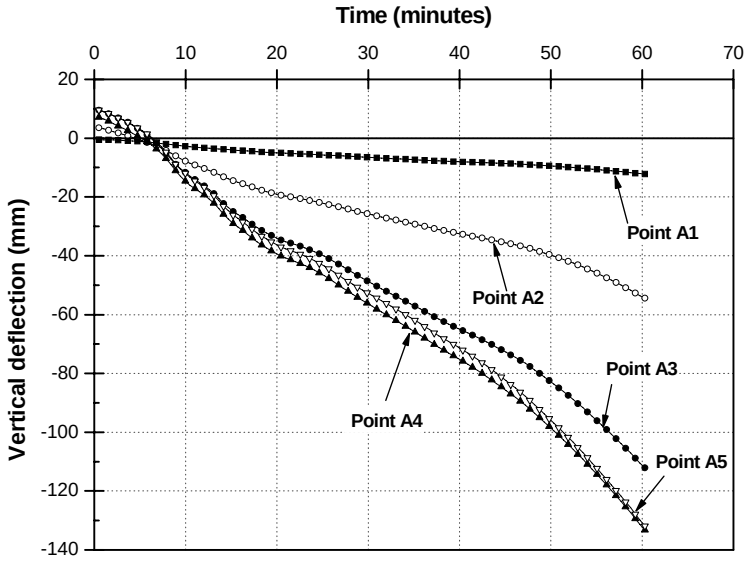

Figure 6.10 Vertical deflection of the multi-bay hollowcore floor at points A1, A2, A3, A4 and A5

Figure 6.11 and Figure 6.12 show x-direction and y-direction horizontal displacements measured at the reference points, A1, B1, B3 and B5 (for the x-direction) and B1, B3, B4 and B5 (for y-direction) (refer to Figure 6.9). Reference points B1, B3 and B5 were defined at column locations while reference point B2 was defined right next to the infill slab and B4 was defined at the mid-point between B3 and B5 as shown in Figure 6.9. The X-direction horizontal movement of point A1 was around 19mm, due to transverse thermal expansion of the hollowcore floors. In addition, X-directional movement of column location points B1, B3 and B5 at the end of the analysis indicated 12, 5 and 0 mm displacement respectively (see Figure 6.11).

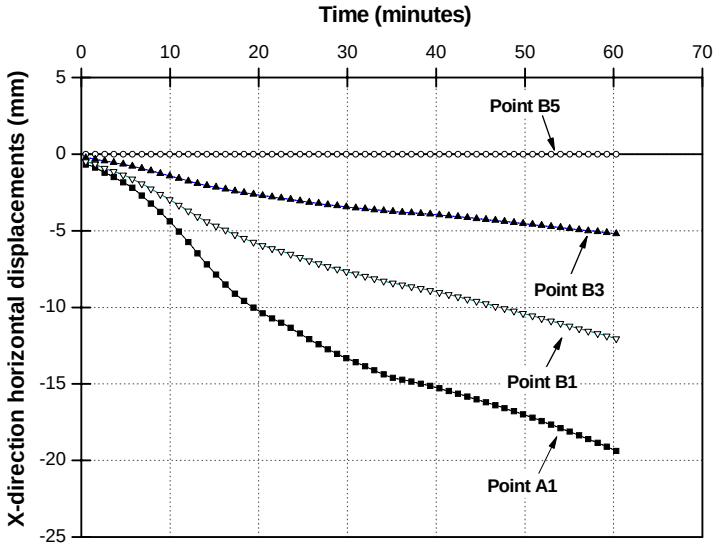

Figure 6.11 X-direction horizontal displacements of the multi-bay hollowcore floor at points A1, B1, B3 and B5

It can be seen from Figure 6.12 that the mid-point between B3 and B5 (point B4) moved slightly outwards from the centre of the hollowcore floor in the first 10 minutes of fire exposure (positive value of Y-direction horizontal displacements), then moved back towards the centre of the hollowcore floor. The corner column (point B1) moved towards the centre of hollowcore floor from the beginning of the fire exposure (negative value). The Y-direction horizontal movement of point B4 was around 8.8mm, due to longitudinal thermal expansion of the hollowcore floor.

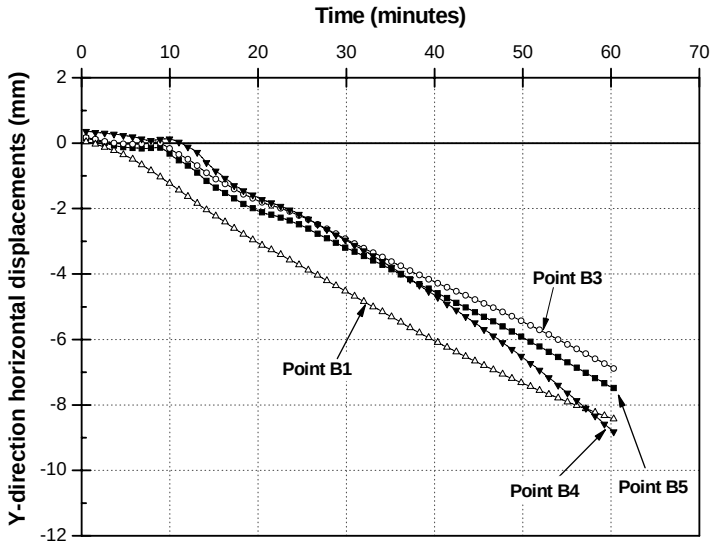

Figure 6.12 Y-direction horizontal displacements of the multi-bay hollowcore floor at points B1, B3, B4 and B5

Figure 6.13 shows an isometric view of the deflected shape at the end of the numerical analysis. The axial force histories of the multi-spring connection elements at hollowcore unit 1, unit 6 and unit 11 (see Figure 6.9) are examined in terms of concrete unfilled and filled parts. With the increase of temperature of hollowcore slabs, the bottom of the hollowcore slabs developed axial compression forces. This can be seen from the axial force histories shown in Figures 6.14 to 6.16. Nevertheless, each bottom concrete spring element does not reach its capacity, due to the rotation restraint of surrounding structures.

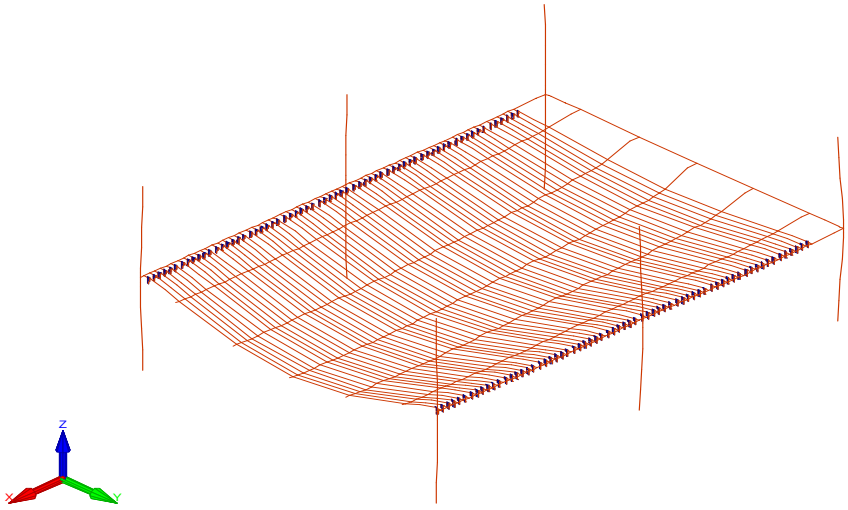

Figure 6.13 Deflected shape of the multi-bay prestressed hollowcore floor, scale factor = 10

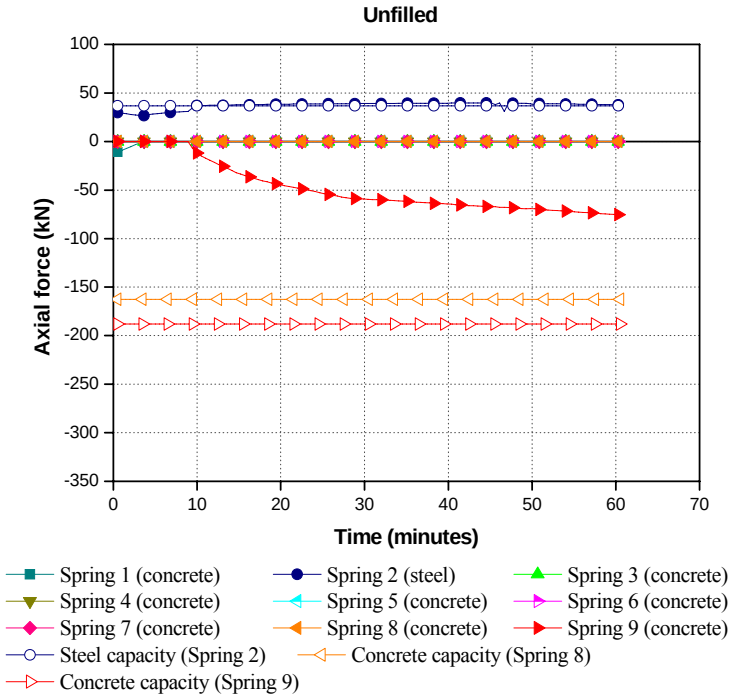

(a) Concrete unfilled multi-spring element

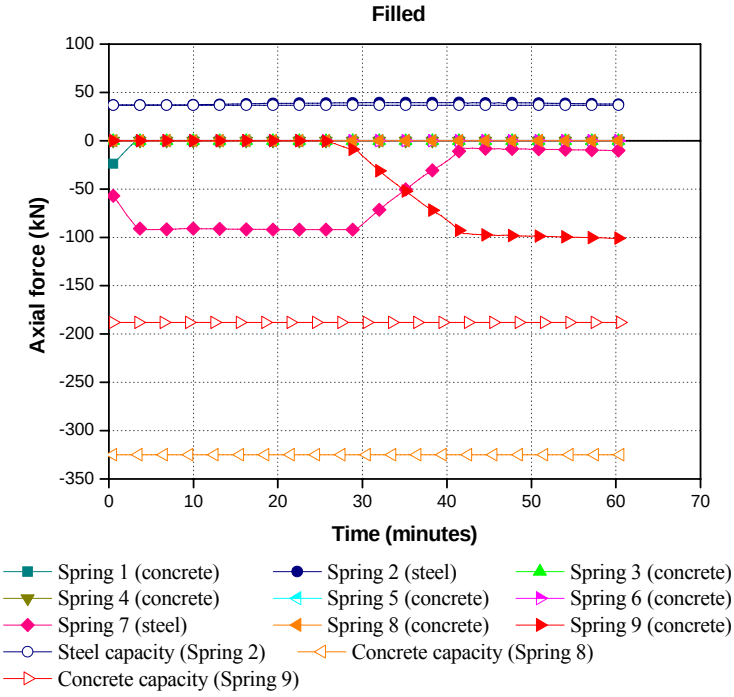

(b) Concrete filled multi-spring element

Figure 6.14 Axial force histories of multi-spring connection elements at unit 11

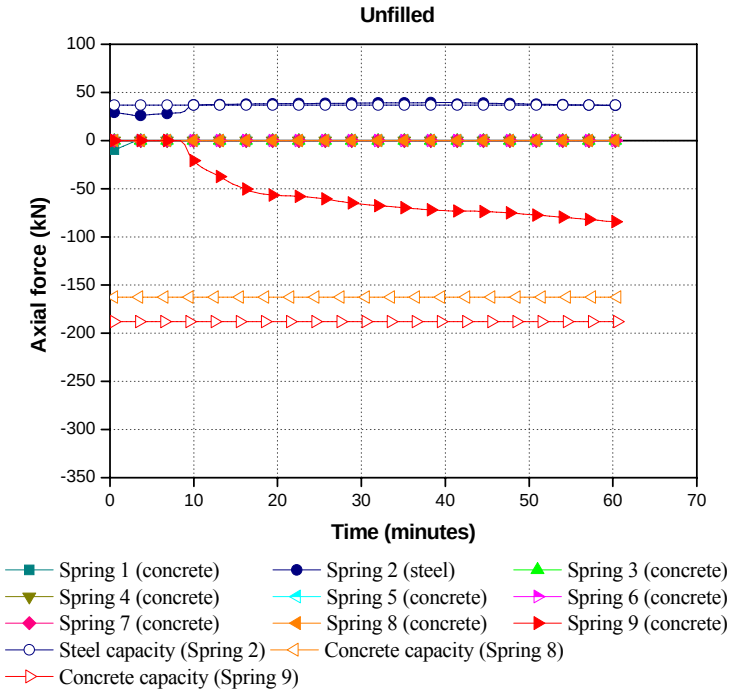

(a) Concrete unfilled multi-spring element

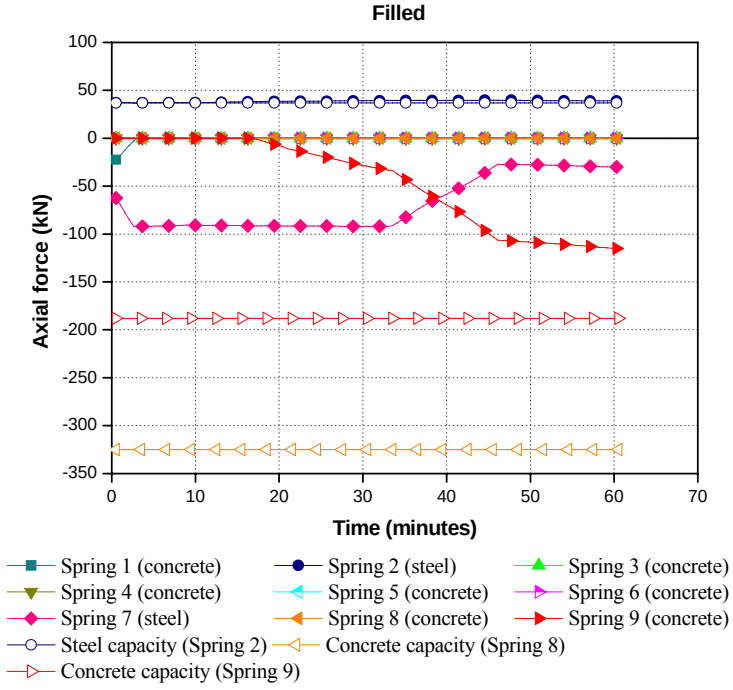

(b) Concrete filled multi-spring element

Figure 6.15 Axial force histories of multi-spring connection elements at unit 6

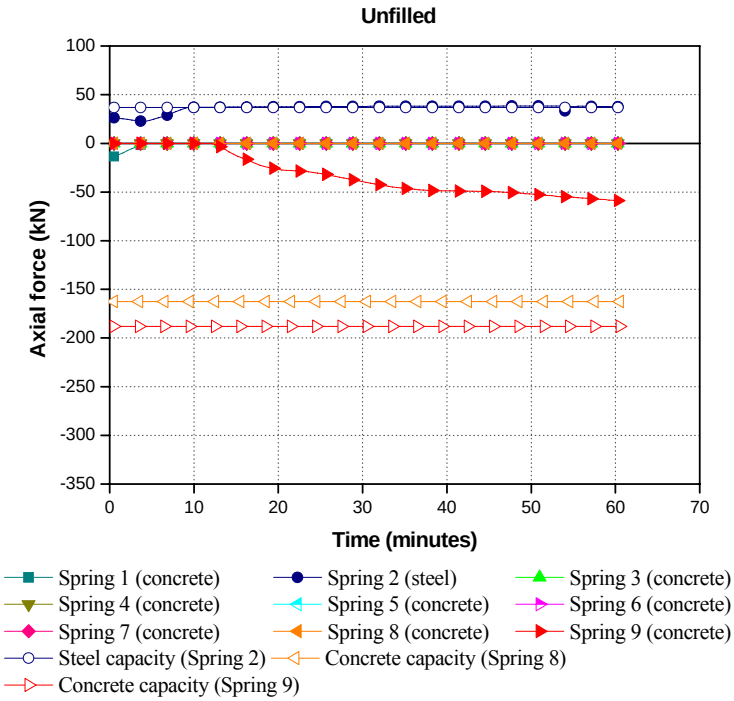

(a) Concrete unfilled multi-spring element

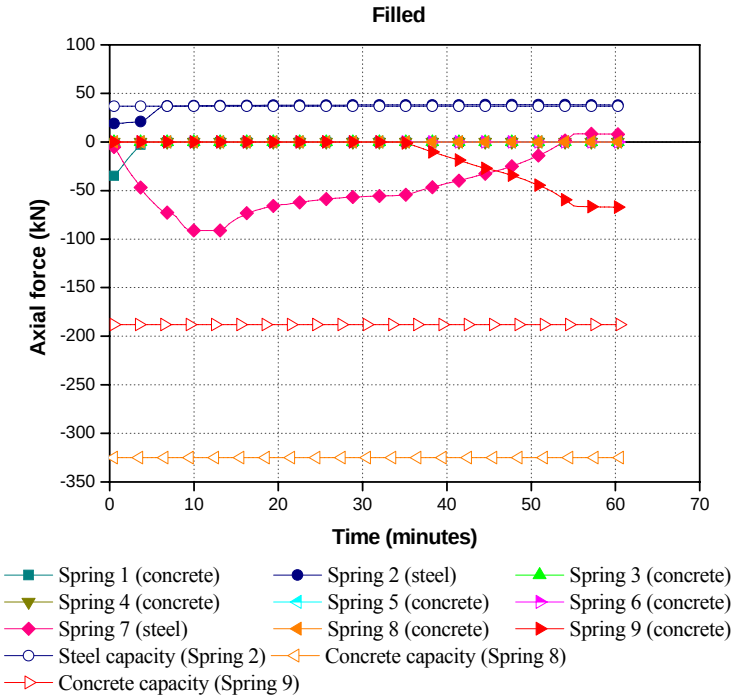

(b) Concrete filled multi-spring element

Figure 6.16 Axial force histories of multi-spring connection elements at unit 1

In order to clarify the effect of starter bars, the multi-bay hollowcore floor model was reanalysed using a special version of the program where the elasto-

plastic steel properties have no unloading phase and the plasticity plateau is "infinite" (i.e. limited to a strain of 10,000%).

Figure 6.17 shows the comparison of structural behaviours between the multi-bay hollowcore floor using 15% strain steel property and infinite strain steel property. With the use of infinite strain steel property, the floor model lasted up to 60 minutes as with the floor model with 15% finite strain steel property. Up to 60 minutes, the structural behaviours of the hollowcore floor model were more or less the same.

The axial force histories of the floor model using infinite strain steel property are presented with respect to hollowcore unit 11 in Figure 6.18. The axial force histories were investigated in terms of same spring elements. As explained previously, the bottom concrete spring elements do not reach their capacity.

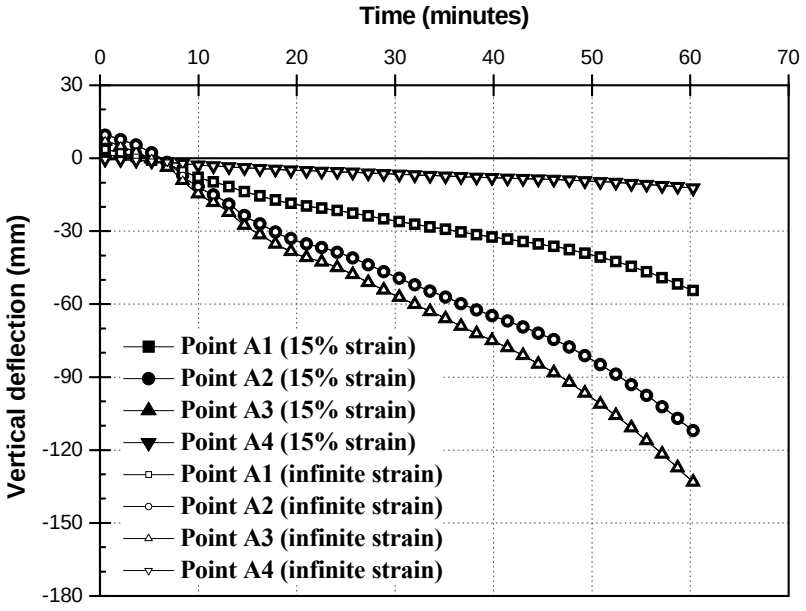

Figure 6.17 Comparison of structural behaviours between the multi-bay hollowcore floor using 15% strain steel property and infinite strain steel property

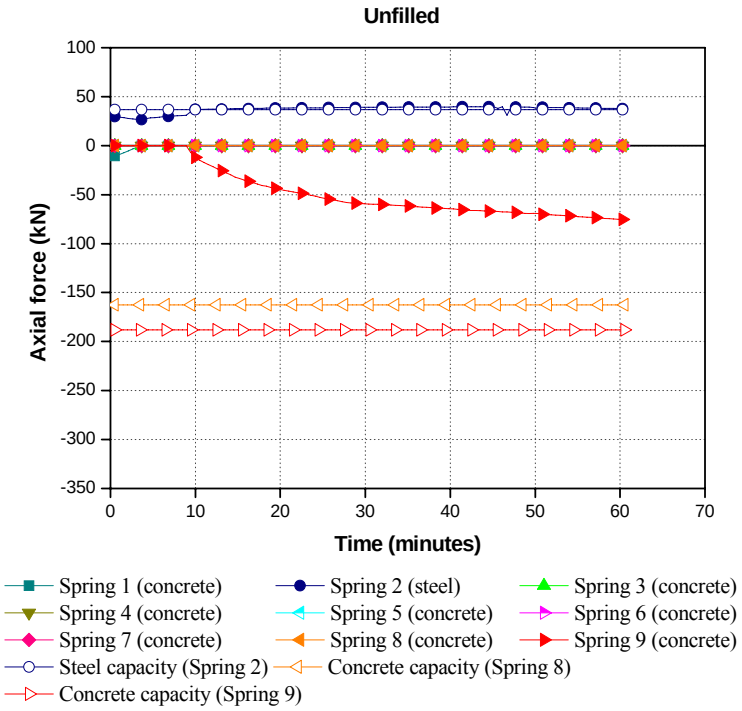

(a) Concrete unfilled multi-spring element

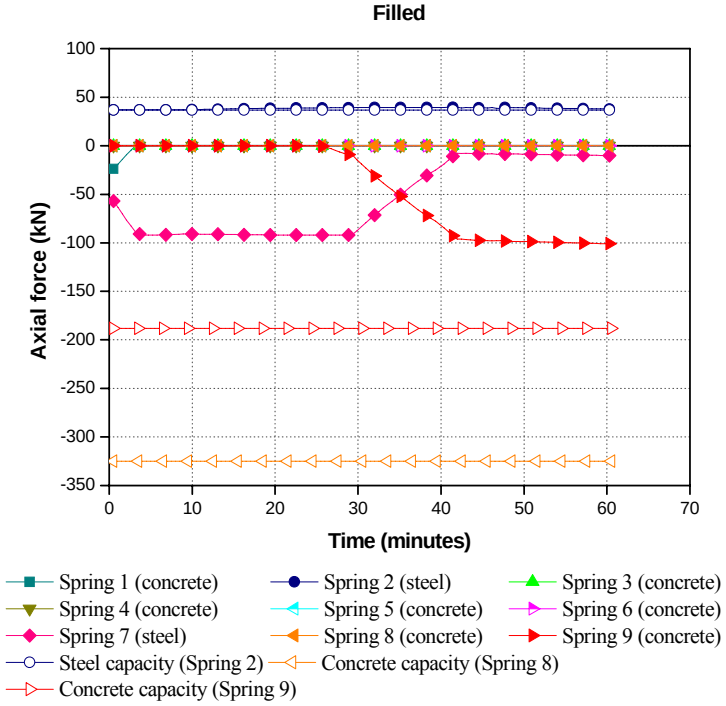

(b) Concrete filled multi-spring element

Figure 6.18 Axial force histories of multi-spring connection elements at unit 11 with respect to a modified Elasto-Plastic option

As explained in Section 6.2.2, the 75mm topping concrete infill strip was not exposed to fire due to the insulation effect of the 25mm timber infill.

Nevertheless, the insulation effect of the timber infill is questionable. In order to assess the effect of topping concrete infill on fire resistance, the floor model incorporating ISO fire exposure of infill strip was numerically analysed and compared with the non fire exposure model with respect to 75mm topping concrete infill. The results are plotted in Figure 6.19 with respect to reference points A1, A2, A3 and A5. It can be seen that, by applying ISO fire exposure to the topping concrete infill, the fire resistance of the floor model is more or less same such that the fire resistance is 60 minutes. In addition, a worse structural behaviour of the floor model was observed particularly at point A2, which is at the end of the infill.

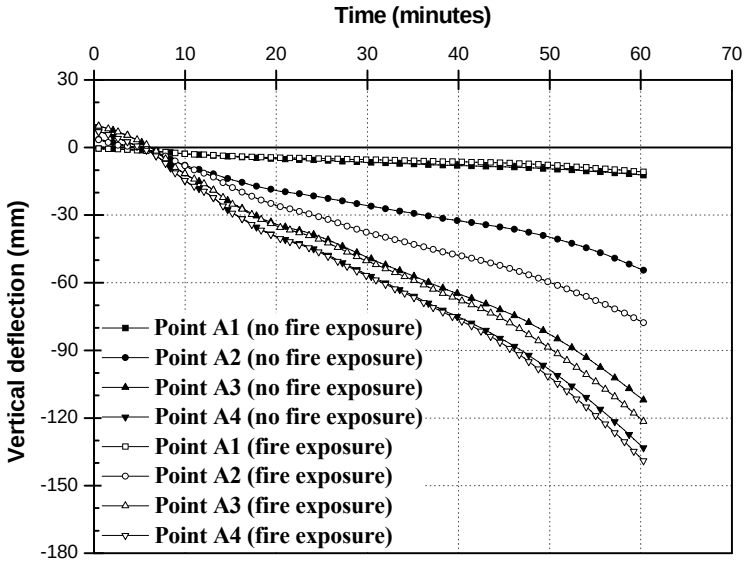

Figure 6.19 Comparison of structural behaviours between the multi-bay hollowcore floor with fire exposure and non fire exposure with respect to topping concrete infill

So far, the multi-bay prestressed concrete hollowcore floor located in the exterior bay of the plan has been analysed and discussed. The behaviour of the fire-exposed floor depends on how it is supported by the surrounding structure. In the case of an interior floor exposed to fire, high thermal expansion of the floor can be restrained by the surrounding structure to improve the fire resistance. Therefore, a scenario of internal multi-bay floors can be considered as shown in Figure 6.20. In this analysis, full horizontal restraints are provided along each edge beam in the shaded area instead of the modelling the entire structure.

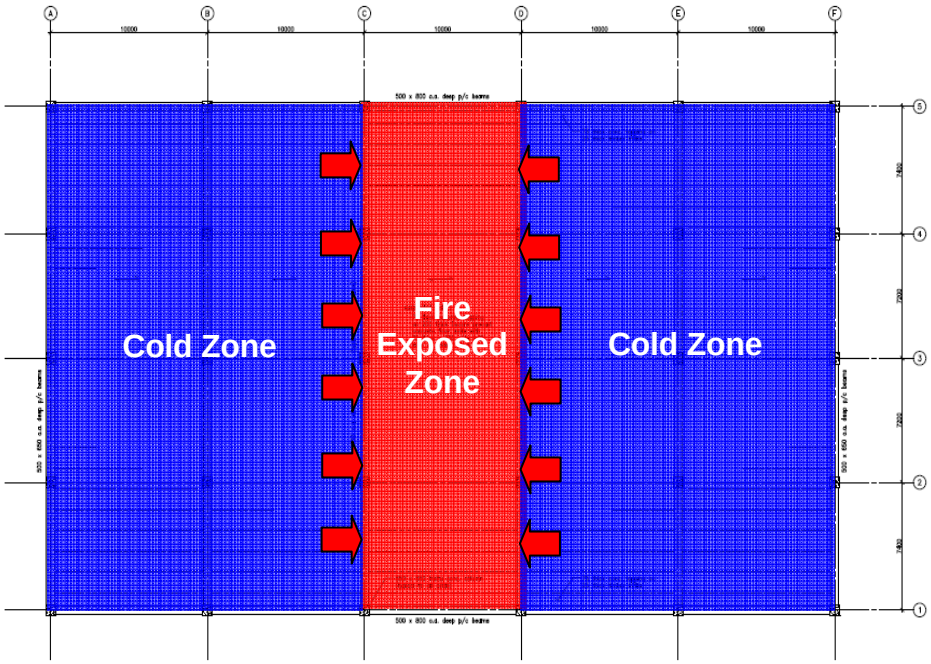

Figure 6.20 Fire exposed interior multi-bay floor used in the analysis

Figure 6.21 shows the comparison of structural behaviours between the exterior and interior multi-bay hollowcore floor. It can be seen that the fire resistance of the interior multi-bay hollowcore floor is improved such that the fire resistance is 82 minutes. It has been shown that the location of the fire exposed multi-bay hollowcore floor should be taken into account for the structural fire design of the hollowcore floors.

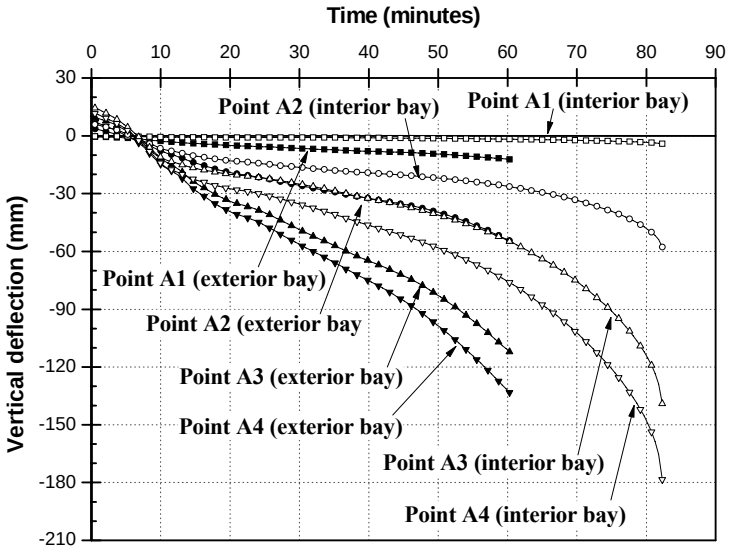

Figure 6.21 Comparison of structural behaviours between the exterior and interior multi-bay hollowcore floor

Figure 6.22 shows the axial force histories of the interior multi-bay hollowcore floor at hollowcore unit 11. For the concrete unfilled and filled hollowcore, the multi-spring connection elements do not reach yield limit until the end of analysis even though the multi-spring connection elements developed higher axial forces compared to the exterior bay floor.

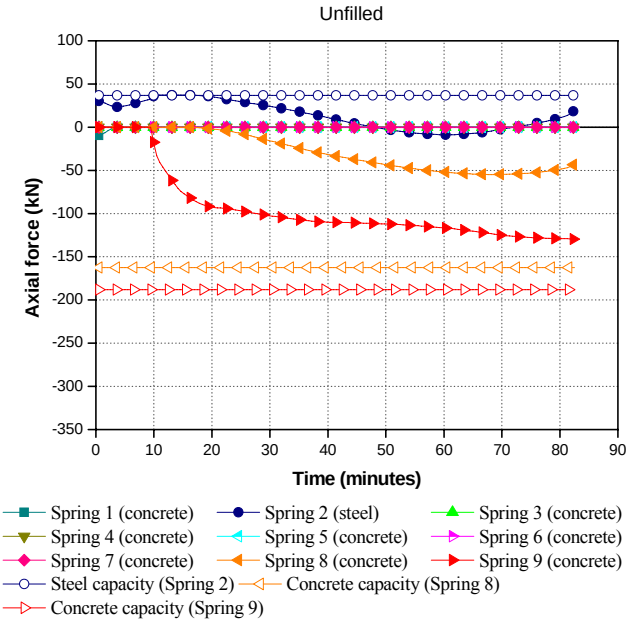

(a) Concrete unfilled multi-spring element

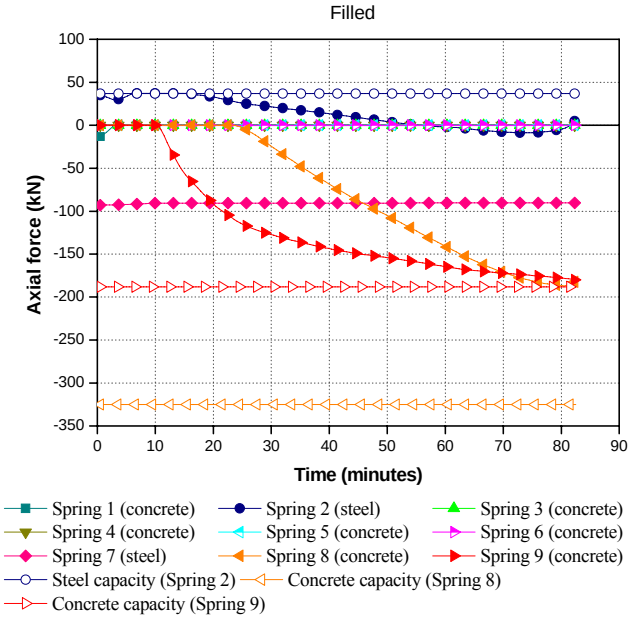

(b) Concrete filled multi-spring element

Figure 6.22 Axial force histories of multi-spring connection elements at unit 11 with respect to an interior bay

6.4.2 Fire performance of multi-bay prestressed hollowcore floor exposed to ISO fire with a decay phase

This section investigates the behaviour of a multi-bay prestressed hollowcore floor subjected to the ISO fire with a decay phase. In order to obtain the Eurocode parametric fire curves, some assumptions have been made. It is assumed that the fire occupies the whole floor area of the modelled floor, so the floor area and height of the fire compartment are 28.4m by 10m and 3.6m respectively. The total internal area of the bounding surfaces (A_t), therefore, is 844m^2. In addition, it is assumed that the area of the window opening (A_v) and the height of the window opening (H_v) are 19.5m^2 and 3m respectively.

According to Eurocode 1 (EC1, 2002), temperature T_s (°C) during the burning period is calculated by the following equation.

$$T_s = 20 + 1325(1 - 0.324e^{-0.2t^*} - 0.204e^{-1.7t^*} - 0.472e^{-19t^*}) \qquad \text{Equation 6-1}$$

where t^* is a fictitious time (hours) given by

$$t^* = t \cdot \Gamma \qquad \text{Equation 6-2}$$

where t is a time (hours) and

$$\Gamma = \frac{(F_v / F_{ref})^2}{(b / b_{ref})^2} \qquad \text{Equation 6-3}$$

where b is $\sqrt{\text{thermal inertia}} = \sqrt{k\rho c_p}$ (Ws$^{0.5}$/m^{2}K), F_v is the ventilation factor ($\sqrt{m}$) given by

$$F_v = A_v \sqrt{H_v} / A_t \qquad \text{Equation 6-4}$$

where A_v is the area of the window opening (m^2), H_v is the height of the window opening (m), A_t is the total internal area of the bounding surfaces (m^2).

Eurocode specifies the value of F_{ref} (0.04) and b_{ref} (1160). However, Feasey and Buchanan (2002) found that the temperature calculated based on the value of b_{ref}, 1160, is often too low. Thus, their recommended value of b_{ref}, 1900, is used in this section.

For the special case where $F_v = F_{ref}$ and $b = b_{ref}$, Equation 6-1 is close to the ISO 834 curve. Therefore, fictitious time (t^*) is same as time (t).

The behaviour of the hollowcore floor is compared for five different fire exposures; the Standard ISO fire for four hours and parametric fires based on the ISO fire with decay phases after 30, 40, 50 and 60 minutes as shown in Figure 6.23. In these parametric fire curves, the reference decay rate $(dT/dt)_{ref}$ introduced in Eurocode 1 was used to determine the decay rate. In Eurocode, a reference decay rate is equal to 625ºC per hour for fires with a burning period less than half an hour, decreasing to 250ºC per hour for fires with a burning period greater than 2 hours. Therefore, parametric fires with decay phases after 30, 40, 50 and 60 minutes have a rate of temperature reduction of 625, 583, 542 and 500ºC per hour respectively.

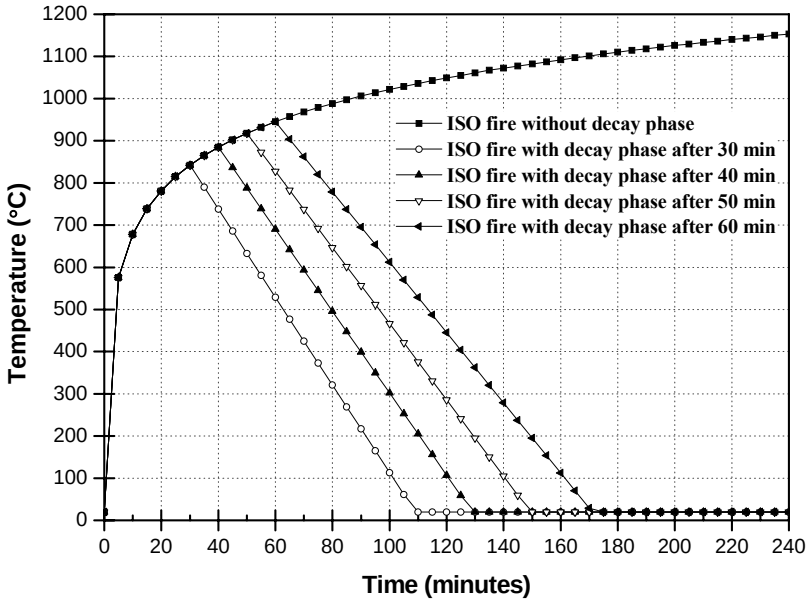

Figure 6.23 Parametric fire curves

The entire prestressed hollowcore floor is assumed to be exposed to an identical parametric fire. The supporting beams were exposed to fire only on the bottom and inner surfaces. The columns were not exposed to the fire. Figure 6.24 shows the temperature development at different locations of a longitudinal beam element of the hollowcore slab, exposed to Standard ISO and parametric fires. It can be seen that the temperature of the underside of the hollowcore elements (point 1) increases up to 900ºC with the longer fire exposure time. The temperature of the prestressing strands reached up to 460 ºC when the hollowcore elements were exposed to ISO fire with decay phase after 60 minutes. The time for reaching the

maximum temperature at point 1 is same as the fire exposure time before cooling down. Points 2, 3 and 4 take some time to attain the maximum temperature due to the heat transfer time. As a result, the temperature of point 1 increases and then decreases quickly after cooling. On the other hand, the points higher than point 1 develop the temperature slowly and cool down with a small decrease rate.

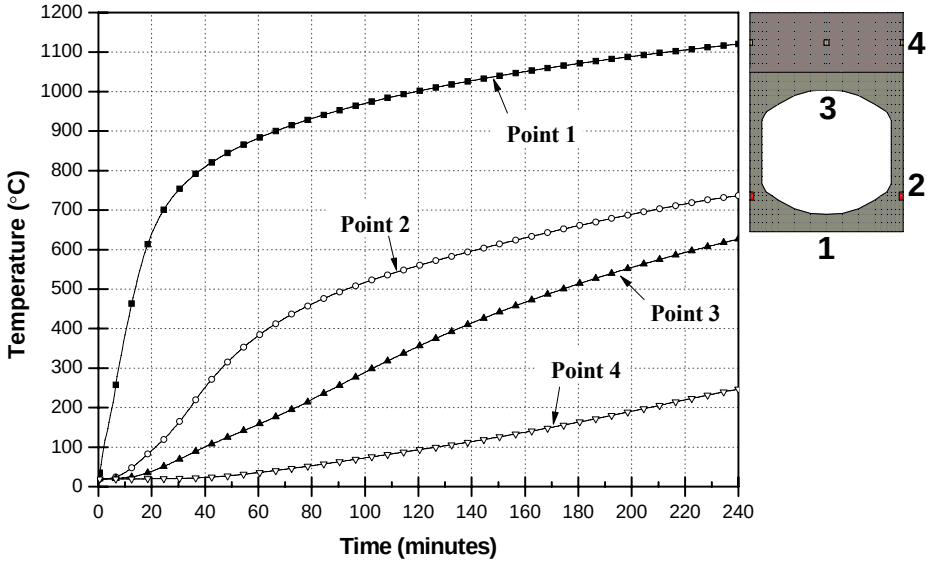

(a) Standard ISO fire exposure

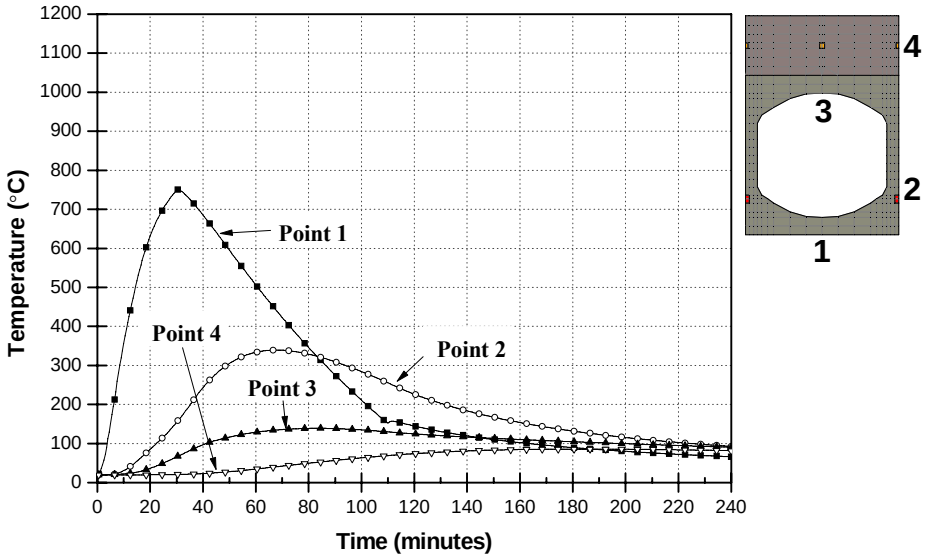

(b) ISO fire exposure with decay phase after 30 minutes

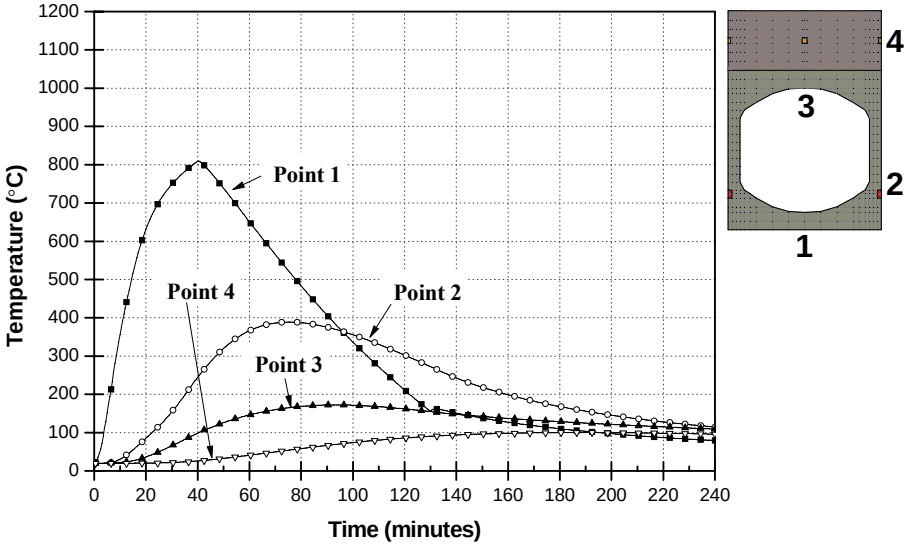

(c) ISO fire exposure with decay phase after 40 minutes

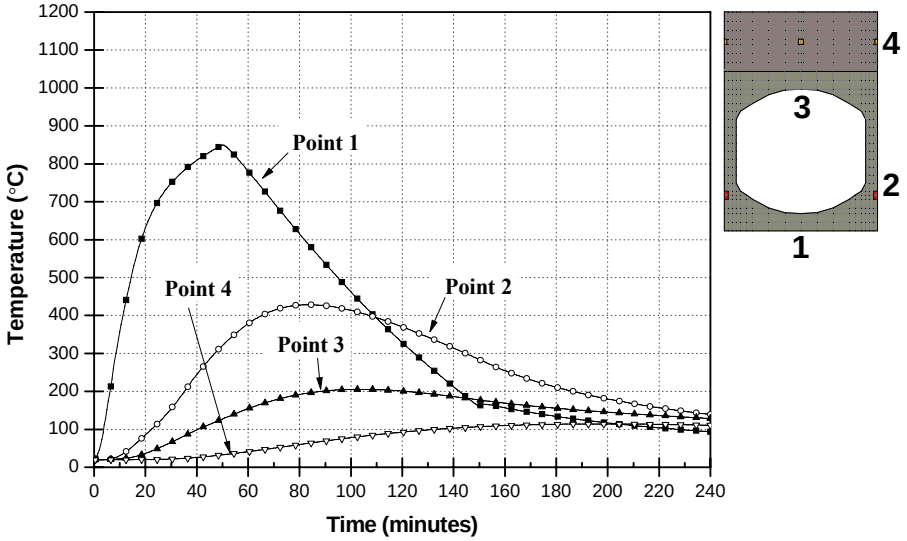

(d) ISO fire exposure with decay phase after 50 minutes

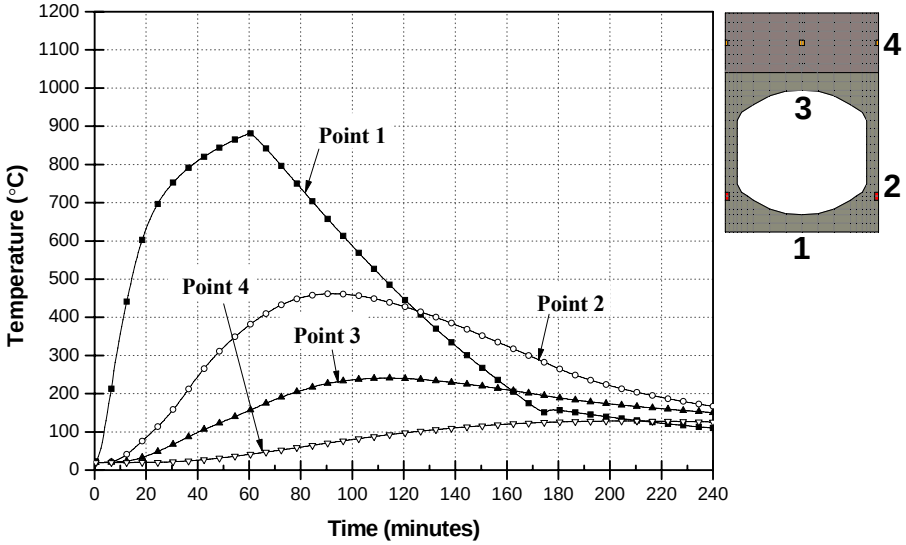

(e) ISO fire exposure with decay phase after 60 minutes

Figure 6.24 Temperature development of longitudinal hollowcore element

In SAFIR program, concrete and steel materials behave at elevated temperature according to the Eurocodes. In addition, for steel materials we need parameters such as the critical temperature (in °C) beyond which the yield strength is not fully recovered during cooling and the rate of decrease of the residual yield strength if the temperature has exceeded the critical temperature. However, the critical temperature for prestressing steels is not confirmed at the moment and the temperature of prestressing steels is less than 500°C after 60 minutes standard fire exposure. Thus, it is assumed that concrete and steel can fully recover their strength during cooling phases.

Figure 6.25 shows a comparison of vertical deflections measured at the centre of the hollowcore floor, for the ISO fire exposure and the four different parametric fire exposures. The numerical results for a parametric fire with decay phase after 60 minutes shows a runaway failure. The hollowcore floors exposed to parametric fires with decay phase after 30, 40 and 50 minutes survived the fire for the entire period while the analysis on the floor exposed to the Stnadard ISO fire terminated around 60 minutes with 133mm vertical deflection. It is obvious, from these results that the failure of multi-bay hollowcore systems is relative to the duration of exposure in the heating phase of the fire.

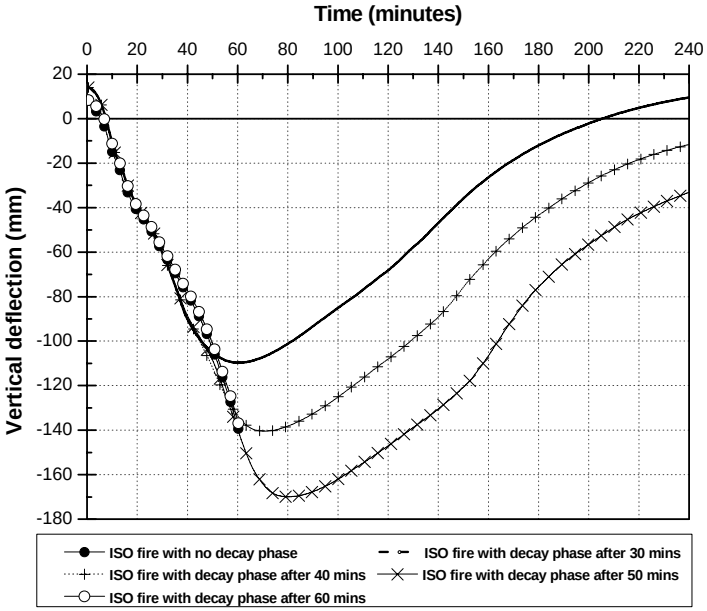

Figure 6.25 Comparisons of vertical deflection of the multi-bay hollowcore floor at point A4

6.4.3 Fire performance of multi-bay prestressed hollowcore floor with 1.5 times starter bars

This section investigates the effect of increasing the area of the starter bars in the concrete topping (1.5 times starter bars) in multi-bay prestressed hollowcore floors subjected to the ISO fire. In Chapter 4, it has been demonstrated that increasing the amount of starter bars with respect to a one unit hollowcore slab can lead to better fire performance. The fire performance of multi-bay prestressed hollowcore floor including 1.5 times starter bars is investigated to identify the increase of fire resistance of multi-bay floors. The amount of starter bars was increased to 1.5 times over the entire prestressed hollowcore floor. Figure 6.26 shows the comparison of structural behaviours between the multi-bay hollowcore floor using normal starter bars and 1.5 times starter bars. It can be seen that the midspan vertical deflections of the multi-bay prestressed hollowcore floor with 1.5 times starter bars reduced slightly compared to that of the multi-bay prestressed hollowcore floor with normal starter bars. As a result, the fire resistance increased from 60 minutes with normal starter bars to 240 minutes with 1.5 times starter bars.

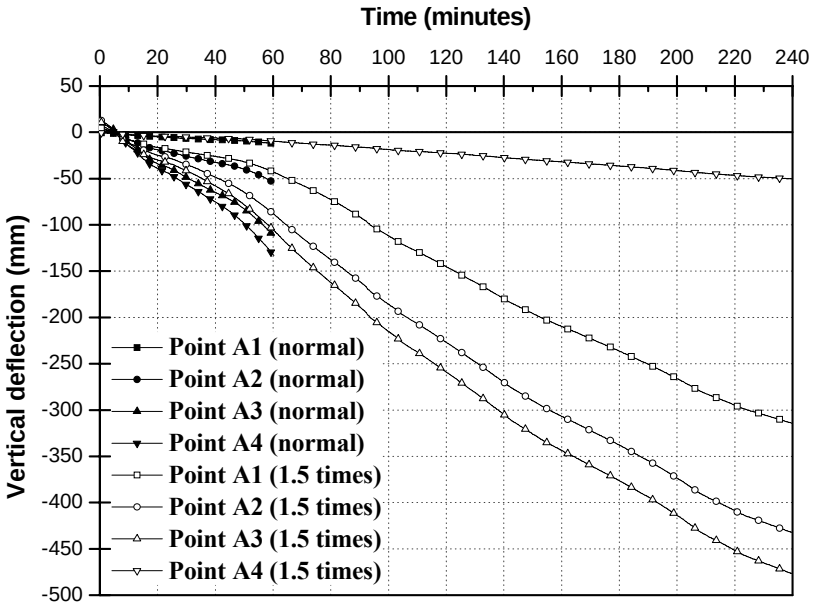

Figure 6.26 Comparison of structural behaviours between the multi-bay hollowcore floor using normal starter bars and 1.5 times starter bars

The axial force histories of the floor model with 1.5 times starter bars in terms of hollowcore unit 1, unit 6 and unit 11 (Figure 6.9) are examined. Figure 6.27 to Figure 6.29 show axial force histories of multi-spring connection elements with respect to concrete unfilled and filled parts. It is evident that any elements such as steel and concrete do not reach the yield limit at the end of analysis.

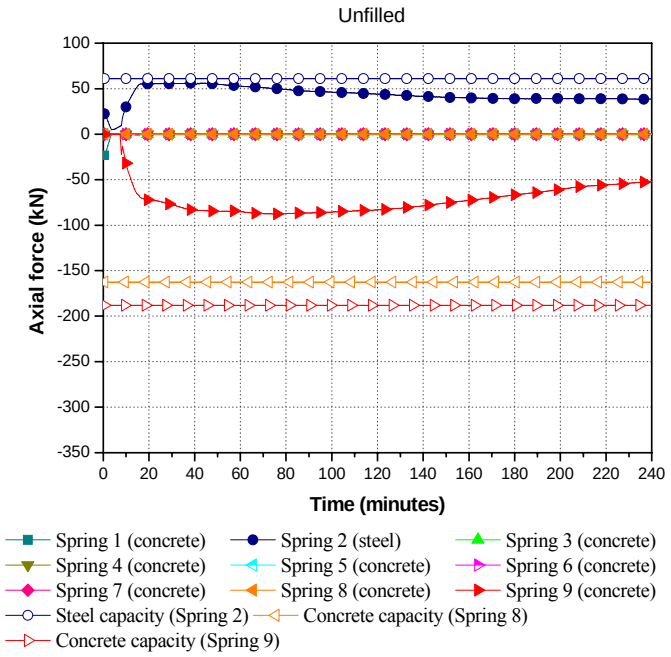

(a) Concrete unfilled multi-spring element

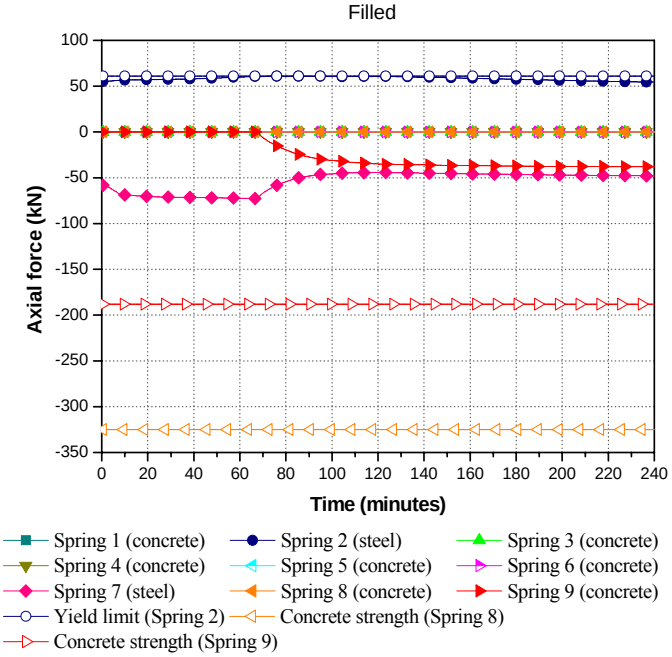

(b) Concrete filled multi-spring element

Figure 6.27 Axial force histories of multi-spring connection elements at unit 11 with respect to the floor model with 1.5 times starter bars

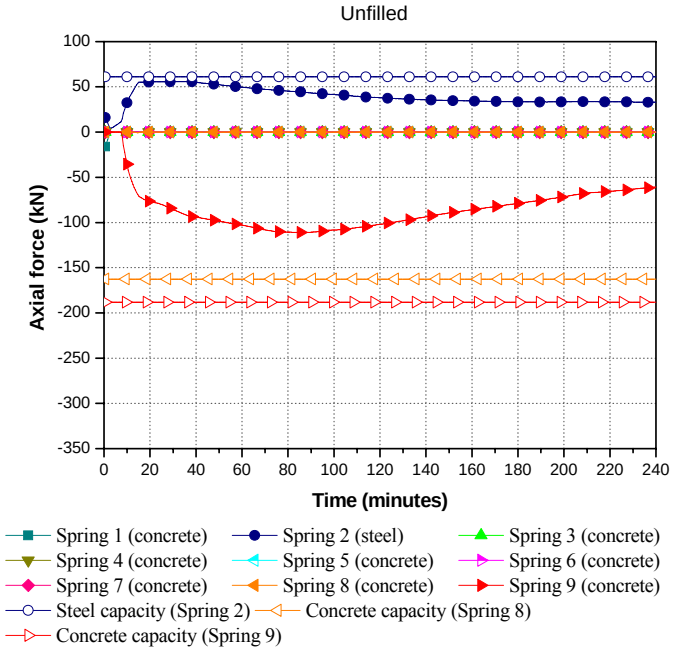

(a) Concrete unfilled multi-spring element

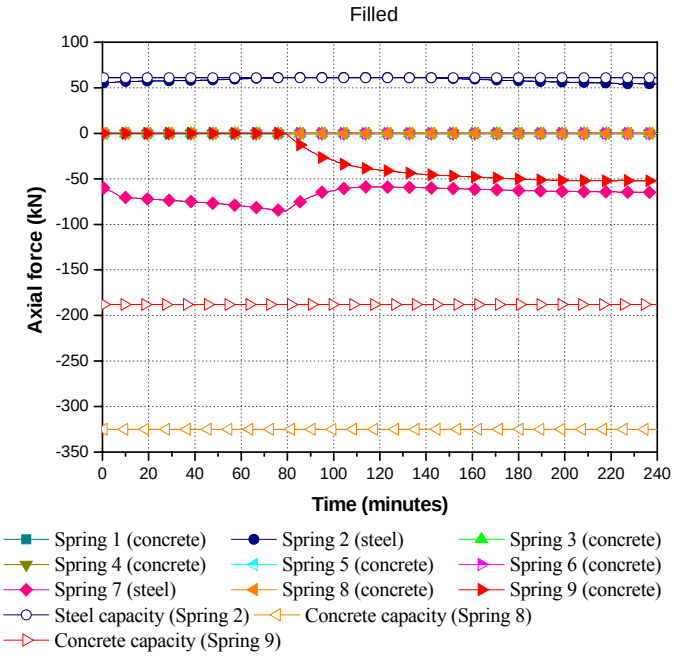

(b) Concrete filled multi-spring element

Figure 6.28 Axial force histories of multi-spring connection elements at unit 6 with respect to the floor model with 1.5 times starter bars

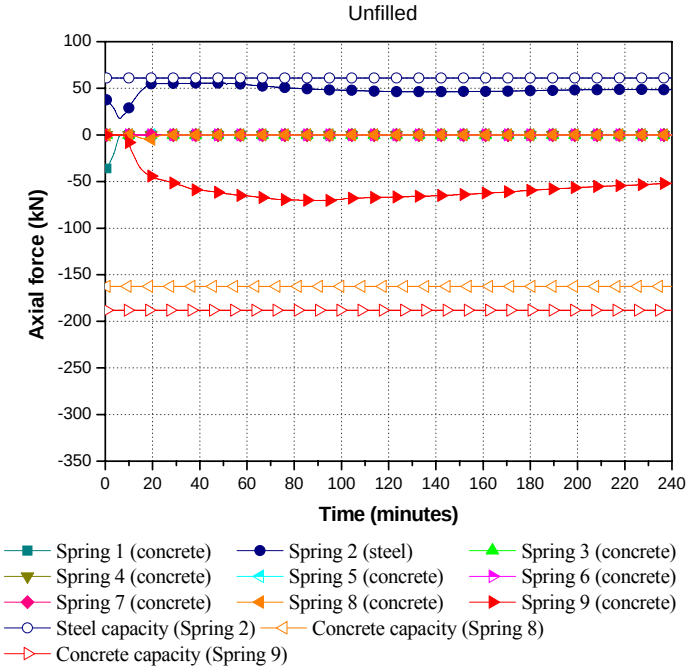

(a) Concrete unfilled multi-spring element

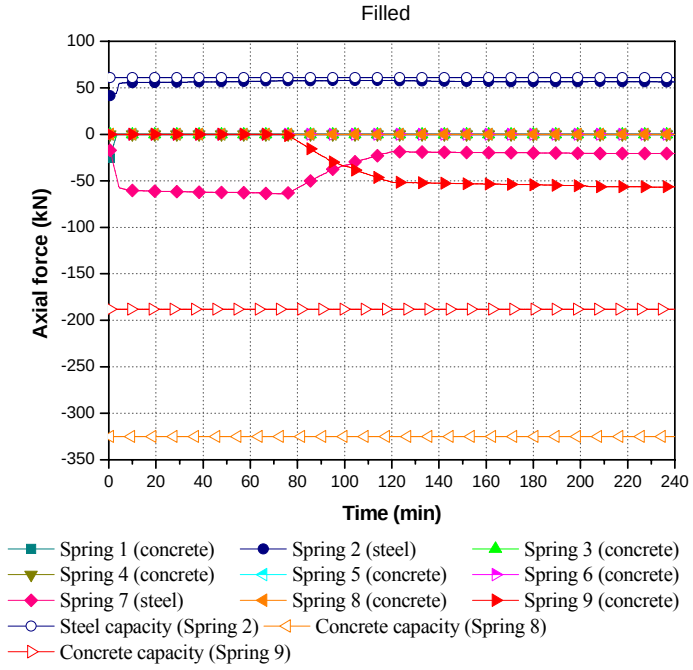

(b) Concrete filled multi-spring element

Figure 6.29 Axial force histories of multi-spring connection elements at unit 1 with respect to the floor model with 1.5 times starter bars

Figure 6.30 shows an isometric view of the deflected shape at the end of the numerical analysis with 1.5 times starter bars. In this simulation, the analysis did not stop until at the end of analysis.

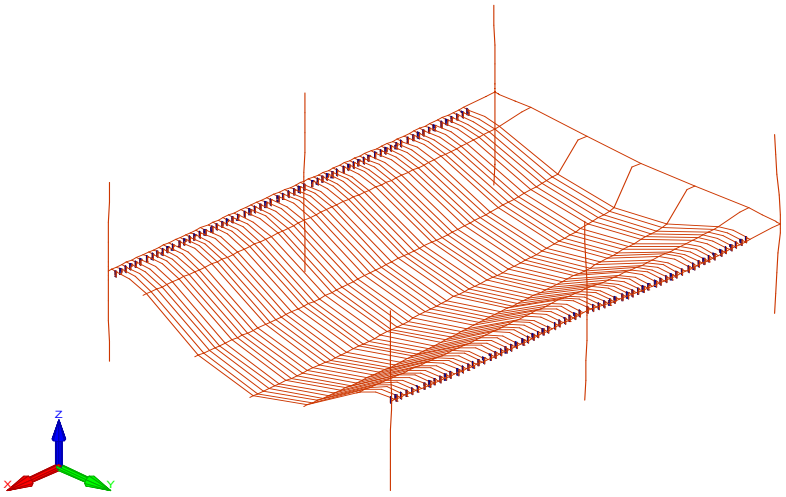

Figure 6.30 Deflected shape of the multi-bay prestressed hollowcore floor with 1.5 times starter bars, scale factor = 5

6.5 Fire performance of multi-bay prestressed hollowcore floor including fire emergency beams

6.5.1 Fire emergency beams

The concept of fire emergency beams has been introduced in recent literature (Chang et al., 2008). Fire emergency beams are defined as extra beams running parallel to the floor slabs, which reduce the transverse curvature of slabs to improve the fire resistance. It has been postulated that fire emergency beams can contribute to an increase of fire resistance of slabs which have a large number of hollowcore units side by side and the extent of the increase in fire resistance depends on the spacing of the fire emergency beams and the fixity between the floor slab and the beams. However, there is no literature that quantifies the influence of fire emergency beams.

6.5.2 Multi-bay prestressed hollowcore floor with fire emergency beams

In order to investigate the effect of emergency beams in fire, the initial model created, based on the Future Building Program System drawings, was modified by adding fire emergency beams as shown in Figure 6.31 and Figure 6.32. The difference between the present analyses and those in the previous section, is the

inclusion of the emergency beams in the multi-bay models. In both cases, the number of hollowcore units is reduced to 20 and 16 in order to introduce infill strips between the emergency beams and the hollowcore units. Even though the emergency beams are added for both models, the total width of the floor was kept at 28.4m. The overall floor dimensions are shown in Figures 6.5, 6.31 and 6.32. The cross section of fire emergency beams used in this study was 400mm by 600mm. It was assumed that the emergency beams were exposed to fire on the sides and the bottom surfaces.

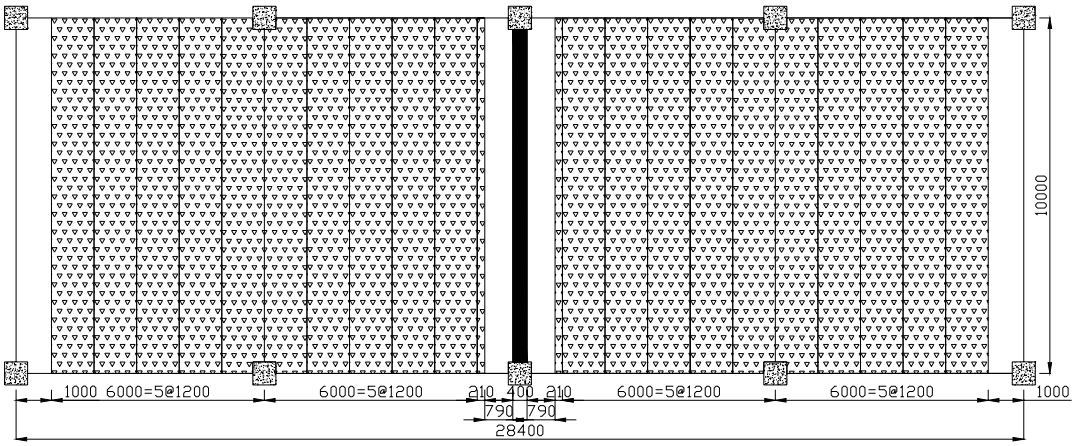

Figure 6.31 The arrangement of hollowcore floors including one emergency beam (20 hollowcore units)

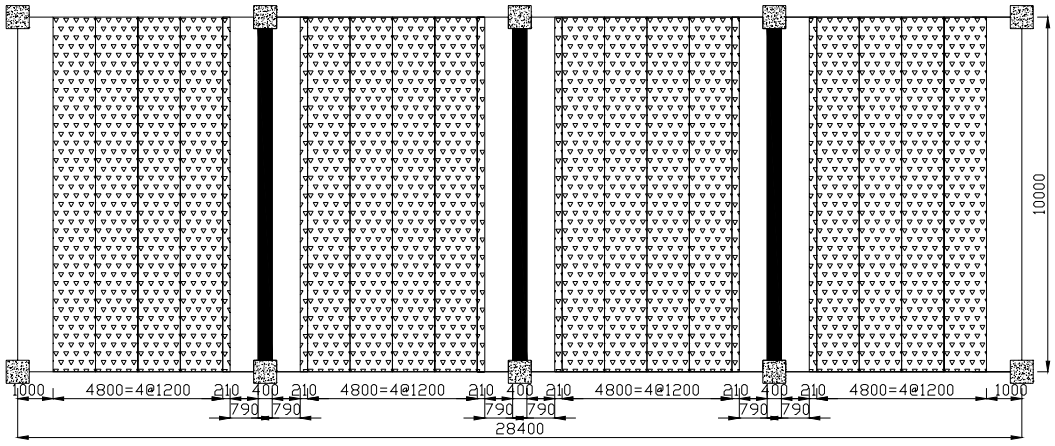

Figure 6.32 The arrangement of hollowcore floors including three emergency beams (16 hollowcore units)

Figure 6.33 and Figure 6.34 illustrate the half model mesh of the multi-bay prestressed hollowcore floors with one emergency beam and three emergency beams, respectively.

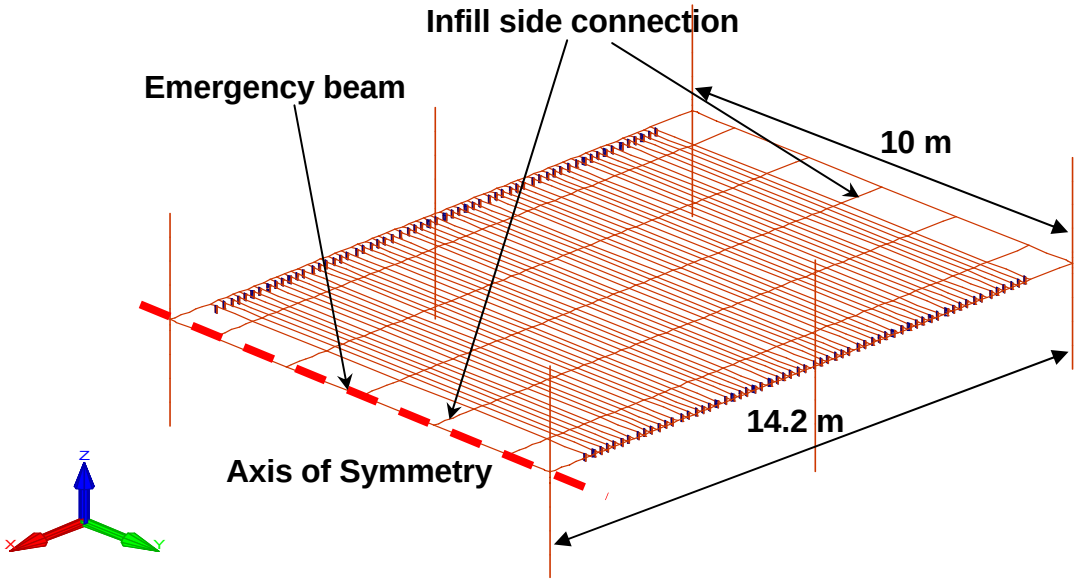

Figure 6.33 The half model mesh used for prestressed hollowcore floors including one emergency beam

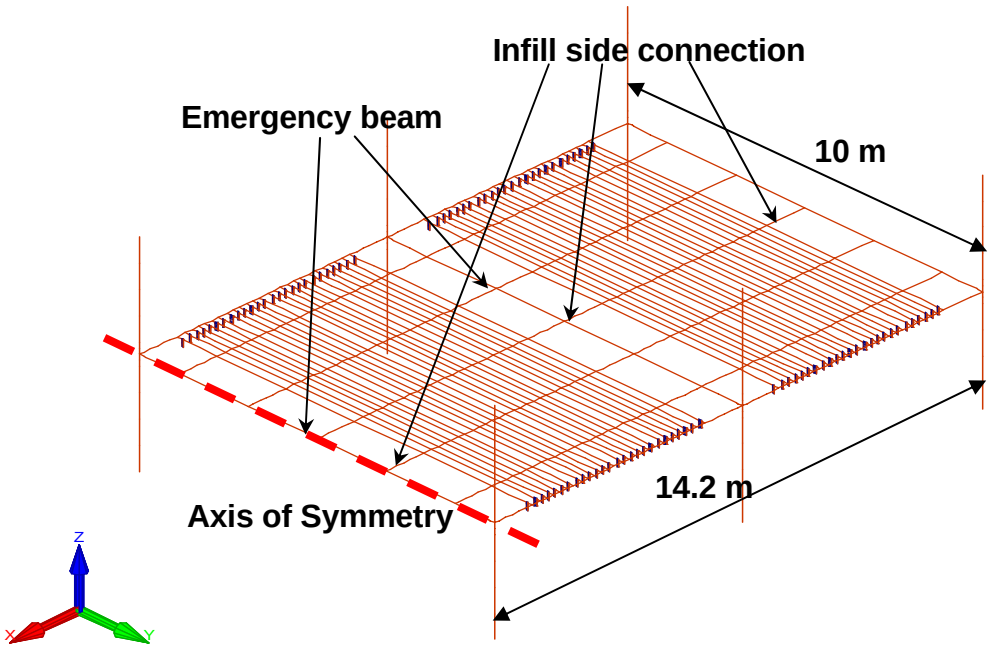

Figure 6.34 The half model mesh used for prestressed hollowcore floors including three emergency beams

6.5.3 Fire performance of multi-bay prestressed hollowcore floor with one fire emergency beam

Figure 6.35 shows the deflected shape at the failure point of the multi-bay prestressed hollowcore floor with one emergency beam. The maximum vertical deflection point is also identified. As in the case of the hollowcore floor with no emergency beam, the analysis terminated due to non-convergence of the non-linear soultion. Furthermore, the failure of the multi-bay prestressed hollowcore floor with one emergency beam also occurred due to numerical instability (Figure 6.35(a)).

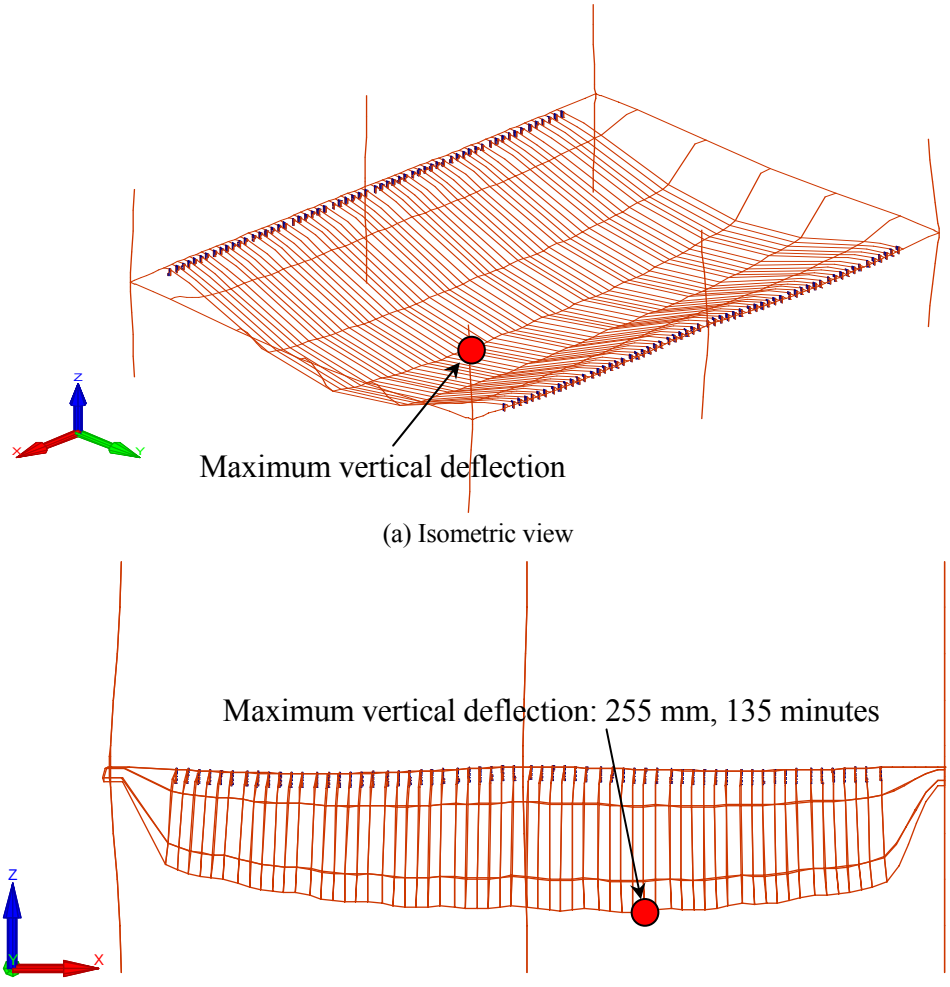

(a) Isometric view

(b) Side view

Figure 6.35 Deflected shape of the multi-bay prestressed hollowcore floor with one emergency beam at 96 minutes, scale factor = 10

6.5.4 Fire performance of multi-bay prestressed hollowcore floor with three fire emergency beams

Figure 6.36 shows the deflected shape of the multi-bay prestressed hollowcore floor with three emergency beams at the end of the analysis. In this analysis the floor failed after 158 minutes due to the numerical instability (Figure 6.36(a)). The maximum vertical deflection point of the multi-bay prestressed hollowcore floor moves closer to the middle of the multi-bays and the maximum vertical deflection of the floor is 174mm.

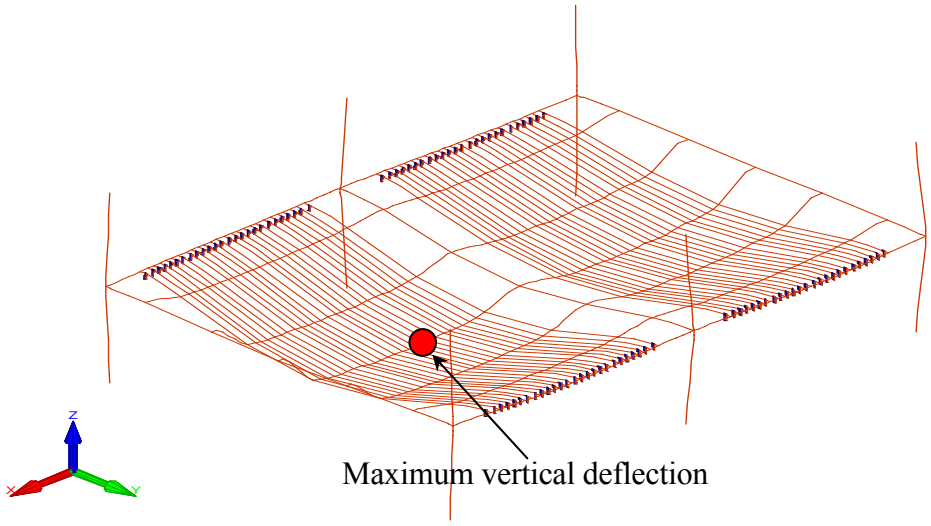

(a) Isometric view

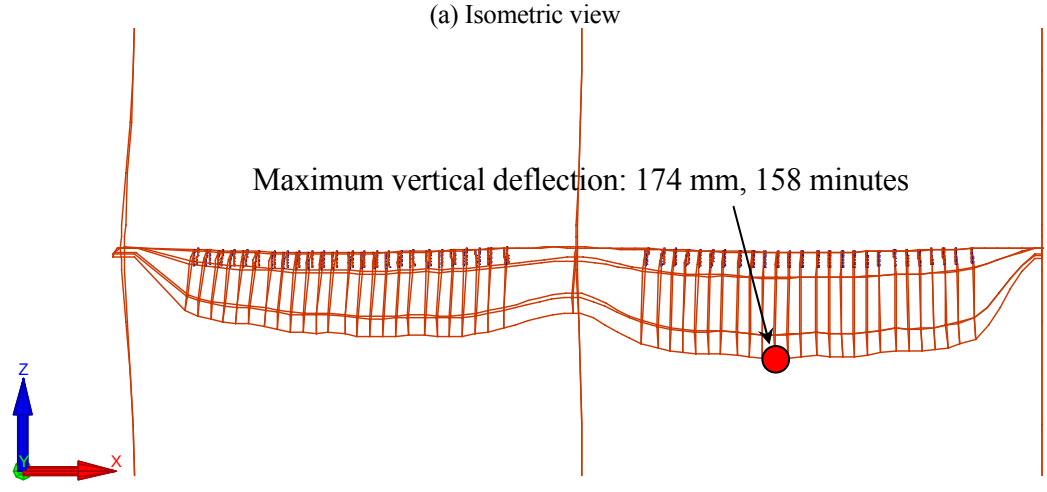

(b) Side view

Figure 6.36 Deflected shape of the multi-bay prestressed hollowcore floor with three emergency beams at the end of analysis, scale factor = 10

6.5.5 Discussion

The maximum vertical deflection of each multi-bay prestressed hollowcore floor, as mentioned in Sections 6.3.1, 6.4.3 and 6.4.4, is plotted against time as shown in Figure 6.37. The floor with no fire emergency beam was seen to deflect 133mm during the fire resistance period, and fail after 60 minutes. The inclusion of one fire emergency beam shows a large increase of fire resistance of 65 minutes, to 98 minutes. However, by reducing the spacing between side beams or fire emergency beams, the floor with three emergency beams showed a significantly increased fire resistance time. These analyses show that the addition of fire emergency beams can be used to increase the fire resistance of hollowcore slabs, if required. The cost of the additional fire emergency beams has not been investigated.

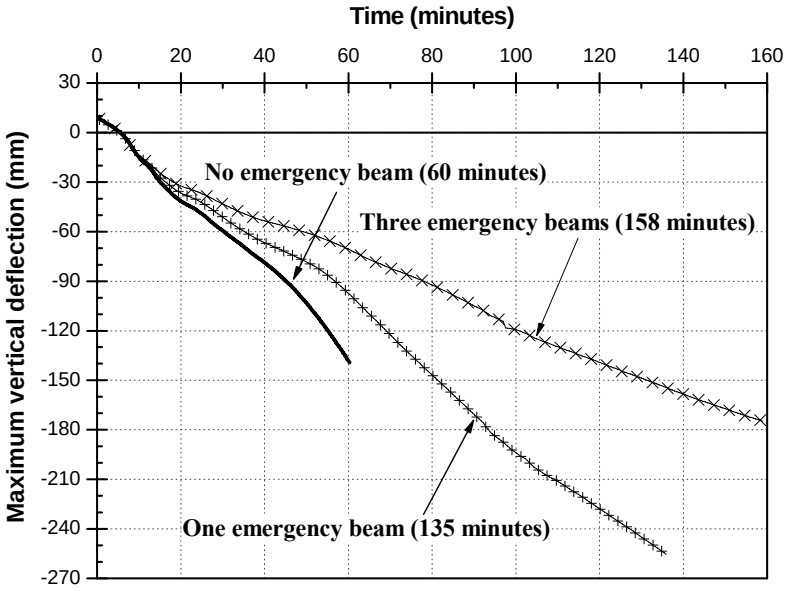

Figure 6.37 Comparison of maximum vertical deflections with no fire emergency beam, one fire emergency beam and three fire emergency beams

6.6 Summary

Numerical analyses of the multi-bay prestressed hollowcore floor in fire were conducted using SAFIR. The hollowcore slabs and connections were modelled using the grillage model and the multi-spring connection. This analysis demonstrates that the multi-bay prestressed hollowcore floor, including 22

hollowcore slabs and side infill connection, provide 60 minutes fire resistance. With respect to parametric fires, the multi-bay hollowcore floor shows much greater fire resistance if the fire goes out after 50 minutes or less, even though larger deflections occur. With respect to the starter bar reinforcing area, it was found that the floor with 1.5 times reinforcement showed better fire resistance and structural behaviour compared to the case of normal reinforcement.

With respect to additional fire emergency beams, the results show that the fire performance of the multi-bay prestressed hollowcore floor with fire emergency beams is much better than the case with no fire emergency beams. The main reason for this appears to be the effect of two way action. This study confirms that the fire performance of multi-bay prestressed hollowcore floors may be significantly improved by utilising fire emergency beams.

Chapter 7

Shear and Splitting Resistance of Hollowcore Slabs in Fire

7.1 Introduction

At ambient conditions, the load bearing capacity of hollowcore slabs can be dominated by four different failure modes, i.e. flexure, anchorage, shear compression and shear tension (Fellinger, 2004). Many researchers have attempted to explain the failure mechanism of hollowcore slabs in fire (Van Acker, 2003; Fellinger, 2004; Jesen, 2005). Nevertheless, failure mechanisms of hollowcore slabs in fire are still not fully understood and require further research.

This chapter outlines the failure modes that are currently believed to be critical for hollowcore exposed to fire. More detailed description of each failure mode is given in Section 7.2. The available calculation models that calculate shear resistance of hollowcore slabs in fire are introduced in Section 7.3. These equations are validated for existing test results and applied to 200mm hollowcore slabs to determine the shear capacity during a fire. Another equation that calculates splitting resistance of hollowcore slabs in fire due to prestressing is introduced in Section 7.4. Thus, splitting resistance calculation with respect to hollowcore slabs subjected to fire is presented.

7.2 Failure modes of a hollowcore slab in fire

7.2.1 Flexure

Figure 7.1 shows the typical structural behaviour of a simply supported hollowcore concrete slab exposed to fire. The deflection process during fire exposure can be divided into three phases as shown in Figure 7.1. Firstly, when hollowcore slabs are

exposed to fire, the hollowcore concrete slab starts to deform downwards as a result of thermal gradients (Phase 1). Then, the yield strength and modulus of elasticity of both steel and concrete in the hollowcore slab reduce steadily (Phase 2). Finally, with further fire exposure, a rapid increase in the deflection is caused by yielding of the prestressing tendons (Phase 3). In this failure mode, the axis distance of the strands to the exposed side plays an important role in determining the fire resistance.

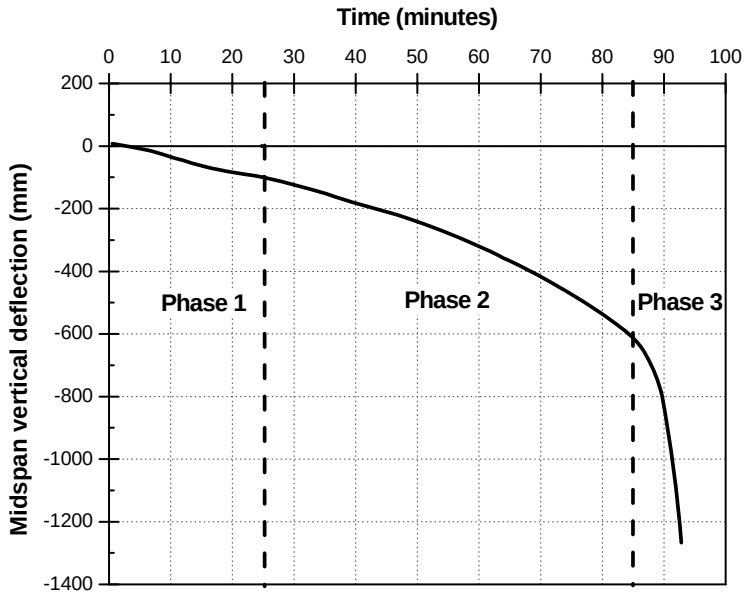

Figure 7.1 Vertical deflection at midspan of a simply supported hollowcore slab

7.2.2 Anchorage

At ambient conditions, the tensile stresses in the concrete drop when a flexural crack appears. To reach a new state of equilibrium, the tensile force in the strand near the crack is increased locally. The tensile force can only build up by bond stresses between the strand and the concrete. The maximum steel stress that can develop depends on the embedment length, i.e. the length over which the steel stress can be transmitted to the concrete cover. So the maximum steel stress decreases towards the end of the slab.

Hertz (1982) investigated the anchorage capacity of a reinforcing bars at high temperatures. In the failure of anchorage, it has shown that two modes of failures are possible: splitting and bond failure. The anchorage capacity of a

reinforcing bar is the minimum of the splitting capacity and the bond capacity. Even though the anchorage failure can occur when the reinforcing bar is the warmest, the anchorage failure of prestressing bars is different as the anchorage failure of prestressing bars in most cases happens much earlier.

Figure 7.2 shows an example of anchorage failure observed in the fire test of hollowcore slabs.

Figure 7.2 Anchorage failure of hollowcore slab (Borgogno, 1997)

7.2.3 Shear

Shear transfer actions and mechanisms in hollowcore slabs are complex and difficult to clearly identify due to the complex stress redistributions that occur after cracking, and which have been shown to be influenced by many factors.

Shear failure occurs in hollowcore slabs with horizontal cracks though the webs (Fellinger, 2004, Van Acker, 2010). The horizontal cracks developed in an early stage of fire exposure. The horizontal cracks were found at the smallest web width at mid depth along the entire length of the specimen, or developed as a splitting crack along a strand. During a fire, the horizontal cracks grew into one crack accompanied by some vertical cracks. The splitting crack either grew only horizontally along the strands which are positioned quite high in the web or from the strand to the nearest void and then down to the exposed soffit. At failure, a combined horizontal and vertical crack opened, and the strands were pulled out.

Figure 7.3 shows the shear failure mode of hollowcore slabs due to fire. After between 20 and 40 minutes ISO fire exposure, vertical thermal cracks appear

in the webs (Figure 7.3(a)). As explained above, horizontal cracks originate in the weakest zone of the cross section due to shear loading from end supports, self-weight, the imposed loading, prestressing and thermal expansion.

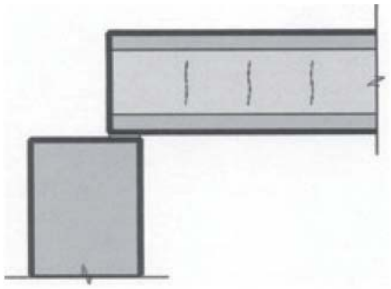

(a) Vertical cracks due to differential thermal deformation over the cross section

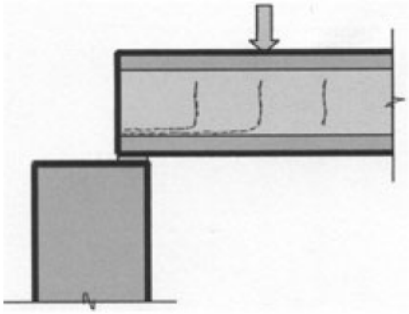

(b) Propagation of the vertical cracks into horizontal cracks due to additional shear loading and thermal effects

Figure 7.3 Failure mode of a hollowcore slab during fire (Van Acker, 2010)

7.2.4 Lateral expansion

Recently, another two possible failure modes of hollowcore floors in New Zealand have been raised by Fenwick *et al.* (2010). The two failure modes are the lateral expansion and the longitudinal expansion.

In Europe, hollowcore slab units are constructed against side beams. As a consequence, lateral expansion of the soffit can be partially restrained by the beam and would reduce or prevent the development of web cracks. On the other hand, in New Zealand hollowcore floor slabs use timber infill with in situ concrete to avoid unexpected displacements under seismic loading. For this New Zealand detail, Fenwick *et al.* (2010) pointed out the possibility of high level of expansion of the concrete below the voids in hollowcore units during the fire. In addition, they

maintained that flexural and shear stressed was induced in the webs as the hollowcore unit was free to distort as illustrated in Figure 7.4.

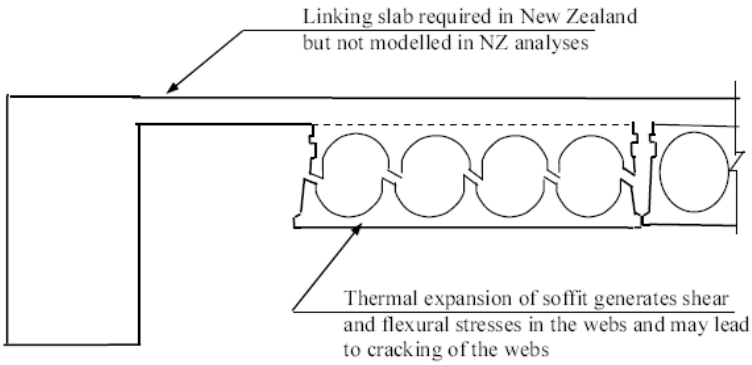

Figure 7.4 Lateral expansion of soffit of hollowcore floor under fire conditions (Fenwick et al., 2010)

7.2.5 Longitudinal expansion

Another possible failure mode is related to thermal expansion of the hollowcore unit in the longitudinal direction. As a result of longitudinal restraint by the supporting structure, a potentially weak section can occur where continuity reinforcement is terminated. Figure 7.5 illustrates a process of the hollowcore failure due to the longitudinal expansion. More details can be found from Fenwick et al. (2010).

In the longitudinal expansion of hollowcore floors, similar results which can capture the failure at the end of starter bars presented in Section 4.7.3.

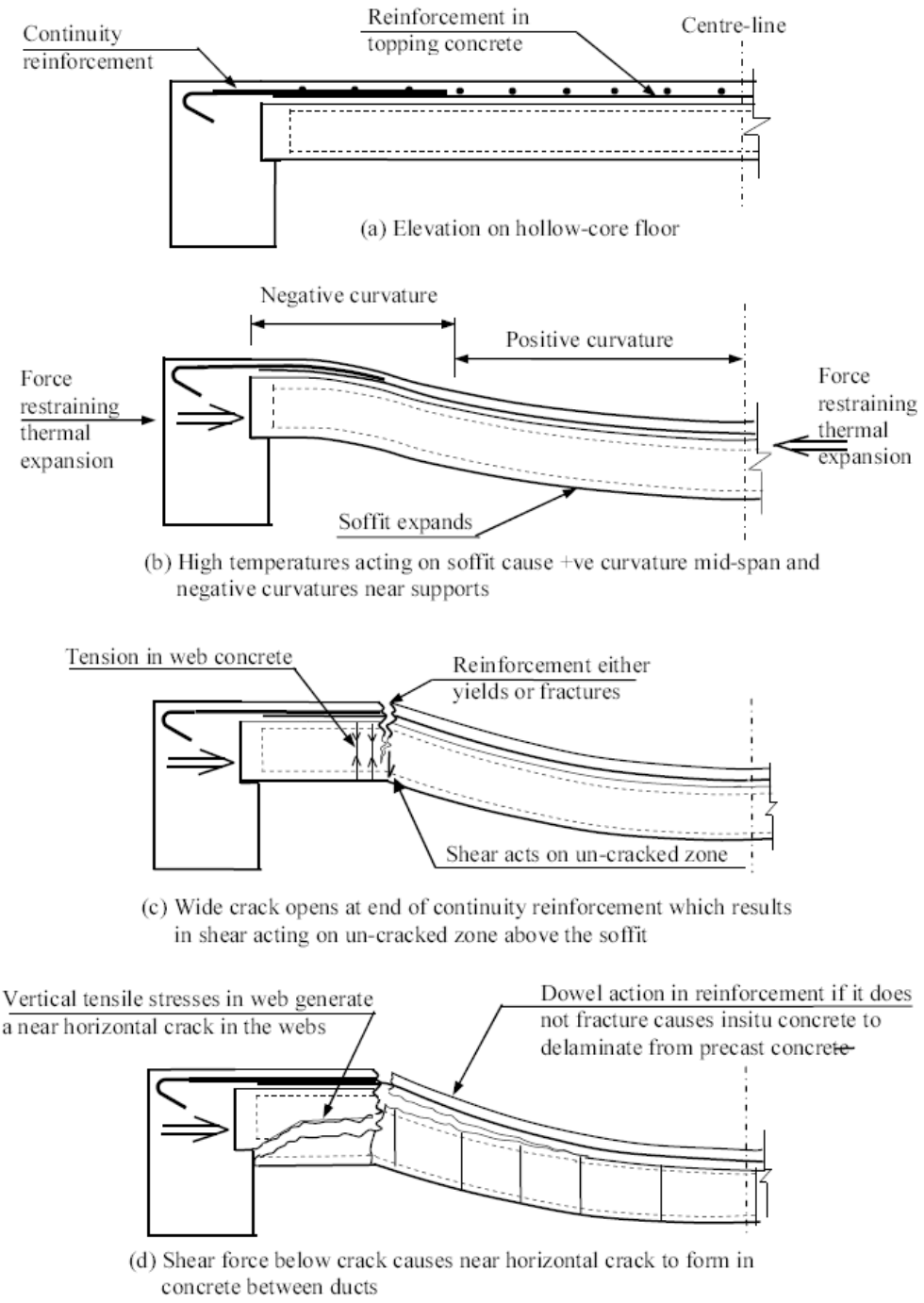

Figure 7.5 Longitudinal expansion of hollowcore unit under fire conditions (Fenwick et al., 2010)

7.3 Calculation method for the shear capacity from the published literature

There are different equations that are able to calculate the shear capacity of hollowcore slabs subjected to fire. These equations are based on FIP recommendations and the Eurocode 2. The main purpose of this section is to evaluate the shear capacity of hollowcore slabs subjected to fire. The results obtained from these different equations are compared and applied to 200mm hollowcore slabs.

7.3.1 FIP

FIP recommendation (1988) provides the equation for predicting the shear resistance of members without reinforcement, such as hollowcore slabs, in the region cracked in flexure at ambient temperature. The shear capacity of the member in the region which is cracked in flexure can be calculated as:

$$V_{uk} = 0.068\ b_w d\xi\left(1+\frac{50A_p}{b_w d}\right)\sqrt{f_c}+\frac{M_0}{M_x/V_x} \qquad \text{Equation 7-1}$$

where,

b_w is the total web width

d is the effective depth

ξ = 1.6 - d (m) ≥ 1 (scale factor) where d is measured in metres

A_p = the total cross sectional area of prestressing strands at the bottom face of the section

M_0 is the decompression moment (the moment that counteracts the prestress)

M_x is the moment in the cross section at a distance x from the theoretical support

V_x is the force in the cross section at a distance x from the theoretical support

Note that equation 7-1 was determined from test results of concrete members which failed in shear at ambient temperature. Borgogno (1997) modified this for high temperature situations to equation 7-2. In equation 7-2, the term $0.068\ \sqrt{f_c}$ stands for the nominal shear strength and the value is dependent on the strength of the concrete. The transfer length which is the length required to develop the full prestress increases with the duration of fire, which also decreases the decompression moment, M_0, in the support areas. Since the flexural shear failure occurs only at mid-length, the decompression moment, M_0, is neglected. Hence,

$$V_{uk} = 0.068\ b_w d\xi\left(1+\frac{50A_p f_{py}(t)}{b_w d f_{py}(20^\circ C)}\right)\sqrt{f_c} \qquad \text{Equation 7-2}$$

In Equation 7-2, f_{py} (20ºC) is the yield strength of prestressing strands and f_{py} (t) is defined as the reduced strength of prestressing strands at elevated temperatures. Therefore, f_{py} (t) can be calculated by using the reduction coefficient given in Table 3.3 of Eurocode EN 1992-1-2 (EC2, 2004).

7.3.2 Eurocode 2

For members not requiring shear reinforcement, the design value for the shear resistance $V_{Rd,c}$ is given by:

$$V_{Rd,c} = [0.12k(100\rho_l f_{ck})^{1/3} + 0.15\sigma_{cp}]\cdot b_w d \qquad \text{Equation 7-3}$$

where,

f_{ck} is in MPa

k $= 1+\sqrt{\frac{200}{d}} \le 2.0$ with d in mm

ρ_l $= \frac{A_{sl}}{b_w d} \le 0.02$

A_{sl} is the area of the tensile reinforcement, which extends ≥ (l_{bd} +d) beyond the section considered, where l_{bd} is a bond development length.

b_w is the smallest width of the cross-section in the tensile area (*mm*)

σ_{cp} $= N_{Ed} / A_c < 0.2 f_{cd}$ (MPa)

N_{Ed} is the axial force in the cross-section due to loading or prestressing in Newtons ($N_{Ed} > 0$ for compression). The influence of imposed deformations on N_{Ed} may be ignored.

A_c is the area of concrete cross section (mm^2)

$V_{Rd,c}$ is in Newtons

The minimum value for the shear resistance is given by the following:

$V_{Rd,c} = (v_{min} + k_1 \sigma_{cp}) b_w d$ where $v_{min} = 0.035 k^{3/2} f_{ck}^{1/2}$

which leads to: $V_{Rd,c} = (0.035 k^{3/2} f_{ck}^{1/2} + 0.15 \sigma_{cp}) b_w d$

$$= [0.035(1 + \sqrt{200/d})^{3/2} f_{ck}^{1/2} + 0.15 \sigma_{cp}) b_w d$$

The Precast Concrete Commission "TC 229" within the European Standard Institute CEN, has set up a Task Group to draft guidelines for the design of hollowcore floors with regard to shear in fire. Within this framework, the French research centre for the precast concrete industry (CERIB) has elaborated a calculation method. It is based on the formula for shear flexure given in the Eurocode EN 1992-1-1 (EC2, 2003), section 6.2.

According to this Standard, the formula is only applicable for single span members without shear reinforcement in the regions cracked by bending. Hollowcore elements exposed to fire are subjected to vertical web cracking over the full span of the slabs, also at the support region. For this reason, the shear flexure formula has been chosen as the basic model rather than the shear tension formula, which is only applicable for non-cracked sections. The formula has been adapted for the fire (i.e. elevated temperatures) situation. The validity has been demonstrated by a finite element analysis and a very good agreement with 9 test results where shear failure occurred (Van Acker, 2010).

The shear flexure equation for the fire situation is given as

$$V_{Rd,c,fi} = [C_{Rd,c} k (100 \rho_{l,fi} f_{c,fi,m})^{1/3} + k_1 \sigma_{cp,fi}] \cdot b_w d \qquad \text{Equation 7-4}$$

where,

$V_{Rd,c,fi}$ is the design shear strength in regions uncracked in flexure in fire

$C_{Rd,c}$ = $0.18/\gamma_c$ (γ_c is partial safety factor for concrete)

k = $1 + \sqrt{\frac{200}{d}} \leq 2.0$ where d is measured in mm

$\rho_{l,fi}$ is the force-equivalent ratio of longitudinal reinforcement $\left(= \frac{\sum F_{R,a,fi}}{500} \frac{1}{b_w d} \right)$

$F_{R,a,fi}$ is the force capacity of prestressing and ordinary reinforcement anchored at the support: $F_{R,a,fi,p} + F_{R,a,fi,s}$)

where, $F_{R,a,fi,p}$ is the force capacity of the prestressing steel anchored at

$$\text{the support} = \min \left(A_p \frac{x f_{bpd,fi}}{\alpha_2 \phi}; A_p 0.9 f_{pk} k_p(\theta) \right)$$

where, A_p is the area of a prestressing tendons

x is the anchorage length of the tendon for the considered section

$f_{bpd,fi}$ is the bond strength for anchorage of the tendon at elevated temperatures $(= f_{bpd} = \eta_{p2} \eta_1 f_{ctd})$

where, η_{p2} is 1.2 for 7- wire strands

η_1 is 1.0 for good bond conditions, or is 0.7 otherwise

f_{ctd} is design tensile strength

α_2 is 0.25 for circular tendons or, 0.19 for 3- or 7-wire strands

ϕ is the diameter of strand

f_{pk} is the characteristic tensile strength of prestressing steel

$k_p(\theta)$ is the strength reduction factor for the prestressing steel at temperature θ, according to EN 1992-1-2, clause 4.2, 4.3

$F_{R,a,fi,s}$ is the force capacity of ordinary reinforcement anchored at the support ($= A_s f_{yk} k_s(\theta)$)

A_s is the cross sectional area of reinforcement

f_{yk} is the characteristic yield strength of reinforcement

$k_s(\theta_m)$ is the strength reduction factor for the ordinary reinforcement at temperature θ_m, according to EN 1992-1-2, clause 4.2, 4.3

$f_{c,fi,m}$ is the average strength of concrete at elevated temperature ($f_{c,fi,m}$ can be taken equal to the strength of concrete for the temperature at mid height of the web)

k_1 = 0.15

$\sigma_{cp,fi}$ is the average stress on the concrete section for fire condition

$$= \min\left(k_p(\theta)\sigma_{cp,20}; \frac{F_{R,a,fi,p}}{A_c}\right)$$

where, $\sigma_{cp,20}$ is the concrete stress due to prestressing force at normal temperature

A_c is the concrete section area

b_w is the total web width

d is the effective depth at ambient temperature

Using the above calculation method the shear capacity at any temperature can be estimated if the geometrical and mechanical properties of the material/member are known. Table 7.1, derived by Van Acker (2010), lists the shear capacity values for hollowcore units for different slab thicknesses and load ratio as a function of the required fire resistance. For instance, for 200mm hollowcore slabs, if the applied shear force does not exceed 65% of the design shear force in normal temperature, no shear failure is likely to happen for 60 minutes. However, the 60 minutes does not exclude the possibility of failure. Even though shear failure may not happen during 60 minutes, flexural bending failure could happen such that a reduced fire resistance time is possible.

Table 7.1 Shear capacity of hollowcore slabs for different fire ratings as a percentage of cold shear strength (Van Acker, 2010)

	Slab depth (mm)				
	160	200	240-280	320	360-400
FRR 60	70	65	60	60	55
FRR 90	65	60	60	55	50
FRR 120	60	60	55	50	50

* FRR: fire resistance rating
** Note: the values of Table 7.1 are given for prestressed hollowcore slabs with strands cut at the ends of the elements, and a section of 1.88 cm²/m of longitudinal tie reinforcement at the support

7.4 Anaysis of shear capacity at elevated temperatures

The main purpose of this section is to evaluate the shear capacity of hollowcore slabs subjected to fire. The results obtained from the above two equations (7-2 and 7-4) are compared and applied to simply supported 200, 300 and 400 mm thick hollowcore slabs.

7.4.1 Hollowcore slabs

In order to investigate the shear capacity predicted by the two different equations, shear capacities of 200, 300, and 400 deep hollowcore slabs (see Figure 2) are calculated and compared. The concrete compressive strength for all hollowcore slabs is 45 MPa, and the strength of the stress relieved 7-wire prestressing strands is 1.87 GPa.

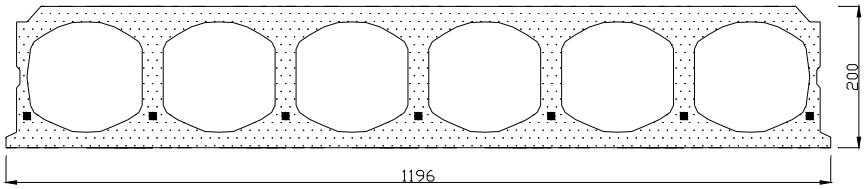

(a) 200 mm

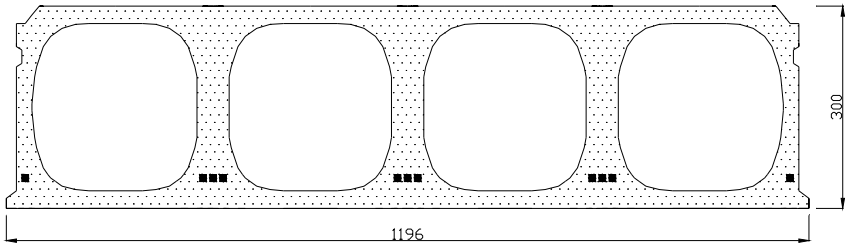

(b) 300 mm

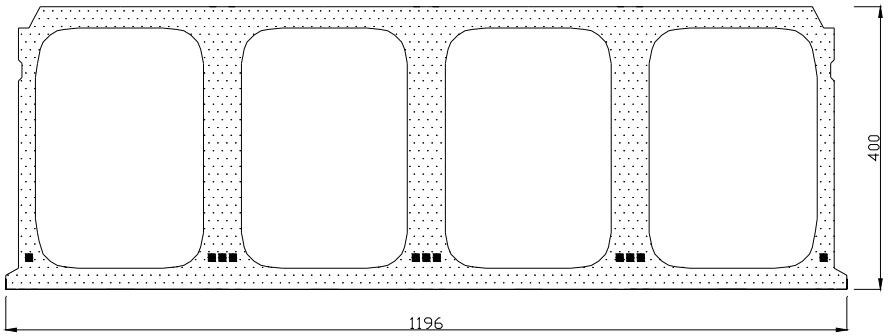

(c) 400 mm

Figure 7.6 Cross section of hollowcore slabs analysed

7.4.2 Heat transfer analysis of hollowcore slabs

The nonlinear finite element analysis program, SAFIR, is used to perform the thermal analyses for the cross sections of a prestressed hollowcore unit in a Standard ISO 834 fire. In the thermal analysis of the SAFIR program, triangular (3 nodes) and quadrilateral (4 nodes) solid elements are used to define the cross

section of the structure. The heat transfer analysis of a prestressed hollowcore slab, taking into account cavities, is crucial because a hollowcore slab has some voids and these voids play an important role in temperature distribution. Therefore convection at the boundaries and radiation in the internal cavities of the cross section are considered. Figure 7.7 shows the thermal gradients across the depth of three different hollowcores at 120 minutes into Standard ISO 834 fire exposure. The temperature at 1 inch (25.4 mm) above the bottom of the 200, 300 and 400 mm thick slabs at different times are obtained from SAFIR thermal analysis results, and compared with the temperatures predicted by PCI guideline (Gustaferro, 1989) and Wickström's formula (Buchanan, 2001) (see Table 7.2). As can be seen, the SAFIR thermal analysis, the PCI method and Wickström's formula give similar temperatures. Even though the PCI method seems to give reasonable prediction of temperature distribution in hollowcore slabs, it covers only a limited depth, and cannot be used to calculate the temperature at the middle of the web. In addition, Wickström's formula is appropriate for linearly temperature increased cross section, but is not proper for hollowcore slab cross section that is the temperature distribution is not uniform across the height. The mid-web temperature obtained from SAFIR thermal analysis, therefore, is used for the calculation of shear capacity using equation 7-4. The temperatures of the prestressing strands and at the middle of the web predicted by SAFIR for the slabs are plotted in Figure 7.8.

Table 7.2 Temperature (°C) comparisons of hollowcore slabs at 25.4mm (= 1in.) height

	Time (minutes)			
	30	60	90	120
200	298 °C	523 °C	629 °C	695 °C
300	274 °C	477 °C	599 °C	678 °C
400	277 °C	479 °C	592 °C	662 °C
PCI document (Gustaferro, 1989)	301 °C	460 °C	560 °C	626 °C
Wickström's formula (Buchanan, 2001)	289 °C	454 °C	563 °C	645 °C

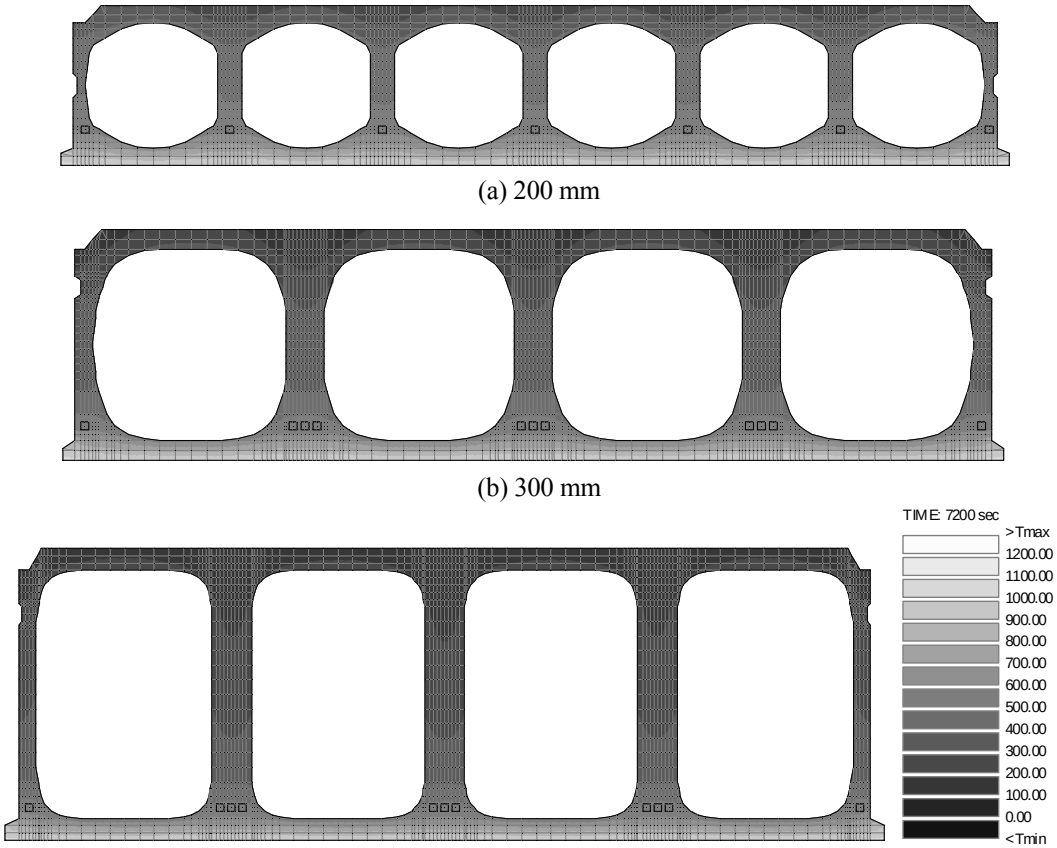

(a) 200 mm

(b) 300 mm

(c) 400 mm

Figure 7.7 Temperature distribution of 200, 300, and 400 deep hollowcore unit at 120 minutes

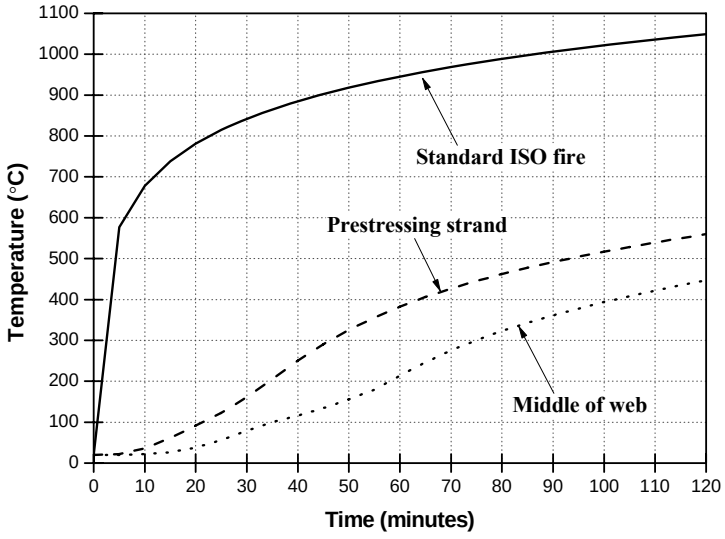

(a) 200 mm

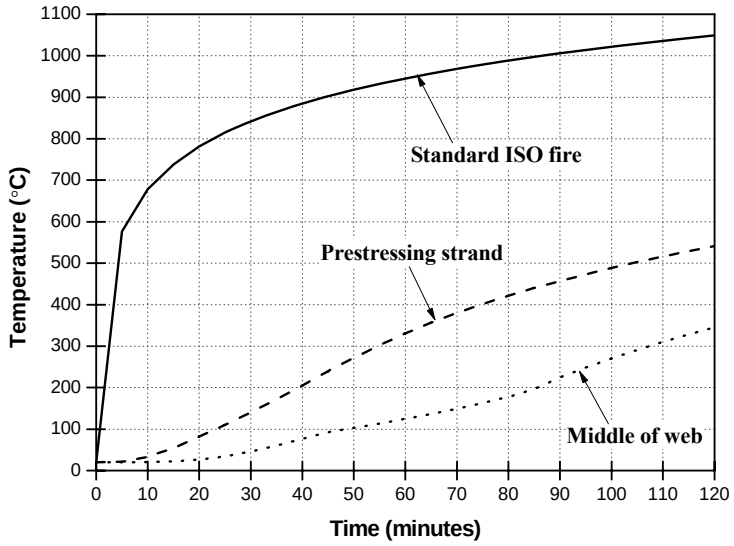

(b) 300 mm

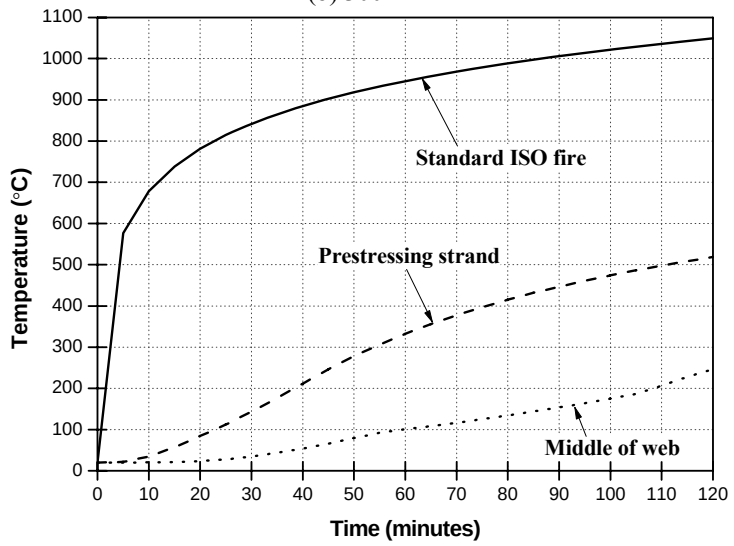

(c) 400 mm

Figure 7.8 Temperature development of prestressing strands and the middle of the web

7.4.3 Calculation of shear capacity

In the calculation of shear capacity, equations 7-2 and 7-4 are used. In equation 7-2, f_{py} (t) is calculated with the reduction factor in accordance with Table 3.3 of Eurocode EN 1992-1-2 (EC2, 2004). Specimen details used for modified FIP method are summarised in Table 7.3. In the application of equation 7-4, it is assumed that prestressed hollowcore slabs have the strands cut at the ends of the elements and a section of 1.88 cm²/m of longitudinal tie reinforcement anchors the units at the support. In addition, the strength reduction factor of reinforcement is not applied as the reinforcement is encased in concrete and located at the mid-depth

of the hollowcore units. For the average strength of concrete ($f_{c,fi,m}$), the strength of concrete for the temperature at the mid height of the web is used. Table 7.4 summarises the specimen details used for the modified Eurocode 2 method.

Table 7.3 Specimen details for modified FIP method

Depth mm	b_w mm	d mm	ξ m	A_p mm^2	$f_{py}(20^\circ C)$ MPa	f_c MPa
200	180	155	1.445	700	1860	50
300	220	255	1.345	1100	1860	50
400	246	355	1.245	1100	1860	50

Table 7.4 Specimen details for modified Eurocode method

Depth mm	$C_{Rd,c}$	k mm	k_1	b_w mm	d mm	A_p mm^2	f_{pk} MPa	A_s mm^2	f_{yk} MPa	A_c mm^2	f_{ck} MPa
200	0.12	2.0	0.15	180	155	700	1860	225.6	450	121x10^3	45
300	0.12	1.88	0.15	220	255	1100	1860	225.6	450	201x10^3	45
400	0.12	1.75	0.15	246	355	1100	1860	225.6	450	235x10^3	45

In terms of both equations 7-2 and 7-4, the shear capacity of the hollowcore slabs is calculated at different times using the analytically predicted time-temperature relationships. Figure 7.9 shows the comparisons of shear capacities of the three different height hollowcore slabs as predicted by equations 7-2 and 7-4. In the 200 mm thick hollowcore slab, the shear force predicted by equation 7-4, which is based on Eurocode 2, is higher than equation 7-2, based on FIP, for up to 70 minutes, but it then drops rapidly with time due to the reduction of concrete strength with increasing time. For the 300 mm and 400 mm hollowcore slabs, the graphs show a similar pattern. Van Acker's suggested allowable shear capacities for a 60 minutes fire ratings are also shown in Figure 7.9 for comparison.

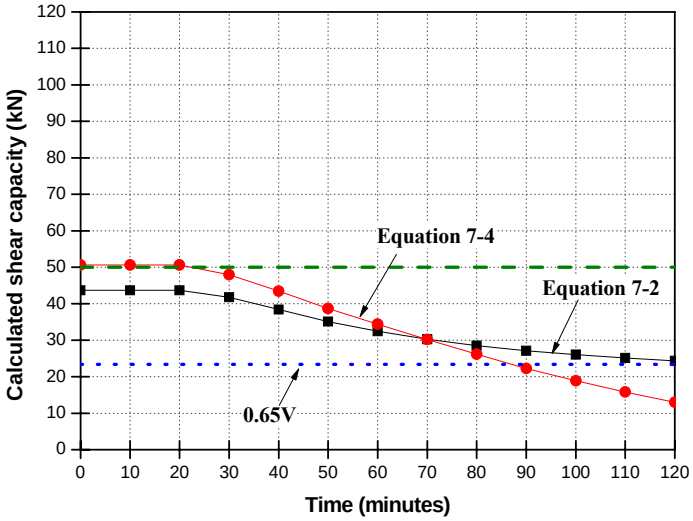

(a) 200 mm

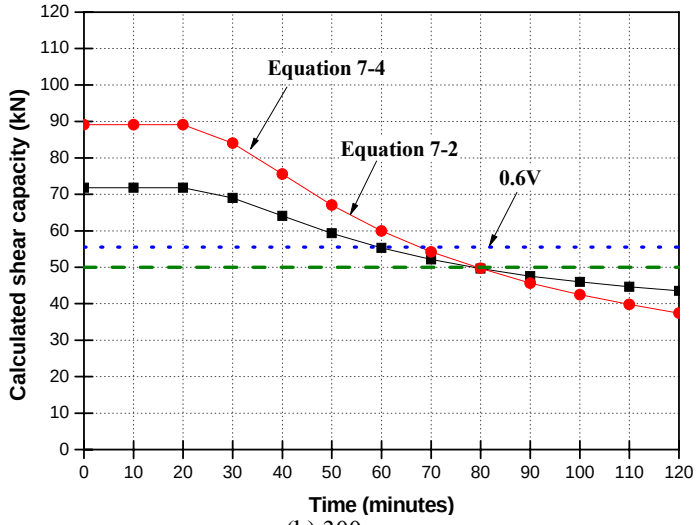

(b) 300 mm

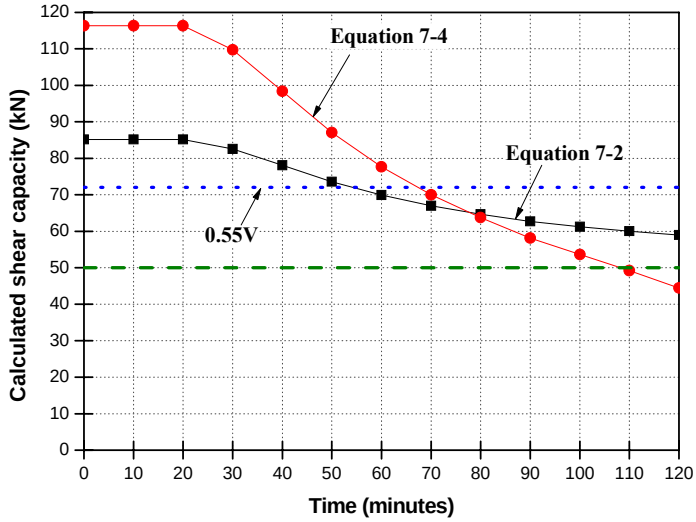

(c) 400 mm

Figure 7.9 Comparison of shear capacity for different methods

If a 50 kN shear force was applied to each of the 200, 300, and 400 mm deep hollowcore slabs, Figure 7.9 shows that the 200 mm hollowcore would have a 20 minute fire resistance based on equation 7-4, whereas equation 7-2 would predict that a shear force of this magnitude exceeded the ambient strength of the slab. For the 300 mm deep slab, equations 7-2 and 7-4 both predict the same fire resistance of just under 80 minutes. In the case of the 400 mm deep hollowcore, equation 7-2 predicts a fire resistance time greater than 120 minutes, while equation 7-4 predicts a shear failure after only 110 minutes of fire exposure.

In tests by Jensen (2005), 265 mm hollowcore slabs were used to ensure fire resistance of 60 minutes for different load levels of 65, 75 and 80% of the ultimate design shear capacity in cold conditions. The hollowcore slabs were exposed to standard fire for up to 60 minutes, followed by a 90 minute cooling phase. The test results show that hollowcore slabs loaded to 80% of ultimate design shear capacity failed at around 45 minutes while the other two other tests were completed without any failure.

These hollowcore slabs were modelled using the SAFIR program. Figure 7.10 shows the results between experiments and numerical predictions for different load levels. Even though the numerical analyses are well matched to the maximum vertical deflection with respect to experimental results, the shear failure prediction for the unit loaded to 80% of its cold capacity was not possible since SAFIR cannot model shear behaviour.

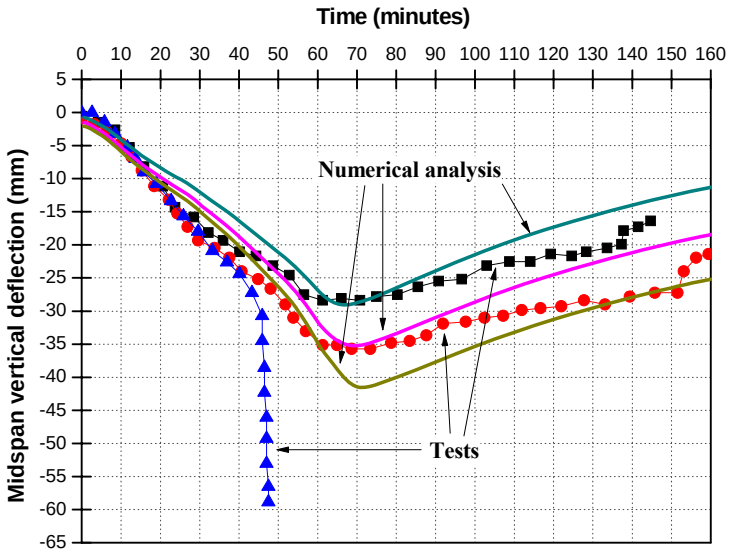

Figure 7.10 Comparisons between experimental and numerical results

The procedure for determining the shear capacity and shear failure time of hollowcore slabs based on the modified Eurocode 2 equation (i.e. equation 7-4), is illustrated by the flow chart of Figure 7-11. This procedure has been used to derive Figure 7.12 showing the comparison between shear capacity and shear force. In this figure, the hollowcore slab with 80% of ultimate design shear capacity showed a shear failure time of around 49 minutes (compared with 45 minutes in the test), while the hollowcore slab with 75% of ultimate design shear capacity failed at around 56 minutes (but did not fail in the tests). On the other hand, the hollowcore slab with 65% of ultimate design shear capacity indicates more than 70 minutes resistance.

From Table 7-1, a 265 mm deep hollowcore slab would have a 60 minute fire resistance based on shear providing the applied shear force is no greater than 60% of the shear capacity at ambient temperature. By comparison with Jensen's test results in figure 7.10, the values of Table 7-1 are more conservative and should provide a safe limit on the temperature dependent shear capacity.

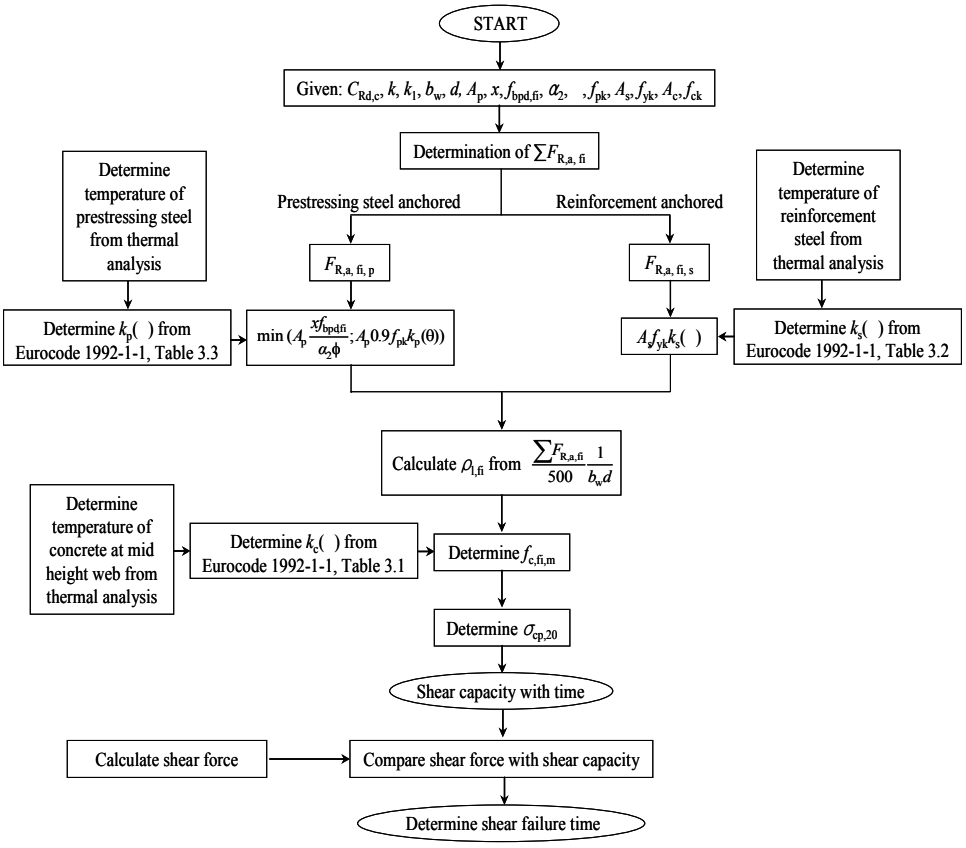

Figure 7.11 Procedure for determining shear capacity and shear failure time of hollowcore slabs

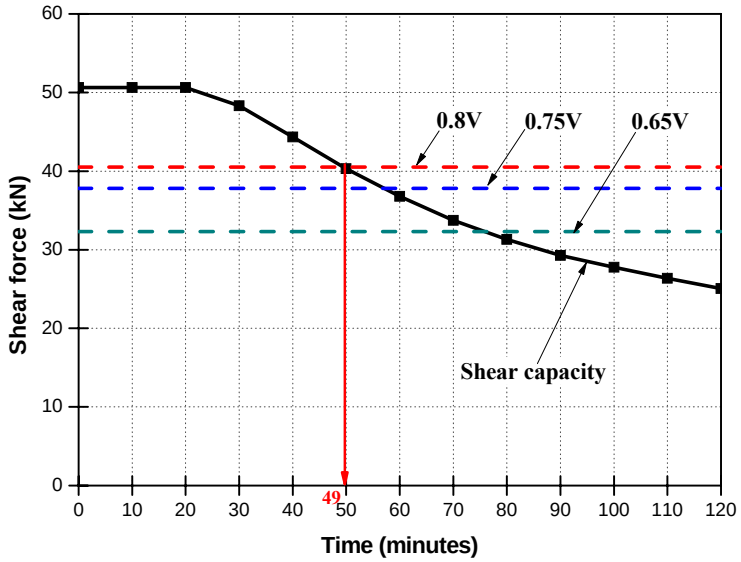

Figure 7.12 Prediction of shear failure for the tests of Jensen (2005) using Equation 7-4

7.5 Splitting resistance of hollowcore slabs in fire

Product Standard EN 1168 on hollowcore units (2004) includes a verification method to avoid the splitting of hollowcore slabs due to high splitting stress. According to the Standard, the splitting stress σ_{sp} shall satisfy the following conditions:

$$\sigma_{sp} \leq f_{ct}$$

where,

f_{ct} is the value of the tensile strength of the concrete deduced at the time that the prestressing is released on the basis of tests

The splitting stress is given as

$$\sigma_{sp} = \frac{P_0}{b_{wi} e_0} \times \frac{15\alpha_e^{2.3} + 0.07}{1 + \left(\frac{l_{pt1}}{e_0}\right)^{1.5} (1.3\alpha_e + 0.1)} \quad \text{and} \quad \alpha_e = \frac{(e_0 - k)}{h} \qquad \text{Equation 7-5}$$

where,

P_0 is the initial prestressing force just after release in the considered web

b_{wi} is the thickness of an individual web

e_0 is the eccentricity of the prestressing steel

l_{pt1} is the lower design value of the transmission length

k is the core radius taken equal to the ratio of the section modulus of the bottom fibre and the net area of the cross section (w_b / A_c)

h is the thickness of a slab

According to Eurocode 2, the transmission length which is the cross section where the prestress is fully introduced over the total concrete cross section is obtained from

$$l_{pt} = \alpha_1 \alpha_2 \phi \frac{\sigma_{pm0}}{\eta_{pl} \eta_1 f_{ctd(t_{rel})}} \qquad \text{Equation 7-6}$$

where,

α_1 is 1.00 (gradual release)

α_2 is 0.19 (7-wire strands);

ϕ is the diameter of a strand;

σ_{pm0} is the stress in the tendon just after release;

η_{pl} is 3.2 (7-wire strand);

η_1 is 1.0 for lower strands and for upper strands in slabs not thicker than 265mm;

η_1 is 0.7 for upper strands in slabs with a thickness of 320mm or more;

t_{rel} is the age of the concrete at release;

Figure 7.13 shows a wide range of test results for the reduction of the tensile strength at elevated temperatures (Fellinger, 2004). In this figure, a large difference exists between the relative decrease of the tensile strength at elevated temperatures

obtained in flexural tests and in direct tension tests. Eurocode 2 (2002) gives a very rough estimate of the decrease of the tensile strength at high temperatures. It is assumed that the strength linearly decreases between 100-600 ^{o}C from 100 % of the strength at ambient temperature to zero, as shown in Figure 7.13.

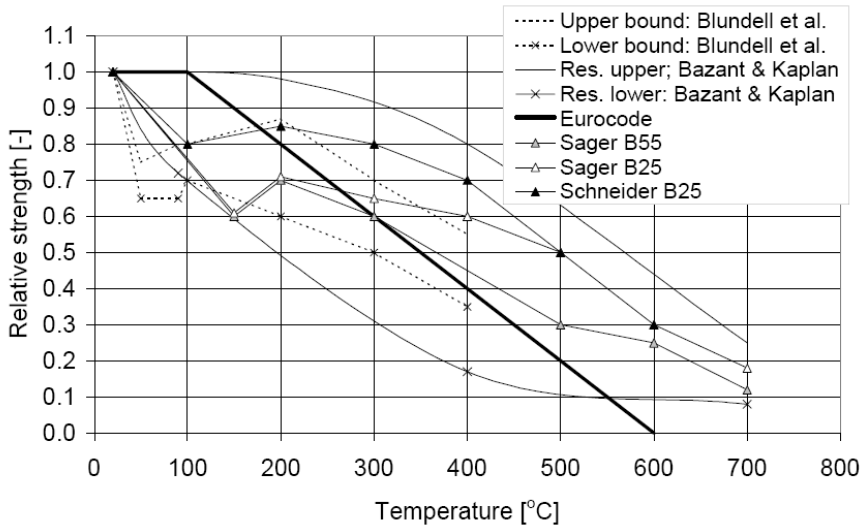

Figure 7.13 Various measurements of the splitting tensile strength of concrete at elevated temperatures (Fellinger, 2004)

Figure 7.14 shows the temperature development in hollowcore slabs at the middle of the web. In NZS 3101 (2006), the design principal tensile strength of the concrete, f_{dt}, is taken as $0.33\sqrt{f_c'}$. With the increase of temperature, the tensile strength at the middle of the web is reduced, as shown in Figure 7.15. Thus, the tensile strength of hollowcore slabs at the middle of the web eventually becomes lower than the splitting stress calculated using equation 7-5, which gives the splitting failure point. For example in Figure 7.15, splitting failure of the analysed 200 mm thick hollowcore slab could occur after about 75 minutes of fire exposure.

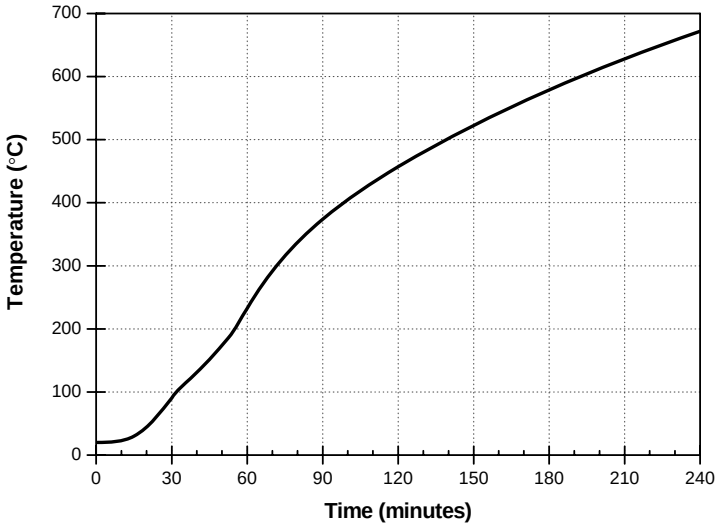

Figure 7.14 Temperature development of 200mm hollowcore web

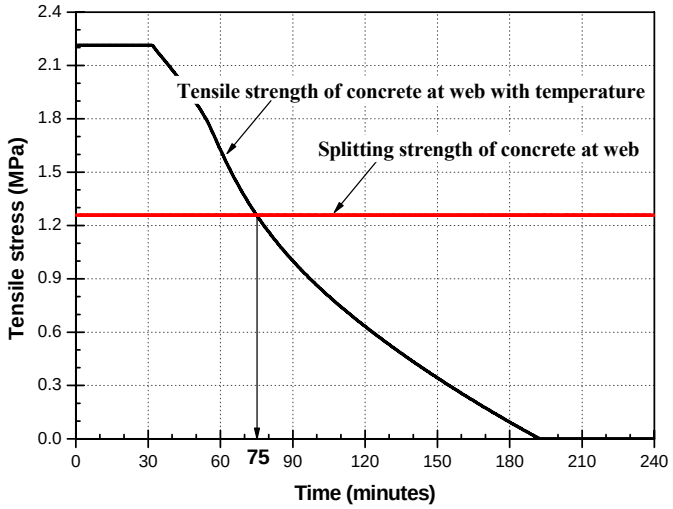

Figure 7.15 Tensile strength vs. splitting strength with time

7.6 Summary

Possible failure modes of simply supported hollowcore slabs in fire were reviewed. In addition, the failure modes which can occur in New Zealand situations were summarised. The available calculation models that calculate shear resistance of hollowcore slabs in fire were introduced and investigated for 200mm hollowcore slabs to determine shear capacity during a fire. Another equation that calculates splitting resistance of hollowcore slabs in fire due to prestressing was introduced and used to evaluate the splitting resistance of 200mm hollowcore slabs.

Deep hollowcore units can fail in shear and this should be taken into account. However, it is difficult to predict the shear capacity of hollowcore units at elevated temperature. Simple equations are preferred by structural engineers rather than having to conduct time-taking finite element analysis for each trial design. Simplified expressions from the literature are presented in this paper to calculate shear capacity of hollowcore slabs at elevated temperature. Using these expressions, the shear capacity can be calculated at different stages during a fire (if the time-temperature relationship is known/found/assumed), which can then be compared to the imposed shear force to predict if, and when, shear failure is likely to occur. The applications of these expressions are shown by applying them to 200, 300, and 400 mm thick hollowcore slabs to determine their shear capacities during fire. Alternatively, the recommendations of van Acker given in Table 7-1 could be used. An expression that calculates the splitting stress due to prestressing in hollowcore members is also introduced and compared with tensile strength of concrete in fire to predict splitting resistance of a typical 200 mm thick hollowcore slab.

Chapter 8

Numerical analysis of Single Tee Slabs Having Different Restraint Mechanisms

---

8.1 Introduction

Precast prestressed single tee slabs are typically supported on the bottom of the webs (Figure 8.1 (a)). They are also supported on a notched web (i.e., web hung) or flange (flange hung) in order to simplify the construction process (Hare *et al.,* 2009) (Figure 8.1 (b) and (c)). Due to the difference in concrete surface exposed to fire, the type of support condition plays a crucial role in the fire resistance of such flooring systems. As a result, concern has been raised with respect to the fire performance of single tee slabs particularly those with notched web or flange supports. This chapter, therefore, analytically investigates the structural behaviour of single tee floor system under the Standard ISO fire. A model of a single tee slab is first created in SAFIR and a sensitivity analysis of a simply supported slab with various prestress levels under a Standard ISO fire regime is carried out. Then, a series of analyses of single tee slabs with different restraint conditions such as web, notched web and flange supports as well as a wide range of axial restraint stiffness is performed. Figure 8.2 shows the organisation of Chapter 8.

(a) Web supported support (USA)

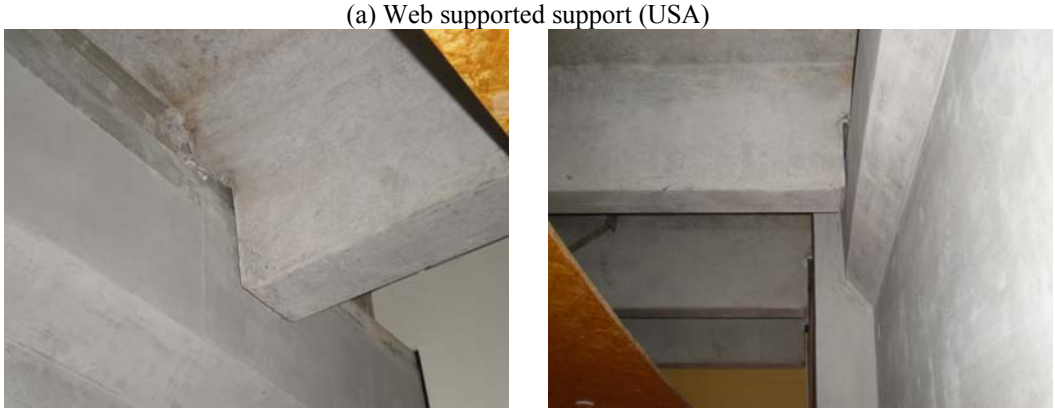

(b) Notched web support (Civil and Mechanical Engineering Building, University of Canterbury)

(c) Flange support (NZi3 Research Centre, University of Canterbury)

Figure 8.1 Various support conditions for single tee slabs

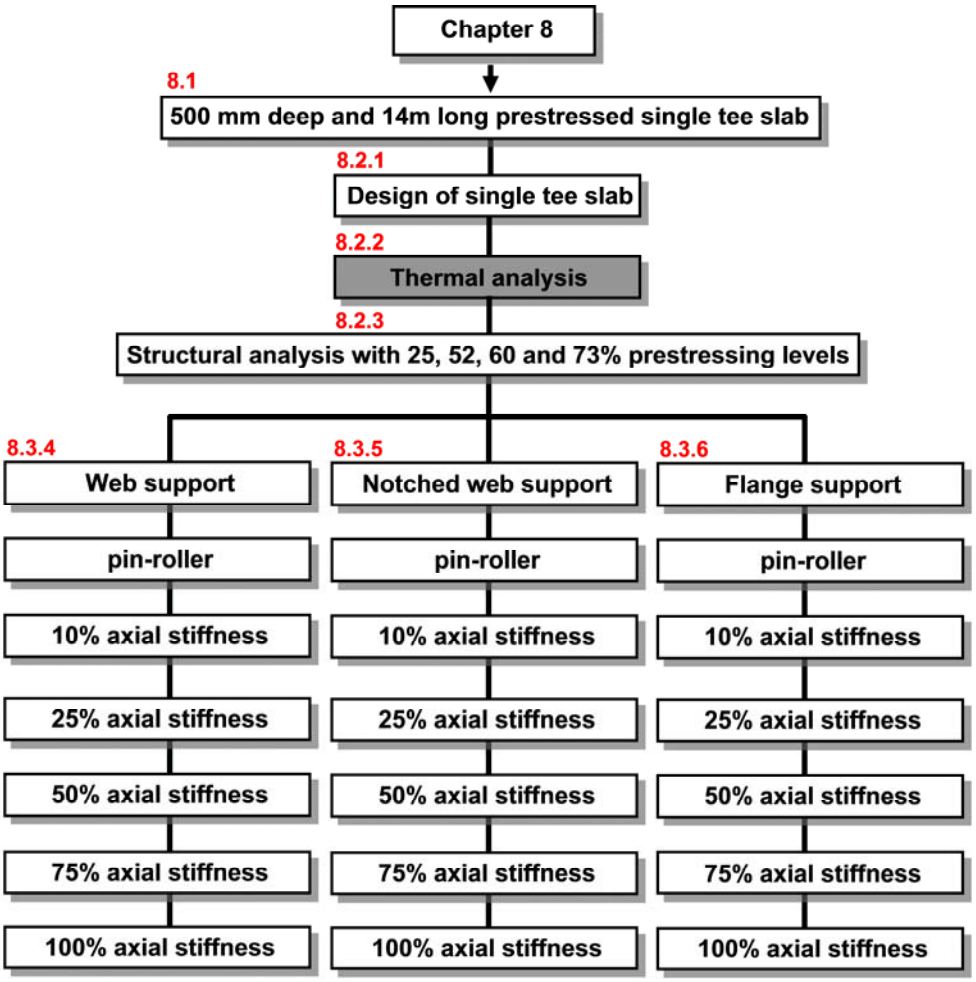

Figure 8.2 Organisation of Chapter 8

8.2 Single Tee slab

8.2.1 Design of a single tee slab at ambient temperature

For this preliminary analysis, a single tee slab of 14m span and 1.2m width, composite with a 75mm reinforced topping slab has been selected from the drawings of the Civil and Mechanical Engineering Building at University of Canterbury (Figure 8.3). The floor system incorporates cast-in-place reinforced concrete topping screed to act as a structural diaphragm and to provide a wearing surface. The single tee slabs were cut out of 500 double tee slabs. The depth of a precast prestressed concrete single tee slab selected is 500mm. The typical 333 mesh (75 x 75 x 6.40mm diameter bars) is used in the concrete topping slab. All relevant material properties are shown in the Table 8.1.

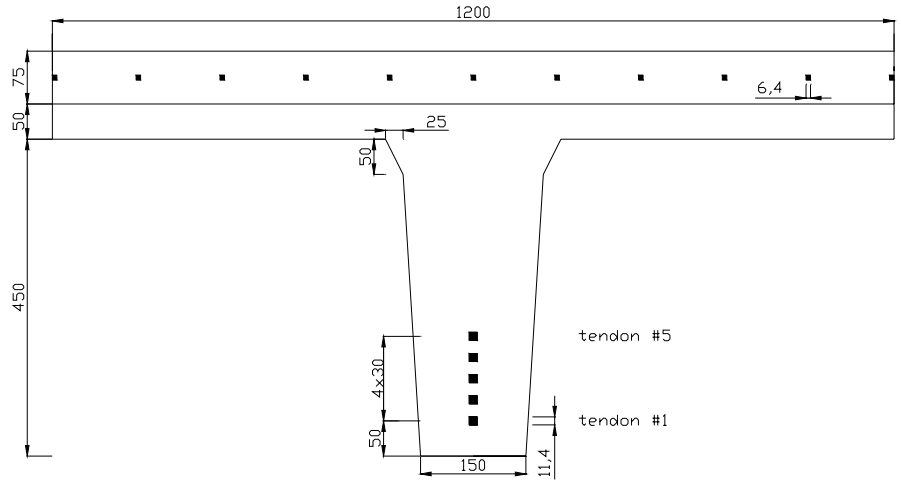

Figure 8.3 Cross section of a 500mm deep single tee slab

Table 8.1 Material properties of a 500mm deep single tee slab selected

500 single tee	
Self weight	4.25 kPa
Compressive strength	45 MPa
Prestressing strands	
Type	Stress relieved 7-wire strand
Strength	1.84 GPa
Prestressing level	73%
Cross sectional area/strand	100 mm^2
Reinforced concrete topping slab	
Concrete compressive strength	25 MPa
Reinforcement strength	450 MPa

Based on the building specification, a 500mm deep single tee slab with 75mm thick concrete topping can sustain a live load (Q) of 3.0 kPa under ambient conditions and it is assumed that there is a superimposed dead load of 0.5 kPa. The self-weight (G) of the slab is 4.25 kPa, as specified in Table 8.1. According to the New Zealand loading code (AS/NZS 1170, 2002), the load combination for the ultimate limit state condition in fire is 1.0G + 0.4Q, where G is the dead load and Q is the live load. The fire design load, therefore, is 5.65 kPa and this value is applied to the 500mm deep single tee slab.

In order to determine the required number of tendons with respect to a double tee slab, a hand calculation has been performed for constant eccentricity tendons as given in Appendix D. In addition, the manufacturer provides details of a precast double tee slabs with two options for the required number of tendons

(Appendix E). In both calculations, ten strands of 12.9mm diameter have been used for a 500mm deep double tee slab. Therefore, five prestressing strands were applied for the 500mm deep single tee slab.

8.2.2 Thermal analysis of a single tee slab

In order to numerically investigate the structural behaviour of a precast prestressed single tee slab under the Standard ISO fire, thermal analysis was carried out to examine the temperature across the single tee slab. In this analysis, a 4 hour ISO Standard fire was used without any decay phase. Due to symmetry, only one half of the cross section was analysed. The variation of the temperature distributions obtained from the thermal analysis was used for the structural analysis. The temperature contours of the 500mm deep single tee slab at 60, 120, 180 and 240 minutes, obtained from SAFIR thermal analysis, are shown in Figure 8.4.

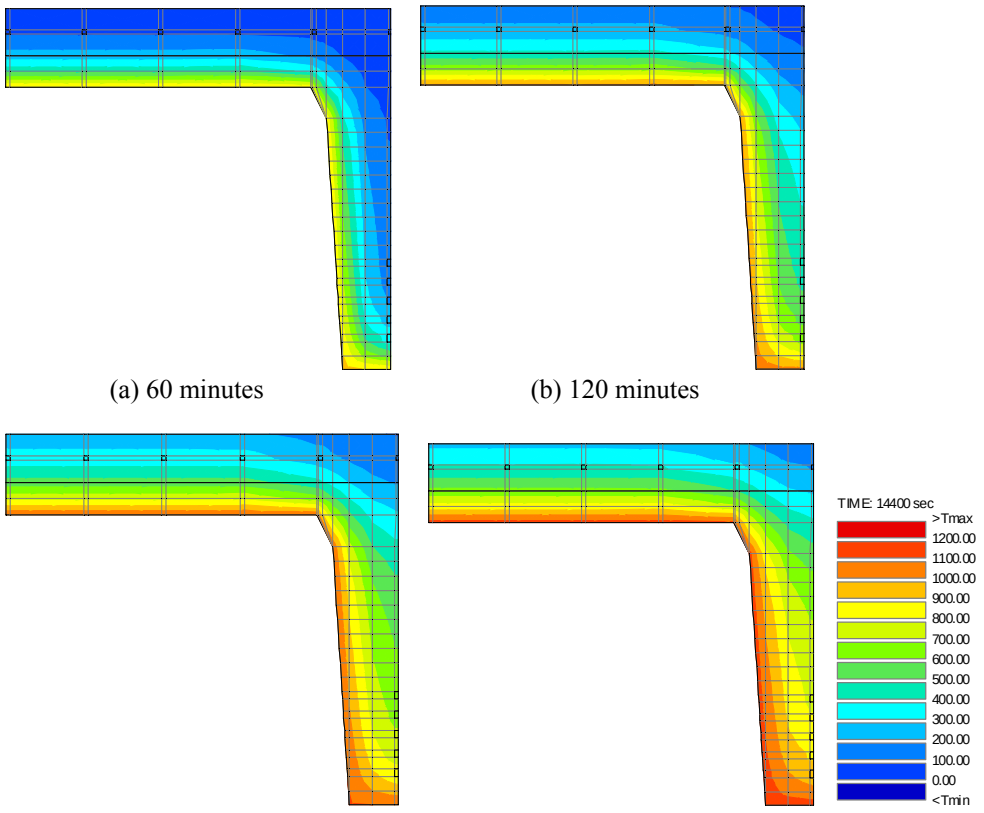

(a) 60 minutes (b) 120 minutes

(c) 180 minutes (d) 240 minutes

Figure 8.4 Temperature contours of the 500mm deep single tee slab at 60, 120, 180 and 240 minutes

It is noted that the concrete topping slab including reinforcement remains below 400 °C during 180 minutes of the ISO fire. In this temperature range, the strength of the material does not decrease substantially. Figure 8.5 shows the temperature assessment at each tendon as well as the ISO 834 fire curve. The rectangular symbol represents the Standard ISO fire up to 4 hours.

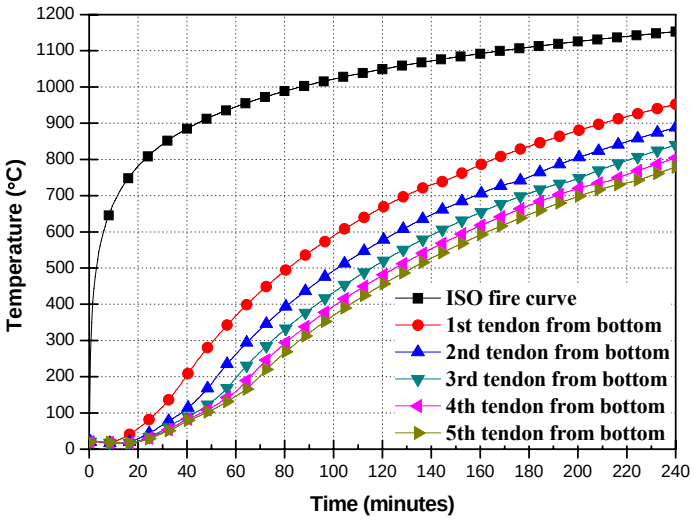

Figure 8.5 Temperature variations with time for each prestressing tendon

8.2.3 Structural analysis of a single tee slab

A single tee slab of 14m length was modelled as a beam using ten 3D beam finite elements and a 3D analysis was conducted (Figure 8.6). The precast single tee slab is assumed to be simply supported on the bottom surface of the webs. The half cross section of the single tee slab is shown in Figure 8.4 and the slab was loaded with a uniformly distributed load along its length.

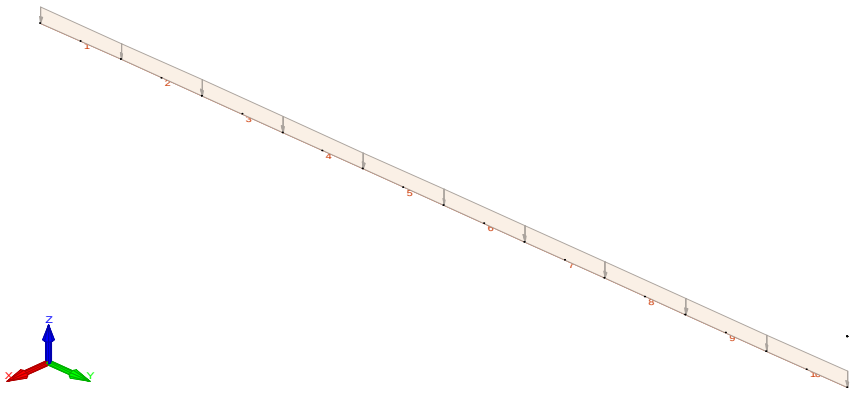

Figure 8.6 Discretisation of the single tee slab with SAFIR for the structural analysis

Even though it is not easy to confirm the level of prestress in precast prestressed units (PCFOG committee, 2009), the level of prestress can be obtained with certainty from manufacturers or literature. In the design of a 500mm deep single tee slab, the manufacturer provides a prestress level of 73% of the ultimate strength of 184 kN. In addition, a 52% prestress level can be found in literature with regard to the double tee slab (Franssen, 1997). In order to examine the effect of prestress level with regard to fire resistance, numerical analyses on 25, 52, 60, 73% prestress level of 184 kN have been carried out. Figure 8.7 shows a comparison of numerical analysis results of a 500mm deep single tee slab. It can be seen that at the beginning the midspan deflection of the single tee slab was upward due to the prestressing tendons at the bottom forcing the slab to bend upwards and the applied load at ambient temperature is not enough to bend the slab in sagging mode. The midspan deflections of the single tee slab did not differ much for different prestress levels and the analyses stopped at around 105 minutes while the required minimum Fire Resistance Rating (FRR) of the slab is 60 minutes.

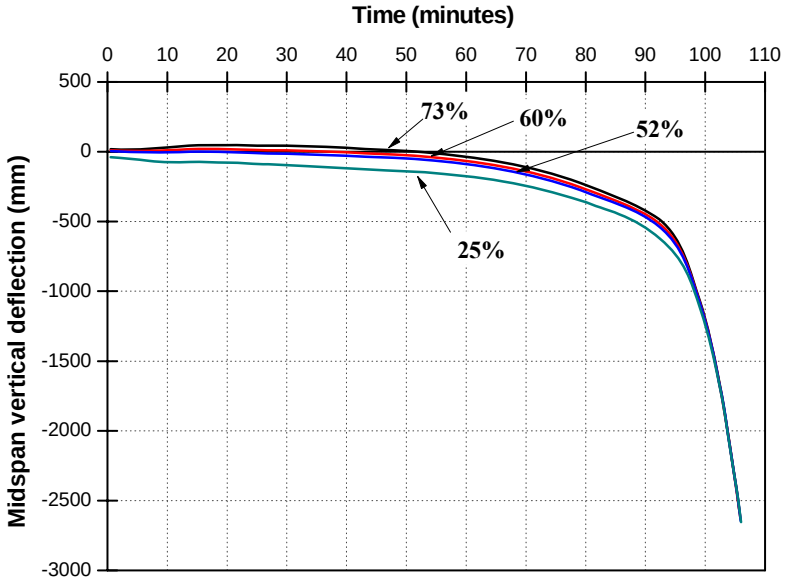

Figure 8.7 Comparison of midspan vertical deflections for various prestressing levels

Figure 8.8 shows the stress history of the prestressing tendons used in the analyses with different prestress levels. Although, depending on the prestress level, the developed stresses at the beginning were different, tendon stresses at the end of

the analyses did not show much difference. For all cases, the tendon stresses increased around 20 minutes due to the effect of thermal gradients, then decreased due to the reduction of the yield strength at higher temperature. As can be seen in the plots, all tendons seemed to reach their yield limits towards the end of the analysis and the analyses stopped due to the failure of tendons #1 and #2. From Figure 8.8, it can be concluded that the stress level of tendons in the later stages of fire does not depend on the prestress level.

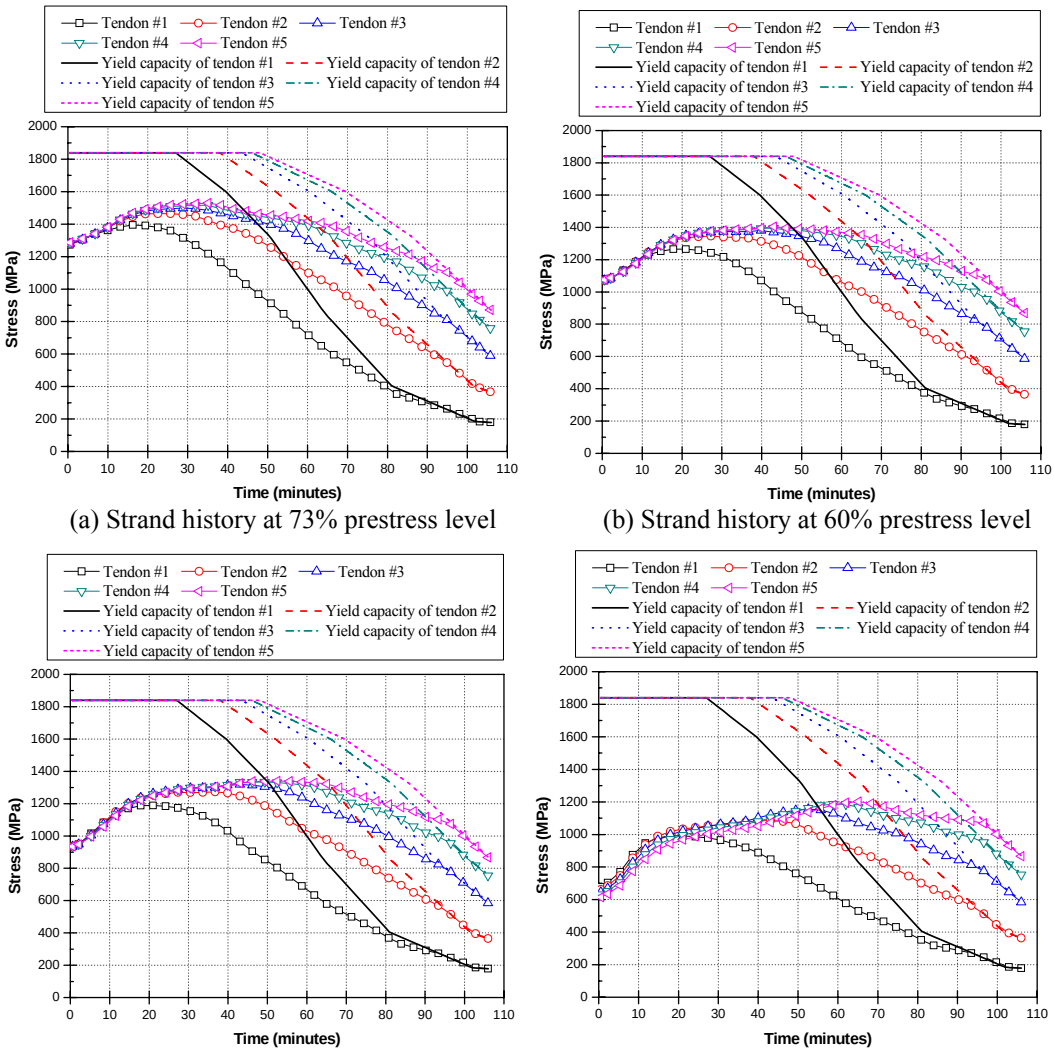

(a) Strand history at 73% prestress level

(b) Strand history at 60% prestress level

(c) Strand history at 52% prestress level

(d) Strand history at 25% prestress level

Figure 8.8 Strand history of a single tee slab at each prestress level

8.3 Pin supported prestressed single tee slabs

In the previous section, the 500mm deep single tee slab was designed and assessed using simply supported end conditions with respect to various prestress levels under the Standard ISO fire. In this section, the fire performance of the single tee slab will be investigated in terms of three different restraint mechanisms, such as web, notched web and flange supports.

8.3.1 Restraint mechanisms

Longitudinal restraint against thermal elongation often develops in single tee slabs during fire and amplifies the effects of continuity. When a fire occurs beneath a single tee slab, the heated portion tends to expand, but it is resisted by adjoining members. As a result, the degree of axial restraint effect can vary depending on the adjoining member conditions. Figure 8.9 shows the possible adjoining members against fire.

8.3.2 Analysis conditions

As shown in Table 8.2, various boundary conditions were used to simulate the interaction between single tee slabs and the supporting structure. Since the aim was to examine the restraining effect with respect to different types of supports, the 500mm deep single tee slab designed in Section 8.2 was used in this analysis series as well. For all cases, the end face of the single tee slabs was represented by rigid elements. In addition, the node line of beam elements was taken to coincide with the centroidal axis of the single tee slabs. Restraints between a single tee slab and a supporting structure need to account for both rotational and axial stiffness. However, in this study, the rotational stiffness was conservatively assumed to be zero. In reality it can be assumed that a single tee slab restrained by rigid surrounding structures can experience a high axial restraint stiffness, close to 100% as specified in Table 8.2. At the other extreme, 1% axial stiffness as well as 0%

axial stiffness (same as a pin-roller support condition) were considered in the parametric analyses.

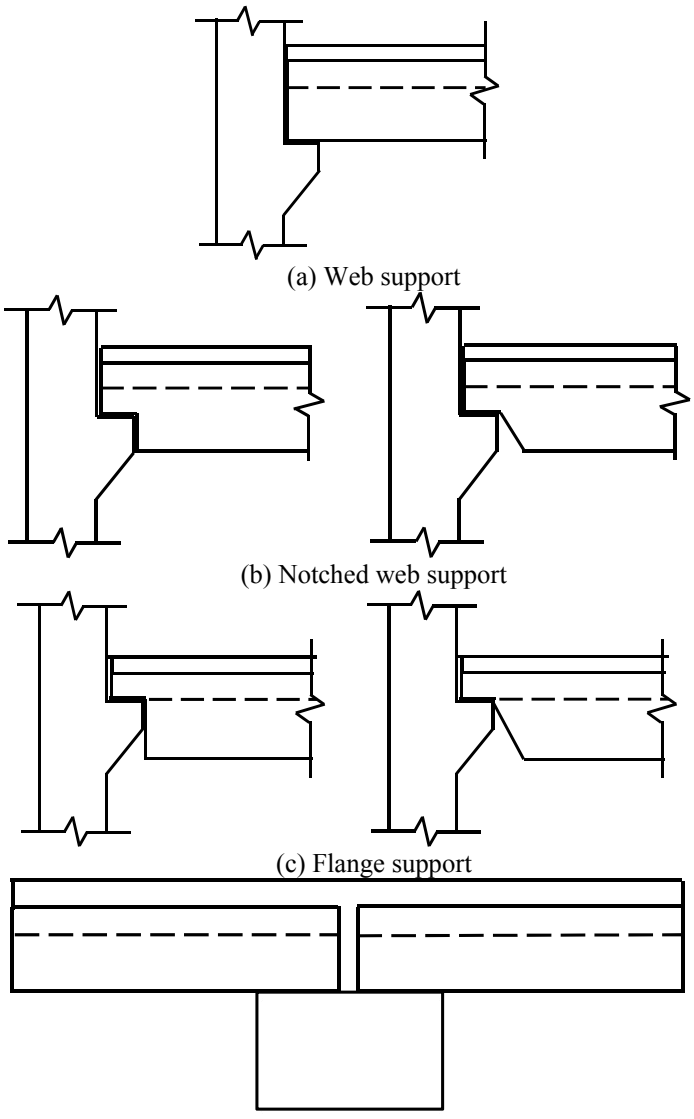

(a) Web support

(b) Notched web support

(c) Flange support

(d) Continuity

Figure 8.9 Possible restraint mechanisms

Table 8.2 Analysis model and spring stiffness used

Support condition	Analysis model	Spring stiffness
Web support	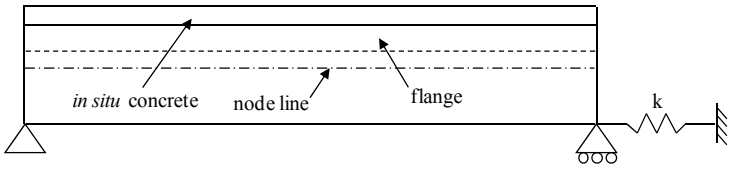	0 % (pin-roller) 1% 5 % 10 % 25 % 50 % 75 % 100 %
Notched web support	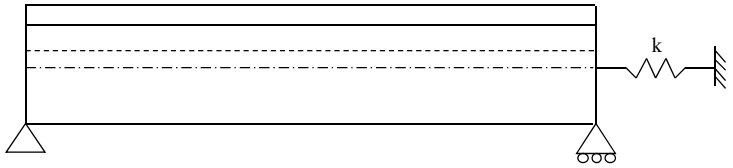	0 % (pin-roller) 1% 5 % 10 % 25 % 50 % 75 % 100 %
Flange support	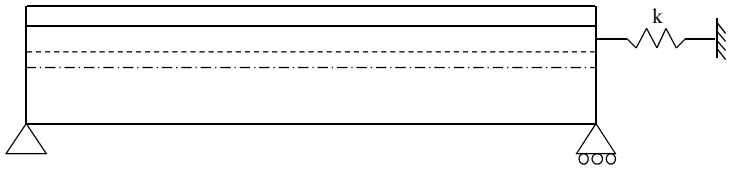	0 % (pin-roller) 1% 5 % 10 % 25 % 50 % 75 % 100 %

8.3.3 Axial restraint stiffness

As explained above, the single tee slabs were modelled with different axial spring stiffnesses. The axial restraint stiffness (k) of the single tee slabs ranged from zero to 100%. The restraint axial stiffness can be calculated as follows:

$$k = \frac{\text{Axial stiffness of adjoining structure}}{\text{Axial stiffness of single tee slab}} \times 100\% \qquad \text{Equation 8-1}$$

For modelling single tee slabs with axial restraint stiffness, spring elements as well as beam elements were used. In the SAFIR program, a spring element is defined by its cross sectional area and the material type as well as the length between its two end nodes. With respect to modelling of spring elements, modified steel material properties were used and the value of elastic modulus was 30.58MPa. In order to avoid failure of spring elements due to thermal expansion, the length between two nodes was assumed to be 500mm.

8.3.4 Web support

The single tee slabs with web support are supported directly on the bottom surface of the web. In the modelling of the single tee slab with web support, an axial restraint spring was located at the bottom of the web in order to capture the restraint effects.

Figure 8.10 shows the comparison of midspan vertical deflections of a single tee slab with various web support conditions. In the case of a single tee slab with 100% axial restraint, the slab remained in hogging shape until the end of the analysis at 197 minutes. The single tee slabs with 75% axial restraint stiffness indicated similar trends up to 85 minutes and then showed a sudden downward deflection due to snap-through of the slab. When the axial restraint stiffness was less than 50 %, the slab behaved in a similar manner to the pin-roller slab (0% axial restraint stiffness) even though the period of the hogging deflection was slightly higher for 25% and 50% axial restraint stiffness cases.

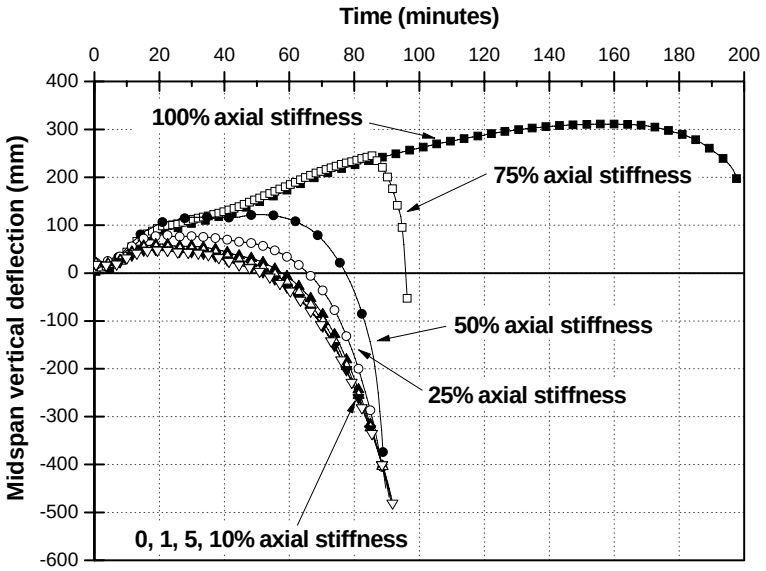

Figure 8.10 Midspan vertical deflections of a single tee slab with web support Condition

The axial force developed in the end restraint spring for a single tee slab supported on the web under a Standard ISO fire is shown in Figure 8.11 as a function of fire exposure time. The magnitude of fire induced axial force varies depending on the stiffness of the axial restraint except for the 100% axial restraint stiffness. The spring element reached its axial capacity in all cases except for the 100% axial restraint case in which the restraining spring did not reach the capacity (603.5kN). This can be attributed to the fact that the axial force of a single tee slab with 100% restraint stiffness is too high. In this case, the failure of the prestressing strands may have led to the failure of the slab. This is investigated further below.

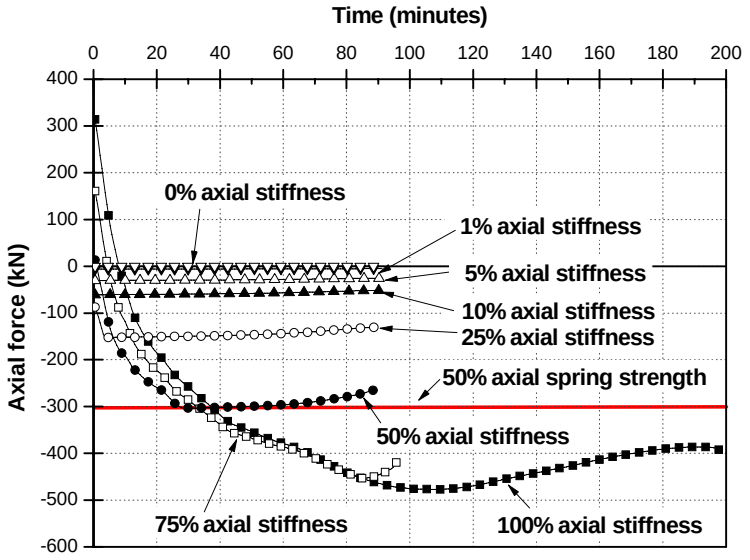

Figure 8.11 Axial force of a single tee slab with web support condition

In order to investigate the failure of prestressing strands of a single tee slab, the deflected shape has been plotted against time. In Figure 8.12, the deflected shape at different time steps, such as the beginning of the analysis (0.5 minutes), the middle of the analysis (102 minutes) and the end of the analysis (197 minutes) is extracted. At the beginning of the analysis, a single tee slab with 100% axial restraint stiffness slightly deflected downward as the prestress of the tendons was not fully developed. After that, with the development of the prestress, the single tee slab deflected upward up to 102 minutes when the maximum axial force developed in the spring (Figure 8.11). Even though the axial force did not reach the axial capacity at the end, the single tee slab started to deflect downwards in the middle (Figure 8.12(c)).

(a) At the beginning of analysis (0.5 minutes)

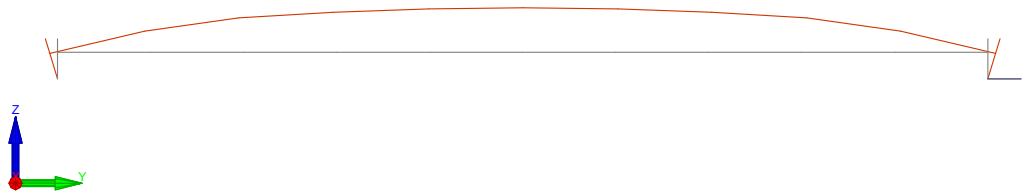

(b) In the middle of analysis (102 minutes)

(c) At the end of analysis (197 minutes)

Figure 8.12 Deflected shape at different times for 100% axial restraint stiffness, scale factor = 5

Figure 8.13 shows the deflected shape of the slab with 75% axial restraint stiffness. In this case, the deflection of the single tee slab shows a similar trend to the slab with 100% axial restraint stiffness until about 86 minutes, after which it fails because the axial spring reaches its capacity and the strain is close to the rupture strain (Note that a steel model is used for the spring).

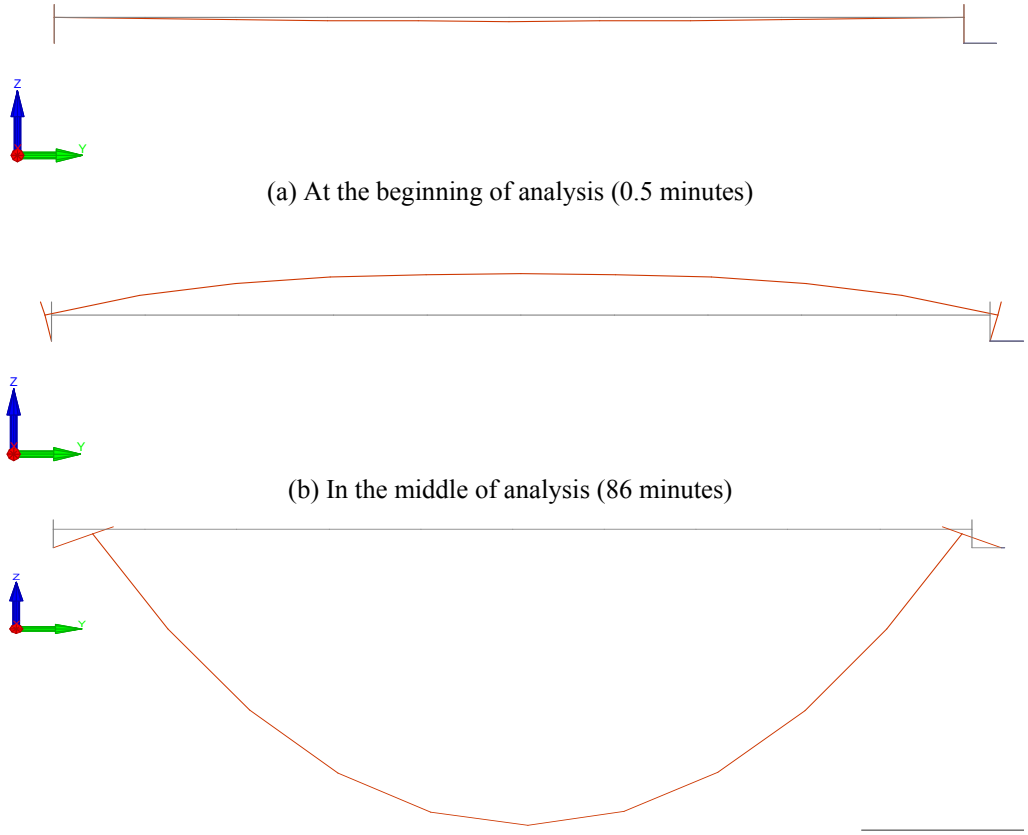

(a) At the beginning of analysis (0.5 minutes)

(b) In the middle of analysis (86 minutes)

(c) At the end of analysis (99 minutes)

Figure 8.13 Deflected shape at different times for slab with 75 % axial restraint stiffness, scale factor = 5

The axial deformation of the end spring (due to thermal expansion of the slab) is shown in Figure 8.14. It can be seen that the behaviour of a single tee slab is significantly affected by the stiffness of the axial restraint provided by the surrounding structure. The 100% axial restraint stiffness does not allow the slab to expand and the horizontal displacement of the slab in this case is almost zero. On the other hand, a single tee slab with low axial restraint stiffness shows up to 76mm horizontal displacement at the end of analysis.

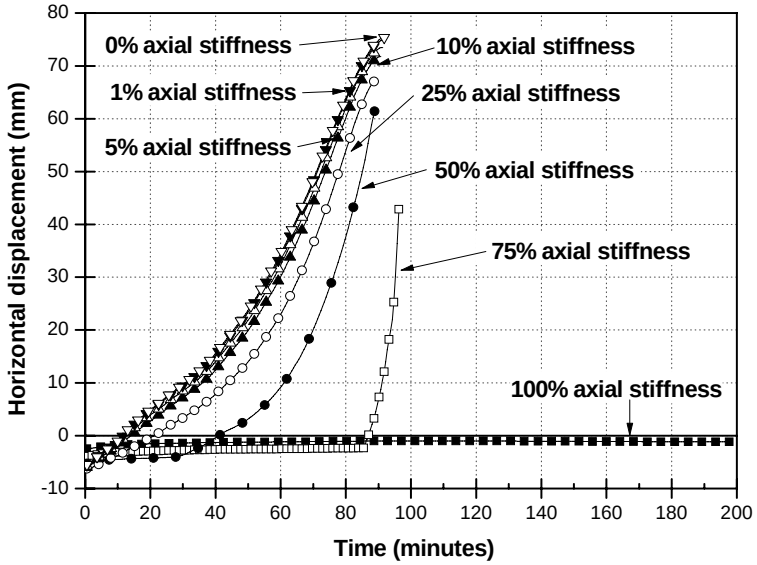

Figure 8.14 Horizontal displacement of a single tee slab with web support condition

8.3.5 Notched web support

In a notched web support, the web is reduced in depth at the end to allow the support level to be raised. Therefore, the support level can be at fixed depths below the floor level. In the modelling of the single tee slab with notched web supports, the axial spring at the end was connected to the centroid of the single tee slab. In this analysis, it is assumed that the webs are tapered at the ends so that the restraint forces only occur at the centroid of the single tee slab and the rotation is free. However, if the webs are not tapered, as shown in Figure 8.15, the structural behaviour of the single tee slab with notched web supports can be close to the structural behaviour of that with web supports during a fire depending on the joint width ($\leq l/500$) as the lower part of the single tee slab can get into contact with the ledge due to deflection and thermal expansion (CTBUH, 1992). Note that l is the span of the single tee slab.

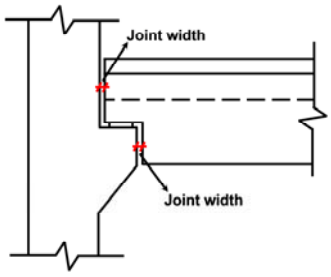

Figure 8.15 Support of single tee slab with non tapered web

Figure 8.16 shows the midspan vertical deflection of a single tee slab with a notched web support. In this graph, the analysis stopped at around 90 minutes. Even though the failure time was similar (90 minutes) in all cases, the behaviour of the slab until the failure time varied significantly with the axial restraint stiffness. The decrease of axial stiffness results in a lower downward deflection and a longer hogging deflection phase.

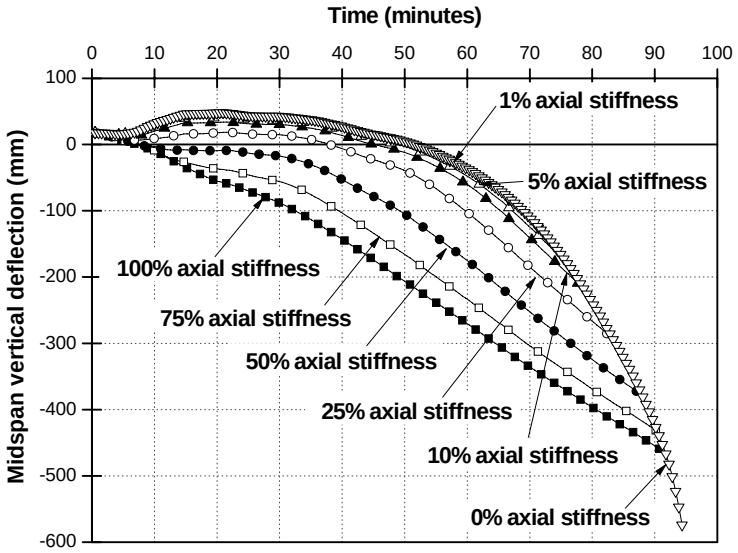

Figure 8.16 Midspan vertical deflection of a single tee slab supported on notched web

In contrast to the tee slab supported on the web, the single tee slab supported on a notched web, for all axial restraint stiffnesses, reached the axial capacity (Figure 8.17). As a result, the degree of axial restraint stiffness did not significantly affect the fire performance of the analysed single tee slab. This can be attributed to the fact that the notched web support cannot lead to arch action as it does not prevent the axial elongation of the bottom of the slab.

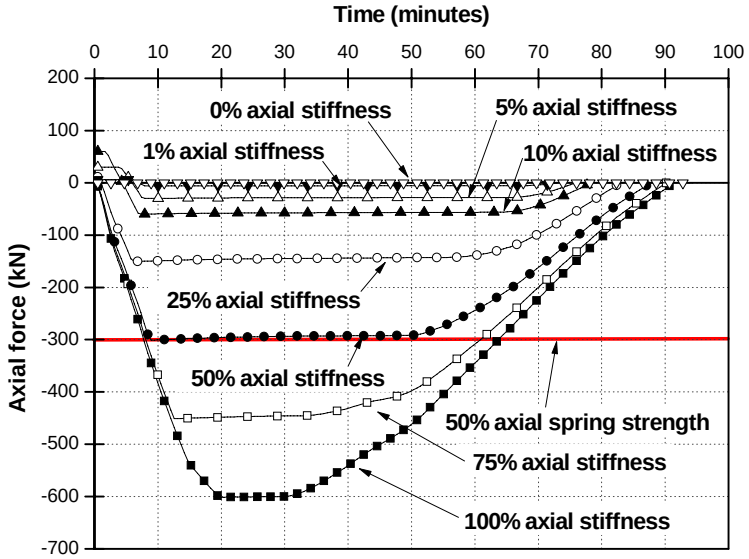

Figure 8.17 Axial force of a single tee slab with notched web support condition

Figure 8.18 shows the horizontal displacement of a single tee slab (i.e., axial deformation of the end spring) with notched web support. Compared to Figure 8.14 (i.e, web support slab), the horizontal displacement of slab at the support on a notched web is only about half that of the web support slab. This is due to the temperature at the centroid increasing more slowly than at the bottom of the web of the tee slab.

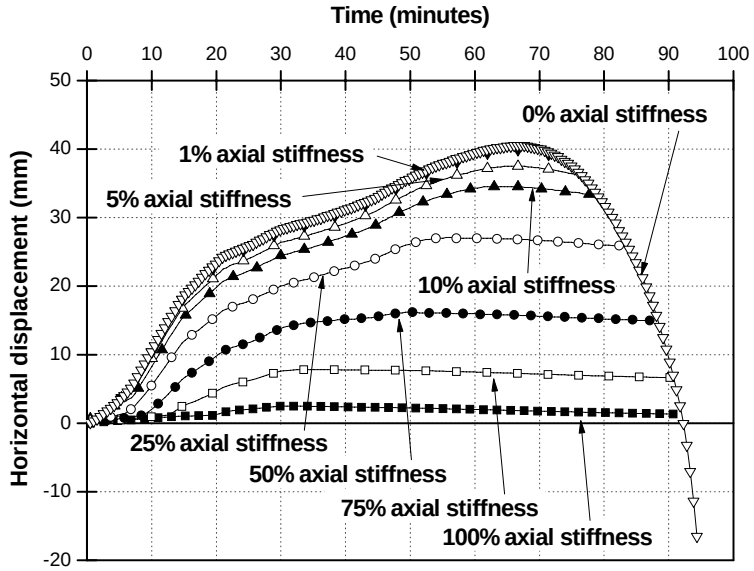

Figure 8.18 Horizontal displacement of a single tee slab with notched web support condition

8.3.6 Flange support

The flange-supported single tee slab was modelled with axial restraint spring at the middle of the flange. As with the case of the notched web support, it is also assumed that the webs are tapered at the ends so that the restraint forces only occurs the centre of the flange and the rotation is free.

The midspan vertical deflection of a single tee slab supported on flange is shown in Figure 8.19. The deflection trend is similar to that of the slab with notched web support. The midspan vertical deflection of tee slab with 75% and 100% axial stiffness are similar. A possible explanation for this is that the axial stiffness does not affect the fire performance of a single tee slab beyond a certain axial restraint stiffness. Figure 8.20 shows the axial force of a flange-hung single tee slab which has a similar to the notched web support of Figure 8.17. The 100% and 75% axial restraint stiffness cases are almost overlapping, otherwise the behaviour of the other cases are similar to what was observed in the case of the slab supported on a notched web (Figure 8.20). Also, there is no restraint to the axial elongation of the slab.

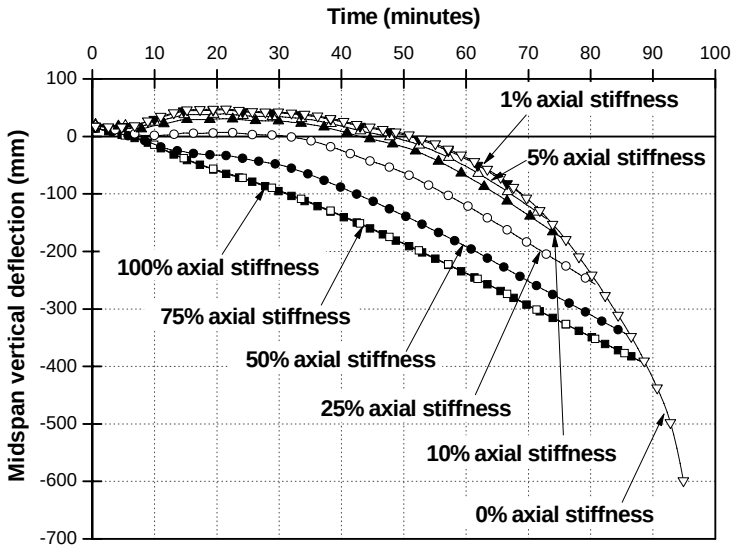

Figure 8.19 Midspan vertical deflection of a single tee slab with flange support condition

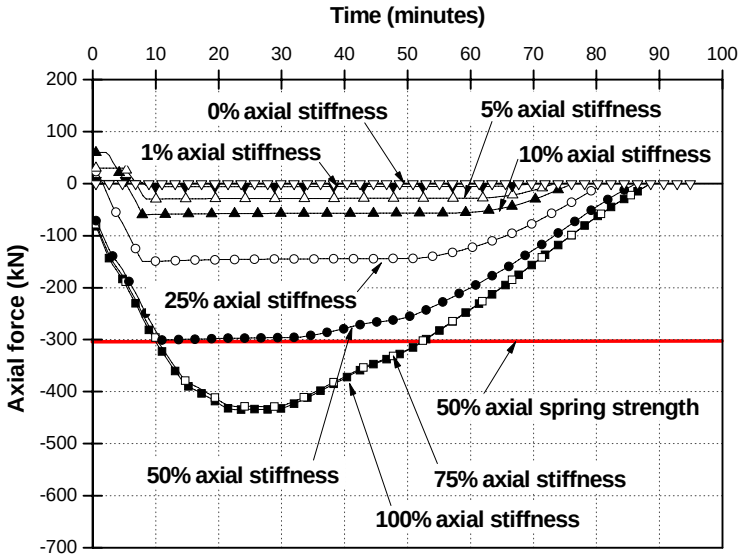

Figure 8.20 Axial force of a single tee slab with flange support condition

The horizontal movement of the end support of the flange-hung tee slab is plotted in Figure 8.21. During the analysis, before the spring element loses its load-carrying capacity, the end support undergoes an outward movement due to the push-out of the single tee slab undergoing thermal expansion. In the second stage, the spring element reaches its capacity and an axial shortening of the slab (i.e., elongation of the end spring) is caused by the large central deflection of the slab.

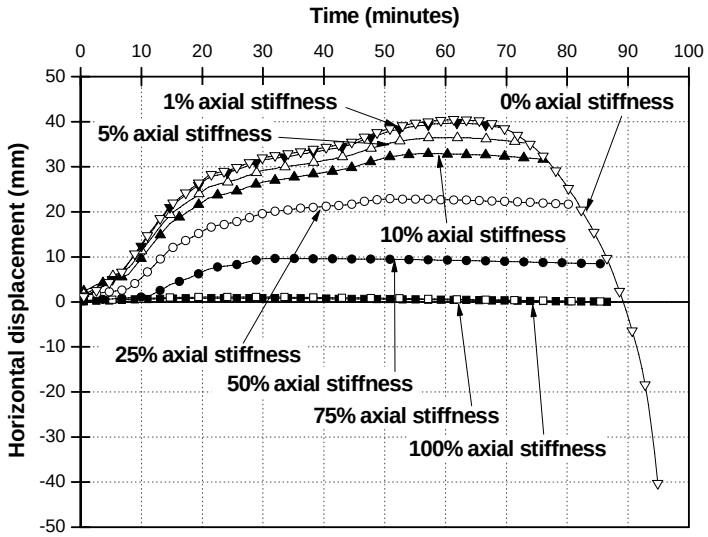

Figure 8.21 Horizontal displacement of a single tee slab with flange support condition

8.4 Summary

A numerical model of a restrained single tee slab was developed and investigated using SAFIR with respect to the location of support and the magnitude of axial stiffness.

Firstly, the effect of prestress levels is investigated. The results show that the prestress level of tendons does not significantly affect the fire performance of a single tee slab.

In addition, a series of analysis of single tee slabs with different restraint mechanisms such as web, notched web and flange supports as well as a wide range of axial restraint stiffness was carried out. It was shown that the fire resistance of the single tee slab is governed by the type of end support. It was also shown that the fire resistance of the single tee slab with web support increases from 90 minutes to 200 minutes depending on the degree of axial restraint stiffness.

Chapter 9

Fire Performance of Prestressed Flat Slabs

9.1 Introduction

This chapter deals with numerical methods for evaluating the structural behaviour of prestressed flat slabs in fire. Numerical analyses using beam elements with simply supported end conditions are validated against a series of physical laboratory test results conducted by Gustaferro (1967). Then, the structural behaviour of prestressed concrete slabs with reinforced topping concrete is compared with test data to investigate the influence of the topping concrete. The multi-spring connection model is used to develop the continuity of prestressed flat slabs and compared to numerical results with simply supported and fully fixed end conditions. Finally, the fire performance of a 75mm deep and 1200mm wide prestressed flat slabs is investigated. Figure 9.1 shows the organisation of Chapter 9.

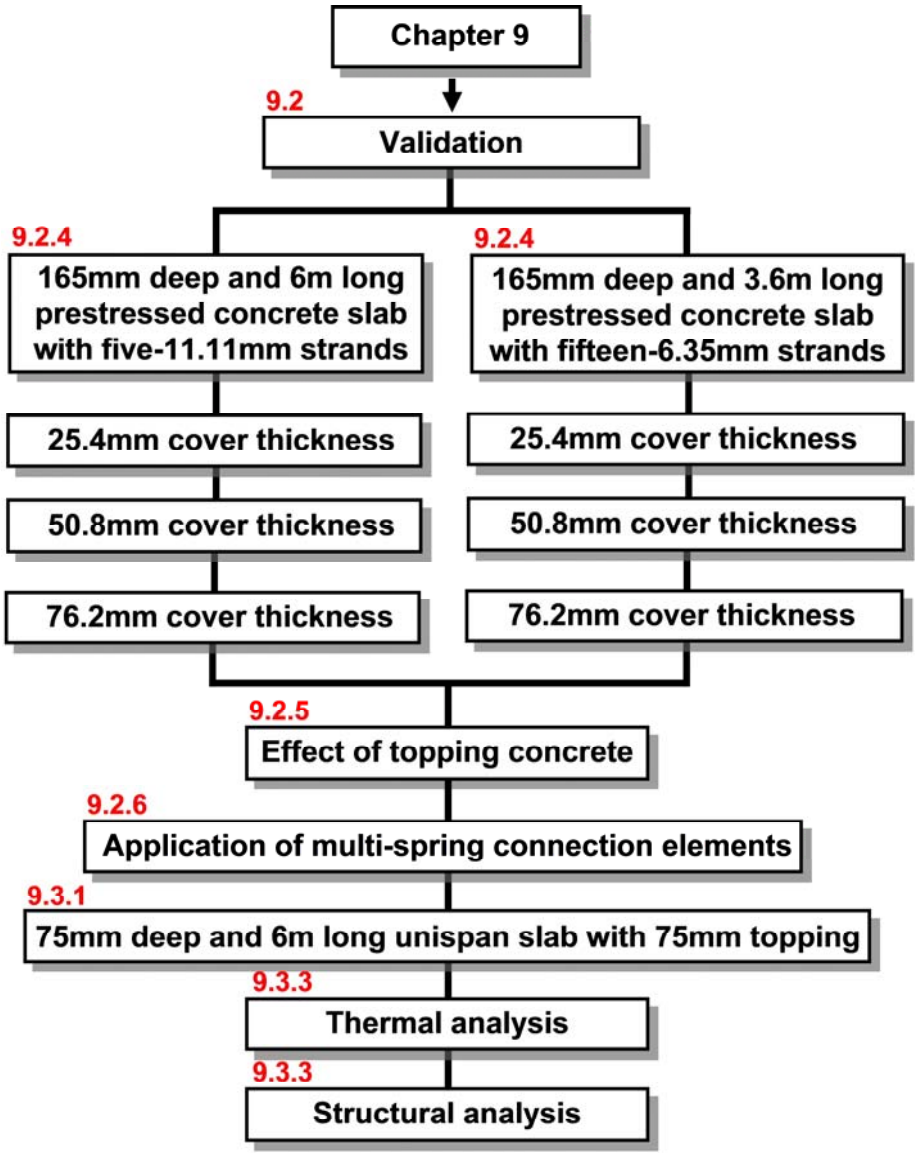

Figure 9.1 Organisation of Chapter 9

9.2 Validation of test and numerical results

9.2.1 Laboratory tests on prestressed concrete slabs

Physical laboratory tests on simply supported prestressed concrete slabs were performed by Gustaferro (1967) in United States. In the tests, a total of eleven prestressed concrete slabs, were tested in accordance with ASTM E119 (ASTM, 1998) fire. Among the test specimens, six of the specimens were made of normal weight concrete, and the rest was made of lightweight concrete. For validation, only

the results of prestressed concrete slabs with normal weight concrete are presented and compared.

Figures 9.2(a) and 9.3(a) show the loading arrangement of specimens which was applied through five equally-spaced hydraulic rams. The three specimens, with five-11.1mm diameter strands, were tested on 6,096mm span as shown in Figure 9.2(a). The other three specimens, with fifteen-6.35mm diameter strands, were tested on 3,661.6mm long span as shown in Figure 9.3(a). In addition, all slabs used in these tests had the same 696.6mm wide and 165mm thick cross section as shown in Figures 9.2(b) and 9.3(b). For each specimen, all strands had the same cover thickness such as, 25.4, 50.8 and 76.2mm.

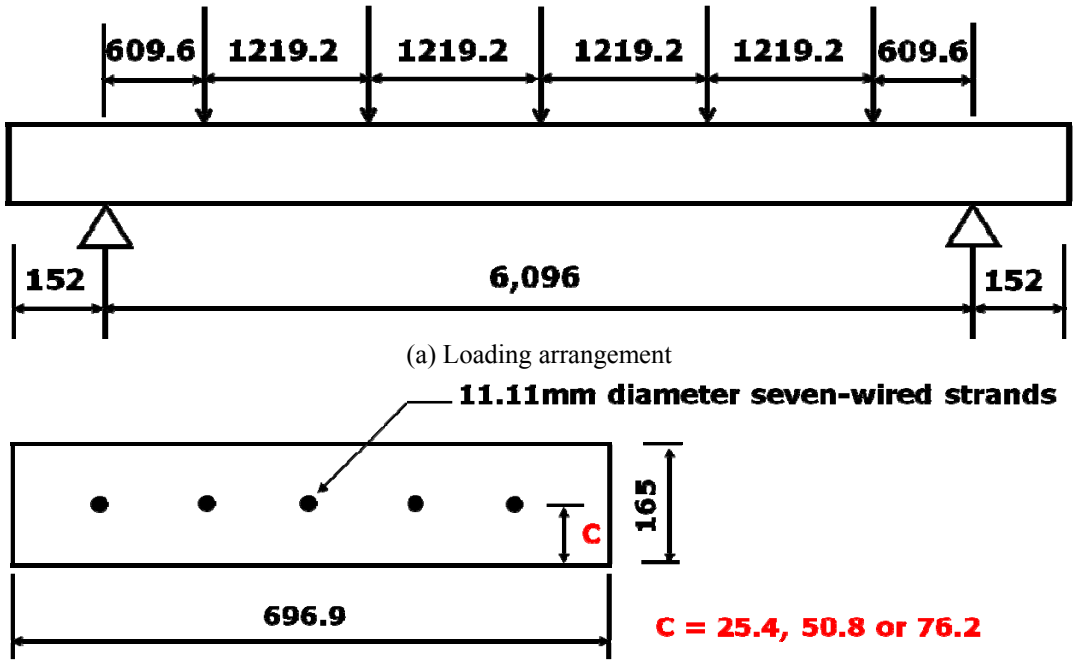

(a) Loading arrangement

(b) Cross section of specimen

Figure 9.2 Specimen details for five-11.11mm tendons and 6,096mm span (Gustaferro, 1967)

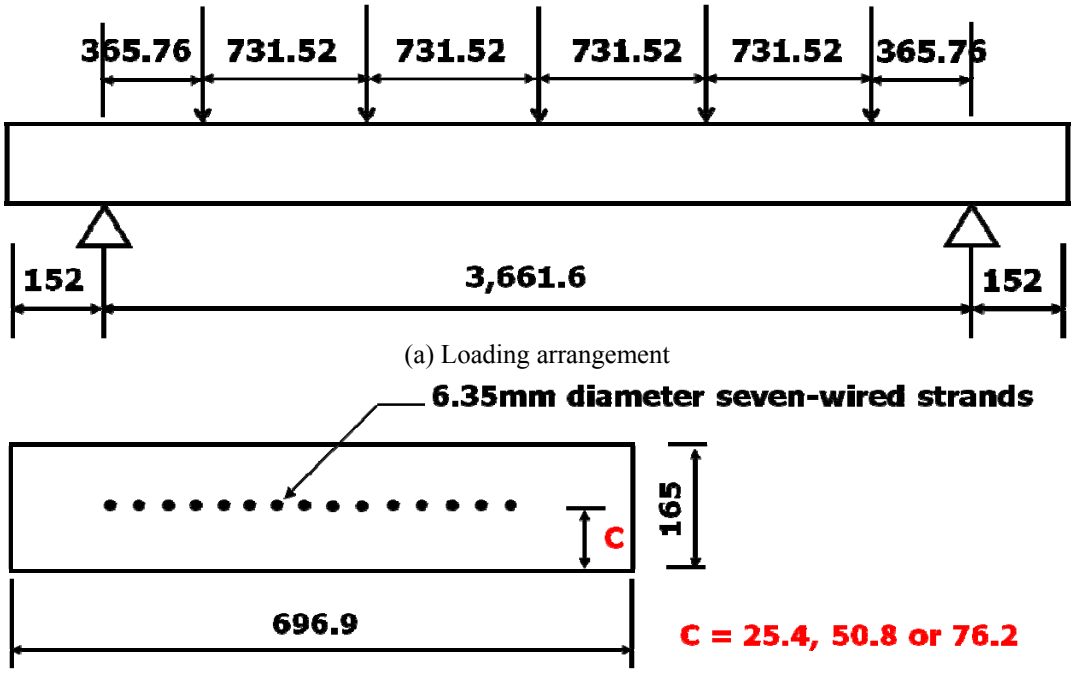

(a) Loading arrangement

(b) Cross section of specimen

Figure 9.3 Specimen details for fifteen-6.35mm tendons and 3,661.6mm span (Gustaferro, 1967)

In terms of material properties and applied load with respect to the specimens, Table 9.1 summarises the details of concrete strengths and loadings. For prestressed strands, the measured ultimate tensile strength for the 11.11mm diameter was 1,806MPa and 1,896MPa for 6.35mm diameter. In addition, partial loss of prestress is assumed to be 18%. The load intensity during the tests ranged between 40 and 60 percent of the calculated ultimate capacities.

Table 9.1 Specimen strength and loading details (Gustaferro, 1967)

Slab Type	Concrete cover, mm	Concrete strength, MPa	Number and size of strands	Applied load, P (N)
NWSLAB1	25.4	37.5	5-11.11mm	5769
NWSLAB2	50.8	34.7	5-11.11mm	4345
NWSLAB3	76.2	43.7	5-11.11mm	2860
NWSLAB7	25.4	35.7	15-6.35mm	11427
NWSLAB8	50.8	53.3	15-6.35mm	9052
NWSLAB9	76.2	37.4	15-6.35mm	6071

9.2.2 Finite element model of the prestressed concrete slabs

The finite element modelling of the prestressed concrete slabs begins with the thermal analysis of the slabs. In the thermal analysis, the whole cross section of each prestressed concrete slab was modelled and analysed. In addition, it was assumed that the specimens were only exposed to fire on the bottom surface. For the structural analysis, the whole length of the specimens was modelled with 10 beam elements using the thermal analysis results.

9.2.3 Temperature distribution

Figure 9.4 shows the numerical results with respect to the exposed and unexposed surfaces as well as the ASTM E119 and ISO 834 fires. The comparison of numerical and test results for the temperature assessment is not presented as the measured temperature results of the test specimens were not available. For the exposed surface temperature, the temperature increased up to 1100°C during a 4 hour fire exposure. On the other hand, the temperature of the unexposed side in numerical analysis was less than 300°C at the end of analysis. As a result, thermal gradients between exposed and unexposed surfaces show a large difference. In addition, the ASTM E119 fire curve was compared with ISO 834 fire. It can be seen that the ISO 834 fire curve is slightly higher than ASTM E119 during the course of the simulated fire.

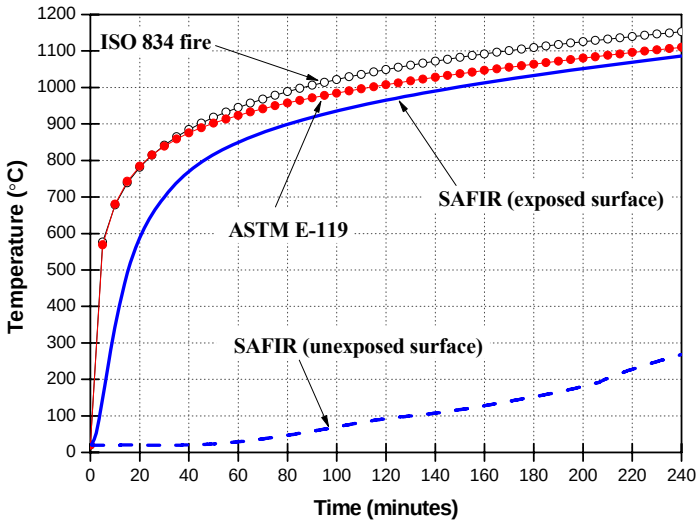

Figure 9.4 Comparison of temperature development between tests and numerical results

9.2.4 Comparison of numerical and test results

Figures 9.5, 9.6 and 9.7 illustrate the comparison of test and numerical results for the central vertical deflection for specimens with five-11.11mm strands and 6,096mm span. The comparison with respect to specimens including fifteen-6.35mm strands and 3,661.6mm span is shown in Figures 9.8, 9.9 and 9.10. All tests lasted until the structural end point was imminent (Gustaferro, 1967).

In terms of the comparison of central vertical deflection with five-11.11mm strands as well as 25.4mm cover thickness, the vertical deflections in numerical results are slightly lower than that in the corresponding test results. On the other hand, with respect to the comparison of central vertical deflection with five-11.11mm strands with 50.8mm and 76.2mm cover thickness, the numerical results show a better agreement with test results. For the earlier part of the fire, the numerical result is stiffer than the test result. This can be attributed to the assumption of a perfect bond in the numerical analysis. In addition, the commonly specified failure criterion (a deflection of 1/20 of a span) is compared with test and numerical results. It can be seen that for both cases, five-11.11mm stands with 50.8mm and 76.2mm cover thickness, the numerical results continue for longer, both test and numerical results meet the failure criterion.

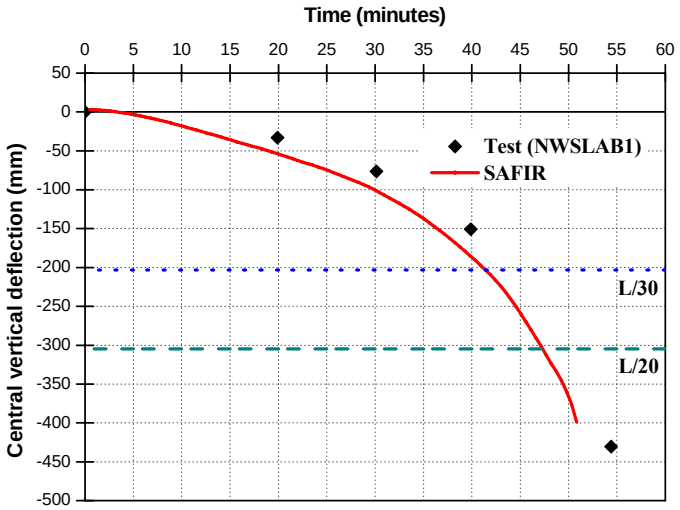

Figure 9.5 Central vertical deflection, 5-11.11mm strands, 25.4mm, 6,096mm span

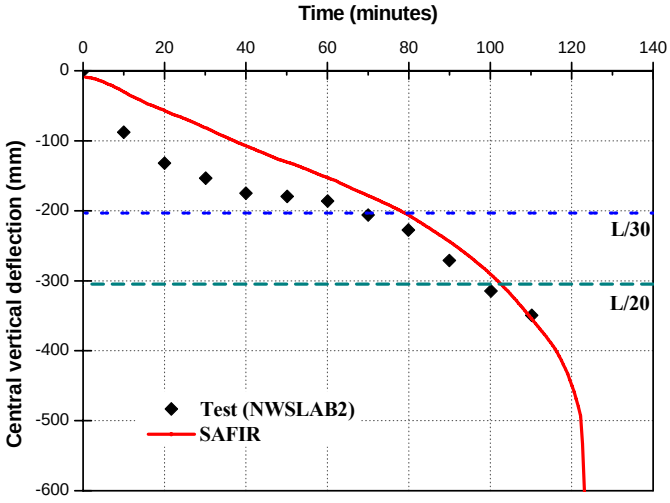

Figure 9.6 Central vertical deflection, 5-11.11mm strands, 50.8mm, 6,096mm span

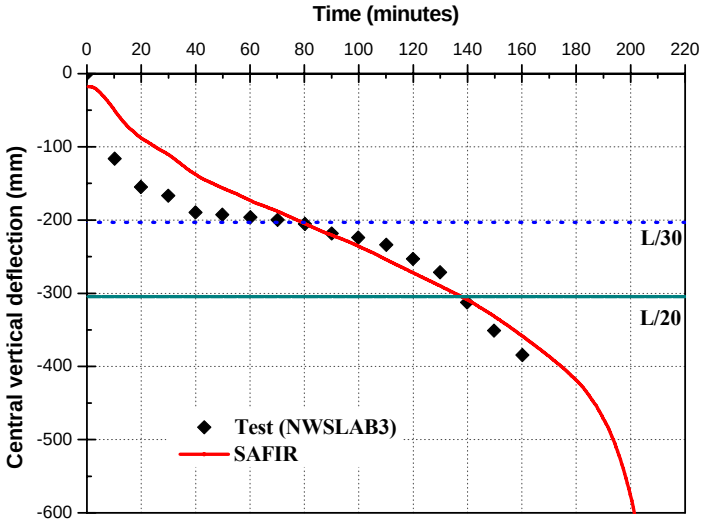

Figure 9.7 Central vertical deflection, 5-11.11mm strands, 76.2mm, 6,096mm span

With respect to the comparison of central vertical deflection of fifteen-6.35mm strands with 25.4mm cover thickness, the numerical results are relatively stiffer than the corresponding test results. On the other hand, the test results on specimens with 6.35mm strands with 50.8 and 76.2mm cover showed a good agreement with numerical results. Nevertheless, there is a discrepancy between the test and numerical results at the end of the analysis.

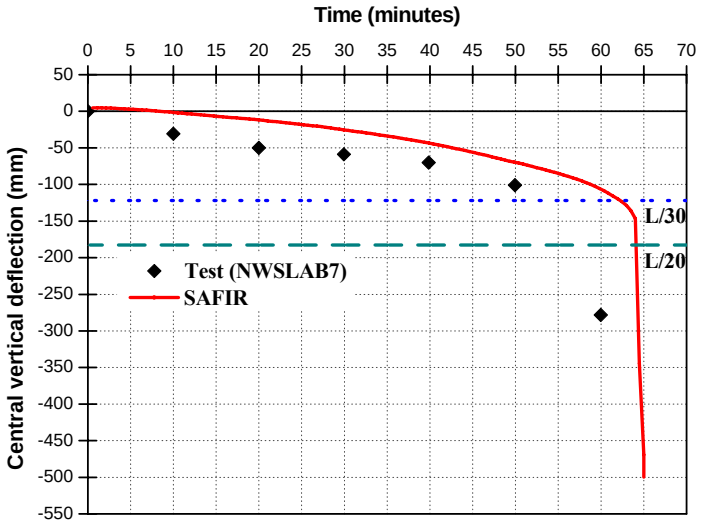

Figure 9.8 Central vertical deflection, 15-6.35mm strands, 25.4mm, 3,661.6mm span

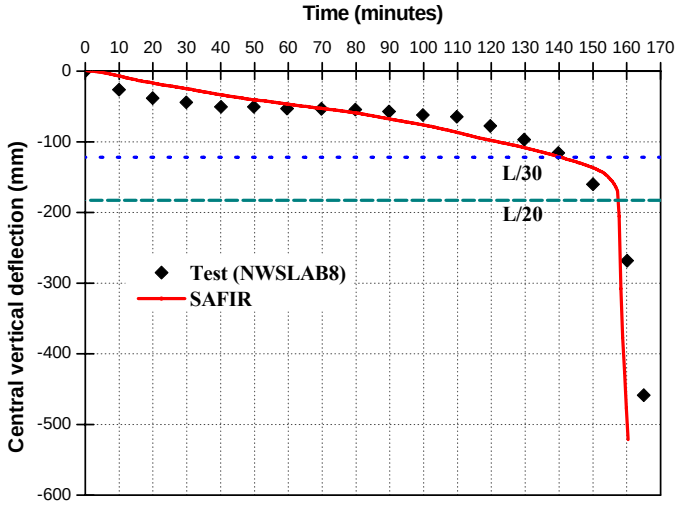

Figure 9.9 Central vertical deflection, 15-6.35mm strands, 50.8mm, 3,661.6mm span

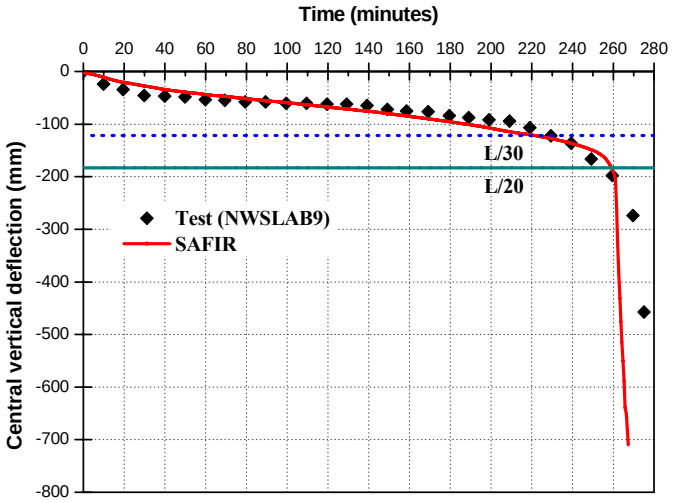

Figure 9.10 Central vertical deflection, 15-6.35mm strands, 76.2mm, 3,661.6mm span

9.2.5 Effect of topping concrete

In New Zealand, prestressed concrete slabs are usually used with 65mm or 75mm topping concrete as well as reinforcement mesh, but the thickness can vary depending on the structural requirements (PCFOG committee, 2009). In order to investigate the effect of reinforced concrete topping with respect to prestressed flat slabs, a numerical analysis on prestressed concrete slabs with reinforced concrete topping was conducted. The thicknesses of the topping concrete used were 65mm and 75mm. The same 333 mesh (75 x 75 x 6.40mm diameter bars) was used for reinforcement. The live loading for the prestressed concrete slabs including topping was kept the same as the prestressed concrete slabs without topping because there is not sufficient information for the loading which includes topping. The self-weight for topping was calculated and considered in the analyses. In addition, the test and numerical results on prestressed concrete slab with five-11.11mm strands were considered for analysis as the arrangement of prestressing steels is more similar to prestressed flat slabs being used in New Zealand.

The comparison of test results, the analysis without topping and analysis with topping of the central vertical deflection, is illustrated in Figures 9.11, 9.12 and 9.13. The results on these figures show an increase of fire resistance due to the contribution of topping. It can be seen that the analysis with topping is stiffer than the analysis without topping. For a prestressed concrete slab with 76.2mm cover thickness, even though the central vertical deflection is beyond L/30 of the span, the slab did not reach the L/20 failure criterion during 4 hours of fire exposure to ASTM E119 (ASTM, 1998).

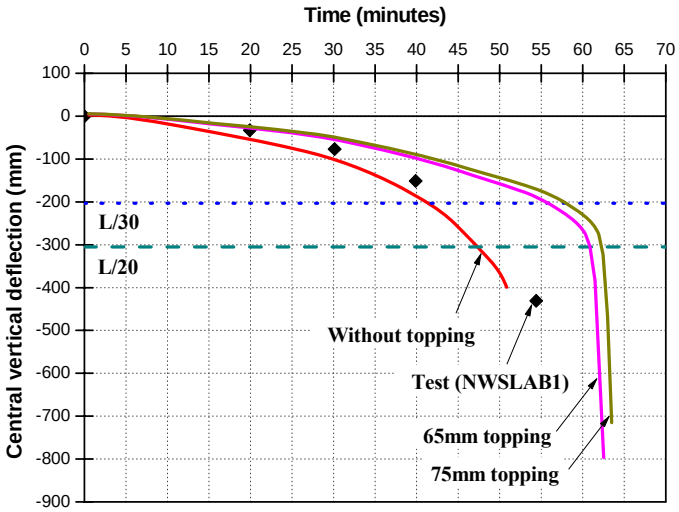

Figure 9.11 Central vertical deflection, 5-11.11mm strands, 25.4mm, 6,096mm span with reinforced concrete topping

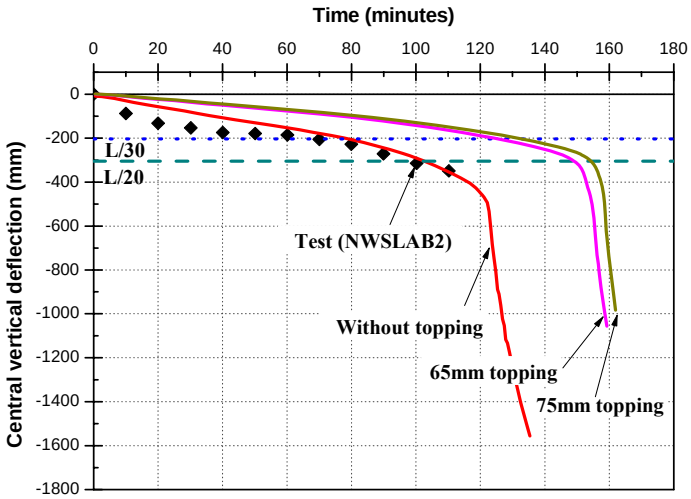

Figure 9.12 Central vertical deflection, 5-11.11mm strands, 50.8mm, 6,096mm span with reinforced concrete topping

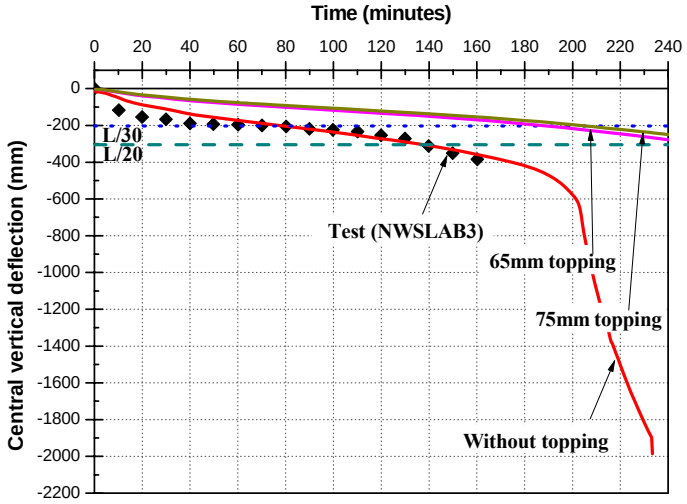

Figure 9.13 Central vertical deflection, 5-11.11mm strands, 76.2mm, 6,096mm span with reinforced concrete topping

9.2.6 Application of multi-spring connection elements

The previously developed multi-spring connection elements (Section 4.3) are useful for evaluating the effect of continuity of prestressed concrete slabs in fire. In order to compare the structural behaviour of prestressed concrete slabs with different end conditions, a numerical model using multi-spring connection elements was analysed. Both Pin-Roller and Fixed-Fixed end conditions incorporating multi-spring connection elements were considered. In terms of Pin-Roller end conditions, a vertical restraint was introduced in the middle of the multi-spring connection elements and a horizontal restraint was applied to the left hand side as shown in Figure 9.14(a). For Fixed-Fixed end conditions, the outer faces of the multi-spring elements were fully fixed and the bottoms of the inner faces were restrained against vertical movements as shown in Figure 9.14(b). In the case of fully fixed end conditions, the support condition represents the situation where prestressed flat slabs in multi-bay floors located in the inner bay with compartment fire.

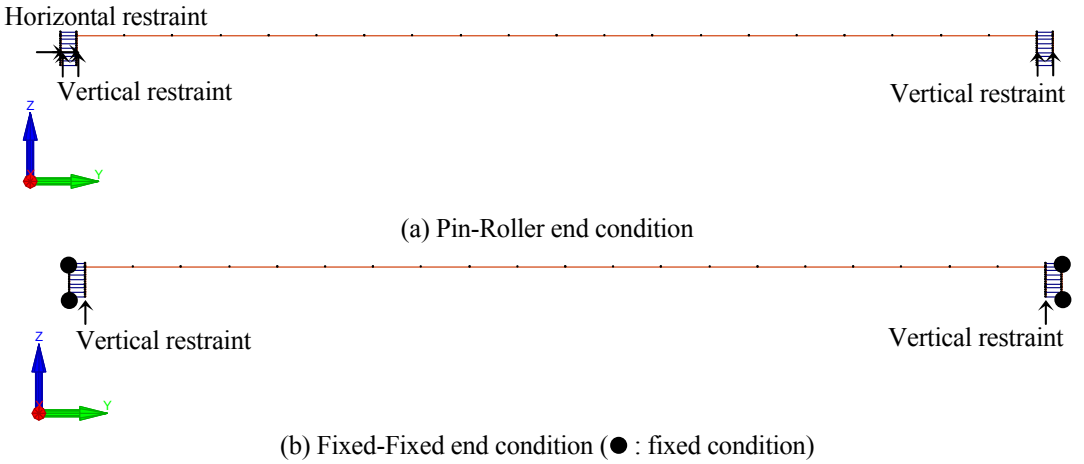

Figure 9.14 End conditions of pretressed concrete slabs using multi-spring connection elements

Figure 9.15 shows the comparison of the structural behaviour of prestressed concrete slab which includes multi-spring connection elements with the previous results. The numerical result regarding the Pin-Roller end conditions shows the same result as that without multi-spring connection elements. On the other hand, the numerical result for Fixed-Fixed end condition shows the significant improvements of the fire resistance and the structural behaviour. The analysis

stopped at around 110 minutes due to the failure of the prestressed concrete slab. Even though both cases are not the same as practical support conditions, multi-spring elements can predict the support conditions of simply supported case and continuously supported case.

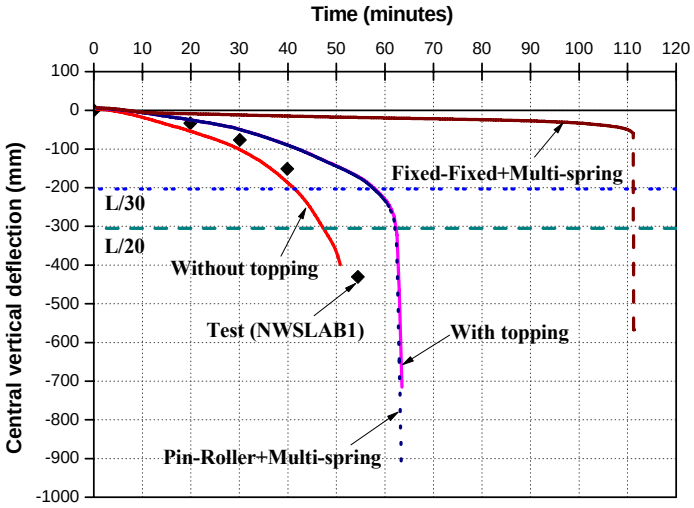

Figure 9.15 Central vertical deflection, 5-11.11mm strands, 25.4mm, 6,096mm span with reinforced concrete topping and multi-spring connection elements

9.3 Fire resistance of prestressed flat slabs

9.3.1 Prestressed flat slabs

Prestressed flat slabs consist of 75mm thick precast, prestressed concrete slabs with a reinforced concrete topping. The slabs are typically 1200mm or 2400mm wide and allow clear spans of up to 8.0 metres. In addition, standard prestressed flat slabs can provide up to 90 minutes fire resistance rating (Stresscrete, 2011).

9.3.2 Dimensions and material specifications of prestressed flat slabs

In order to investigate the fire performance of prestressed flat slabs, a model of a prestressed flat slab with 6m span and 1.2m width, composite with a 75mm topping slab has been selected as shown in Figure 9.16. 333 mesh (75 x 75 x 6.40mm diameter bars), was used in the concrete topping slab. All of the relevant material properties are shown in Table 9.2.

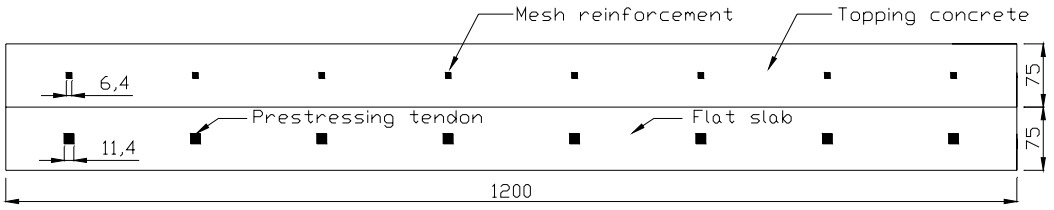

Figure 9.16 Cross section of a prestressed flat slab

Table 9.2 Material properties of a 75 mm deep prestressed prestressed flat slab

Prestressed flat slab	
Self weight	3.77 kPa
Compressive strength	40 MPa
Prestressing strands	
Type	Stress relieved 7-wire strand
Strength	1.84 GPa
Prestressing level	73%
Cross sectional area/strand	100 mm^2
Reinforced concrete topping screed	
Concrete compressive strength	20 MPa
Reinforcement strength	450 MPa

From the load/span table of the manufacturer (Stresscrete, 2011), a 75mm deep prestressed flat slab with 75mm thick concrete topping can sustain a live load (Q) of 4.0 kPa under the ambient conditions and it is assumed that any other superimposed dead load is 0 kPa. The self-weight (G) of a 75mm deep prestressed flat slab is 3.77 kPa, as specified in Table 9.2. According to the New Zealand loading code (AS/SNZ, 2002), the load combination for the ultimate limit state condition in fire is 1.0G + 0.4Q, where G is dead load and Q is live load. The fire design load, therefore, is 5.37 kPa and this value is applied to the 75mm prestressed flat slab.

9.3.3 Numerical analysis of prestressed flat slabs

Finite element model for the thermal analysis of the 75mm deep prestressed flat slabs was performed using one half of the slab width as shown in Figure 9.17. The Standard ISO 834 fire was applied to the bottom of the prestressed flat slab. In terms of structural analysis, the 6m long prestressed flat slab was modelled with 10

beam elements. Simply supported boundary conditions were applied for the structural analysis.

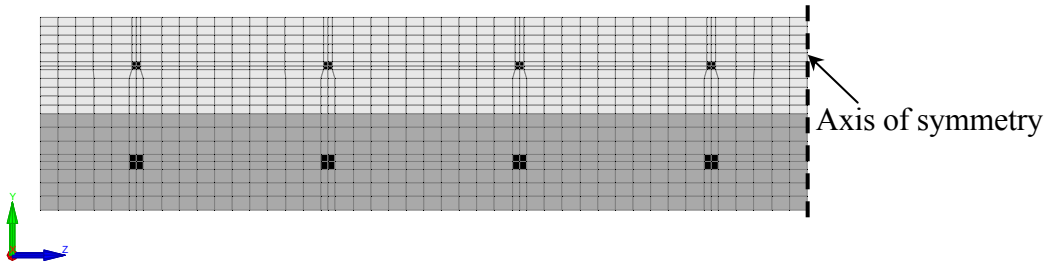

Figure 9.17 Cross section mesh model of a 75mm prestressed flat slab

The calculated temperature distribution for four points, the bottom and top of the prestressed flat slab, the prestressing tendon, and the reinforcement, as well as the Standard ISO 834 fire is presented in Figure 9.18. During 4 hours fire exposure time, the top of prestressed flat slab reached 480ºC while the temperature of the bottom of the prestressed flat slab directly exposed to fire was 1130ºC. The temperature of the prestressing tendon that has 37.5mm axis distance was just over 700ºC.

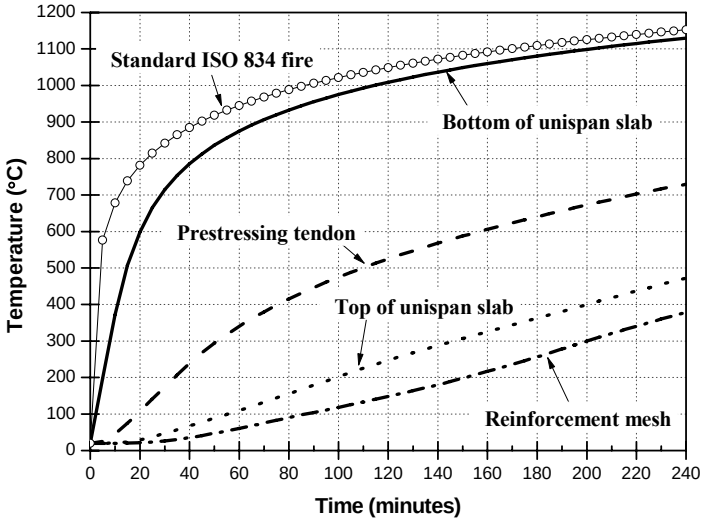

Figure 9.18 Temperature development of a 75mm prestressed flat slab

Figure 9.19 shows the numerical result of a 75mm deep and 6m long prestressed flat slab with 75mm reinforced concrete topping. The numerical analysis lasted for around 150 minutes. With respect to the failure criteria for fire

resistance testing, a deflection of 1/20 of the span was reached at 104 minutes. Nevertheless, the fire resistance of 90 minutes provided by the manufacturers is more conservative than the numerical result.

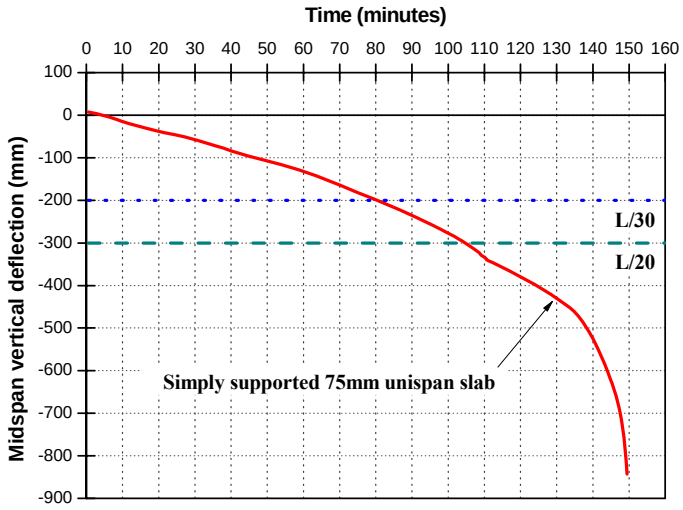

Figure 9.19 Structural behaviour of a 75mm deep prestressed flat slab in fire

9.4 Summary

A series of laboratory test results on prestressed concrete slabs which were tested at standard fire testing facility with ASTM E119 fire being used. In order to investigate the validity and applicability of the numerical model, the predicted structural behaviour of the prestressed concrete slabs were compared with the results obtained from fire tests using ASTM E119.

The simply supported numerical model using beam elements is capable of predicting the response of prestressed concrete slabs exposed to elevated temperature. In terms of comparisons of structural response, the numerical model shows a good agreement with the test results.

For the application of multi-spring connection elements, the numerical model is capable of modelling the continuity of prestressed concrete slabs. The consideration of end support conditions, such as Fixed-Fixed arising from continuity, can result in significant improvement in the fire performance of prestressed concrete slabs.

In accordance with the fire resistance rating provided by manufacturers, the current numerical model on prestressed flat slabs is capable of predicting fire resistance rating.

Chapter 10

Conclusions and Recommendations

10.1 Introduction

This research was conducted to develop numerical models for assessing the fire performance of precast prestressed concrete flooring systems in concrete framing structures. The present work has been primarily concerned with the numerical modelling of the structural behaviour of prestressed hollowcore flooring systems incorporating variable parameters, such as end beams, side beams, infill concrete toppings and columns, in fire. An investigation into the fire performance of a single tee slab was also performed, taking into account the various possible axial restraints depending on the end shape of the single tee slab, and seating conditions. The numerical prediction of structural behaviour of prestressed flat slabs in fire was also investigated, with the validation of a series of experimental results which were found in the published literature.

10.2 Development of finite element model for precast prestressed hollowcore concrete flooring systems

A numerical study carried out into the structural behaviour of a single hollowcore concrete slab subjected to Standard ISO fire on the underside. In addition, the development of multi-spring connection model has been made. The main findings of the research on the single hollowcore slab in fire and the development of multi-spring connection model are follows:

10.2.1 Single unit hollowcore slab in fire

- The application of ideal support conditions in simulating prestressed hollowcore slabs using grillage methods had some limitations in modelling the gap between hollowcore slabs and the end beams and representing the end conditions for the prestressing tendons of the precast flooring units.
- The pinned and fixed end conditions are inappropriate to represent reality in prestressed hollowcore floors.

10.2.2 Development of multi-spring connection elements

- A multi-spring connection model can be used to predict the structural behaviour of prestressed hollowcore slabs in fire. The validation of hollowcore floors using multi-spring elements showed reasonable agreement with an experimental result found in the published literature.
- An increase of topping thickness (from 65mm to 75mm) with same loading conditions improved the structural behaviour slightly while the addition of top prestressing stands reduced the fire resistance due to the reduced lever arm length.
- The numerical results showed that the number of starter bars is important for enhancing fire resistance of prestressed hollowcore slabs.

10.3 Investigation of fire performance for hollowcore flooring systems connected with surrounding structures

The study into prestressed hollowcore flooring systems restrained by surrounding structures was conducted with 3D finite element analyses. The extensions of numerical model developed with multi-spring connection element have been made. The main findings of the research on prestressed hollowcore flooring systems restrained by surrounding structures are follows:

10.3.1 One bay hollowcore floors in fire

- Without the considerations of side beams and columns, an increase in the number of hollowcore units did not affect the fire resistance significantly.
- One bay hollowcore floors with side beams have much greater fire resistance than one bay hollowcore floors with no side beam.
- One bay hollowcore floor restrained by side beams supported the applied loads for the entire duration of the fire without collapse even though one bay hollowcore floor connected next to the side (Figure 5.20(a)) beam showed better structural behaviour rather than the latest lateral connection detail (Figure 5.20(b)) due to the reduction of the transverse curvature.

10.3.2 Multi-bay hollowcore floors in fire

- The fire resistance of 4x1 bay hollowcore floors, including 22 hollowcore slabs and side infill connections, achieved 60 minutes fire resistance. This result is noticeably worse than the fire resistance of one bay hollowcore floors.
- Fire resistance of interior multi-bay hollowcore floors can be improved by the axial restraint from the surrounding structures which are not exposed to fire.
- For parametric fires, the multi-bay hollowcore floor showed much greater fire resistance than the floor exposed to increasing Standard ISO fire if the fire goes out after 50 minutes or less, even though larger deflections occur.
- The numerical model with 1.5 the number of starter bars is able to increase the fire resistance as well as show better structural performance than the floor with normal number of starter bars. However, more investigations are required as hollowcore floors can fail while the topping slab remains intact during the course of the fire.
- The numerical results showed that the addition of fire emergency beams which reduce the transverse curvature is important for improving the fire resistance of prestressed hollowcore floors. In the 4x1 bay hollowcore flooring system, the floor with one emergency beam and three emergency beams achieved 135 minutes and 158 minutes fire resistance, respectively.

10.3.3 Shear and splitting resistance of hollowcore slabs in fire

- The code based calculation equations for the shear resistance of hollowcore slabs are helpful to determine the shear resistance of simply supported hollowcore slabs in fire.
- The Eurocode equation (6.2.a) which is not requiring design shear reinforcement can be modified with high temperature material properties to estimate the shear capacity of a hollowcore slab.
- With respect to 200mm hollowcore slabs, the splitting of hollowcore slabs due to fire exposure could occur at around 75 minutes in a Standard ISO fire.

10.4 Extension of numerical modelling for precast prestressed single tee and flat slabs

The numerical study carried out into the structural behaviour of single tee slabs having different axial restraint stiffness as well as the variation of axial thrust under Standard ISO fire. In addition, the study into prestressed flat slabs was conducted with the validation of a series of test results using ASTM E119 fire in the published literature. The main findings of the research on single tee slabs in fire are follows:

10.4.1 The structural behaviour of single tee slabs under fire conditions

- The prestressing levels of steel strands in prestressed concrete slabs do not significantly affect the fire performance even though the structural behaviour of prestressed concrete slabs is related to the prestressing levels during the course of the fire.
- For web supported single tee slabs, the effect of only high axial restraint stiffness against single tee slabs is significant to varying fire resistance of the single tee slab.
- In terms of notched web and flange supports, the prediction of the structural behaviour under Standard ISO fire regardless the variation of axial restraint

stiffness showed worse fire resistance than a simply supported single tee slab. The predicted structural behaviour may be conservative compared to the actual behaviour due to the lack of consideration of friction between the single tee slabs and the supporting beams.

10.4.2 The structural behaviour of prestressed flat slabs under fire conditions

- A numerical model using beam elements has been validated against physical laboratory testing data and showed good agreement with the actual structural behaviour.
- The developed multi-spring connection element is useful in predicting the structural behaviour of continuous prestressed concrete slabs subjected to elevated temperatures.
- Proprietary ratings for the fire resistance of prestressed flat slabs are more conservative than the numerical prediction of prestressed flat slabs.

10.5 Recommendations for design and construction of precast prestressed concrete slabs

This section presents the recommendations for design and construction of precast prestressed concrete slabs based on finite element analyses of the slabs conducted in this study.

- Hollowcore floors show excellent fire behaviour with the increase of starter bars. In order to mobilise the catenary action, the supporting beams must be able to withstand high strains due to the large rotation.
- NZS 3101 (concrete code) requires infill adjacent to frames, which will give less damage in earthquake, but will reduce the benefits of membrane action in fire exposure, compared with no infill.
- The fire performance of prestressed hollowcore floors may be enhanced by considering more realistic restraint conditions such as side beams. However, in

the case of multi-bay hollowcore floors, more attention to the arrangement for the fire emergency beam is required.

- The SAFIR program cannot predict the shear behaviour of hollowcore slabs. Nevertheless, the shear checks for hollowcore slabs should be undertaken when determining the fire resistance of hollowcore slabs using simple equations which are presented in Chapter 7.
- Fire resistance of prestressed flat slabs can be improved by the use of the web supported seating detail with high axial restraint stiffness. Web hung and flange supports should be used with care.

10.6 Recommendations for future studies

In order to improve the applicability of the developed numerical models in practice and to improve their accuracy, the following topics are recommended for future research.

- Investigate the fire performance of hollowcore floors which are not restrained by side beams as mentioned in Section 7.2.4. The SAFIR program was not able to model shear deformation, web splitting, bond and spalling using solid elements at elevated temperatures. Therefore, some other commercial software packages, such as ABAQUS or DIANA, are needed to examine the lateral thermal expansion of hollowcore floors.
- Investigate the fire performance of the structure with different cross sections. The failure modes of hollowcore slabs in fire can vary depending on the height of the specimens, the arrangement of strands, and the shape of the hollow cores. Therefore, more detailed information on hollowcore slabs in fire is required for designers.
- Fire induced spalling is not included in the analysis. Nevertheless, fire induced spalling is one of the major concerns with new types of concrete. Therefore, fire test data on new types of precast prestressed concrete flooring systems is needed.

References

Abram, M. S., and Gustaferro, A. H. (1972). Fire Endurance of Prestressed Concrete Units Coated with Spray-Applied Insulation. *PCI Journal*, 17(1), 82-103.

ACI 216.1 (2007). *Code Requirements for Determining Fire Resistance of Concrete and Masonry Construction Assemblies.* American Concrete Institute. Farmington Hills, MI, USA.

ACI 318 (2005). *Building code requirements for structural concrete and Commentary.* American Concrete Institute. Detroit, MI, USA.

Anchor, R. D., Malhotra, H. L., and Purkiss, J. A. (1986). *Design of Structures against Fire*. Elsevier Applied Science Publishers, London, England.

Andersen, N. E., and Lauridsen, D. H. (1998). *Danish Institute of Fire Technology Technical Report X 52650 Part 1 – TT-roof slabs*. Danish Institute of Fire Technology, Denmark.

Andersen, N. E., and Lauridsen, D. H. (1999). *Danish Institute of Fire Technology Technical Report X 52650 Part 2 – Hollowcore Concrete Slabs*. Danish Institute of Fire Technology, Denmark.

AS/NZS (2002). AS/NZS 1170:2002, *Structural design actions*. Standards New Zealand, Wellington, NZ.

ASTM E119-98 (1998). *Standard test methods for fire tests of building construction and materials.* American Society for Testing and Materials International.

Bailey, C. G., and Lennon, T. (2008). Full-scale fire tests on hollowcore floors. *The Structural Engineer*, 86(6), 33-39.

Bazant, Z. P., and Kaplan, M. F. (1996). *Concrete at High Temperatures: Material Properties and Mathematical Models*. Longman, UK.

BEF (2005). *Hollow Core Slabs and Fire - Documentation on Shear Capacity.* Birch & Krogboe A/S, Denmark.

Bilow, D. N., and Kamara, M. E. (2008). Fire and Concrete Structures. *Proceedings of the 2008 Structures Congress*, Vancouver, Cananda.

Borgogno, W. (1997). Tragverhalten von Slim Floor Decken mit Betonhohlplatten bei Raumtemperatur und Brandeinwirkungen. PhD Thesis, Eidgenössische Technische Hochschule Zürich (in German).

Breccolotti, M., and Materazzi, A. L. (2004). Fire behaviour of HPLWC hollowcore slabs: full scale furnace tests and numerical modelling. *Workshop on: Fire design of concrete structures: What now? What next?*, fib Task Group 4.3, Milan, Italy.

Breccolotti, M., Materazzi, A. L., and Venanzi, I. (2006). Fire performance of HPLWC hollow core slabs. *Proceedings of the Fourth International Workshop Structures in Fire SiF'06*, Aveiro, Portugal.

BSI (1987). *Fire Tests on Building Materials and Structures, BS 476 (Parts 1 to 23).* British Standards Institution, UK.

BSI (2004). *Precast concrete products - Hollow core slabs.* BS EN 1168, British Standards Institution, London, UK.

Buchanan, A. H. (2001). *Structural Design for Fire Safety*. John Wiley & Sons Ltd, Chichester, UK.

Buchanan, A. H. (2008). The Challenge of Predicting Structural Performance in Fires, *International Association for Fire Safety Science*, Invited Lecture, Karlsruhe, GERMANY.

Carlson, C. C., Selvaggio, S. L., and Gustaferro, A. H. (1965). A Review of Studies of the Effects of Restraint on the Fire Resistance of Prestressed Concrete. *Proceedings, Symposium on Fire Resistance of Prestressed Concrete*, Braunschweig, Germany, International Federation for Prestressing (F.I.P.), Bauverlag GmbH, Wiesbaden, PCA Research Department Bulletin 206, pp. 32-42.

Chang, J. J. (2007). Computer simulation of hollowcore concrete flooring systems exposed to fire. PhD Thesis, University of Canterbury, Christchurch, New Zealand.

Chang, J. J., Buchanan, A. H., Dhakal, R. P., and Moss, P. J. (2008). Hollowcore concrete slab exposed to fire. *Fire and Materials*, 32(6), 321-331.

Council on Tall Buildings and Urban Habitat (CTBUH). Committee 8A (1992). *Fire Safety in Tall Buildings*. McGraw-Hill, New York, USA.

Concrete Reinforcing Steel Institute (CRSI) (1980). *Reinforced concrete fire resistance.* Chicago, USA.

Dotreppe, J., and Franssen, J. (2004). Precast Hollow Core Slabs in Fire: Numerical Simulations and Experimental Tests. *Proceedings of the Third International Workshop Structures in Fire SiF'04*, Ottawa, Canada.

DS 411 (1999). *Code of practice for the structural use of concrete*, 4th Edition, Dansk Standard (in Danish).

EC1 (2002) *Eurocode 1: Actions on structures. PrEN 1991-1-2: Actions on structures exposed to fire*. European Committee for Standardization, Brussels.

EC2 (1995). *Eurocode 2: Design of Concrete Structures. ENV 1992-1-1: General Rules and Rules for Buildings*, European Committee for Standardization, Brussels.

EC2 (2003). *Eurocode 2: Design of Concrete Structures. prEN 1992-1-1: General Rules and Rules for Buildings*, European Committee for Standardization, Brussels.

EC2 (2004). *Eurocode 2: Design of Concrete Structures. prEN 1992-1-2: General Rules, Structural Fire Design*, European Committee for Standardization, Brussels.

EC3 (2004). *Eurocode 3: Design of Steel Structures. prEN 1993-1-2: General Rules, Structural Fire Design*, European Committee for Standardization, Brussels.

Elliott, K. S. (2000). Research and development in precast concrete framed structures. *Progress in Structural Engineering and Materials*, 2(4), 405-428.

Federal Emergency Management Agency (FEMA) (2002). *World Trade Center Building Performance Study: Data Collection, Preliminary Observations, and Recommendations*. FEMA Region Ⅱ, New York, USA.

Fédération internationale du béton. FIB Commission 6, Prefabrication (2000). *Special Design Considerations for Precast Prestressed Hollow Core Floors: Guide to Good Practice*. International Federation for Structural Concrete, Lausanne, Switzerland.

Fédération internationale du béton. Task Group 4.3 (2008). *Fire Design of Concrete Structures – Structural Behaviour and Assessment: state-of-art report*. International Federation for Structural Concrete, Lausanne, Switzerland.

Fédération internationale du béton. Working Party 4.3-1 (2007). *Fire Design of Concrete Structures – Materials, Structures and Modelling: state-of-art report*. International Federation for Structural Concrete, Lausanne, Switzerland.

Fellinger, J. H. H. (2004) *Shear and Anchorage Behaviour of Fire Exposed Hollow Core Slabs*. DUP Science, Delft, Netherlands.

Fellinger, J., Stark. J., and Walraven, J. (2005) Shear and anchorage behaviour of fire exposed hollow core slabs. *Heron*, 50(4), 279-301.

Fenwick, R., Bull, D. K., and Gardiner, D. (2010). *Assessment of hollow-core floor for seismic performance*. University of Canterbury.

FIP/CEB Recommendations (1975). *The design of reinforced and prestressed concrete structural members for fire resistance*.

FIP Recommendations (1988). *Precast Prestressed Hollow Core Floors*.

Franssen, J.–M., and Bruls, A. (1997). Design and Tests of Prestressed Concrete Beams. *Proc. 5th International Symposium on Fire Safety Science (Melbourne)*, pp 1081-1092.

Franssen, J.–M., Kodur, V., and Mason, J. (2002). *Elements of theory for SAFIR 2001: A computer program for analysis of structures submitted to the fire.* Department Structures du Génie Civil, Service Ponts et Charpentes, University of Liége, Belgium.

Franssen, J.–M., and Gens, F. (2004). Dynamic analysis used to cope with partial and temporary failures. *Proceedings of the Third International Workshop Structures in Fire SiF'04*, Otawa, Canada.

Franssen, J.–M. (2005a). SAFIR. A Thermal/Structural Program Modelling Structures under Fire. *Engineering Journal, AISC*, 42 (3), 143–158.

Franssen, J.–M., and Raul, Z. (2005b). *Design of Steel Structures subjected to Fire: Background and Design Guide to Eurocode 3*. Éditions de l'Université de Liège, Liège, Belgique.

Franssen, J.–M. (2007). *User's Manual for SAFIR 2007: A Computer Program for Analysis of Structures Subjected to Fire.* Liège: University of Liège, Belgium.

Gustaferro, A. H. (1967). Fire Endurance of Simply Supported Prestressed Concrete Slabs. *PCI Journal*, 12(1), 37-52.

Gustaferro, A. H. (1973). Design of Prestressed Concrete for Fire Resistance, *PCI Journal*, 18(6), 102-116.

Gustaferro, A. H., and Martin, L. D. (1989). *Design for Fire Resistance of Precast Prestressed Concrete*, 2nd Ed., Prestressed Concrete Institute, Illinois, USA.

Hare, J., Fewnwick, R., Bull, D., and Built, R. (SESOC Sub Committee) (2009). Precast Double Tee Support Systems. *SESOC journal*, 22(1), 10-44.

Harmathy, T.Z. (1986). *Evaluation and Repair of Fire Damage to Concrete*. American Concrete Institute, Michigan, USA.

Harmathy, T. Z. (1993). *Fire Safety Design and Concrete*. Longman Scientific and Technical, UK.

Herlihy, M. D. (1999). Precast concrete floor support and diaphragm action. PhD Thesis, University of Canterbury, Christchurch, New Zealand.

Hertz, K. (1982). The anchorage capacity of reinforcing bars at normal and high temperatures. *Magazine of Concrete Research*, 34(121), 213-220.

International Code Council (ICC) (2006). *International Building Code*. Falls Church, VA, USA.

ISO (1975). *Fire resistance tests – Elements of building construction. ISO 834-1975*. International Organization for Standardization.

Issen, L. A., Gustaferro, A. H., and Carlson, C. C. (1970). Fire Tests of Concrete Memebers: An Improved Method for Estimating Thermal Restraint Forces. *Fire Test Performance*, ASTM STP No. 464, American Society for Testing and Materials, pp. 153-185.

Jensen, J. F. (2005). *Hollowcore Concrete Slabs – Documentation on shear capacity*. Danish Institute of Fire Technology, Denmark.

Jensen, J. P. (2006). The seismic behaviour of existing hollowcore seating connections pre and post retrofit. Master Thesis, University of Canterbury, Christchurch, New Zealand.

Kirby, B. R. (1997). Large Scale Fire Tests: the British Steel European Collaborative Research Programme on the BRE 8-Storey Frame. *Fifth International Symposium on Fire Safety Science*, Melbourne, Australia.

Kirby, B. R. (2000). *British Steel data on the Cardington fire tests*. Technical report, British Steel, UK.

Lennon, T. (2003). Precast Concrete Hollowcore Slabs in Fire. *The Structural Engineer*, 81(8), 30-47.

Liew, H. Y. (2004). Performance of hollowcore floor seating connection details. Master Thesis, University of Canterbury, Christchurch, New Zealand.

Lim, L. (2003). Membrane action in fire exposed concrete floor systems. PhD Thesis, University of Canterbury, Christchurch, New Zealand.

Lin, T. Y. (1963). *Design of Prestressed Concrete Structures*. Wiley, New York, USA.

Lindsay, R. (2004). Experiments on the seismic performance of hollow-core floor systems in precast concrete buildings. Master Thesis, University of Canterbury, Christchurch, New Zealand.

MacPherson, C. (2005). Seismic performance and forensic analysis of a precast concrete hollow-core floor super-assemblage. Master Thesis, University of Canterbury, Christchurch, New Zealand.

Malhotra, H. L. (1982). *Design of Fire-Resisting Structures*. Surrey University Press, UK.

Matthews, J. (2004). Hollow-core floor slab performance following a severe earthquake. PhD Thesis, University of Canterbury, Christchurch, New Zealand.

Mbwambo, J. W. (1995). Structural response of prestressed concrete members subjected to elevated temperatures. PhD Thesis, University of Florida, USA.

Mejia-McMaster, J. C. (1994) Precast concrete hollow-core floor unit support and continuity. Master Thesis, University of Canterbury, Christchurch, New Zealand.

Moss, P. J., Dhakal, R. P., Buchanan, A. H., Min, J-K, and Chang, J. J. (2009). Modelling hollowcore concrete slabs subjected to fire, in Aravithan, Karunasena & Wang (Eds), *Futures in Mechanics of Structures and Materials being Proc 20th Australasian Conference on the Mechanics of Structures and Materials*, Toowoomba, Australia, 2-5 Dec. 2008, CRC Press/Balkema, pp205-209.

Overbeek, T. V., Breunese, A., Gijsbers, J., Both, J., Maljaars, J., and Noordijk, L. (2010). New Regulations for Hollow Core Slabs After Premature Partial Collapse. *Proceedings of the Sixth International Workshop Structures in Fire SiF'10*, Michigan, USA.

PCFOG committee. (2009). *Seismic Performance of Hollow Core Floor Systems – Guidelines for Design Assessment and Retrofit*, Preliminary report, Depatrment of Building and Housing, New Zealand (retrieved from http://www.dbh.govt.nz/UserFiles/File/Consulting/pdf/2009/Seismic-Performance-of-Hollow-Core-Floor- Systems.pdf).

Precast/Prestressed Concrete Institute (2004). *PCI Design Handbook 6th edition: precast and prestressed concrete*. Chicago, IL, USA.

Rombach, G. A. (2004). *Finite Element Design of Concrete Structures: Practical*

Problems and Their Solutions. Thomas Telford, London, UK.

Schepper, L., and Anderson, N. E. (2000). *Danish Institute of Fire Technology & COWI Technical Report PG 10724 – Fire Test of Deck Elements*. COWI and Danish Institute of Fire Technology, Denmark.

Selvaggio, S. L., and Carlson, C. C. (1962). Effect of Restraint on Fire Resistance of Prestressed Concrete, *Symposium on Fire Test Methods*, ASTM STP No. 344, American Society for Testing and Materials, pp. 91-115.

Selvaggio, S. L., and Carlson, C. C. (1967). Restraint in Fire Tests of Concrete Floors and Roofs. *Fire Test Methods – Restraint of Smoke*, ASTM STP No. 422, American Society for Testing and Materials, pp. 21-39.

Sesoc News (2008). (retrieved from http://sesoc.org.nz/Journals/newsletters/SESOC_Issue04_September2008.pdf)

SNZ (2004). Amendment No. 3 to NZS 3101:1995 Standards New Zealand, wellington, NZ.

SNZ (2006a). NZS 3101:Part 1:2006, *The Design of Concrete Structures.* Standards New Zealand, Wellington, NZ.

SNZ (2006b). NZS 3101:Part 2:2006, *Commentary on The Design of Concrete Structures.* Standards New Zealand, Wellington, NZ.

Stollard, P., and Abrahams, J. (1995). *Fire from Fire Principles: a design to building fire safety*. E & FN Spon, London, UK.

Stahlton (2011). (retrieved from http://www.stahlton.co.nz/idc/groups/web_stahlton/documents/webcontent/nz_00016547.pdf, http://www.stahlton.co.nz/idc/groups/web_stahlton/documents/webcontent/nz_00016542.pdf and http://www.stahlton.co.nz/idc/groups/web_stahlton/ documents/webcontent/nz_00016543.pdf).

Stresscrete products (2011). (retrieved from http://www.stresscrete.co.nz/ downloads/35 % 20 -%2040%20Hollowcore.pdf, http://www.stresscrete.co.nz/ downloads/41%20-%2043%20Double%20Tee.pdf and http://www.stresscrete.co.nz/downloads/ 26%20-%2031%20Unispan.pdf).

Technical reports (2007). (retrieved from http://www.dbh.govt.nz/UserFiles/File/Publications/Building/Technical-reports/hollowcore-floor-overview-report.pdf).

Van Acker, A. (2003). Shear Resistance of Prestressed Hollow Core Floors exposed

to Fire. *Structural Concrete*, 4(2), 65-74.

Van Acker, A. (2010). Fire safety of prestressed hollowcore floors. *Concrete Plant International*, 2010(1), 182-196.

Appendix A

Fire resistance of a simply supported hollowcore slab (PCI method)

Determine the fire resistance of a simply supported (unrestrained) hollowcore slab, 200mm deep, 1200mm wide, reinforced with seven 11.2mm, 1.87GPa strands centered 45mm above the bottom of the slab. The span is 10m, the dead load is 3.88kPa, and the live load is 3.3kPa. Concrete is made with siliceous aggregate with f_c=45MPa. The topping thickness is 65mm and its strength is 30MPa. Therefore, the transformed cross section using modulas ratio for topping concrete is used.

Bending moment

$$M = \frac{\mathrm{wl}^2}{8} = \frac{(3.88+3.3)\times 1.2\times(10)^2}{8} = 107{,}700 Nm$$

Nominal moment strength

$$M_n = A_{ps} f_{ps} (d - \frac{a}{2})$$

where, A_{ps} : the cross sectional area of prestressing steel

f_{ps} : stress in prestressing steel in flexural member at ultimate load

d: distance between centroid of reinforcement and extreme

compression fibre

a: the depth of the equivalent rectangular stress block at ultimate load and is equal to $A_{ps}f_{ps}/0.85f_cb$, where f_c is the compressive strength of the concrete and b is the width of the slab

$$A_{ps} = 7 \times 100^2 = 700mm^2$$

$$d = 243.55 - 45 = 198.55mm$$

$$f_{ps} = f_{pu}(1 - \frac{0.5A_{ps}f_{pu}}{bdf_c})$$

$$= 1870 \times \left[1 - \frac{0.5 \times 700 \times 1870}{1200 \times 198.55 \times 45}\right] = 1755.93MPa$$

$$a = \frac{A_s f_y}{0.85 \times f_c \times b} = \frac{700 \times 1870}{0.85 \times 45 \times 1200} = 28.52mm$$

$$M_n = A_{ps}f_{ps}(d - \frac{a}{2}) = 700 \times 1755.93 \times (198.55 - 14.26) = 226,520Nm$$

Moment intensity

$$M/M_n = 107,700 / 226,520 = 0.475$$

$$\overline{\omega_P} = \frac{A_{ps}f_{pu}}{bdf_c} = \frac{700 \times 1870}{1200 \times 198.55 \times 45} = 0.122$$

From Figure A.1 with $M/M_n = 0.475$, $\overline{\omega_P} = 0.122$, and $u = 45mm$, the fire resistance is about **2hr 15min**.

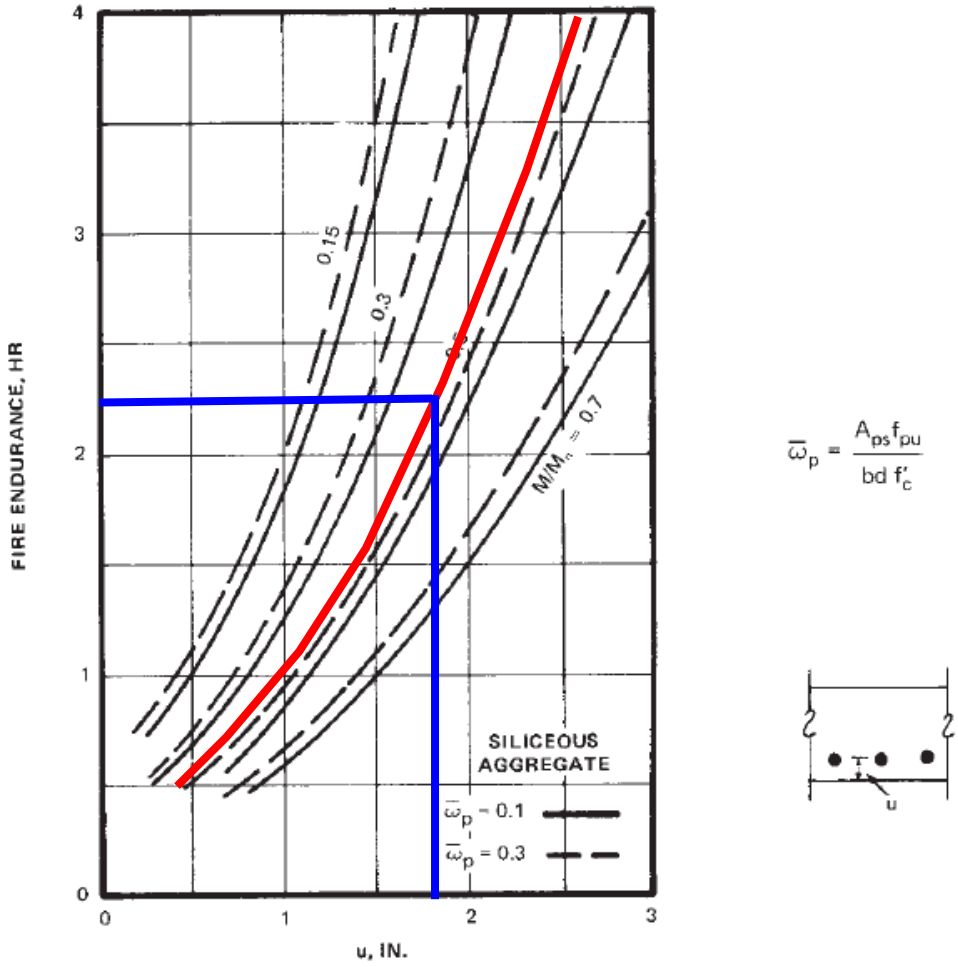

Figure A.1 Fire resistance of prestressed concrete slabs as affected by moment intensity, $\overline{\omega_p}$, and u, SILICEOUS AGGREGATE (Gustaferro, 1989)

Appendix B

Fire resistance of a simply supported hollowcore slab (Simple hand calculation: step-by-step method (Buchanan, 2001))

Determine the fire resistance of a simply supported (unrestrained) hollowcore slab, 200mm deep, 1200mm wide, reinforced with seven 11.2mm, 1.87GPa strands centered 45mm above the bottom of the slab. The span is 10m, the dead load is 3.88kPa, and the live load is 3.3kPa. Concrete is made with siliceous aggregate with f_c=45MPa. The topping thickness is 65mm and its strength is 30MPa. Therefore, the transformed cross section using modulas ratio for topping concrete is used.

1) Calculation of steel temperature against time using spreadsheet

Table B.1 Spread sheet calculation

Time		Fire temperature	Surface temperature	Concrete temperature	Steel temperature	Reduction factor	Reduced yield stress
Minute (t)	Hour (t_h)	(T_f)	(T_w)	(T_c)	(T_s)	-	($f_{y,T}$)
1	0.02	349	-440	190	190	1.00	1870
10	0.17	678	476	-8	-8	1.00	1870
20	0.33	781	655	71	71	1.00	1870
30	0.50	842	746	136	136	0.96	1793
40	0.67	885	807	188	188	0.89	1665
50	0.83	918	852	233	233	0.82	1538
60	1.00	945	887	272	272	0.75	1411
70	1.17	968	916	306	306	0.69	1288

80	1.33	988	941	337	337	0.63	1184
90	1.50	1006	963	365	365	0.58	1080
100	1.67	1022	982	391	391	0.52	977
110	1.83	1036	999	415	415	0.48	888
120	2.00	1049	1014	437	437	0.43	810
130	2.17	1061	1028	458	458	0.39	732
140	2.33	1072	1041	478	478	0.35	655
150	2.50	1082	1053	496	496	0.31	577
160	2.67	1092	1064	514	514	0.28	524
170	2.83	1101	1074	530	530	0.26	478
180	3.00	1110	1084	546	546	0.23	432
190	3.17	1118	1093	562	562	0.21	386
200	3.33	1126	1101	576	576	0.18	340
210	3.50	1133	1110	590	590	0.16	294
220	3.67	1140	1117	604	604	0.14	257
230	3.83	1146	1125	617	617	0.13	241
240	4.00	1153	1132	629	629	0.12	217

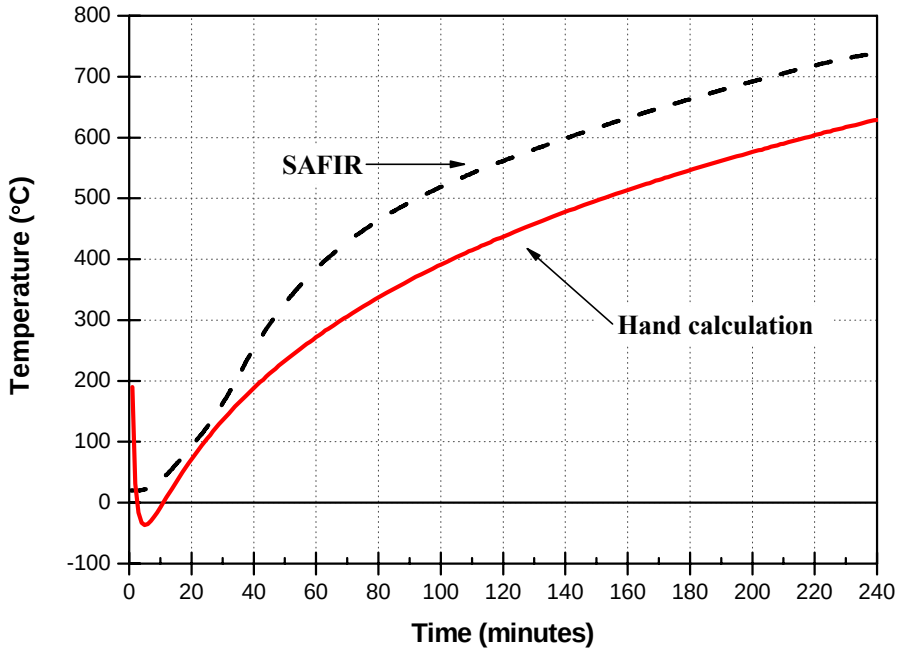

Figure B.1 Comparison of temperature developments for presteressing strand

Figure B.1 shows the comparison between SAFIR thermal analysis and hand calculation using Wickström's fomula.

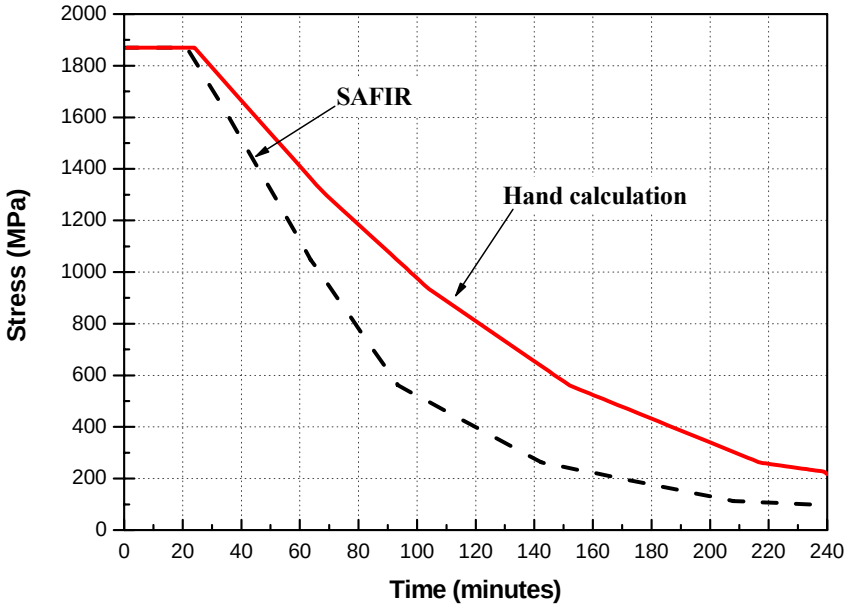

Figure B.2 Comparison of prestressing yield stress

2) Calculation of prestressing tensile stress capacity

FIRE CALCULATIONS

Bending moment

$$M^*_{fire} = w_f L^2 / 8$$

where, w_f : fire design load

L : span

$$M^*_{fire} = w_f L^2 / 8 = \frac{6.24 \times 10^2}{8} = 78\,\text{kNm}$$

Tensile stress capacity

d : effective depth $(= h - c_v - D_b / 2)$

$$d = 243.55 - 40 - \frac{10}{2} = 198.55\,\text{mm}$$

jd : internal lever arm $(= d - a/2)$

$$jd = 198.55 - \frac{28.52}{2} = 184.29\,\text{mm}$$

$$a = (700 \times 1870)/(0.85 \times 45 \times 1200) = 28.52\,\text{mm}$$

$$M^*_{fire} = A_s \sigma_s jd$$

$$\sigma_s = \frac{78000000}{700 \times 184.29} = 604.64\ \text{N/mm}^2 = 604\text{MPa}$$

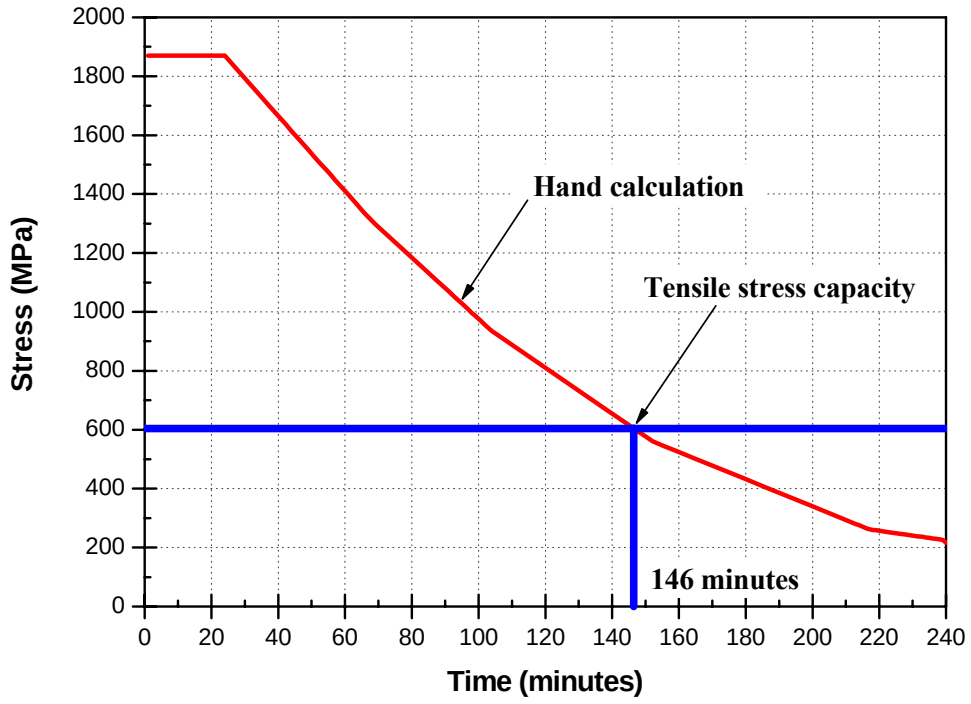

Figure B.3 Tensile stress capacity of prestressing strand

Appendix C

Fire resistance of a simply supported hollowcore slab (Simple hand calculation: moment capacity method)

Determine the fire resistance of a simply supported (unrestrained) hollowcore slab, 200mm deep, 1200mm wide, reinforced with seven 11.2mm, 1.87GPa strands centered 45mm above the bottom of the slab. The span is 10m, the dead load is 3.88kPa, and the live load is 3.3kPa. Concrete is made with siliceous aggregate with f_c=45MPa. The topping thickness is 65mm and its strength is 30MPa. Therefore, the transformed cross section using modulas ratio for topping concrete is used.

1) Fire calculations (1hr 30min. fire exposure)

Revised strength reduction factor $\phi = 1.0$

Design load (fire) $w_f = G + 0.4Q = 5.2\text{kN/m}$

Bending moment $M^*_{fire} = w_f L^2/8 = \dfrac{5.2\times 10^2}{8} = 65\,\text{kNm}$

After 90 minutes of standard fire exposure $t = 90\,\text{min}$ (t_h=1.5 hours)

Fire temperature $T_f = 20 + 345\log(8t+1) = 1006\,^\circ\text{C}$

Surface temperature $T_w = [1 - 0.0616 t_h^{-0.88}]\ T_f = 963\,^\circ\text{C}$

Concrete temperature $T_c = [0.18\ln(t_h/C_e^{\,2}) - 0.81]\ T_w = 365\,^\circ\text{C}$

Steel temperature $T_s = T_c = 365\,°C$

Reduced yield stress $f_{y,T} = 1080\,\text{MPa}$ (from table B.1)

Stress block depth $a = A_s f_{y,T} / 0.85 f_c' b$

$= 700 \times 1080 / 0.85 \times 45 \times 1200 = 16.47\,\text{mm}$

Internal lever arm $jd = d - \frac{a}{2} = 155 - \frac{16.47}{2} = 146.8\,\text{mm}$

Bending strength $M_{nf} = A_s f_{y,T} jd = 700 \times 1080 \times \frac{146.8}{10^6}$

$= 111\,\text{kNm}$

$\phi M_{nf} = 1.0 \times 111 = 111\,\text{kNm}$

$\phi M_{nf} \rangle M^*_{fire}$ so design is OK.

2) Fire calculations (2hr fire exposure)

Revised strength reduction factor $\phi = 1.0$

Design load (fire) $w_f = G + 0.4Q = 5.2\,\text{kN/m}$

Bending moment $M^*_{fire} = w_f L^2 / 8 = \frac{5.2 \times 10^2}{8} = 65\,\text{kNm}$

After 90 minutes of standard fire exposure $t = 120\,\text{min}$ (t_h= 2 hours)

Fire temperature $T_f = 20 + 345\log(8t + 1) = 1049\,°C$

Surface temperature $T_w = [1 - 0.0616 t_h^{-0.88}]\ T_f = 1014\,°C$

Concrete temperature $T_c = [0.18\ln(t_h / C_e^{\,2}) - 0.81]\ T_w = 437\,°C$

Steel temperature $T_s = T_c = 437\,°C$

Reduced yield stress $f_{y,T} = 810\,\text{MPa}$ (from table B.1)

Stress block depth $a = A_s f_{y,T} / 0.85 f_c' b$

$= 700 \times 810 / 0.85 \times 45 \times 1200 = 12.35\,\text{mm}$

Internal lever arm $jd = d - \frac{a}{2} = 155 - \frac{12.35}{2} = 148.8\,\text{mm}$

Bending strength $M_{nf} = A_s f_{y,T} jd = 700 \times 810 \times \frac{148.8}{10^6}$

$= 84.36\,\text{kNm}$

$\phi M_{nf} = 1.0 \times 84.36 = 84.36\text{kNm}$

$\phi M_{nf} \rangle M^*_{fire}$ so design is OK.

3) Fire calculations (2hr 30min. fire exposure)

Revised strength reduction factor $\phi = 1.0$

Design load (fire) $w_f = G + 0.4Q = 5.2\text{kN/m}$

Bending moment $M^*_{fire} = w_f L^2 / 8 = \frac{5.2 \times 10^2}{8} = 65\,\text{kNm}$

After 90 minutes of standard fire exposure $t = 150\,\text{min}$ (t_h= 2.5 hours)

Fire temperature $T_f = 20 + 345\log(8t + 1) = 1082\,^\circ\text{C}$

Surface temperature $T_w = [1 - 0.0616 t_h^{-0.88}]\ T_f = 1053\,^\circ\text{C}$

Concrete temperature $T_c = [0.18\ln(t_h / C_e^2) - 0.81]\ T_w = 496\,^\circ\text{C}$

Steel temperature $T_s = T_c = 496\,^\circ\text{C}$

Reduced yield stress $f_{y,T} = 577$ MPa (from table B.1)

Stress block depth $a = A_s f_{y,T} / 0.85 f'_c b$

$= 700 \times 577 / 0.85 \times 45 \times 1200 = 8.8\,\text{mm}$

Internal lever arm $jd = d - \frac{a}{2} = 155 - \frac{8.8}{2} = 150.6\,\text{mm}$

Bending strength $M_{nf} = A_s f_{y,T} jd = 700 \times 577 \times \frac{150.6}{10^6}$

$= 60.8\,\text{kNm}$

$\phi M_{nf} = 1.0 \times 60.8 = 60.8\text{kNm}$

$\phi M_{nf} \langle M^*_{fire}$ so design is FAIL.

Appendix D

Determination of required number of tendons (Constant eccentricity tendons)

● **Given conditions**:

Span	L: 14 m
Self-weight	w_s: 4.25 kPa
Dead load	w_d: 0.5 kPa
Live load	w_l: 3.0 kPa
Depth of unit	h: 500 mm
Cross sectional area of concrete	A_c: 288x10^3 mm^2
Distance from the centroid to the top surfaces	y_t: 163 mm
Distance from the centroid to the bottom surfaces	y_b: 337 mm
Second moment of area	I: 6.929x10^9 mm^4
Section modulus of top surfaces	Z_t: 42.5x10^6 mm^3
Section modulus of bottom surfaces	Z_b: 20.6x10^6 mm^3
Radius of gyration	$r_c^2\left(=\frac{I}{A_c}\right)$: 24.06x10^3 mm^2

1) **Stress limits**

At transfer stage (unloaded state):

$$f_{ci} = -0.6f_{ci} = -0.6 \times 31.5 = -18.9 \text{ MPa}$$

$$f_{ti} = 0.5\sqrt{f_{ci}} = 0.5\sqrt{31.5} = 2.8 \text{ MPa}$$

At service load stage (loaded state):

$$f_{cs} = -0.45f_c^{'} = -0.45 \times 45 = -20.25 \text{ MPa}$$

$$f_{ts} = 0.5\sqrt{f_c^{'}} = 0.5\sqrt{45} = 3.4 \text{ MPa}$$

2) **Determination of cross section**

The self-weight of the 500 mm double tee will be estimated at 4.59 kN/m. The moments due to transverse loading are

$$M_0 = \frac{w_s l^2}{8} = \frac{1}{8} \times 4.25 \times 14^2 = 104.125 \text{ kNm} = 104.125 \times 10^6 \text{ Nmm}$$

$$M_d + M_l = \frac{(w_d + w_l)l^2}{8} = \frac{1}{8} \times (0.5 + 3.0) \times 14^2 = 85.75 \text{ kNm} = 85.75 \times 10^6 \text{ Nmm}$$

The required section moduli with respect to the top and bottom surfaces of the double tee are found

$$Z_t \geq \frac{M_0 + M_d + M_l}{Rf_{ti} - f_{cs}} = \frac{104.125 \times 10^6 + 85.75 \times 10^6}{0.85 \times 2.8 + 20.25} = \frac{189{,}875{,}000}{22.63} = 8.39 \times 10^6 \text{ mm}^3$$

$$Z_b \geq \frac{M_0 + M_d + M_l}{f_{ts} - Rf_{ci}} = \frac{104.125 \times 10^6 + 85.75 \times 10^6}{3.4 \times 0.85 + 18.9} = \frac{189{,}875{,}000}{21.79} = 8.71 \times 10^6 \text{ mm}^3$$

3) The **<u>concrete centroidal stress</u>** under initial conditions is given by

$$f_{cci} = f_{ti} - \frac{y_t}{h}(f_{ti} - f_{ci})$$

where, $f_{ti} = 0.5\sqrt{f_{ci}} = 0.5\sqrt{31.5} = 2.8 \text{ MPa}$

$$f_{ci} = -0.6f_{ci} = -0.6 \times 31.5 = -18.9 \text{ MPa}$$

Therefore,

$$f_{cci} = f_{ti} - \frac{y_t}{h}(f_{ti} - f_{ci}) = 2.8 - \frac{163}{500}(2.8 + 18.9) = -4.3 \text{ MPa} = -4.3 \text{ N/mm}^2 \qquad (1)$$

4) From equation (1), the **initial prestress force** is

$$P_i = A_c f_{cci} = 288 \times 10^3 \times 4.3 = 1{,}238 \ \text{kN}$$

5) The **required constant eccentricity** is

$$e = (f_{ti} - f_{cci})\frac{Z_t}{P_i} = \{2.8 - (-4.3)\}\frac{42{,}500{,}000}{1{,}238{,}000} = 244 \ \text{mm}$$

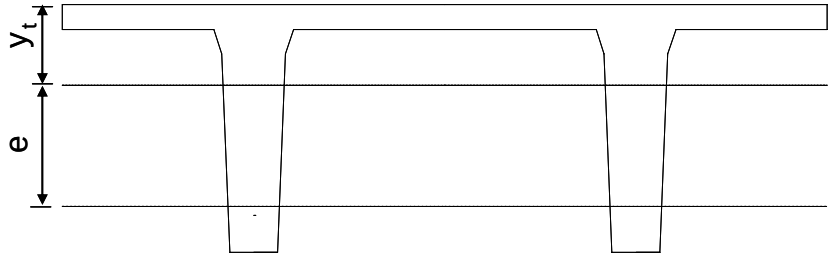

※ Use of 12.7 mm diameter seven-wire stress relieved wires

The required initial prestress force of 1,238 kN will be provided using tendons consisting of 12.7 mm diameter seven-wire stress-relieved wires. The minimum tensile strength is f_{pu}=1,840 MPa, and for normal prestressing wire, the yield strength may be taken as f_{py}= 0.85xf_{pu} =1,564 MPa

The permissible stress in the wire immediately after transfer must not exceed 0.82f_{py} =1,282 MPa or 0.74f_{pu} =1,361 MPa. The first criterion controls.

6-1) The **required area of prestressed steel** is

$$A_p = \frac{P_i}{0.82 f_{py}} = \frac{1{,}238{,}000}{1{,}282} = 965 \ \text{mm}^2$$

7-1) The cross sectional area of one 12.7 mm diameter wire is 98.71 mm^2; hence, the **number of wires required** is

$$\text{Number of wires} = \frac{965}{98.71} = 9.77 = 10 \ \text{ea}$$

※ Use of 15.2 mm diameter seven-wire stress relieved wires

The required initial prestress force of 3,398.4 kN will be provided using tendons consisting of 15.2 mm diameter seven-wire stress-relieved wires. The minimum tensile strength is f_{pu}=1,840 MPa, and for normal prestressing wire, the yield strength may be taken as f_{py}= 0.85xf_{pu} =1,564 MPa

The permissible stress in the wire immediately after transfer must not exceed 0.82f_{py} =1,282 MPa or 0.74f_{pu} =1,361 MPa. The first criterion controls.

6-2) The **required area of prestressed steel** is

$$A_p = \frac{P_i}{0.82f_{py}} = \frac{1{,}238{,}000}{1{,}282} = 965 \ \text{mm}^2$$

7-2) The cross sectional area of one 15.2 mm diameter wire is 138.7 mm^2; hence, the **number of wires required** is

$$\text{Number of wires} = \frac{965}{138.7} = 6.95 = 8 \,\text{ea}$$

A total of 10 wires is required as before, 12.7 mm each tendon.

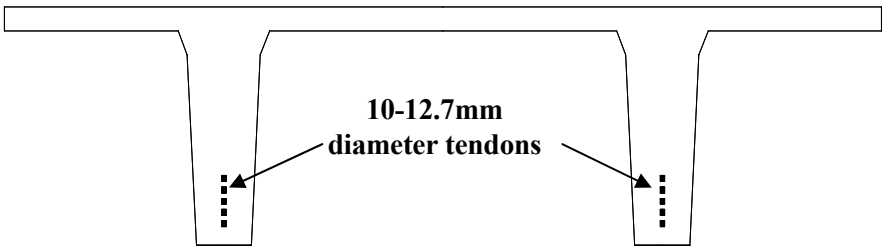

8) **Verification of stresses**

The calculations will be checked by verifying concrete stresses at the top and bottom of the beam for the critical load stages. The component stress contributions are

P_i: $$f_t = -\frac{P_i}{A_c} + \frac{P_i e}{I} y_t = -\frac{P_i}{A_c}\left(1 - \frac{e y_t}{r_c^2}\right) = -\frac{1{,}238{,}000}{288 \times 10^3}\left(1 - \frac{244}{24{,}060} \times 163\right)$$

$$= 2.81 \text{ MPa (tension)}$$

$$f_b = -\frac{P_i}{A_c} + \frac{P_i e}{I} y_b = -\frac{P_i}{A_c}\left(1 - \frac{e y_b}{r_c^2}\right) = -\frac{1{,}238{,}000}{288 \times 10^3}\left(1 + \frac{244}{24{,}060} \times 337\right)$$

$$= -18.99 \text{ MPa (compression)}$$

P_e: $$f_t = 0.85 \times 2.81 = 2.39 \text{ MPa}$$

$$f_t = 0.85 \times 18.99 = -16.14 \text{ MPa}$$

M_0: $$f_t = -\frac{M_0}{Z_t} = -\frac{104.125 \times 10^6}{42.5 \times 10^6} = -2.45 \text{ MPa}$$

$$f_b = \frac{M_0}{Z_b} = \frac{104.125 \times 10^6}{20.6 \times 10^6} = 5.05 \text{ MPa}$$

$M_d + M_l$: $$f_t = -\frac{M_d + M_l}{Z_t} = -\frac{85.75 \times 10^6}{42.5 \times 10^6} = -2.01 \text{ MPa}$$

$$f_b = \frac{M_d + M_l}{Z_b} = \frac{85.75 \times 10^6}{20.6 \times 10^6} = 4.16 \text{ MPa}$$

Superimposing the appropriate stress contributions, the stress distributions in the concrete at midspan and at the supports are obtained. When the initial prestress force of 1,238 kN acts alone, as at the supports, the stresses at the top and bottom surfaces are

$$f_t = 2.81 \text{ MPa}$$

$$f_b = -18.99 \text{ MPa}$$

At midspan the beam weight is immediately superimposed, and stresses resulting from P_i plus M_0 are

$$f_t = 2.81 - 2.45 = 0.36 \text{ MPa}$$

$$f_b = -18.99 + 5.05 = -13.94 \text{ MPa}$$

When the full service load acts, together with P_e, the midspan stresses are

$$f_t = 2.39 - 2.45 - 2.01 = -2.07 \text{ MPa}$$

$$f_b = -16.14 + 5.05 + 4.16 = -6.93 \text{ MPa}$$

If we check against the specified limiting stresses, it is evident that the design is satisfactory in this respect at the critical load stages and locations.

Appendix E

Details of a precast double tee slab

In this appendix, details of a precast double tee slab are provided for the same cross section. Some differences exist depending on the number of prstressing steels and strand patterns.

FULTON HOGAN PRECAST
MDES SUMMARY SHEET

Christchurch Branch
133 Waterloo Road,Christchurch, N.Z
Phone 03 344 3014
Fax 03 344 3018

Page :
Date : 25-Feb-10
Time : 3:57 p.m.
Job No : CHQ012
Initials : MRL

Title: FIRE TESTING

PRECAST UNIT NAME : 500 x 2400 Double Tee
MANUFACTURED AT : Christchurch
GRID/FLOOR LOCATION : OPTION 1

Shop Drawing Check Required : No
Special Supervision Required : No
Calculation Sheets Attached : No No. off : 0

Span	:	14.000	m	$w_{(Odl)}$	:	6.72	kN/m
P.C. Depth	:	500	mm	$w_{(topp)}$	:	4.25	kN/m
Topping Depth	:	75	mm	Line DL	:	0.00	kN/m
Width	:	2.400	m	Super DL	:	0.50	kPa
Spacing	:	2.400	m	Live Load	:	3.00	kPa
				Other Load	:		
P.C. Unit f'_c	:	45.0	MPa (28 day)	P.C. f'_{ci}	:	28.0	MPa
Topping f'_c	:	25.0	MPa	P.C. Density	:	23.6	kN/m^3
Fire Rating	:	1.0	hrs	Unit Handled at	:	Ends	

Final Deflection	:	-15	mm	Allowable L/300	:	47	mm
LL Deflection	:	10	mm	Allowable L/500	:	28	mm

PRESTRESS : 10 - 12.9 mm Dia. @ 110 mm above soffit

STRAND PATTERN :

No.	Dia.(mm)	$Y_{s(mm)}$
2	12.9	200.0
2	12.9	150.0
2	12.9	100.0
4	12.9	50.0

73 % of 184 kN

ESTIMATE

COMMENTS :

4R6 STIRRUPS @ 50 EE

R6 STIRRUPS @ 300 CENTRES

FULTON HOGAN PRECAST
PARTIAL PRESTRESS SUMMARY SHEET

Christchurch Branch
133 Waterloo Road,Christchurch, N.Z
Phone 03 344 3014
Fax 03 344 3018

Page :
Date : 25-Feb-10
Time : 3:58 p.m.
Job No : CHQ012
Initials : MRL

Title: FIRE TESTING

PRECAST UNIT NAME : 500 x 2400 Double Tee
MANUFACTURED AT : Christchurch
GRID/FLOOR LOCATION : OPTION 2

Shop Drawing Check Required : No
Special Supervision Required : No
Calculation Sheets Attached : No No. off : 0

Span	:	14.000	m	$w_{(Odl)}$	:	6.72	kN/m
P.C. Depth	:	500	mm	$w_{(topp)}$	:	4.25	kN/m
Topping Depth	:	75	mm	Line DL	:	0.00	kN/m
Width	:	2.400	m	Super DL	:	0.50	kPa
Spacing	:	2.400	m	Live Load	:	3.00	kPa
				Other Load	:		
P.C. Unit f'_c	:	45.0	MPa (28 day)	P.C. f'_{ci}	:	28.0	MPa
Topping f'_c	:	25.0	MPa	P.C. Density	:	23.6	kN/m^3
Fire Rating	:	1.0	hrs	Unit Handled at	:	Ends	

Final Deflection	:	-5	mm	Allowable L/300	:	47	mm
LL Deflection	:	14	mm	Allowable L/500	:	28	mm

PRESTRESS : 8 - 12.9 mm Dia. @ 88 mm above soffit

STRAND PATTERN :

No.	Dia.(mm)	$Y_{s(mm)}$
2	12.9	150.0
2	12.9	100.0
4	12.9	50.0
[2	U12.9	50.0

73 % of 184 kN

ESTIMATE

Unstressed steel ~ 6m centred]

COMMENTS :

4R6 STIRRUPS @ 60EE

R6 STIRRUPS @ 250 CENTRES

Appendix E Details of a precast double tee slab